AD-A130 687 PROCEEDINGS OF THE STIP (STUDY OF TRAVELLING INTERPLANETARY PHENOMENA) SY..(U) AIR FORCE GEOPHYSICS LAB HANSCOM AFB MA M A SHEA ET AL. 27 DEC 82 1/3

UNCLASSIFIED AFGL-TR-82-0390 F/G 3/2 NL

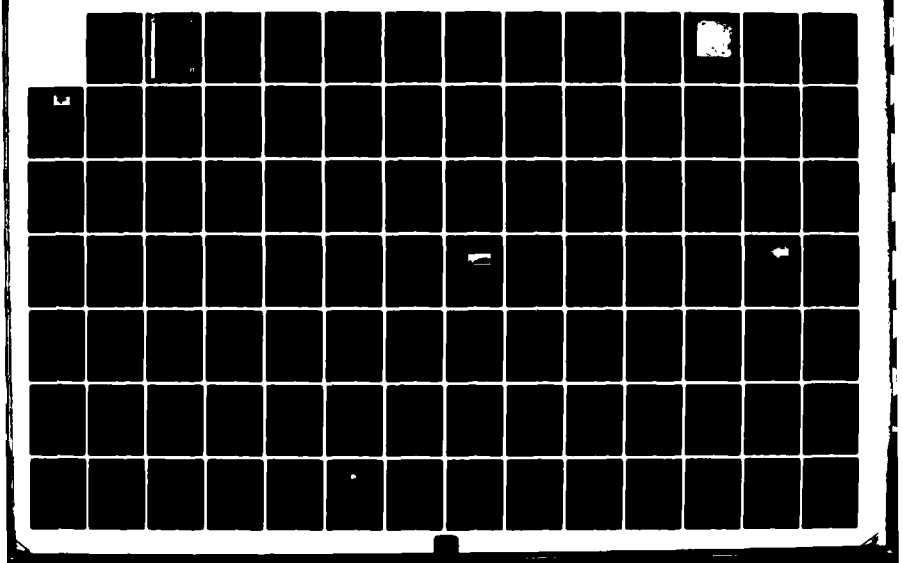

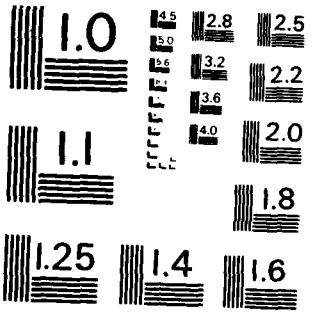

MICROCOPY RESOLUTION TEST CHART
NATIONAL BUREAU OF STANDARDS - 1963 - A

AFGL-TR-82-0390
SPECIAL REPORTS, NO. 233

Proceedings of the STIP Symposium on Solar Radio Astronomy, Interplanetary Scintillations and Coordination With Spacecraft

Editors:

M.A. SHEA
D.F. SMART
D.J. McLEAN
G.J. NELSON

27 December 1982

SPACE PHYSICS DIVISION PROJECT 2311
AIR FORCE GEOPHYSICS LABORATORY
HANSCOM AFB, MASSACHUSETTS 01731

AIR FORCE SYSTEMS COMMAND, USAF

This report has been reviewed by the ESD Public Affairs Office (PA) and is releasable to the National Technical Information Service (NTIS).

This technical report has been reviewed and is approved for publication.

Alva T Stair, Jr.

DR. ALVA T. STAIR, Jr
Chief Scientist

Qualified requestors may obtain additional copies from the Defense Technical Information Center. All others should apply to the National Technical Information Service.

COMPONENT PART NOTICE

THIS PAPER IS A COMPONENT PART OF THE FOLLOWING COMPILATION REPORT:

(TITLE): Proceedings of the STIP (Study of Travelling Interplanetary Phenomena) Symposium on Solar Radio Astronomy, Interplanetary Scintillations and Coordination with Spacecraft Held at Narrabri, N.S.W., Australia on 28-30 November 1979.

(SOURCE): Air Force Geophysics Lab., Hanscom AFB, MA.

TO ORDER THE COMPLETE COMPILATION REPORT USE AD-A130 687.

THE COMPONENT PART IS PROVIDED HERE TO ALLOW USERS ACCESS TO INDIVIDUALLY AUTHORED SECTIONS OF PROCEEDINGS, ANNALS, SYMPOSIA, ETC. HOWEVER, THE COMPONENT SHOULD BE CONSIDERED WITHIN THE CONTEXT OF THE OVERALL COMPILATION REPORT AND NOT AS A STAND-ALONE TECHNICAL REPORT.

THE FOLLOWING COMPONENT PART NUMBERS COMPRISE THE COMPILATION REPORT:

AD#:	TITLE:
P001 435	Radio and X-Ray Evidence for Electron Acceleration in Solar Flares.
P001 436	Magnetohydrodynamic (MHD) Description of Solar Radio Bursts.
P001 437	Profiles of Coronal MHD (Magnetohydrodynamic) Disturbance Associated with the Solar Flare on April 27, 1979.
P001 438	Fine Structure in Metre-Wave Solar Radio Bursts.
P001 439	The Mechanism of the U-Shaped Spectrum of Type IV Solar Radio Bursts.
P001 440	The Proton Flare of 1976 April 30.
P001 441	Relativistic Solar Particle Events during STIP (Study of Travelling Interplanetary Phenomena) Intervals II and IV.
P001 442	Thermal Cyclotron Radiation from Solar Active Regions.
P001 443	Observations of the Quiet Sun at Decametre and Metre Wavelengths.
P001 444	The Rise, Decline, and Possible Relationship between two Flare Producing Regions Including Details of the Activity Patterns of Their Known Antecedent and Descendant Plages.
P001 445	Theoretical MHD (Magnetohydrodynamic) Simulations of Coronal Transients and Interplanetary Observations.
P001 446	Three-Dimensional Distribution of the Solar Wind Velocity Deduced from IPS (Interplanetary Scintillation) Observations.
P001 447	Interplanetary Scintillations at 103 MHz.
P001 448	Analysis of IPS (Interplanetary Scintillation) Data Using a Periodic Phase Screen Model for the Solar Wind.
P001 449	STIP (Study of Travelling Interplanetary Phenomena) VII Observations of the Northern Solar Corona - A First Report on the Scope of Data and the Early Results.
P001 450	Unusually Intense Jovian Decametric Emission Observed on 1979 March 7, 1920 - 2040 UT.

COMPONENT PART NOTICE (CON'T)

AD#: TITLE:

Unclassified

SECURITY CLASSIFICATION OF THIS PAGE (When Data Entered)

REPORT DOCUMENTATION PAGE

READ INSTRUCTIONS BEFORE COMPLETING FORM

1. REPORT NUMBER: AFGL-TR-82-0390	2. GOVT ACCESSION NO.: AD-A130 687
3. RECIPIENT'S CATALOG NUMBER	
4. TITLE (and Subtitle): PROCEEDINGS OF THE STIP SYMPOSIUM ON SOLAR RADIO ASTRONOMY, INTERPLANETARY SCINTILLATIONS AND COORDINATION WITH SPACECRAFT	5. TYPE OF REPORT & PERIOD COVERED: Scientific, Interim
	6. PERFORMING ORG. REPORT NUMBER: SR, No. 233
7. ~~AUTHOR(s)~~: Editors: M. A. Shea, D. F. Smart, D. J. McLean* and G. J. Nelson**	8. CONTRACT OR GRANT NUMBER(s)
9. PERFORMING ORGANIZATION NAME AND ADDRESS: Air Force Geophysics Laboratory (PHG) Hanscom AFB, Massachusetts 01731	10. PROGRAM ELEMENT, PROJECT, TASK AREA & WORK UNIT NUMBERS: 61102F 2311G108
11. CONTROLLING OFFICE NAME AND ADDRESS: Air Force Geophysics Laboratory (PHG) Hanscom AFB, Massachusetts 01731	12. REPORT DATE: 27 December 1982
	13. NUMBER OF PAGES: 229
14. MONITORING AGENCY NAME & ADDRESS(if different from Controlling Office)	15. SECURITY CLASS. (of this report): Unclassified
	15a. DECLASSIFICATION/DOWNGRADING SCHEDULE

16. DISTRIBUTION STATEMENT (of this Report)

Approved for Public Release, Distribution Unlimited.

17. DISTRIBUTION STATEMENT (of the abstract entered in Block 20, if different from Report)

18. SUPPLEMENTARY NOTES

* Division of Radiophysics, CSIRO, P. O. Box 76, Epping, N.S.W., 2121, Australia

** CSIRO Solar Radio Observatory, Culgoora, P. O. Box 94, Narrabri, N.S.W. 2390, Australia

19. KEY WORDS (Continue on reverse side if necessary and identify by block number)

Solar physics	Solar particles
Solar radio astronomy	Interplanetary medium
Interplanetary scintillations	Cosmic rays
Solar wind	Jupiter radio emission

20. ABSTRACT (Continue on reverse side if necessary and identify by block number)

This report is a compilation of 16 papers presented at the Study of Travelling Interplanetary Phenomena (STIP) Symposium on Solar Radio Astronomy, Interplanetary Scintillations, and Coordination with Spacecraft, held 28-30 November 1979 at the Culgoora Radio Observatory in Narrabri, N.S.W., Australia. These papers span a range of multi-disciplinary studies of various solar emissions propagating from the sun through the interplanetary medium to the earth and beyond to Jupiter. This includes papers on solar radio emissions, solar region evolution, solar particle propagation, the

DD FORM 1 JAN 73 1473 EDITION OF 1 NOV 65 IS OBSOLETE

Unclassified

SECURITY CLASSIFICATION OF THIS PAGE (When Data Entered)

modeling of solar induced disturbances in the interplanetary medium; and the use of radio measurements to probe the turbulence of the interplanetary medium. Theoretical studies and analyses, computer simulation and in situ measurements of these phenomena are included. The subjects covered are solar physics, solar radio astronomy, interplanetary scintillation measurements, cometary studies, direct spacecraft measurements and energetic solar particle propagation in the interplanetary medium.

Foreword

The Study of Travelling Interplanetary Phenomena (STIP) is one of the interdisciplinary studies established by the International Council of Scientific Union's Scientific Committee on Solar-Terrestrial Physics (SCOSTEP). The scientific objectives of STIP are the study of phenomena that propagate through the interplanetary medium and a search for understanding of these phenomena during both quiet (i.e. normal) and active periods.

About 300 scientists are actively participating in STIP, their interests ranging from solar physics (insofar as it concerns the initiation of phenomena which moves out from the Sun) to the observation and study of comets and planetary magnetospheres and ionospheres. Solar radio astronomy and interplanetary scintillations of discrete radio sources, solar and galactic cosmic rays, solar wind plasma and interplanetary magnetic fields, and interstellar interactions are among the topics of interest.

The STIP Symposium on Solar Radio Astronomy, Interplanetary Scintillations and Coordination with Spacecraft was held in November 1979 at the site of the CSIRO Culgoora radioheliograph in Narrabri, N.S.W., Australia. This specialized symposium, co-sponsored by the IAU, COSPAR, and IAGA, was attended by ~35 scientists from 10 countries. A total of 21 papers were presented allowing ample time for discussion. In addition, a tour of the radioheliograph and other on site CSIRO radio astronomy equipment was conducted by the CSIRO personnel.

Sixteen of the papers presented at the symposium are contained in this proceedings. Although some of the manuscripts were prepared in camera-ready format by the authors, most of the papers were edited and re-typed after review by the referees. The editors are most grateful to Ms. Marie Vickery for her careful review and typing of eight of these manuscripts. The editors also thank Ms. Karen Flaherty, Ms. Anne A. Bathurst, Ms. Louise C. Gentile, and Ms. Stacey A. Horning for their assistance in typing and reference searches.

Finally, on behalf of all the participants, we wish to thank the CSIRO group for their work in providing the conference facility and the local arrangements for this symposium.

M. A. Shea
D. F. Smart
D. J. McLean
G. J. Nelson

Contents

Foreword iii

1. Radio and X-ray Evidence for Electron Acceleration in Solar Flares 1
   R.T. Stewart

2. Magnetohydrodynamic (MHD) Description of Solar Radio Bursts 19
   S.T. Wu

3. Profiles of Coronal MHD Disturbance Associated with the Solar Flare on April 27, 1979 37
   R.V. Bhonsle, S.S. Degaonkar, and S.K. Alurkar

4. Fine Structure in Metre-Wave Solar Radio Bursts 43
   D. McConnell and G.R.A. Ellis

5. The Mechanism of the U-shaped Spectrum of Type IV Solar Radio Bursts 49
   Li Chun-sheng, Zheng Wing-wu, and Yao Jin-xing

6. The Proton Flare of 1976 April 30 65
   S.I. Avdjushin, N.K. Perejaslova, V.V. Fomichev, and I.M. Chertok

7. Relativistic Solar Particle Events During STIP Intervals II and IV 71
   M.A. Shea and D. F. Smart

8. Thermal Cyclotron Radiation from Solar Active Regions 85
   V.V. Zheleznyakov and E. Ya. Zlotnik

9. Observations of the Quiet Sun at Decimetre and Metre Wavelengths 97
   A.A. Abranin, L.L. Bazeljan, and R.A. Duncan

10. The Rise, Decline and Possible Relationship Between Two Proton Flare Producing Regions Including Details of the Activity Patterns of their Known Antecedent and Descendant Plages 107
    Susan M.P. McKenna-Lawlor

Contents

11. Theoretical MHD Simulations of Coronal Transients and Interplanetary Observations 137
M. Dryer, R.S. Steinolfson, and Z.K. Smith

12. Three-dimensional Distribution of the Solar Wind Velocity Deduced from IPS Observations 153
T. Kakinuma, H. Washimi, and M. Kojima

13. Interplanetary Scintillations at 103 MHz 163
S.K. Alurkar and R.V. Bhonsle

14. Analysis of IPS Data Using a Periodic Phase Screen Model for the Solar Wind 167
A. Basu and S.K. Alurkar

15. STIP VII Observations of the Northern Solar Corona--A First Report on the Scope of Data and the Early Results 183
Thomas A. Croft

16. Unusually Intense Jovian Decametric Emission Observed on 1979 March 7, 1920-2040 UT 209
K. Bullough and W. Gibbons

THE CULGOORA RADIOHELIOGRAPH

This unique instrument consistes of 96 antenna (each antenna being a steerable paraboloid about 45 feet in diameter) arranged in a circular array 1.86 miles in diameter. This radioheliograph has been the world standard for meter wave length solar observations since it began operation in 1967.

PROCEEDINGS OF THE STIP SYMPOSIUM ON SOLAR RADIO ASTRONOMY, INTERPLANETARY SCINTILLATIONS AND COORDINATION WITH SPACECRAFT

1. Radio and X-Ray Evidence for Electron Acceleration in Solar Flares

R. T. Stewart
Division of Radiophysics, CSIRO,
P.O. Box 76, Epping, N.S.W. 2121, Australia

Abstract

Radio and X-ray observations, as well as γ-ray and interplanetary electron observations, are briefly reviewed for evidence of electron acceleration during solar flares. The evidence collected so far suggests that in some large flares a second stage of particle acceleration takes place where ions and electrons are accelerated to very high energies. This second stage follows no more than several minutes after the first or impulsive stage, which occurs during the initial minute or so of the solar flare. During the impulsive phase electrons are accelerated to energies ~10-100 keV, probably by bulk energization, where stored magnetic energy is converted into thermal energy. Energy-loss arguments favour the electrons having a quasi-thermal (near-Maxwellian) electron velocity distribution. During large flares second-phase electrons are accelerated to much higher energies, ~10 MeV, and appear to have a power-law velocity distribution. The second-stage acceleration mechanism may be associated with a coronal shock wave, but so far there is no clear evidence that electrons with energies ≥100 keV are directly associated with a shock wave.

1. INTRODUCTION

The problem of particle acceleration in solar flares has been studied for many years now but is still not fully understood. Evidence for electron acceleration comes from direct measurements of streams of high-energy electrons in interplanetary space and from indirect manifestations, such as burst emission from the Sun at radio, EUV, X-ray and γ-ray wavelengths. Radio bursts at metre wavelengths appear to be due mainly to plasma radiation excited by electrons with energies ~10-100 keV and those at microwave wavelengths to gyro-synchrotron radiation from electrons with energies $\geqslant$100 keV to 1 MeV. Hard X-ray bursts appear to be due to bremsstrahlung from electrons with energies ~10-100 keV and γ-ray continuum to bremsstrahlung from relativistic electrons with energies ~1-10 MeV.

Because energetic ions $\leqslant$10 GeV and relativistic electrons $\leqslant$10 MeV are ejected from the Sun during large flares it is generally believed that these high-energy particles are accelerated in a second-stage process. During the first stage, which occurs during the impulsive phase of the flare, electrons are accelerated to energies ~10-100 keV. Most of the accelerated electrons have energies $\leqslant$30 keV and it has been suggested that these first-stage electrons might come from a quasi-thermal source region where the electron temperature is ~$2\text{-}4 \times 10^8$ K. In the second stage electrons and ions are accelerated to relativistic energies and appear to have non-thermal power-law distributions. It is thought that some form of stochastic process such as Fermi acceleration is responsible.

2. FIRST-STAGE ACCELERATION

This occurs during the first 10 s to 1 min of a solar flare. The radio signature is a group of Type III bursts at metre and decimetre wavelengths and an impulsive microwave burst. Hard and soft X-ray bursts, Hα and EUV flashes also occur. Sometimes fine structures with durations ~1 s are observed in the microwave and hard X-ray bursts and seem to be associated with individual Type III bursts at metre and decimetre wavelengths (Figure 1). This suggests that the acceleration process is very short ($\leqslant$1 s) and repeated. Impulsive bursts are also closely associated with interplanetary electron streams with energies ~10-100 keV but not with proton streams (Lin, 1974). Only a small fraction of the electrons accelerated in the lower corona near the hard X-ray source region escape to interplanetary space (Lin and Hudson, 1971), giving rise to Type III and Type V radio bursts as they travel through the corona (Figure 1); the remaining electrons are either trapped on closed magnetic field lines, where they give rise to microwave bursts by gyro-synchrotron emission, or are lost by collisions and give rise to hard X-ray bursts by bremsstrahlung.

Most of the flare-accelerated electrons seem to be associated with emission of the hard X-ray burst. For example, Hoyng et al. (1976) estimate that ~10^{36} electrons per second with energies $\geqslant$25 keV are needed for a non-thermal electron distribution with spectral index ~-4 to explain a strong impulsive hard X-ray burst by thick-target bremsstrahlung. The corresponding energy input for a burst lasting 10 s is ~10^{30} ergs, which is an appreciable fraction of the total flare energy. The reason for the high-energy requirement in non-thermal electrons is that most of their energy is lost by collisions in the target area and only a small fraction ~10^{-5} goes into bremsstrahlung (Hoyng et al., 1976). This had led a number of investigators to consider thermal or quasi-thermal source models for impulsive hard

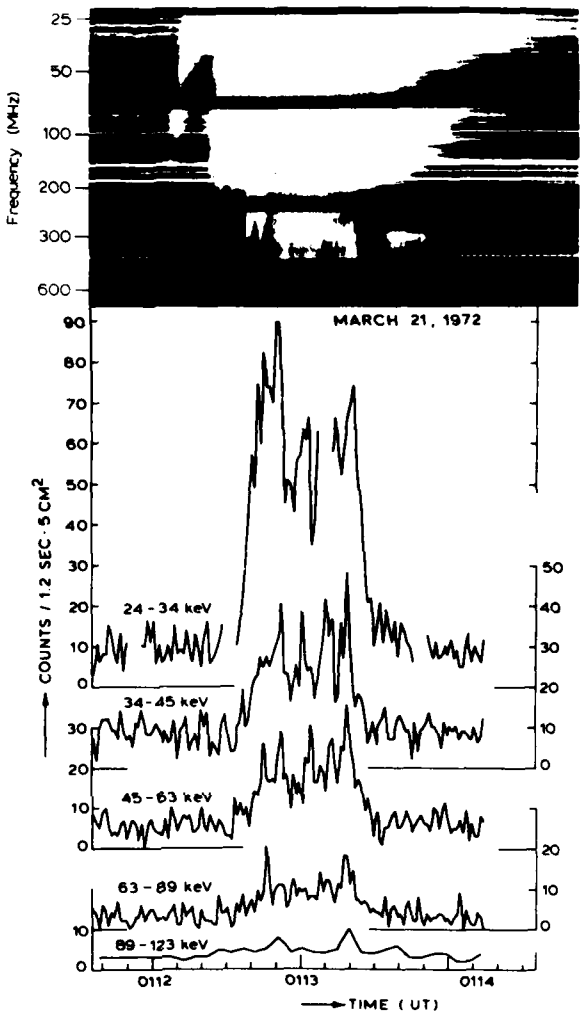

Figure 1. Example of a metre-wavelength Type III-V burst (upper) associated with a hard X-ray burst (lower). The lower figure is a copy of Figure 2 of Hoyng (1975). The Type III-V burst was recorded by the Culgoora radio spectrograph with a time resolution of 0.25 s. The hard X-ray burst was recorded by the Utrecht hard X-ray spectrometer on board the ESRO TD-1A satellite with a time resolution of 1.2 s. The energy ranges of the five X-ray channels and the observed frequency range of the radio burst are indicated (Stewart, 1978).

X-ray bursts. In these models the electrons are impulsively heated in a small source region and relax to a near-Maxwellian distribution where the electron temperature T_e is ~1-4 × 10^8 K and the ion temperature T_i is considerably less ($T_e \gtrsim 10\ T_i$) (Brown et al., 1979; Ramaty et al., 1979; Smith and Lilliequist, 1979). Considerable energy is lost from the source region by conduction to the surrounding plasma but even so the models are considered to be 10-100 times more efficient in producing X-rays than the non-thermal thick-target model.

Some observational support for the thermal model has been presented by Crannell et al. (1978), who show that the impulsive hard X-ray burst profile often has a symmetrical rise and fall (Figure 2) which could be caused by a reversible

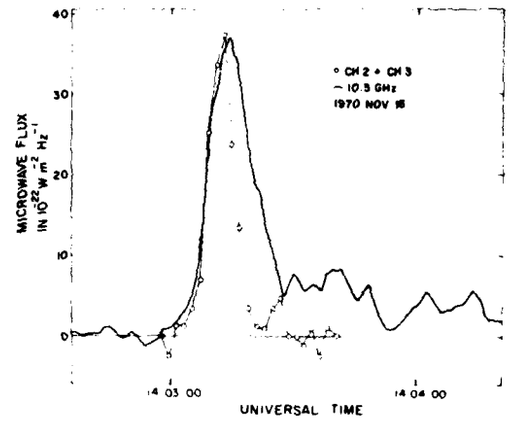

Figure 2. The time profiles of the sum of the X-ray flux in channels 2 (28-55 keV) and 3 (55-82 keV) of the OSO-X-ray spectrometer (NASA Goddard Space Flight Center) and the 10.5 GHz microwave flux (Institute of Applied Physics, University of Bern). The X-ray profile has been normalized to the same peak height as the microwave profile (Crannell et al., 1978).

process such as adiabatic compression (heating) and expansion (cooling) of a small source region (Matzler et al., 1978). They also show that impulsive microwave bursts are closely correlated with hard X-ray bursts (Figure 2). This suggests that hard X-rays and microwaves are emitted from the same source of thermal electrons. Combining the two sets of observations, Matzler et al. (1978) and Dulk et al. (1979) find electron temperatures $T_e \approx 10^8$ K, emission measures $n_e^2 V \approx 10^{45}$ cm^{-3}, source sizes $A \approx 10^{18}$ cm^2, electron densities $n_e \approx 10^9$ cm^{-3}, and magnetic fields with $B \approx 100$-400 G (Figures 3a and 3b). We note that the electron and ion densities derived from these observations are considerably less than the values ~10^{11} cm^{-3} used in the theoretical models mentioned above.

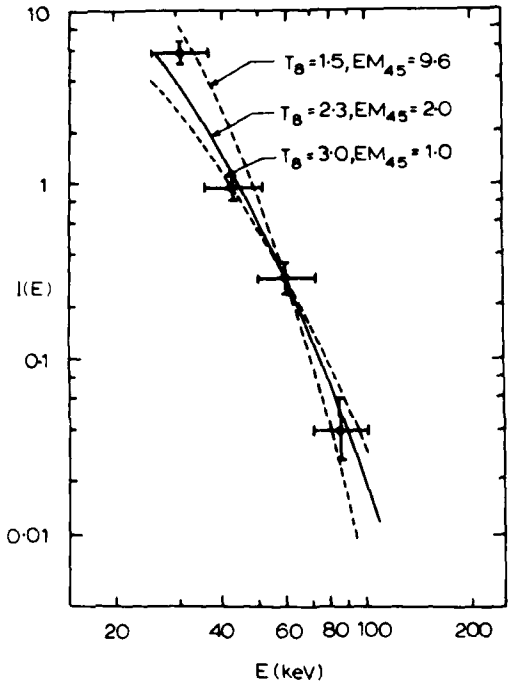

Figure 3(a). X-ray spectrum of the impulsive burst of 1972 May 18, $14^h06^m09^s$ UT. The datum points are from Hoyng and Stevens (1973). The solid and dashed curves represent X-ray spectra derived from electron thermal distributions with the parameters indicated on the figure. T_8 is the electron temperature in 10^8 K and EM_{45} the emission measure in 10^{45} cm^{-3} (Dulk et al., 1979).

So far there have not been routine spatial observations of hard X-ray bursts. It is hoped that during the solar maximum mission such observations will settle the question of whether the X-ray electrons are thermal or non-thermal and whether these electrons are located primarily in the chromospheric-corona transition region, where the ion density n_i is $\sim 10^{11}$ cm^{-3}, or in the low corona, where n_i is $\sim 10^9$ cm^{-3}. A recent stereo-spacecraft observation reported by Kane et al. (1979) indicates that the coronal contribution for one hard X-ray impulsive burst is 600 times less than the chromospheric contribution.

Lin and Hudson (1971) and Stewart (1978) have estimated that 10^{33} to 10^{35} electrons with energies $\geq$10 keV escape from the flare region during the impulsive phase. If the total number of accelerated electrons is represented by the hard X-ray burst then as many as 10^{38} non-thermal electrons or $\geq 10^{36}$ thermal electrons are accelerated during the impulsive phase. It would appear that <10% thermal or <1% non-thermal electrons escape to the higher corona to produce the Type III-V burst and the interplanetary electron event.

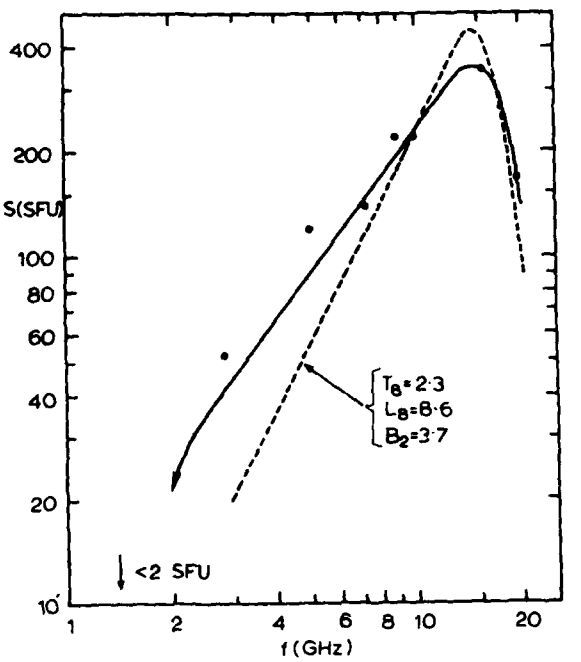

Figure 3(b). Microwave spectrum of the event of Figure 3(a). The datum points are from Hoyng and Stevens (1973). The solid curve is a hand-drawn fit to the datum points. The dashed line was computed by Dulk et al. (1979) using the parameters L_8 and B_2 indicated on the figure, where L_8 is the source size in 10^8 cm and B_2 the magnetic induction in 10^2 G. T_8 = 2.3 and EM_{45} = 2.0 were derived from Figure 3(a) (Dulk et al., 1979).

The impulsive phase electrons are thought to be accelerated by some form of bulk energization where stored magnetic energy is converted into electron energy during the flare. Various processes involving the acceleration of electrons by induced electric fields caused by magnetic field line motion have been reviewed by Smith (1974) and Ramaty et al. (1979).

3. SECOND-STAGE ACCELERATION

In very large flares there appears to be a second stage of acceleration where electrons reach energies of ~10 MeV and protons and ions even higher energies, ~10 GeV. Interplanetary particle observations suggest that energetic ions and

relativistic electrons are released from the Sun a few minutes after the 10-100 keV impulsive-phase electrons are accelerated (Lin, 1970). Microwave and hard X-ray bursts show a distinct first and second phase (Frost and Dennis, 1971) with the X-ray spectrum becoming harder in the second phase corresponding to an increase in the proportion of high-energy electrons as second-phase acceleration takes place (see Figure 4 and also Hoyng et al. (1976)). Gamma-ray observations of the 1972

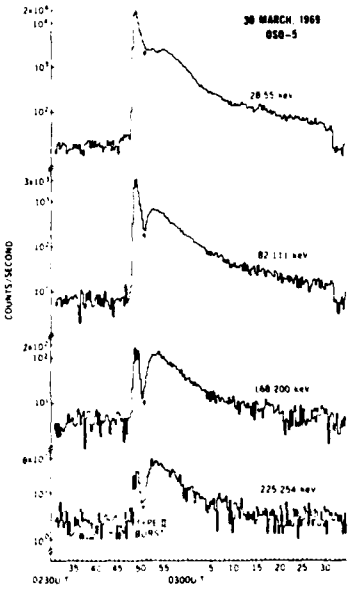

Figure 4(a). Time profiles of the hard X-ray flux for different energy ranges during the two-stage event of 1969 March 30 (Frost and Dennis, 1971). The second stage began near the starting time of a Type II burst indicated by the vertical arrow.

August 4 flare (Chupp et al., 1975) indicate that the relativistic electrons ($E \approx 1$-10 MeV) producing γ-ray continuum (0.35-8 MeV) by electron-electron and electron-ion bremsstrahlung and the high-energy protons ($E \approx 10$-100 MeV) producing γ-ray line emission (2.2 MeV) by nuclear reactions are accelerated several minutes after the 10-100 keV impulsive phase electrons (Figure 5) (Bai and Ramaty, 1976). Both escaping and trapped flare electrons appear to have power-law spectra up to energies ~10 MeV (Lin et al., 1978; Bai and Ramaty, 1976).

The high proton-to-electron ratio (at, say, 10 MeV) observed in large flares is consistent with the particles being accelerated in a stochastic process such as

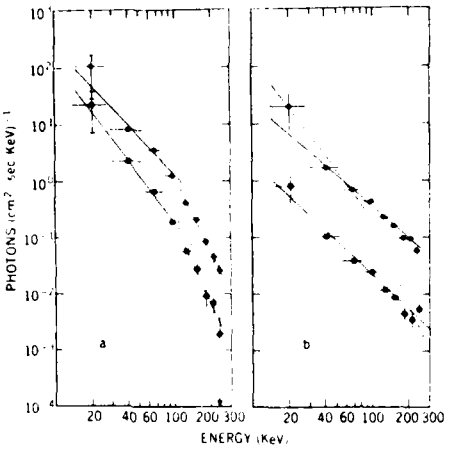

Figure 4(b). The hard X-ray photon energy spectrum at two times during the impulsive burst (a) and during the second-stage burst (b) of 1969 March 30. The impulsive burst spectrum shows a steepening above ~100 keV which is fairly typical of flash phase events. The second-stage spectrum is harder than the first stage and fits a single power law up to the maximum energy of the detector. (After Frost and Dennis (1971) and Lin (1974).)

Fermi acceleration (Ramaty et al., 1979). The energy gained by repeated reflections off magnetic field irregularities is greater than the energy lost by collisions for electrons with energies $\geq$100 keV and for protons with energies $\geq$0.5 keV (Ramaty et al., 1979). Hence a high-energy tail is required for the inital electron distribution if Fermi acceleration is to occur. This high-energy tail could be provided by the first-stage acceleration of electrons during the impulsive phase of the flare. Protons, on the other hand, could be accelerated from thermal energies directly during the second stage (Ramaty et al., 1979).

4. EXTENDED MICROWAVE BURSTS

Stewart and Nelson (1979) have found that the second-stage microwave burst is closely correlated with the hard X-ray burst (Figure 6a). These extended microwave bursts have a flatter spectrum (below the turnover frequency) than impulsive bursts (compare Figures 3b and 6b) and this can be explained by assuming that the radiating electrons are trapped in a non-uniform magnetic source region such as a dipole magnetic field. In such a source similar numbers of electrons with energies ~100 keV are required to explain the microwave and hard

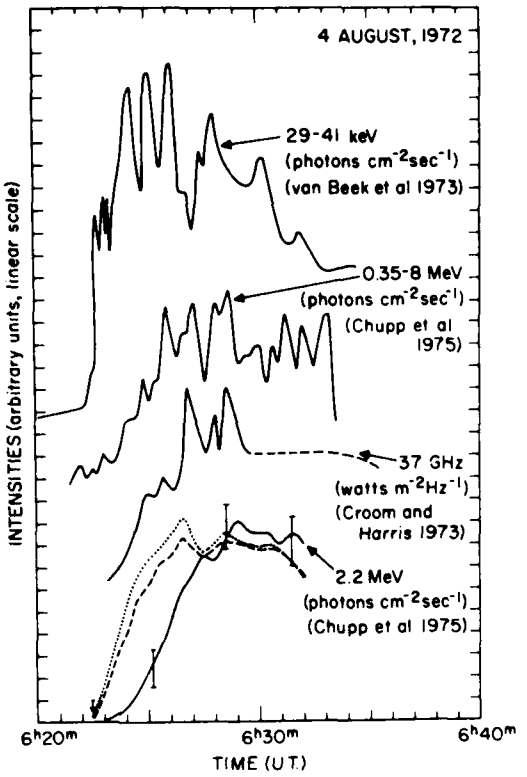

Figure 5. Time dependences of radiations of the flare of 1972 August 4. The three upper lines are the measured time profiles of X-rays (29-41 keV), gamma rays (0.35-8 MeV), and microwaves (37 GHz). The error bars in the lower part of the figure represent the measured intensities of the 2.2 MeV line. The solid, dashed, and dotted lines are calculated time profiles of the 2.2 MeV line. The solid line is obtained by assuming that the instantaneous number of nuclei in the flare region has the same time dependence as that of the observed 0.35 to 8 MeV gamma rays. The dashed and dotted lines are obtained by assuming that the time dependence of the nuclei is the same as that of the 29 to 41 keV X-rays. (For the solid and dotted lines the photospheric ^{3}He abundance ratio ^{3}He/H equals 5×10^{-5}; for the dashed line, ^{3}He/H equals 0.) Note that the solid line fits the 2.2 MeV data better than the dashed or the dotted line. Hence both the 1-10 MeV electrons emitting the 0.35-8 MeV γ-continuum and the 10-100 MeV protons responsible for the 2.2 MeV γ-line are accelerated several minutes after the 10-100 keV impulsive hard X-ray burst electrons. (After Bai and Ramaty (1976).)

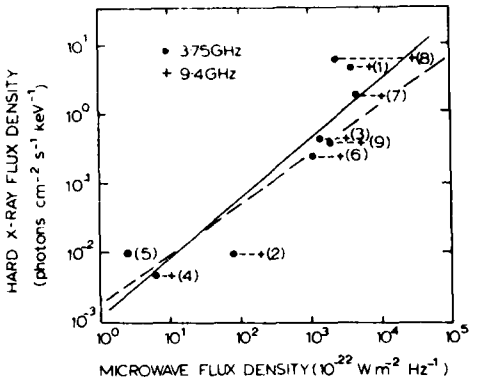

Figure 6(a). Observed correlation between the 100 keV hard X-ray and 3.75 GHz or 9.4 GHz microwave flux densities at the time of X-ray maximum in nine extended (second-stage) flare events. The full line shows the least-mean-squares fit (logarithmic) to the 9.4 GHz data and the short dashed line the fit to the 3.75 GHz data. The nine events are listed in Table 1 of Stewart and Nelson (1979).

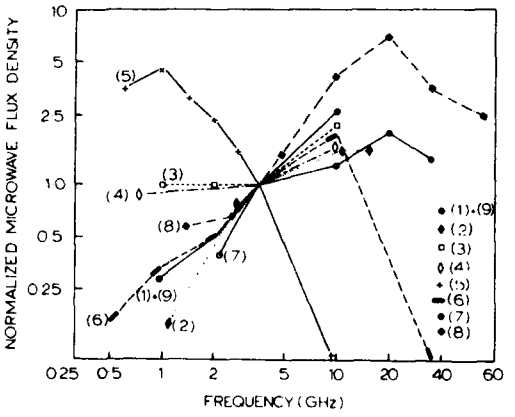

Figure 6(b). Microwave spectra at the time of 100 keV hard X-ray maximum for the nine events of Figure 6(a). Each spectrum is normalized to the 3.75 GHz value (Stewart and Nelson, 1979).

X-ray emission (Nelson and Stewart, 1979; Takakura, 1972). The turnover frequencies of extended microwave bursts are usually ~10-20 GHz (Figure 6b) and indicate maximum values for the magnetic induction B ≈ 500-1500 G (Nelson and Stewart, 1979). With the above source model we expect to find larger source sizes and stronger magnetic fields for second-stage microwave and hard X-ray bursts than for impulsive phase events. We also expect the size of the microwave burst to increase with decreasing frequency. At present there are not enough high spatial resolution observations to test this model.

5. RADIO EVIDENCE FOR SHOCK WAVE ACCELERATION

Second-stage stochastic acceleration of particles in shock waves has been considered by several authors, including Schatzman (1963) and Gubchenko and Zaitsev (1978). The clearest evidence for the presence of a shock wave in the corona during a solar flare is the Type II radio burst (Wild et al., 1953). These bursts usually occur during proton flares (Van Hollebeke et al., 1975) near the start of the second-stage hard X-ray event (see arrow of Figure 4a). The Type II burst is thought to be due to plasma emission from mildly relativistic electrons (E ≈ 20 keV) accelerated by the shock wave. Sometimes these electrons escape from the Type II shock wave and produce herringbone features, which are rib-like bursts with fast-frequency drift rates similar to those of Type III bursts. The high circular polarization of fundamental herringbone bursts (Suzuki et al., (1980) indicate that the electron streams travel along ordered magnetic field lines. Electron streams of this kind have also been observed by spacecraft to travel along magnetic field lines away from the Earth's bow shock (R.P. Lin, 1979 - personal communication) and away from interplanetary shock waves (Richter et al., 1979).

Type II shock waves probably also accelerate electrons to produce flare continuum (FC II) bursts at metre wavelengths (Robinson and Smerd, 1975). The high brightness temperature observed in some of these bursts, $\geq 10^{10}$ K (Duncan et al., 1980; Magun et al., 1975), suggests that the flare continuum is coherent plasma emission from electrons with energies ≥10 keV. According to Dulk et al. (1978), a flux of at least 10^{34} electrons per second is required in the flare continuum source region located at a height ≥0.6 $R_\odot$ above the photosphere. For a typical burst of ~1000 s duration this means that $\sim 10^{34}$ to 10^{37} electrons with energies ≥10 keV must be accelerated by the shock wave as it passes through the corona, assuming that the electrons are not trapped in the source region but escape over times ≥1 s. This number is considerably less than the value $\sim 10^{39}$ required for the 10-100 keV electrons in the extended hard X-ray source region.

It was originally thought that moving Type IV bursts were due to synchrotron emission from relativistic electrons with energies ≥1 MeV (Boischot and Denisse, 1957). The possibility of large populations ($\sim 10^{33}$ particles) of high-energy electrons at the large source heights of moving Type IV bursts created a considerable interest in these events. However, later observations with the Culgoora radioheliograph showed that moving Type IV bursts at 80 and 160 MHz were often polarized in the circular sense. This led Dulk (1973) and others to consider models in which the radio emission was attributed to low-harmonic gyro-synchrotron radiation from mildly relativistic electrons (~10-100 keV). More recent observations, especially at 80 and 43 MHz, have shown that the moving Type IV burst in its early stages can have brightness temperatures $\geq 10^{10}$ K (Figure 7) (Stewart et al., 1978a; Duncan et al., 1980). Such high brightness temperatures, together with the observed circular polarization, suggest that the moving Type IV burst, at least in its early stage of development, is due to coherent plasma emission from 10-100 keV electrons.

There is little direct evidence to suggest that these electrons are accelerated by shock waves. Indeed, the close association found between eruptive prominences and moving Type IV sources (Stewart et al., 1978b) would seem to exclude the possibility of shock wave acceleration.

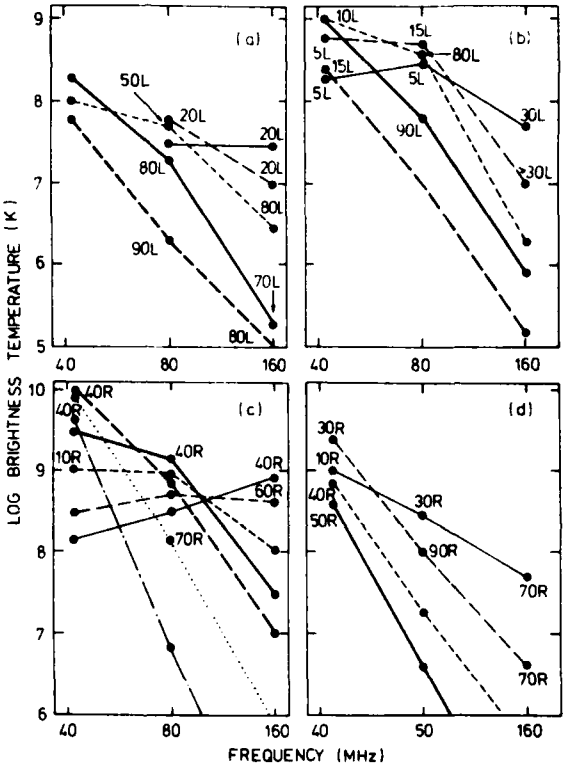

Figure 7. Observed source brightness temperature and degree of circular polarization of moving Type IV bursts at 160, 80 and 43 MHz. Source heights (solar radii above the centre of the Sun) and times (UT) are shown in the following table.

Table to Figure 7

(i) ———— (iv) ————

(ii) — — — (v) — — —

(iii) - - - - - (vi) .....

(vii) —·—·—

(a) 1975 Aug. 22 (i) 01^h30^m at 1.4 $R_\odot$;
(ii) 01^h40^m at 1.7 $R_\odot$; (iii) 02^h00^m at 2.4 $R_\odot$;
(iv) 02^h20^m at 2.7 $R_\odot$; (v) 02^h40^m at 3.0 $R_\odot$.

(b) 1977 Oct. 4/5 (i) 23^h50^m at 1.3 $R_\odot$;
(ii) 00^h08^m at 1.7 $R_\odot$; (iii) 00^h46^m at 2.2 $R_\odot$;
(iv) 01^h13^m at 2.5 $R_\odot$; (v) 01^h30^m at 3.0 $R_\odot$.

(c) 1977 Sept. 20 (i) 03^h14^m at 1.3 $R_\odot$;
(ii) 03^h19^m at 1.4 $R_\odot$; (iii) 03^h25^m at 1.6 $R_\odot$;
(iv) 03^h35^m at 1.8 $R_\odot$; (v) 03^h40^m at 2.1 $R_\odot$;
(vii) 03^h50^m at 2.6 $R_\odot$; (viii) 04^h00^m at 3.1 $R_\odot$.

(d) 1977 Oct. 3/4 (i) 23^h35^m at 2.1 $R_\odot$;
(ii) 23^h51^m at 2.3 $R_\odot$; (iii) 00^h03^m at 2.6 $R_\odot$;
(iv) 00^h24^m at 3.0 $R_\odot$.

L and R refer to LH and RH circular polarization. At 43 MHz the degree of circular polarization is accurate to ±5% for 0-15% and ±10% for 15-50%. The maximum source velocities are (a) 400, (b) 300, (c) 600 and (d) 400 km s^{-1}. Only the later part of event (d) was recorded.

6. CONCLUSION

Radio and X-ray observations indicate that the bulk of the electrons accelerated during the impulsive phase of the solar flare have energies in the range 10-1000 keV. During very large flares there is evidence from interplanetary particle measurements and from γ-ray observations that electrons are accelerated to much higher energies, ≲10 GeV. It is still not clear how the particles are accelerated during these two stages. A popular idea is that during the impulsive phase the electrons are impulsively heated to very high temperatures, ~10^8 K, by some form of bulk energization where stored magnetic energy is converted into thermal energy. These hot electrons then relax to form a quasi-thermal (near-Maxwellian) distribution and produce the hard X-ray burst near the base of the corona by bremsstrahlung. A few per cent of the hot electrons then escape to higher regions of the corona to produce Type III-V bursts and interplanetary electron events. Shock-wave acceleration is still an attractive possibility for the second-stage process, although there is no clear evidence to show that a coronal shock wave is capable of accelerating electrons and ions to the very high energies attained by second-stage particles.

References

Bai, T., and Ramaty, R.: 1976, "Gamma-ray and microwave evidence for two phases of acceleration in solar flares", Solar Phys., 49, 343.

Boischot, A., and Denisse, J.F.: 1957, "Les émissions de type IV et l'origine des rayons cosmiques associés aux éruptions chromosphériques", C. R. Acad. Sci. Paris, 245, 2194.

Brown, J.C., Melrose, D.B., and Spicer, D.S.: 1979, "Production of a collisionless conduction front by rapid coronal heating and its role in solar hard X-ray bursts", Astrophys. J., 228, 592.

Chupp, E.L., Forrest, D.J., and Siri, A.N.: 1975, "High energy gamma-ray radiation above 300 keV associated with solar activity", in Solar, Gamma, X and EUV Radiations (Proc. IAU Symp. 68) (ed. S. Kane), p. 341 (Reidel, Dordrecht).

Crannell, C.J., Frost, K.J., Mätzler, C., Ohki, K., and Saba, J.L.: 1978, "Impulsive solar X-ray bursts", Astrophys. J., 223, 620.

Croom, D. L., and Harris, L. D. J.: 1973, "Solar radio events at 9.4 to 71 GHz in the period 26 July - 14 August 1972" in Collected Data Reports on the August 1972 Solar-Terrestrial Events (ed. Helen E. Coffey), UAG-28, Part 1, p. 210, (U. S. Department of Commerce, NOAA, Boulder).

Dulk, G.A.: 1973, "The gyro-synchrotron radiation from moving type IV sources in the solar corona", Solar Phys., 32, 491.

Dulk, G.A., Melrose, D.B., and Smerd, S.F.: 1978, "Radio evidence on the particle distribution functions", Proc. Astron. Soc. Aust., 3, 243.

Dulk, G.A., Melrose, D.B., and White, S.M.: 1979, "The gyrosynchrotron emission from quasi-thermal electrons and applications to solar flares", Astrophys. J., 234, 1137.

Duncan, R.A., Stewart, R.T., and Nelsen, G.J.: 1980, "Recent very bright type IV solar metre-wave radio emissions", in Solar and Interplanetary Dynamics (Proc. IAU Symp. 91) (eds. M. Dryer and E. Tandberg-Hanssen) p. 381 (Reidel, Dordrecht).

Frost, K.J., and Dennis, B.R.: 1971, "Evidence from hard X-rays for two-stage particle acceleration in a solar flare", Astrophys. J., 165, 655.

Gubchenko, V.M., and Zaitsev, V.V.: 1978, "On proton and electron acceleration by shock waves during large solar flares", Proc. Astron. Soc. Aust., 3, 296.

Hoyng, P.: 1975, "Studies on hard X-ray emission from solar flares and on cyclotron radiation from a cold magneto-plasma", Ph.D. Thesis, University of Utrecht.

Hoyng, P., and Stevens, G.A.: 1973, "Interpretation of a hard solar X-ray burst", in Solar Activity and Related Interplanetary and Terrestrial Phenomena, (Proc. First European Astron. Meeting, Athens, Sept. 4-9, 1972) (ed. J. Xanthakis), Vol. 1, p. 97 (Springer-Verlag, N.Y.).

Hoyng, P., Brown, J.C., and van Beek, H.F.: 1976, "High time resolution analysis of solar hard X-ray flares observed on board the ESRO TD-1A satellite", Solar Phys., 48, 197.

References

Kane, S.R., Anderson, K.A., Evans, W.D., Klebesadel, R.W., and Laros, J.: 1979, "Observation of an impulsive solar X-ray burst from a coronal source", Astrophys. J. (Lett.), 233, L151.

Lin, R.P.: 1970, "The emission and propagation of ~40 keV solar flare electrons", Solar Phys., 12, 266.

Lin, R.P.: 1974, "Non relativistic solar electrons", Space Sci. Rev., 16, 189.

Lin, R.P., and Hudson, H.S.: 1971, "10-100 keV electron acceleration and emission from solar flares", Solar Phys., 17, 412.

Lin, R.P., Mewaldt, R.A., Stone, E.C., Vogt, R.E., Paizis, C., and Van Hollebeke, M.A.I.: 1978, "Spectral and temporal characteristics of solar electrons from 20 keV to 20 MeV", Bull. Am. Phys. Soc., 23, 4-AJ7.

Magun, A., Stewart, R.T., and Robinson, R.D.: 1975, "Three-frequency radioheliograph observations of solar continuum events", Proc. Astron. Soc. Aust., 2, 367.

Mätzler, C., Bai, T., Crannell, C.J., and Frost, K.J.: 1978, "Adiabatic heating in impulsive solar flares", Astrophys. J., 223, 1058.

Nelson, G.J., and Stewart, R.T.: 1979, "Interpretation of a correlation between the flux densities of extended hard X-ray and microwave solar bursts", Proc. Astron. Soc. Aust., 3, 392.

Ramaty, R., Colgate, S.A., Dulk, G.A., Hoyng, P., Knight, J.W., Lin, R.P., Melrose, D.B., Orrall, F., Paizis, C., Shapiro, P.R., Smith, D.F., Van Hollebeke, M.: 1979, "Energetic particles in solar flares", in Solar Flares (ed. P. A. Sturrock) p. 117 (Colorado Associate University Press).

Richter, A.K., Van Hollebeke, M.A.I., Hsich, K.C., Denskat, K.U., Keppel, E., McDonald, F.B., and Schwenn, R.: 1979, Max-Planck-Institut für Aeronomic Preprint SP5-31.

Robinson, R.D., and Smerd, S.F.: 1975, "Solar flare continua at the metre wavelengths", Proc. Astron. Soc. Aust., 2, 374.

Schatzman, E.: 1963, "On the acceleration of particles in shock fronts", Ann. Astrophys., 26, 234.

Smith, D.B.: 1974, "Mechanisms for flash phase phenomena in solar flares", in Coronal Disturbances (Proc. IAU Symp. 57) (ed. G. Newkirk, Jr.) p. 253 (Reidel, Dordrecht).

Smith, D.F., and Lilliequist, C.G.: 1979, "Confinement of hot, hard X-ray producing electrons in solar flares", Astrophys. J., 232, 582.

Stewart, R.T.: 1978, "Relationship between Type III-IV radio and hard X-ray bursts", Solar Phys., 58, 121.

Stewart, R.T., and Nelson, G.J.: 1979, "An observed correlation between the flux densities of extended hard X-ray and microwave solar bursts", Proc. Astron. Soc. Aust., 3, 390.

Stewart, R.T., Duncan, R.A., Suzuki, S., and Nelson, G.J.: 1978a, "Observations of high brightness temperatures in moving Type IV solar radio bursts", Proc. Astron. Soc. Aust., 3, 247.

References

Stewart, R.T., Hansen, R.T., and Sheridan, K.V.: 1978b, "Estimates of the magnetic energy densities of two eruptive prominences from their close association with moving Type IV radio bursts", in Physics of Solar Prominences (Proc. IAU Colloq. 44) (eds. E. Jensen, P. Maltby and F.Q. Orrall), p. 315 (Inst. Theor. Astrophys. Blindern, Oslo).

Suzuki, S., Stewart, R.T., and Magun, A.: 1980, "Polarization of herringbone structure in Type II bursts", in Radio Physics of the Sun (Proc. IAU Symp. 86) (eds. M.R. Kundu and T.E. Gergely) p. 241 (Reidel, Dordrecht).

Takakura, T.: 1972, "The self-absorption of gyro-synchrotron emission in a magnetic dipole field: microwave impulsive burst and hard X-ray burst", Solar Phys., 26, 151.

van Beek, H. F., Hoyng, P., and Stevens, G. A.: 1973, "Solar flares observed by the hard X-ray spectrometer on the ESRO TD-1A satellite" in Collected Data Reports on the August 1972 Solar-Terrestrial Events (ed. Helen E. Coffey), UAG-28, Part II, p. 319, (U. S. Department of Commerce, NOAA, Boulder).

Van Hollebeke, M.A.I., Ma Sung, L.S., and McDonald, F.B.: 1975, "The variation of solar proton energy spectra and size distribution with heliolongitude", Solar Phys., 41, 189.

Wild, J.P., Murray, J.D., and Rowe, W.C.: 1953, "Evidence of harmonics in the spectrum of a solar radio outburst", Nature, 172, 533.

Discussion

Schwenn: There have been recent direct measurements at 1 AU of the electrons causing Type III bursts. How do these electron numbers compare with the hard X-ray data?

Stewart: Lin and Hudson (1971) estimated that ~1% of the non-thermal electrons in the hard X-ray source escape to interplanetary space. If the hard X-rays are due to thermal electrons the number of electrons escaping to space might be as high as 10^{7}.

Gelfreich: Were there any bursts when all four possible methods to estimate the number of fast electrons were used?

Stewart: Lin and Hudson's (1971) list includes several events where hard X-ray and Type III-V bursts were observed to be associated with interplanetary electron events (see also Stewart 1978).

Alurkar: Do Type II burst structures show a high degree of polarization?

Stewart: Only the herringbone features are polarized in the circular sense. The ordinary Type II burst with its narrow-frequency bands showing slow drift in frequency with time, i.e. the "backbone" component of the herringbone Type II burst, does not appear to be polarized.

Giovanelli: At what level was the 370 G field found by Dulk?

Stewart: Dulk's model for the impulsive microwave source region had an electron density of $2 \cdot 10^{9}$ cm^{-3}, so it was presumably near the base of the corona.

Discussion

Croft: You mentioned that 10^8 K is needed to fit your data by invoking a thermal mechanism, but you added that no temperature so high has been measured. Yet your phenomenon would last only about 30 s, would have a small area, and would occur only rarely. I am not familiar with the operational history of those scientists who measure solar temperature, but their methods might not work well in the search for such a transient. Do you know if this is true? If so, then the lack of an existing observation doesn't necessarily preclude the thermal mechanism.

Stewart: I am not familiar with the technical problems involved in detecting line emission at such high temperatures.

Note added later. Line observations of Fe XXV at 1.9 Å during a solar flare indicate a temperature ~2-3 × 10^7 K. This is the highest temperature I have seen quoted in the literature.

2. Magnetohydrodynamic (MHD) Description of Solar Radio Bursts

S. T. Wu
The University of Alabama in Huntsville
Huntsville, Alabama 35807 U.S.A.

Abstract

The nature of solar radio bursts and their dynamic spectra usually are discussed in terms of a static, semi-quiet corona. In particular, the value of the electron density and the general topological nature of the magnetic field, necessary for a proper description of the radio bursts, are deduced from undisturbed coronal models. On the other hand we know that Type II and moving Type IV bursts are related to flare-generated disturbances in the corona; as the disturbances pass through the atmosphere, all plasma properties are changed.

In order to take these disturbed coronal conditions into consideration we have used a two-dimensional MHD model to compute the properties of the disturbed corona. Given these spatial and temporal properties, we have then deduced the resulting dynamic spectra of Type II and moving Type IV radio bursts. Three different initial magnetic field topologies have been considered: closed-field, open-field, and coronal streamer configurations. While the model is unable to specify the particular form of radiation mechanism present in any given

observation, the results strongly suggest that temporal collective MHD behavior must be considered regardless of the mechanism (plasma oscillations or gyro-synchrotron emission).

1. INTRODUCTION

Generally, moving solar radio bursts are usually believed to be caused by one (or, in some cases, both) of the following mechanisms: (1) synchrotron radiation from magnetized structures moving through the corona (see for example, Kundu, 1965; Wild and Smerd, 1972) which is called gyromagnetic emission and classified as moving Type IV, and (2) electron density enhancement in the corona wherein the plasma emission energy in Langmuir waves is converted into energy in escaping radiation either at the fundamental or the second harmonic of the plasma frequency. The evidence for fundamental plasma emission comes from harmonic structure, first reported in Type II and Type IV bursts by Wild, Sheridan and Trent (1959), and Wild, Smerd and Weiss (1963). Smerd and Dulk (1971) note, in particular, that the moving Type IV has three distinctive types, namely: (i) an expanding magnetic arch, (ii) an advancing front, and (iii) an isolated plasmoid. In addition, they have suggested certain coronal magnetic field configurations related to these moving Type IV radio sources as shown in Figure 1. Later, Kai (1978) has investigated further details for the relation between circular polarization of the moving Type IV bursts and polarity of the photospheric magnetic field. This study is based on two-dimensional, high-resolution observations (see, for example, Table 1 in Kai, 1978). Other data concerning this subject have been given by Sheriden, Labrum and Payton (1973), Schmahl (1973), Kai (1975), Stewart (1980), and Stewart et al. (1974). However, all of these works are based entirely on observational data. Smerd and Dulk (1971) have suggested that the second classification can be explained by magnetohydrodynamic (MHD) theory, but no systematic theoretical study has been performed for this or the other classifications.

In this study, we shall present an ideal, two-dimensional, time-dependent, MHD model which preserves the basic topology suggested by all three morphological suggestions made by Smerd and Dulk (1971) as noted above. The important parameters in this model are: (i) the initial topology of the magnetic field (Nakagawa, Wu, and Han, 1978; Wu et al., 1978); and (ii) a characteristic plasma β_o, where β_o is defined as the ratio of initial plasma pressure to magnetic pressure at the lower boundary on the axis of symmetry. In Section II, the brief description of the governing equations will be given, and numerical results are presented in Section III. We will discuss the results in the context of the observations, together with the concluding remarks, in Section IV. It will be shown that certain observed features are reflected in the numerical results. However, we will make it clear that the model is unable to specify the specific form of radiation mechanism (plasma oscillations vis-à-vis gyro-synchrotron emission) present in any particular event.

2. BASIC THEORY

It has been recognized that the collective dynamical behavior of plasma and magnetic field interaction can be described by magnetohydrodynamic (MHD) theory. The MHD, two-dimensional and time-dependent planar theory was first suggested by Nakagawa, Wu and Han (1978) and Wu et al. (1978) to explain certain features of coronal transients which constitute certain observational manifestations of mass motion and shock waves resulting from a solar flare. It has been concluded that the density enhancement in the corona, leading to the observed white-light coronal transient, is due to the interaction of fast- and slow-mode MHD waves. This model is defined in the equatorial plane (governing equations are shown in Appendix I). Subsequently, Steinolfson and Wu (1980) and Steinolfson (1982) have extended this planar model to the meridional plane (governing equations shown in Appendix II) to examine further characteristics of coronal transients. It should be emphasized that the equations differ only in the choice of the plane of analysis and that the physical processes are the same; that is, the coronal response to a perturbation within it is one of collective MHD temporal and spatial reaction.

This model was compared with some success with the general characteristics of observed white-light coronal transients. More specifically, Dryer et al. (1979) have used an observed eruptive prominence as the forcing function in a model, which incorporated the observed electron density and temperature profile, to produce some basic features of the white-light transient observed 1973 August 21, 13:19 UT. Recently, Dryer and Maxwell (1979) made a comparison between radio data and the fast-mode MHD shock wave computed from this model. In their study, the computed trajectory of the fast-mode MHD shock matched the trajectory of the shock wave in the corona deduced from data on a radio Type II burst observed 1973 September 5 for a flare which started at 18:26 UT. In this event, the forcing function was a 10 min. square-wave temperature pulse, the magnitude of which was varied on an iterative basis until the matched trajectory was accomplished. Although this phenomenological simulation is not unambiguous, the final temperature peak magnitude at the "flare" coronal base site was representative of that measured in large flares. In this study, we will present computation results for plasma frequencies based on these suggested self-consistent MHD models with various initial magnetic field configurations as suggested by Smerd and Dulk (1971). Then we will utilize these results to interpret some observed radio signals.

3. COMPUTATIONAL RESULTS

In all of these computations, the steady state conditions for the system (both physical and mathematical aspects) must be established. Therefore, the solar corona before the introduction of disturbances is chosen to be an atmosphere in hydrostatic equilibrium with an isothermal temperature $T_o = 1.5 \times 10^6$ °K, the number density at the bottom of the atmosphere, $n_o = 2.7 \times 10^8$ particles cm^{-3}; and the polytropic index $\gamma = 1.2$. In the following, the specifics of the computational results are discussed.

3.1 Closed Field Case

As suggested by Smerd and Dulk (1971), the background magnetic field configuration related to observed moving Type IV can be represented by three basic types of the magnetic field configuration as shown in Figure 1. We direct attention, in this section, to the first configuration depicted in Figure 1a. We may represent this configuration by (Wu et al., 1978)

$$B_r = C_1 r^{-C_2} \cos \phi,$$

$$B_\phi = C_3 r^{-C_2} \sin \phi, \qquad (1)$$

with $C_3 = 0.619\ C_1$ and $C_2 = 2.619$, where C_1 is an arbitrary constant to be determined by the choice of the surface intensity of the magnetic field strength.

With this field configuration and the initial atmospheric conditions mentioned earlier, the numerical computation is started with the introduction of an impulsive temperature increase of magnitude $T = 10\ T_o$, in mid atmosphere (i.e., 20,000 km above the lower boundary). Physically, this enhancement corresponds to an impulsive release of energy in a flare, about 10^{29} ergs in this calculation.

Figure 2 shows the contours of plasma (fundamental) frequency which changes both temporally and spatially after introduction of the prototype "flare" pulse. This calculation, made at t = 200, 400 and 600 sec, was made for the case when $\beta_o = 0.34$, with β_o being the initial ratio of the plasma pressure to magnetic pressure at the coronal base on the axis of symmetry. Obviously, β_o will initially be different at other locations; thus the beta, as just given, is simply characteristic of the initial quiescent state of the low corona. As time increases, beta will also change significantly everywhere. Also, some energy, resident initially as magnetic and thermal, will be converted to kinetic; hence, the Alfven Mach number will exceed one. In this result, it is clearly indicated that plasma frequency enhancement contours form a loop-like structure which expands as a function of time. Figure 3 shows the initial magnetic field lines (dashed line) and disturbed magnetic field lines (solid lines) 600 sec after introduction of the pulse; also shown are the local velocity vectors. This figure corresponds to the plasma frequency enhancement contours shown in Figure 2c. Comparison of these two figures shows that the loop-like emission structure in the latter figure does not conform directly to the magnetic flux tubes shown in Figure 3. Instead, the emission structure must, by definition, conform to the density enhancement loop.

Figure 4 shows, in a different format, the plasma frequency as a function of time at two heights of 20,000 km and 35,000 km, respectively. (Note that the frequency increases downward along the ordinate of the figure.) At a height of 20,000 km, the plasma frequency slowly increases monotonically with time; however, at 35,000 km, the plasma frequency shows an increase initially but then a decrease after about 400 sec. Physically, this difference in response at the two representative altitudes may be interpreted in the following way. At the lower heights (i.e., 20,000 km), which are near the explosive site, both the fast and slow MHD waves propagate initially at almost the same speed. Mathematically, this corresponds to a signal speed, $C = \vec{v} \cdot \vec{n}$ (see Eq. (15) in Nakagawa, Wu and Han, 1978). On the other hand at the higher levels (i.e., 35,000 km), the fast

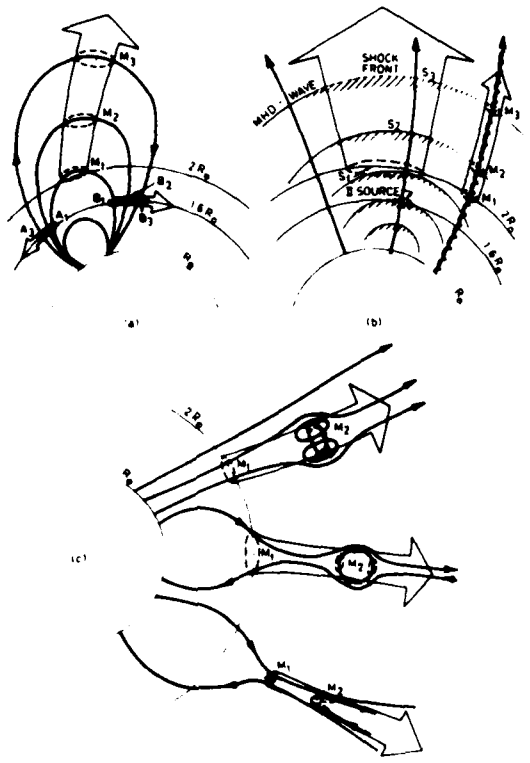

Figure 1. Schematic diagram of the magnetic field structure in three models of moving Type IV sources as suggested by Smerd and Dulk (1971). The magnetic field lines are shown as thick arrow lines, the paths of the moving IV sources by broad arrows. The optical disk, the 80 MHz plasma level and the average starting height of the moving IV sources are shown by thin arcs at $R_\odot$, 1.6 $R_\odot$ and 2 $R_\odot$, respectively. The subscripts 1, 2 and 3 refer to the source positions at three successive times (Smerd and Dulk, 1971).

and slow MHD waves are now propagating, at the later times, with their own separate characteristic speeds (see, Equations (12) and (13) in Nakagawa, Wu and Han, 1978). Therefore, the temporal variation at the lower altitudes of plasma frequency are due to the interactions of fast and slow MHD waves.

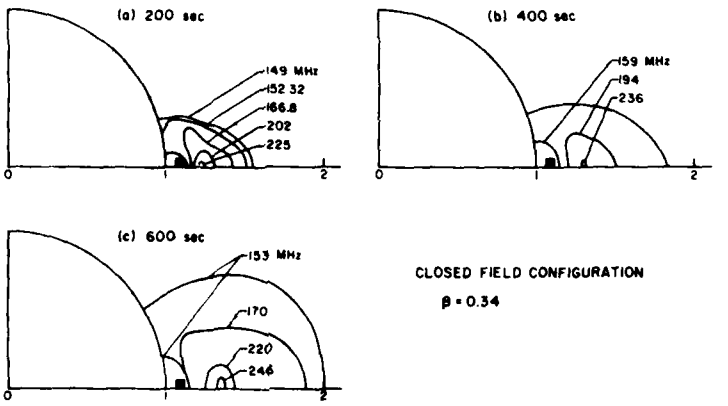

Figure 2. The contours of plasma frequency enhancements at time 200s, 400s, and 600s after the introduction of the disturbance for $\bar{P}$ = 0.34 and closed field configuration.

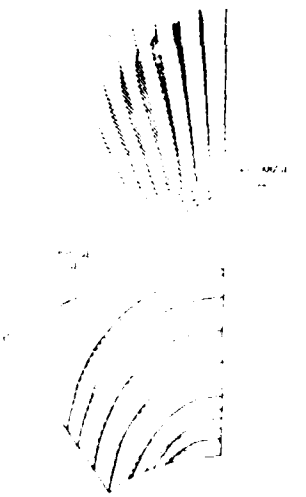

Figure 3. Velocity field and magnetic field configurations 600s after introduction of the disturbance for closed field configuration. Note that the equatorial axis (vertical in this figure) corresponds to the horizontal axis in Figure 2 (Wu et al., 1978).

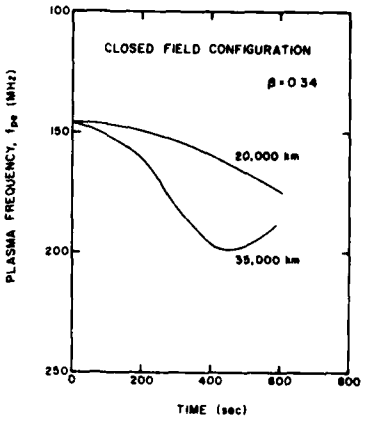

Figure 4. Plasma frequency versus time at heights of 20,000 km and 35,000 km for β_o = 0.34 and closed field configuration.

3.2 Open Field Case

We now turn our attention to the second magnetic field configuration suggested by Smerd and Dulk (1971), as shown in Figure 1b. This topology, essentially an open (radial) field configuration, may be represented by the following representative equations:

$$B_r = C_1 r^{-C_2} \sin \phi,$$

$$B_\phi = -C_3 r^{-C_2} \cos\phi, \qquad (2)$$

where C_1, C_2 and C_3 are constants defined as shown previously in Eq. (1).

With this initial magnetic field configuration, together with an atmosphere in hydrostatic equilibrium as mentioned previously, the numerical computation again started with the introduction of an impulsive temperature pulse (as in the case of the closed field topology discussed before). The contours of plasma frequency for β_o = 0.34 are plotted in Figure 5a, b, c, respectively, at t = 200, 400 and 600 seconds after introduction of the pulse. The corresponding magnetic and velocity fields are shown in Figure 6, in which the dashed curves represent the magnetic field lines at t = 0, and the solid curves indicate the magnetic field lines at t = 600 sec. From these results, we note that the "prototype" emission coming from the fundamental (or even second harmonic) plasma frequency has formed as a plasma cloud-like structure preceeded by a quasi-parallel shock. This is in contrast to the loop-like structure appearing for the closed-field case. Also, we note that the field has been pushed sideways by this enhanced plasma cloud ahead of which the quasi-parallel shock has formed. Figure 7 shows the plasma frequency as a function of time for β_o = 0.34 at the two different altitudes which were considered previously for the closed-field topology. It shows that the emission source has a minimum frequency at 20,000 km. At 34,000 km, the emission is essentially constant for ~400 sec, after which it rapidly increases in frequency to ~ 300 MHz at t = 600 sec. Eventually, however, this will return to the background level after the disturbance passes through.

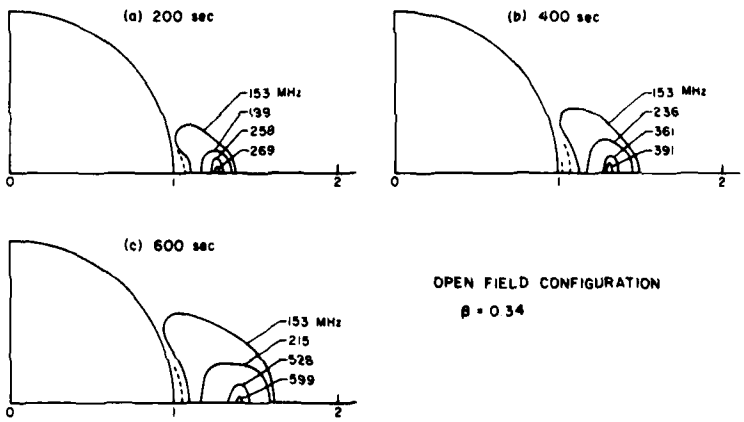

Figure 5. The contours of plasma frequency enhancement (solid line) and depletion (dashed line) at time 200s, 400s, and 600s after introduction of disturbance for β_o= 0.34 and open field configuration.

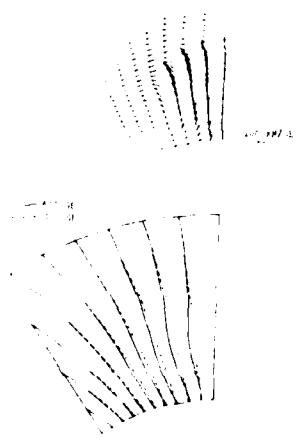

Figure 6. Velocity field and magnetic field configuration 600s after introduction of the disturbance for open field configuration (Wu et al., 1978). Note again, that the equatorial axis (vertical in this figure) corresponds to the horizontal axis in Figure 5.

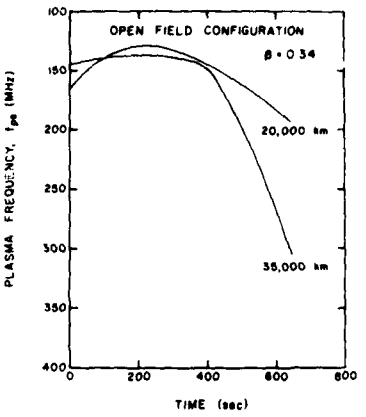

Figure 7. Plasma frequency versus time at heights of 20,000 km and 35,000 km for β_o = 0.34 and open field configuration.

3.3 Coronal Streamer Case

According to the suggestion of Kai (1975), some radio sources were observed in a region which apparently consisted of a background magnetic field which had a configuration of a coronal streamer as shown in Figure 8. In this section, we will discuss the temporal and spatial variations of the plasma and magnetic field results, obtained from precisely such a configuration, in more detail. The coronal streamer configuration is obtained by solving the set of governing equations shown in Appendix II together with a predetermined solar wind. The detailed account of this work can be found in Steinolfson and Wu (1980) and Steinolfson, Suess and Wu (1982). A typical solution of the coronal streamer β_o = 0.5 (defined in the same way as before) is shown in Figure 9. Shown in this figure are the following: (a) magnetic field lines, (b) pressure distribution, (c) velocity vectors and (d) density contours. The vertical axis is the equator and the horizontal axis is the pole, both extending from 1 to 5 R_s (R_s being solar radius). The short dashed line in Figure 9(a) represents the Alfvén mach number (u/V_A) being unity, where u is the flow velocity, $(V_r^2 + V_\theta^2)^{1/2}$, and V_A is the Alfven velocity $\frac{B}{\sqrt{4\pi\rho}}$. The longer dashed line represents the sonic Mach number (u/a) being unity, where a is the sonic velocity $(\gamma RT)^{1/2}$. It is seen that a steady-state, self-consistent solution for both a coronal (or helmet) streamer, together with a polar coronal hole, is provided.

With this solution as our initial condition, the "prototype flare" computation was carried out by introduction of a thermal pressure pulse at the lower boundary of the corona (i.e., R_s = 1). This thermal pressure pulse has a magnitude of 10 in which the temperature is increased by a factor of 5, and the density by a factor of 2. This pulse is kept "on" during the entire computation. In Figures 10 and 11, we show the coronal magnetic field and density responses at 80 and 180 minutes after introduction of the pulse. In these figures several interesting features are worthy of mention:

(i) In the closed magnetic field region, the field has been pushed up by this pulse, thereby enabling its interpretation as a rising arch;

(ii) This closed magnetic field region eventually is pushed open at later times (see Figure 11) while the plasma pressure and kinetic energy density become greater than the magnetic pressure; this condition will relax back to the sun

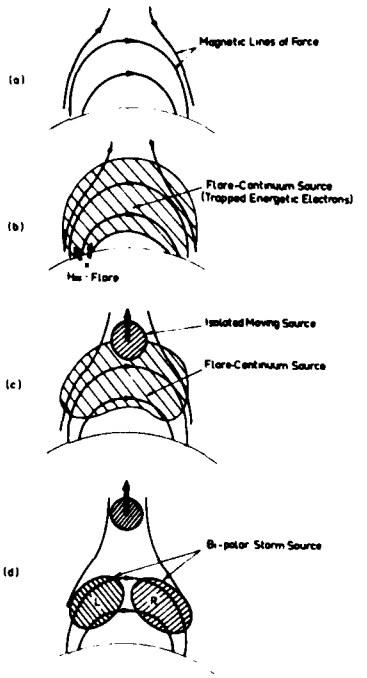

Figure 8. A schematic model showing the successive appearance of a flare-continuum source, an isolated moving source and a storm-continuum source with bi-polar structure (Kai, 1975).

following cessation of the pulse;

(iii) A MHD fast shock is formed and propagates outward;

(iv) A high density region forms behind the shock as suggested by the speculation of Smerd and Dulk (1971) shown in Figure 1. This high density region forms a loop-like structure; however, the maximum density enhancement (i.e., plasma frequency enhancement) is immediately behind the normal shock, and decreases somewhat along the optical, loop-like transient's legs. This phenomena shows features similar to the model (see Figure 8c) suggested by Kai (1975) based, phenomenologically, on the observations.

(v) At a later time (i.e., 180 minutes after introduction of the pulse), most of the original closed field region has become open, and the center part of the density enhancement has propagated out of the computational field of view (i.e., beyond 5 R_S). The density-enhanced leg (within the two short-dashed lines) remains as shown in Figure 11.

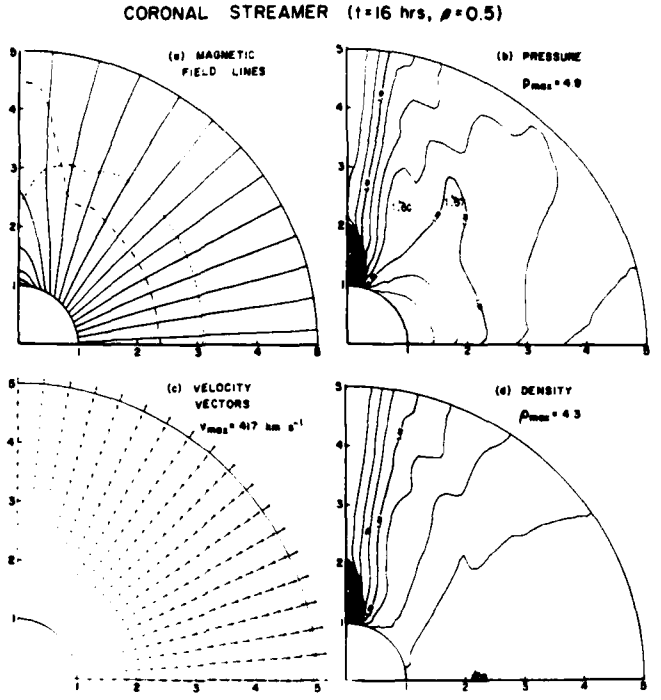

Figure 9. Planar maps of the magnetic field configuration and plasma properties in the coronal streamer for β_o=0.5 (Steinolfson and Wu, 1980).

(t=80 min, β_o=0.5)

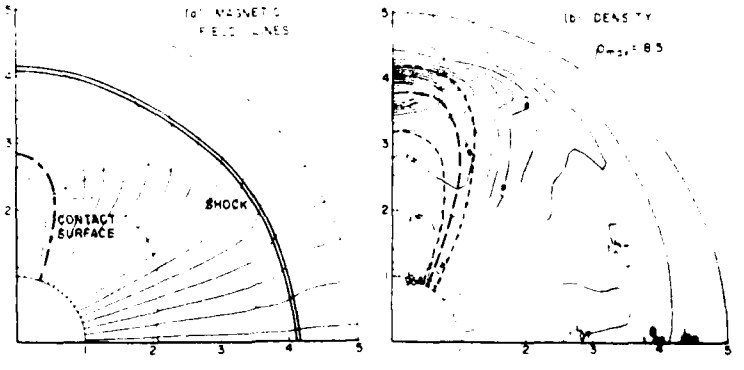

Figure 10. The magnetic field configuration and density distribution 80 minutes after introduction of the disturbance for β_o=0.5. The long dashed line in (a) represents the sonic line; the short dashed line represents the Alfven Mach line. In (b) the short dashed curves enclose the maximum density region, and the curve with longer dashes traces out the approximate location of the maximum density in this region (Steinolfson, 1982).

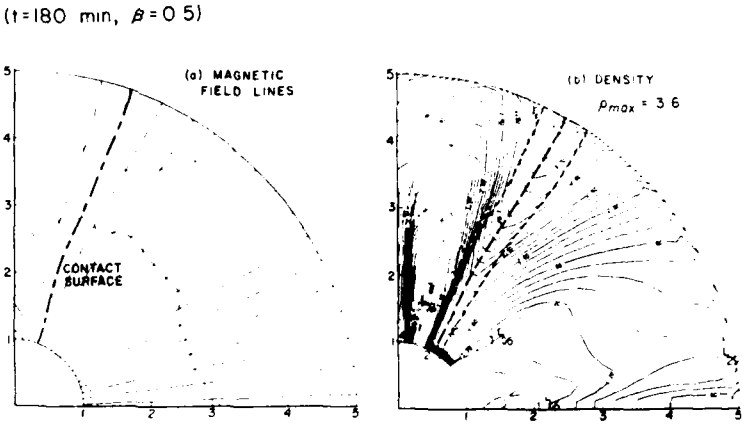

Figure 11. The magnetic field configuration and density distribution 180 minutes after introduction of the disturbance for $\beta_o = 0.5$. The other symbols are the same as Figure 10 (Steinolfson and Wu, 1980).

4. CONCLUDING REMARKS

In this study, we have presented a two-dimensional, time-dependent MHD computation for three types of magnetic field configurations. These topologies have been suggested by a number of radio astronomers to explain several classes of observations. We have started with these topologies to describe the different classes of coronal responses due to a thermal pressure disturbance. Physically, this disturbance may be interpreted as a "prototype flare" or a similar solar disruptive activity. The time evolution of the plasma parameters (i.e., density, temperature, velocity and magnetic field) in the corona has been obtained. In particular, those parameters (i.e., density and magnetic field) which we believe to be relevant to several classes of radio sources are presented. We have referred to the fundamental plasma frequency, although our results, in terms of density enhancement, do not preclude consideration of the second (or higher) harmonics. The important characteristics may be summarized as follows:

(i) From this calculation, we learned that the initial magnetic field configuration has the dominant effect on the spatial character of the radio sources. For example, the closed-field configuration shows that the emission source (i.e., described herein as a density or, equivalently, plasma frequency enhancement forms a loop-like structure which propagates outward as shown in Figure 2. The behavior has the characteristic of a rising arch. For the open field configuration computation, the emission source resulted as a bubble-like plasma cloud which propagates outward, as shown in Figure 5. Further, we may note that behind the bubble, a void (or density depletion) region is shown. These calculated results resembled the case suggested by Smerd and Dulk (1971) based on observation as shown in Figure 1b. Finally, the coronal streamer calculation shows that the emission sources have a two-fold characteristic. Part of the sources propagate outward, while the other portion remains behind within the leg region close to the foot point as shown in Figures 10 and 11. These calculations resemble the morphological case suggested by Kai (1975) as shown in Figure 8.

(ii) By presenting the computed results of plasma frequency versus time at several representative altitudes, we show how the plasma frequency (fundamental or, equivalently, its harmonics) behaves after the disturbance passes through the corona. These results demonstrate, once again, that the magnetic field configuration in the pre-flare state plays an important role. For example, the closed-field case shows a U-shape behavior at 35,000 km; whereas, the open-field case shows an inverted U-shape behavior at the same altitude. (Note, here we used the "U-shape" in a frequency-time context which does not imply U-shape intensity burst.) A word of caution concerning further interpretation of our model is warranted. Because of the limitation of the one-fluid MHD theory, we have no way to discriminate between mechanisms of various radio emission; that is, we cannot specify whether plasma oscillation or gyro-synchrotron emission is responsible for a given case. However, some gross behavior of radio emission, using the plasma oscillations as a working hypothesis, has been demonstrated through this type of calculation. Gyro-cyclotron frequency (or its harmonics) could equally be employed by referring to the temporal and spatial magnetic fields. Further study should include this latter point at well as a model in the form of multi-fluid MHD theory in which the detailed gross dynamical interaction between ions and electrons can be studied. In this latter case, polarization effects can be shown. Thus, some detailed characteristics of radio emission sources resulting from theoretical calculations such as that discussed here may be compared directly with observations.

Acknowledgments

The author is indebted to fruitful discussions with Drs. M. Dryer, R. Stewart, K. Sheriden, Y. Nakagawa and E. Tandberg-Hanssen. In particular, Dr. M. Dryer read the manuscript and gave many valuable suggestions; Dr. R. Stewart brought to the author's attention many valuable references when the author visited CSIRO, Division of Radiophysics in Sydney. This work was supported in part by NSF Grant ATM77-22484 and in part by NASA/MSFC Contract NAS8-28097.

Appendix I

The basic ideal MHD (without dissipation except at the shock) equations for numerical computation are written in the following form in spherical coordinates (r, θ, ϕ) and specialized for the equatorial plane ($\theta = 90^{o}$).

Mass conservation:

$$\frac{\partial \rho}{\partial t} + \frac{1}{r^2}\frac{\partial}{\partial r}(r^2 \rho V_r) + \frac{1}{r}\frac{\partial}{\partial \phi}(\rho V_\phi) = 0 \qquad \text{(AI-1)}$$

Momentum conservation:

$$\frac{\partial V_r}{\partial t} + V_r \frac{\partial V_r}{\partial r} + \frac{V_\phi}{r}\frac{\partial V_r}{\partial \phi} - \frac{V_\phi^2}{r}$$

$$= -\frac{1}{\rho}\frac{\partial p}{\partial r} + \frac{1}{\rho}\frac{B_\phi}{r}\frac{\partial B_r}{\partial \phi} - \frac{1}{\rho}\frac{B_\phi}{r}\frac{\partial}{\partial r}(rB_\phi) - \frac{GM_s}{r^2} \qquad \text{(AI-2)}$$

$$\frac{\partial V_\phi}{\partial t} + V_r \frac{\partial V_\phi}{\partial r} + \frac{V_\phi}{r}\frac{\partial V_\phi}{\partial \phi} + \frac{V_r V_\phi}{r}$$

$$= -\frac{1}{\rho r}\frac{\partial p}{\partial \phi} - \frac{1}{\rho}\frac{B_r}{r}\frac{\partial B_r}{\partial \phi} + \frac{1}{\rho}\frac{B_r}{r}\frac{\partial}{\partial r}(rB_\phi) \qquad \text{(AI-3)}$$

Induction equations:

$$\frac{\partial B_r}{\partial t} = -\frac{1}{r}\frac{\partial}{\partial \phi}[r(B_r V_\phi - B_\phi V_r)], \qquad \text{(AI-4)}$$

$$\frac{\partial B_\phi}{\partial t} = \frac{1}{r}\frac{\partial}{\partial r}[r(B_r V_\phi - B_\phi V_r)], \qquad \text{(AI-5)}$$

Energy conservation:

$$\frac{\partial}{\partial t}\left[r^2\left\{\frac{p}{\gamma-1} + \frac{1}{2}\rho(V_r^2 + V_\phi^2) + \frac{1}{2\mu}(B_r^2 + B_\phi^2)\right\}\right]$$

$$+ \frac{\partial}{\partial r}\left[r^2 V_r\left\{\frac{\gamma p}{\gamma-1} + \frac{1}{2}\rho(V_r^2 + V_\phi^2)\right\}\right.$$

$$\left. + \frac{r^2}{\mu}(V_r B_\phi^2 - V_\phi B_r B_\phi)\right]$$

(Equation (AI-6) continued on next page.)

$$+ \frac{1}{r} \frac{\partial}{\partial \phi} \left[r^2 V_\phi \left\{ \frac{\partial}{\gamma - 1} p + \frac{1}{2} \rho (V_r^2 + V_\phi^2) \right\} \right.$$

$$\left. + \frac{r^2}{\mu} (V_\phi B_r^2 - V_r B_r B_\phi) \right]$$

$$+ V_r \rho G M_s = 0 \qquad \text{(AI-6)}$$

Here, the dependent variables are the density ρ, radial velocity V_r, azimuthal velocity V_ϕ, thermal pressure p, radial magnetic field B_r, and azimuthal magnetic field B_ϕ; the constants are the polytropic index γ, the gravitational constant G, and the solar mass M_s. In addition, the equation of state is used, namely, $p = \rho RT$, where T is the temperature and R is the gas constant.

Appendix II

The two-dimensional, time-dependent ideal MHD equations in the meridional plane are written in the following form:

Mass conservation:

$$\frac{\partial \rho}{\partial t} + \frac{\partial}{\partial r} (\rho V_r) + \frac{\partial}{\partial \theta} \frac{\rho V_\theta}{r} = - \frac{2 \rho V_r}{r} - \frac{\rho V_\theta}{r} \cot \theta, \qquad \text{(AII-1)}$$

Momentum conservation:

$$\frac{\partial V_r}{\partial t} + V_r \frac{\partial V_r}{\partial r} + \frac{V_\theta}{r} \frac{\partial V_r}{\partial \theta} - \frac{V_\theta^2}{r}$$

$$= - \frac{1}{\rho} \frac{\partial p}{\partial r} + \frac{B_\theta}{\mu \rho r} \frac{\partial B_r}{\partial \theta} - \frac{B_\theta}{\mu \rho} \frac{\partial B_\theta}{\partial r} - \frac{B_\theta^2}{\mu \rho r} - \frac{G M_s}{r^2}, \qquad \text{(AII-2)}$$

$$\frac{\partial V_\theta}{\partial t} + V_r \frac{\partial V_\theta}{\partial r} + \frac{V_\theta}{r} \frac{\partial V_\theta}{\partial r} + \frac{V_r V_\theta}{r}$$

$$= - \frac{1}{\rho r} \frac{\partial p}{\partial \theta} + \frac{B_r}{\mu \rho} \frac{\partial B_\theta}{\partial r} - \frac{B_r}{\mu \rho r} \frac{\partial B_r}{\partial \theta} + \frac{B_r B_\theta}{\mu \rho r}, \qquad \text{(AII-3)}$$

Induction equations:

$$\frac{\partial B_r}{\partial t} - \frac{1}{r\sin\theta}\frac{\partial}{\partial\theta}\left(\frac{V_r B_\theta - V_\theta B_r}{r}\right) = \frac{1}{r}\left(V_r B_\theta - V_\theta B_r\right)\cot\theta, \tag{AII-4}$$

$$\frac{\partial B_\theta}{\partial t} + \frac{1}{r}\frac{\partial}{\partial r}\left(V_r B_\theta - V_\theta B_r\right) = -\frac{1}{r}\left(V_r B_\theta - V_\theta B_r\right), \tag{AII-5}$$

Energy conservation

$$\frac{\partial p}{\partial t} + \gamma p\frac{\partial V_r}{\partial r} + V_r\frac{\partial p}{\partial r} + \frac{\gamma p}{r}\frac{\partial V_\theta}{\partial\theta} + \frac{V_\theta}{r}\frac{\partial p}{\partial\theta} \tag{AII-6}$$

$$= -\frac{\gamma p}{r}\left(2V_r + V_\theta\cot\theta\right). \tag{AII-6}$$

Here, all symbols have the same meaning as we have defined in Appendix I. In addition, the V_θ and B_θ represent the meridional velocity and meridional magnetic field, respectively.

References

Dryer, M. and Maxwell, A.: 1979, "Radio data and a theoretical model for the fast-mode MHD shock wave generated by the solar flare of 1973 September 5, 13:26 UT", *Astrophys. J., 231*, 945.

Dryer, M., Wu, S. T., Steinolfson, R. S., and Wilson, R. M.: 1979, "Magnetohydrodynamic models of coronal transients in the meridional plane. II. Simulation of the coronal transient of 1973 August 21", *Astrophys. J., 227*, 1059.

Kai, Keizo: 1975, "A model for the development of a solar outburst based on observations with the Culgoora radio spectograph and heliograph", *Solar Phys., 45*, 217.

Kai, Keizo: 1973, "Relation between circular polarization of moving Type IV bursts and polarity of photospheric magnetic fields", *Solar Phys., 56*, 417.

Kundu, M. R.: 1965, *Solar Radio Astronomy*, Interscience, New York.

Nakagawa, Y., Wu, S. T., and Han, S. M.: 1978, "Magnetohydrodynamics of atmospheric transients. I. Basic results of two-dimensional plane analyses", *Astrophys. J., 219*, 314.

References

Nakagawa, Y., Wu, S. T., and Han, S. M.: 1981, "Magnetohydrodynamics of atmospheric transients. III. Basic results of non plane two-dimensional analysis", *Astrophys. J., 244,* 331.

Schmahl, E. J.: 1973, "Catalogue of nine moving Type IV radio sources observed with the Culgoora radioheliograph", *Australian J. Phys., Astrophys. Suppl., 29,* 1.

Sheridan, K. V., Labrum, N. R., and Payten, W. J.: 1973, "Three-frequency operation of the Culgoora radioheliograph", *Proc. Inst. Elec. Electron. Engrs., 61,* 1312.

Smerd, S. F. and Dulk, G. A.: 1971, "80 Mhz radioheliograph evidence on moving Type IV bursts and coronal magnetic fields", in R. Howard (ed.), *Solar Magnetic Fields,* IAU Symp. 43, D. Reidel, Dordrecht, 616-641.

Steinolfson, R. S. and Wu, S. T.: 1980, "Dynamic simulation of coronal mass ejections", *UAH Research Report No. 240,* University of Alabama in Huntsville, Huntsville, Alabama.

Steinolfson, R. S.: 1982, "Coronal loop transients in streamer configurations", *Astron. and Astro.* (in press).

Steinolfson, R. S., Suess, S. T., and Wu, S. T.: 1982, "The steady global corona", *Astrophys. J., 255,* 730.

Stewart, R. T.: 1980, "Transient disturbances of the outer corona", in M. Dryer and E. Tandberg-Hanssen (eds.), *Solar and Interplanetary Dynamics,* IAU Symp. 91, D. Reidel, Dordrecht, 333.

Stewart, R. T., McCabe, M. K., Koomen, M. J., Hansen, R. T., and Dulk, G. A.: 1974, "Observations of coronal disturbances from 1 to 9 R_0", *Solar Phys., 36,* 203.

Wild, J. P. and Smerd, S. F.: 1972, "Radio bursts from the solar corona", *Ann. Rev. Astron. Astrophys., 10,* 159.

Wild, J. P., Sheridan, K. V., and Trent, G. A.: 1959, "The transverse motions of the sources of solar radio bursts", in R. N. Bracewell (ed.), *Paris Symp. Radio Astron.,* Stanford University Press, p. 176.

Wild, J. P., Smerd, S. F., and Weiss, A. A.: 1963, "Solar bursts", *Ann. Rev. Astron. Astrophys., 1,* 291.

Wu, S. T., Dryer, M., Nakagawa, Y., and Han, S. M.: 1978, "Magnetohydrodynamics of atmospheric transients. II. Two-dimensional numerical results for a model solar corona", *Astrophys. J., 219,* 325.

Discussion

Gelfreich: How could you get twisted magnetic fields? Is it due to initial conditions or is it a solution you have obtained?

Wu: In this calculation, the twisted magnetic field is caused by a rotational discontinuity. Details are shown in a paper by Nakagawa, Wu and Han (1981) who show the twist in a self-consistent MHD model which considers the time-dependent evolution of all three components of the magnetic topology and plasma velocity. Yes, the initial field is being twisted.

Discussion

Zlotnik: You believe gyroresonance emission to be responsible for Type IV bursts. What about electron velocities: are the electrons relativistic or not? And how can you explain fine structure on Type IV bursts in the framework of gyrofrequency radio emission?

Wu: In this simple fluid MHD model, we cannot explain those fine structures; however, we plan to move ahead to extend this model to two fluids and non-plane analyses. Then, it should be able to demonstrate, in part, what you are asking. That is, we expect to show the localized regions of locally-compressed magnetic fields which, in principle, could - together with the few electrons in our (assumed) Maxwellian distribution function - conspire to produce gyroresonance emission.

Croft: In theoretical studies such as yours, one must approximate in order to make the mathematics tractable. The difficulty lies in finding which kinds of simplifications can be made without thereby eliminating some of the more important phenomena. One way to meet this problem is to perform calculations (as you have) and then to look for similarities between the derived results and the corresponding physical events experimentally observed. How well do your methods perform, when judged by this approach?

Wu: The purpose of this paper is to utilize the previously-published results of a series of papers by our group on this subject. In several of these papers (please see the reference list to the written version of this talk as well as my reply to Dr. Schwenn) we demonstrate: (a) shock development and velocity as measured by typical Type II radio bursts; (b) density enhancements, followed by rarefactions, as measured by coronograph observations of K corona scattering of sunlight from transiently-disturbed electrons; and (c) shape of coronal transients as also determined for a number of cases by the coronagraph.

Schwenn: The "bomb" in these calculations was just a local temperature increase. Did you ever consider, as an alternative, the injection of new material?

Wu: Yes, we have considered various alternatives. I may refer you to the paper by Steinolfson et al., to appear in the Proceedings of the Burghausen conference (1978), Solar Wind IV. In that paper we used emerging magnetic flux as our disturbance. In several other papers in the Astrophysical Journal, we used various combinations of enhanced density (to simulate injection of new plasma from the chromosphere into the base of the corona) and temperature pulses. In one of these papers (Dryer et al., Astrophys. J., 227, 1979) we used a long-lasting density and temperature enhancement as measured by the NASA/MSFC-Aerospace soft X-ray instrument aboard Skylab during the 21 August 1973 limb event. The result simulated main features of the observed coronal transient as observed by the NCAR/HAO coronograph.

Giovanelli: It is difficult to see how such a field system could develop, given that the lines of force all originate from two magnetic poles in the model used; or that, as in Wu's case, such a model field could develop an explosive instability. However a simple change in model could be devised to provide an instability, without any significant change to Dr. Li's analysis of the physics involved.

Wu: It is essential to correct a misinterpretation which I may have unintentionally left with you (as implied in your remark). We do not assume that an explosive instability occurs in our model equilibrium (i.e., ambient) magnetic field and atmosphere. Rather, we simulate an energy conversion process (as, for example, by reconnection) by assuming various thermodynamic consequences - a pressure pulse (with variously-assumed temporal profiles) or a magnetic pulse (e.g., by an emerging magnetic flux). The first two cases we have shown may not be realistic; however, they do exhibit fundamental physics. Our third case (i.e., coronal streamer configuration) may resemble Dr. Li's observational analysis.

3. Profiles of Coronal MHD Disturbance Associated With the Solar Flare on April 27, 1979

R. V. Bhonsle, S. S. Degaonkar and S. K. Alurkar
Physical Research Laboratory
Ahmedabad-380009, India

Abstract

A solar flare of importance 1B which occurred at 0636 UT on April 27, 1979 in region 1705 (McMath No. 15967) on the solar disk (N20, E16) produced intense radio bursts. An impulsive microwave event was also recorded at 2800 MHz at Ahmedabad, beginning at 0642 UT, and showing about 10-12 peaks in intensity in a time duration of 20 minutes. The most interesting feature of this event is the observation of a strong continuum radiation (Type IV) starting at 0653 UT and lasting for about 10 minutes as recorded by the wide band spectrograph operating in the 45 - 25 MHz range. This continuum radiation displayed sharp low frequency cut-off, which varied from about 40 to 30 MHz in a quasi-periodic manner. The sharp low frequency cut-off in the continuum radiation is attributed to "Razin effect". The perturbation of this cut-off frequency is interpreted as that induced by the passing MHD shock wave through the magnetic flux tube where the continuum radiation is generated by the synchrotron mechanism from trapped energetic electrons. Assuming a spherically symmetric electron density model and using the observed cut-off frequency, the magnitude of the coronal magnetic field around 2 $R_\odot$ above the photosphere had a value of about 6 gauss.

1. INTRODUCTION

A wide band decametric spectrograph with medium resolution (~ 50 kHz recently began operating at Ahmedabad, India (23° 02'N, 72° 36'E) for the purpose of recording burst spectra in the range 45 - 25 MHz. As the radio bursts in this frequency range originate from the coronal region 1 - 2 solar radii above the photosphere where transition from closed magnetic field lines to open field lines is believed to take place, it is interesting to deduce properties of the region from the characteristics of the burst spectra just as the microscopic features of coronal density irregularities were deduced from high resolution decametric spectroscopy (Sawant et al., 1976; Bhonsle et al., 1979). In the present paper, we report on an interesting solar event which was recorded on April 27, 1979 with our wide band spectrograph.

2. OBSERVATION

A solar flare of optical importance 1B and type X-1 in X-rays occurred at 0652 UT on April 27, 1979 in region 1705 (McMath No. 15967, location N18, E17). Though the Boulder Solar and Geophysical Data reports (1979) indicated that the flare was not spectacular optically it produced intense Type IV radio emission which lasted for about 10 minutes starting from 0653 UT. Figure 1 shows the first minute of the Type IV burst spectral record which reveals some interesting features. Following the solar flare at 0652 UT, no conventional Type II burst was seen on the spectrograph record but a strong Type IV continuum radiation was evident from 0653 UT to 0702 UT.

It can be seen from Figure 1 that the Type IV radiation appears with a sudden large decrease in cut-off frequency from about 44 MHz in a time duration of about 8 seconds beginning 0653 UT. Then the cut-off frequency increased to 42 MHz after which the radiation spread again slowly to the low frequency side to about 33 MHz. In addition it can be seen that the observed cut-off frequency of Type IV emission, while it was slowly decreasing, underwent a quasi-periodic perturbation with small amplitude. This is seen more clearly in Figure 2 which is the tracing of Figure 1. Thus, the initial sudden change in cut-off frequency is of the order of 9 MHz and the average frequency change and period of the perturbation as determined from the record are $\pm$ 0.3 MHz and 5 seconds respectively.

3. INTERPRETATION AND DISCUSSION

The perturbation seen on the low frequency side of the Type IV continuum appears to be the result of the dynamic interaction between the magnetic field and the material ejected during a solar event. Numerical solution of the time dependent magneto-hydrodynamic (MHD) equations of motions have been obtained in some simple situations to understand how a disturbance propagates upward and laterally through the corona with the leading edge of the disturbance having the shape of an expanding loop (Steinolfson et al., 1978). The leading portion of the disturbance contains only coronal material whose properties have been altered by the preceding

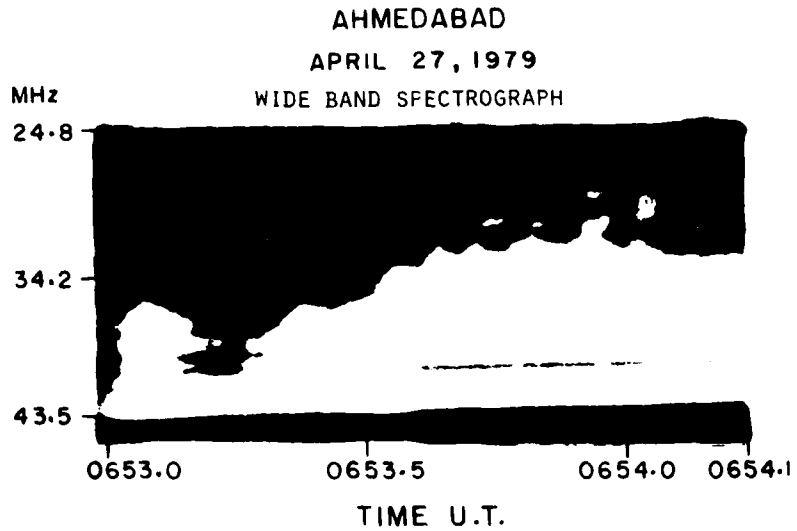

Figure 1. Dynamic spectrum of Type IV burst observed on April 27, 1979 starting at 0653 UT. Note sharp low frequency cut-off of continuum radiation and its quasi-periodic variation.

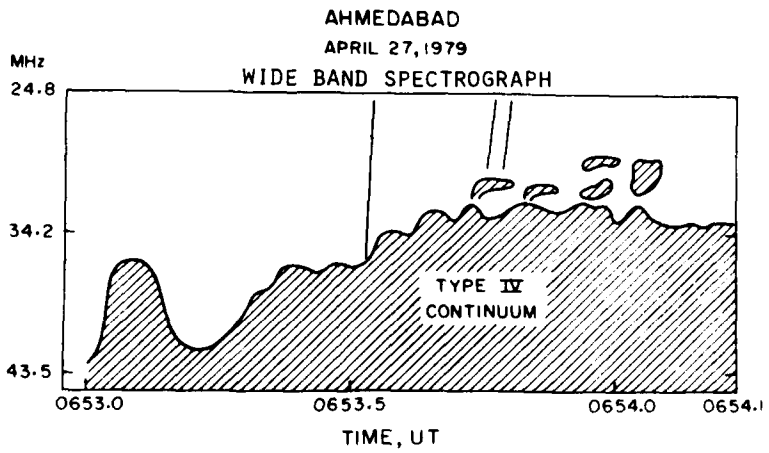

Figure 2. Sketch of burst spectrum shown in Figure 1.

3.

waves (which may strengthen into shocks) created by the explosive nature of the solar event. Hence we may assume that the perturbations seen in Figures 1 and 2, caused by the MHD disturbance along the closed field lines forming the magnetic bottle in which energetic electrons are trapped, give rise to Type IV emission by synchrotron processes (Takakura, 1966; Wild and Smerd, 1972). Such perturbations can be expected to produce magnetic field fluctuations which in turn modulate the cut-off frequency of Type IV continuum (Ramaty and Lingenfelter, 1967).

Ramaty and Lingenfelter (1967) have shown that the sharp low frequency cut-off in Type IV continuum may be explained as due to Razin effect rather than on the basis of cut-off imposed by the local plasma frequency. The latter possibility does not arise in the present situation because the generating mechanism of Type IV bursts is a synchrotron process which is independent of the local plasma frequency. The Razin effect is seen only when the parameter $\alpha = 466B/Ne^{1/2}$) is less than 1. Here B is the magnetic field in gauss and Ne the number of electrons per cm^3 in the source region.

Newkirk (1971) and Dulk and McLean (1978) have reviewed the coronal magnetic field estimates. However, we can estimate the magnetic field value in the corona from the observed Razin cut-off frequency from the relation given by Ramaty and Lingenfelter (1967).

$$\upsilon_R = 20 \frac{Ne}{B} \qquad (1)$$

where υ_R is the low frequency cut-off of the continuum in Hz. Putting υ_R $\sim 35 \times 10^6$ Hz and Ne $\sim 10^7$ per cm^3 at $2R_\odot$, using Newkirk's model (1961), we find that B has a value of ~ 6 gauss which is in agreement with the estimates given by Newkirk (1971) and Dulk and McLean (1978). The initial sudden impulsive change in cut-off frequency at 0653 UT of about 9 MHz and the average amplitude of perturbation of the cut-off frequency of $\pm$ 0.3 MHz makes the percentage change of ~ 30 and ~ 1 at the observed cut-off freqency (~ 30 MHz). Hence, the change from 1 to 30% in the magnetic field, B, is due to a MHD wave at that level in the corona.

Another interesting feature seen from Figures 1 and 2 is that four "puffs" of radiation appear to emerge when the cut-off frequency of Type IV radiation reaches minimum. This shows that energetic electrons are ejected in bunches from the magnetic bottle when the magnetic field is quasi-periodically strengthened. The released electrons subsequently caused radiation by a plasma oscillation process.

4. CONCLUSION

From the observed low frequency cut-off of Type IV continuum burst in the decameter range, we have obtained estimates of the coronal magnetic field (~ 6 gauss) around 2 solar radii and the magnitude of its perturbation (from 1 to 30%) as a result of an MHD wave propagating through that region.

Acknowledgments

Our thanks are due to Prof. D. Lal, F.R.S., Director of PRL for his interest in this work. The cooperation of the field staff in the maintenance of the equipment is very much appreciated. This program is supported by the Department of Space, Government of India.

References

Bhonsle, R.V., Sawant, H.S., and Degaonkar S.S.: 1979, "Exploration of the solar corona by high resolution solar decametric observations", *Space Sci. Rev., 24,* 259.

Dulk, G.A., and McLean, D.G.: 1978, "Coronal magnetic fields", *Solar Phys., 57,* 279.

Newkirk, G.: 1961, "The solar corona in active regions and the thermal origin of the slowly varying component of solar radio radiation", *Astrophys. J., 133,* 983.

Newkirk, G.: 1971, "Large scale solar magnetic fields and their consequences", in R. Howard (ed.) *Solar Magnetic Fields,* Proc. IAU Symp. No. 43, D. Reidel, Holland, p. 547.

Ramaty, R., and Lingerfelter, R.E.: 1967, "The influence of the ionized medium on synchrotron emission spectra in the solar corona", *J. Geophys. Res., 72,* 879.

Sawant, H.S., Bhonsle, R.V., and Alurkar, S.K.: 1976, "Microscopic spectral features in solar decametric burst and coronal irregularities", *Solar Phys., 50,* 481.

Solar-Geophysical Data: 1979, U.S. Department of Commerce, NOAA, Boulder, Colorado, 417-I, p. 7.

Steinolfson, R.S., Wu, S.T., Dryer, M., and Tandberg-Hanssen, E.: 1978, "Magneto-hydrodynamic models of coronal transients in the meridional plane. I. The effect of the magnetic field", *Astrophys. J., 225,* 259.

Takakura, T.: 1966, "Implications of solar radio bursts for the study of the solar corona", *Space Sci. Rev., 5,* 80.

Wild, J.P., and Smerd, S.F.: 1972, "Radio bursts from the solar corona", *Ann. Rev. Astron. Astrophys., 10,* 159.

Discussion

Dryer: What is the reason for the cutoffs which gave the results of multiple "puffs" at the lower frequency?
Alurkar: This may be due to the energetic electrons released in bunches from the magnetic field bottle when the latter is quasi-periodically perturbed by the M.H.D. disturbance.

Gelfreich: Was there any evidence of a Type II burst in this event?
Alurkar: No, there was no evidence of a Type II burst.

Wu: While you determine the magnetic field strength from the observed $f_R \approx 20\ N_e/B$, you need the disturbed number density. How do you get this disturbed number density?
Alurkar: Newkirk's values of N_e give a rough estimate during undisturbed conditions. For more precise values number density in the source region should be used.

4. Fine Structure in Metre-Wave Solar Radio Bursts

D. McConnell and G. R. A. Ellis
Department of Physics, University of Tasmania,
Box 252C, G.P.O., Hobart, Tasmania 7001, Australia

Abstract

Observations with high time resolution (<1 ms) have been made in the frequency range 30-82 MHz. During June 1979 several thousand bursts with bandwidth ~100 kHz and duration at a single frequency of about 50 ms were recorded. Their frequency drift rates were between -1.5 and -5 MHz s^{-1}. They belong to the classification "fast-drift storm bursts" (FDS bursts). Approximately 1% of the bursts in the present observations showed bands or fringes in the frequency-time plane almost parallel to the time axis and with a frequency separation of about 100 kHz. Figures 1 and 2 show examples of FDS bursts and FDS bursts with fringes.

In this discussion the presence of fringes and their short duration at a single frequency are considered.

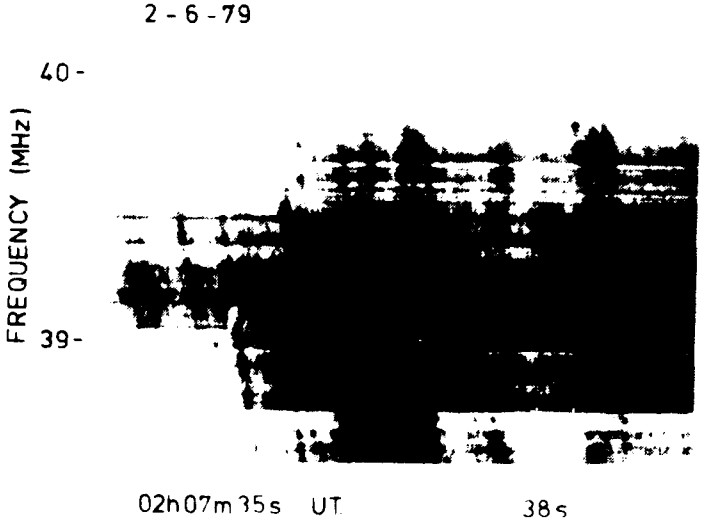

Figure 1. Dynamic spectrum of FDS bursts. A fringed FDS burst can be seen above 39.6 MHz a little after $02^h07^m38^s$.

1. FRINGES

We consider two possible generation mechanisms.

(i) The fringes may be due to the solar radiation having a strong linearly polarized component, being subject to Faraday rotation in the corona and ionosphere and being observed with a linearly polarized antenna. From the fringe spacing the path integral $D = \int N_e B_{\parallel} d\ell$ (where N_e is electron density, $B_{\parallel}$ is the longitudinal magnetic field and ℓ is the path length) was estimated. It was found that near 40 MHz $D = 3.8 \pm 0.2 \times 10^{13}$ G m^{-2}. From simultaneous ionosonde data the contribution to D from the ionosphere was $D_I \simeq 4 \times 10^{12}$ G m^{-2}, leaving the residual, presumably of solar origin, of $D_C \simeq 3.4 \pm 0.2 \times 10^{13}$ G m^{-2}. This corresponds to a total Faraday rotation in the corona of 503 ± 30 rad at 40 MHz.

(ii) The second alternative considered involves an idea from a theory (Takakura and Yousef, 1975) for the generation of Type IIIb bursts. According to Melrose (1974) the brightness temperature T of a source of fundamental plasma emission is related to the electron density gradient as follows:

$$T \propto \exp(\alpha L - 1) ,$$

where

$$\alpha \propto f^2 \frac{\langle T_p \rangle \Delta\Omega}{T_i} \quad \text{cm}^{-1} ,$$

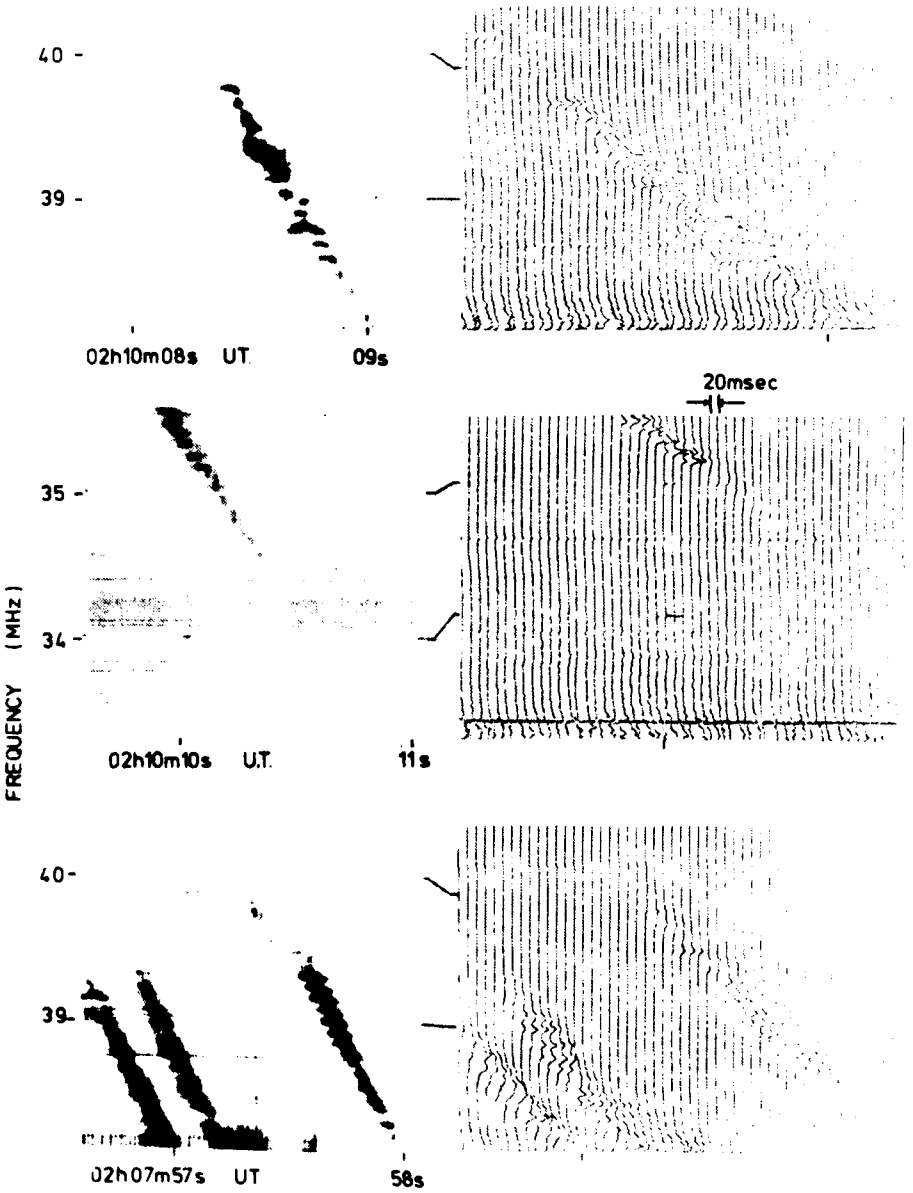

Figure 2. Dynamic spectra of solar radio bursts which show fringes. The spectrum of each burst is shown twice, recorded with a 256-channel filter bank (left) and with a time expansion sweep frequency analyser (right). The sweep frequency analyser has a time expansion ratio of 1500 and simulates a 1500-channel filter bank analyser with individual filters of 2 kHz bandwidth. Each sweep of the analyser is 20 ms apart and displays the power spectrum. All bursts were recorded on 1979 June 2.

where f is in megahertz, T_i is the ion temperature, T_p is the effective temperature of plasma waves confined in a limited range of solid angle $\Delta\Omega$, and L is the effective distance over which amplification is possible. Now

$$L \propto \frac{1}{\text{grad } \omega_p} \quad ,$$

where ω_p is the plasma frequency and $\omega_p \propto N_e^{\frac{1}{2}}$. Thus the brightness temperature is strongly dependent upon the electron density gradient in the source. An electron stream travelling through a region of the corona with a spatial periodicity in electron density might therefore generate fringed bursts similar to those observed. Figure 3 shows the observed profile of brightness temperature with frequency for a pair of fringes and the profile expected from a sinusoidal variation in electron density. The observed fringe separation implies a wavelength of the density variation of 1000 km, assuming the variation is superimposed upon a 2 × Baumbach Allen coronal density model.

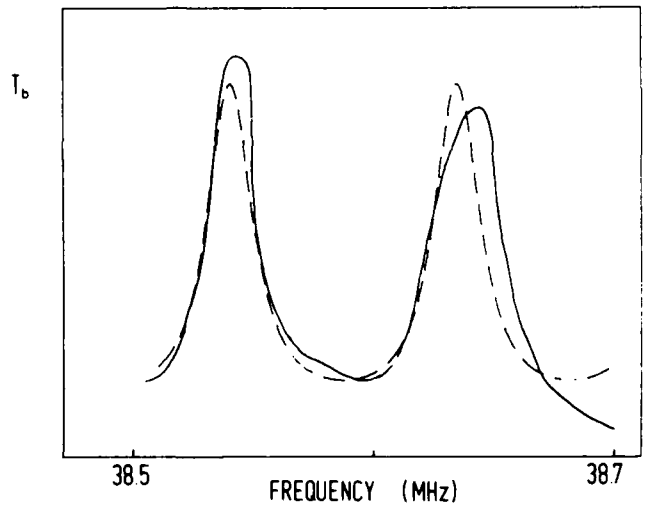

Figure 3. Variation of brightness temperature T_b (arbitrary, linear scale) with frequency for a pair of fringes. The solid line gives the observed variation and the dotted curve is derived from a sinusoidal electron density variation as described in Section 1(ii).

2. DURATION

Figure 4 shows the distribution of fringe durations. The burst duration sets an upper limit to the size of the source of emission. A duration of 33 ms limits the source size to 10^4 km The short duration also sets a limit on the amount of scattering of radiation within the corona. Numerical calculations of the expected amount of scattering give minimum burst durations. Riddle (1974) has calculated the expected time smearing of short bursts of 80 MHz radiation. His calculations give minimum durations of about 0.1 and 0.5 s for emission at second-harmonic and fundamental plasma frequency respectively. In view of the short durations measured in the present observations, it seems important to repeat these calculations for 40 MHz radiation.

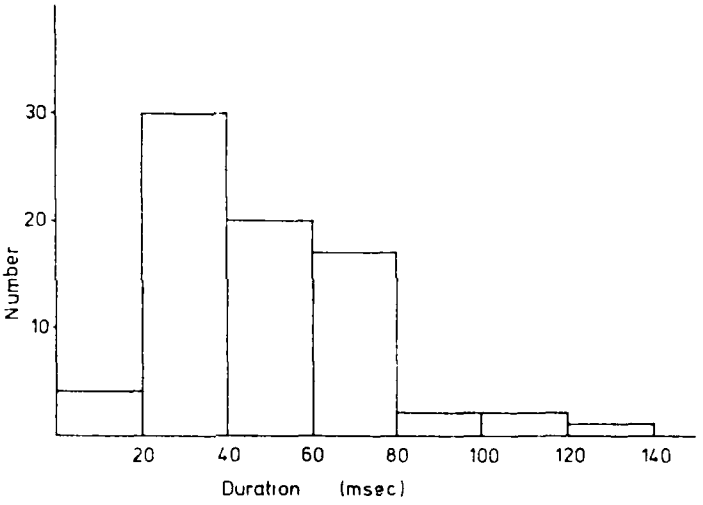

Figure 4. Distribution of durations of the fringes in FDS bursts.

It should be noted with regard to coronal scattering that the short duration of FDS bursts suggests that the radiation must be emitted at the second harmonic of the plasma frequency. However, the coronal irregularity model proposed above for the generation of FDS fringes requires radiation to be at the fundamental plasma frequency. In order to resolve this problem further study of these bursts must aim to determine which harmonic is being observed.

References

Melrose, D.B.: 1974, "A relationship between the brightness temperatures for Type III bursts", Solar Phys., 35, 441.

Riddle, A.C.: 1974, "On the observations of scattered radio emission from sources in the solar corona", Solar Phys., 35, 153.

Takakura, T., and Yousef, S.: 1975, "Type IIIb radio bursts: 80 MHz source position and theoretical model", Solar Phys., 40, 421.

Discussion

Stewart: The Faraday rotation interpretation assumes the stria bursts are linearly polarized. We know that Type IIIb stria bursts are unpolarized so I suspect that the same is true for the fine-structure bursts you described.

McConnell: We have set up an antenna with crossed dipoles sensitive to two perpendicular linear polarizations to try and resolve the question. We have not yet observed any of these bursts in this way.

Nelson: Given that you have an estimate of the size of the source, have you calculated its brightness temperature?

McConnell: The flux from these bursts is comparable with that from the thermal solar background. A source size of 10^4 km then implies a source temperature of $\sim 10^{11}$ K.

Dryer: Your assumption of the sinusoidal density profile suggests that fast-mode MHD waves may have been propagating upward.

McConnell: Yes, the implied period of such a wave, with wavelength of ~5000 km, would be 1-10 s, depending on the model corona used.

Croft: Is it possible that nothing is travelling but that the longer delay at lower frequencies is due to dispersion in the medium, and that the source was a single, wide-band outburst?

McConnell: We considered that possibility, but the delay at lower frequencies does not follow the correct law. Furthermore, we observe some bursts which show a reverse-frequency drift.

5. The Mechanism of the U-Shaped Spectrum of Type IV Solar Radio Bursts

Li Chun-sheng and Zheng Wing-wu
Department of Astronomy, Nanjing University
Nanjing, China

Yao Jin-xing
Purple Mountain Observatory
Academia Sinica
Nanjing, China

Abstract

A mechanism is suggested to account for the U-shaped spectrum of the Type IV solar radio burst during the explosive phase of a proton flare. The U-shaped spectrum consists of two parts, namely the part of Type IV-μ burst and that of Type IV-dm burst. Each of them is believed to be produced by gyro-synchrontron radiation of non-thermal electrons (100 keV $\leq \varepsilon \leq$ 2 Mev) being accelerated simultaneously with protons in the explosive phase and gyro-resonance absorption of thermal electrons.

Numerical calculations are presented for the flux densities of Type IV-μ burst and Type IV-dm burst during the 1972 August 7 event, assuming a cylindrical volume of these burst sources. It is shown that the computed results are consistent with that of observations. In addition, we also discuss the relation between the U-shaped spectrum of a Type IV radio burst and the occurrence of a proton event.

1. INTRODUCTION

The peak flux density spectrum of Type IV solar radio bursts is generally continuous broad-band, particularly those associated with PCA (Polar Cap Absorption) events having a distinctive U-shaped spectral signature (Fig. 1). There is high intensity in the meter range, a minimum at 500-4000 MHz, a peak near 10 GHz, and a decline toward higher frequencies. Such spectra were first constructed by Castelli et al. (1967) who showed that this U-shaped spectrum is a characteristic feature of all flares producing strong proton fluxes in space. Since, however, a well-developed Type IV burst is a typical characteristic of all proton flares, this spectrum shape is in fact characteristic for all strong and well-developed Type IV bursts. A series of well-known U-shaped spectral criteria for proton events were formulated (Sarris, 1971; Castelli and Guidice 1976). These criteria, being used as a yes-no forecasting tool for proton events, clearly had predictive or warning value, since the delay from the observance of the burst (and the identification of the spectral signature) to the first onset of the particles at the earth could be anywhere from 10 minutes to 20 hours.

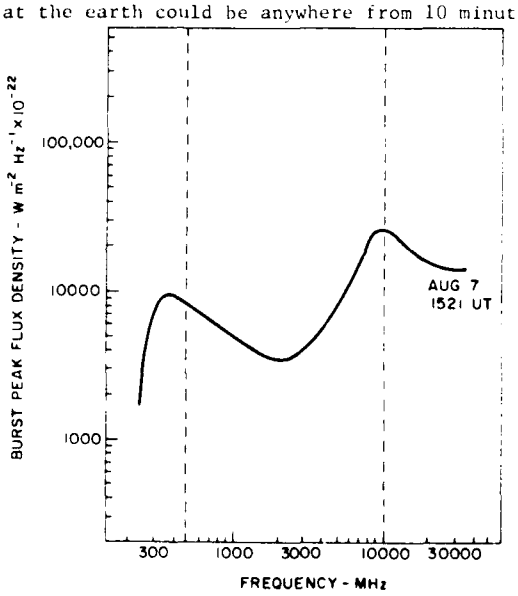

Figure 1. The U-shaped spectrum of Type IV solar radio bursts on 7 August 1972.

During the period 2-7 August 1972, four unusually intense solar flare-burst events occurred in the McMath plage region 11976. All of them were associated with the U-shaped spectrum and proton events. Moreover, those on August 4 and 7 were ascertained as ground level events (GLE's). During this period extensive observations of the spectacular solar events were made by all available means such as spacecraft, balloons, lunar-based instruments, and rockets in addition to numerous ground-based solar observations both in optical and radio regions.

The data of radio observations over wavelengths ranging from millimeter to meter for the U-shaped spectrum of the Type IV radio bursts on 7 August 1972 at the same place (Sagamore Hill) and the information of related observations were provided (Castelli et al., 1973).

We also utilize the observational data published in Solar Geophysical Data 7 August 1972 by Academia Sinica. It is, therefore, appropriate that we utilize this extensive data set to study the physical mechanisms of the U-shaped spectrum of Type IV radio bursts.

2. MODEL OF SOLAR FLARE-BURST SOURCES PRODUCING THE U-SHAPED SPECTRUM OF TYPE IV RADIO BURSTS

In this study, the U-shaped spectrum is considered to be formed at the peak radiation of Type IV radio bursts during the explosive phase of a proton flare. The range from the valley on the curve of the U-shaped spectrum to higher frequencies is the spectrum of Type IV-μ bursts. The range from the valley to lower frequencies is that of Type IV-dm bursts. These two spectra are believed to be produced by the sources of Type IV-μ bursts and Type IV-dm bursts, respectively.

During the explosive phase of a proton flare, the ejected plasma cloud, frozen in the magnetic field, seems to be the source of Type IV-dm bursts. The magnetoactive plasma cloud captures numerous high energy electrons ejected upward continuously with arbitrary angles from the solar flare explosive region.

In the course of gyrating around magnetic field lines, the high energy electrons emit electromagnetic waves, generally known as gyrosynchrotron radiation to form the Type IV-dm bursts. Similarly, at the same time those ejected downward continuously will also send out gyrosynchrotron emission to form the type IV-μ bursts.

All the high energy electrons mentioned above and those high energy protons escaping into the space during the explosive phase of a proton flare may be accelerated simultaneously by the same accelerating mechanism, thus a close correlation may exist between the U-shaped spectrum of type IV radio bursts and the proton events.

The model described above is analogous to that of Sturrock (1968). For simplicity, the magnetic field due to a bipolar sunspot is illustrated by two independent axially symmetric dipole fields which have opposite polarities plotted in Fig. 2. The magnetic field-strength along the axis with height is given by Takakura and Scalise (1970),

$$H = \left(\frac{d}{d+h}\right)^3 H_o \qquad (1)$$

where H_o is the magnetic field strength at the photosphere and is set to 3000 G (Castelli et al., 1967; Solar Geophysical Data, 1972). H is the magnetic field strength at the height h above the photosphere. The depth of the vertical dipole below the photosphere, d, equals 3.5×10^4 km in the present model (Takakura and Scalise, 1970).

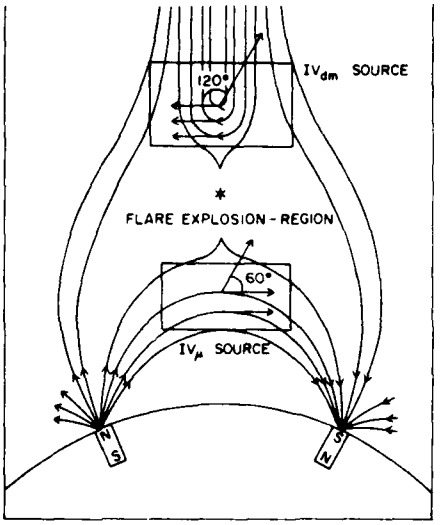

Figure 2. Model with a bipolar sunspot for solar flare-burst sources.

In the sources of Type IV-μ bursts and Type IV-dm bursts, the magnetic field lines are approximately antiparallel to each other, but all are taken to be parallel to the photospheric surface.

For computational simplification, the volume of these bursts' sources are assumed to be cylinders, and their bases are all parallel to the photospheric surface. Thus for the active region McMath 11976 (N14°, W36°) on 7 August 1972, the 3B flare meridian distance can be adopted as 30°. If θ represents the angle between the direction of observation and the magnetic field in the source, then it will be 60° for the Type IV-μ burst source and 120° for Type IV-dm burst source in this case. Hence it follows that the quasi-longitudinal propagation of radio wave from the above radio sources under consideration is valid.

3. THE COMPUTING FORMULAE FOR U-SHAPED SPECTRUM

According to the theory of radiative transfer, the spectrum of the emission from the solar radio source is given by

$$ds(f,\theta) = \frac{dV}{R^2}\,\eta(f,\theta)\,e^{-\tau(f,\theta)} \qquad (2)$$

where f is the frequency of emission under consideration and $ds(f,\theta)$ is the flux density received at the distance R to the earth due to the gyrosynchrotron emission with volume emissivity $\eta(f,\theta)$ from a volume dV. $\tau(f,\theta)$ is the optical depth of the background plasma in the source for a volume dV and is supposed to be due mainly to thermal gyro-absorption in the present model. (The self-absorption in the

sources is assumed to be small).

3.1 The Volume Emissivity

We will use the gyrosynchrotron volume emissivities in a magnetoactive plasma given by Ramaty (1969) and the corrected ones by Trulsen and Fejer (1970) and Ko et al. (1973). We consider the distribution of pitch angle ψ of energetic electrons to be isotropic, the energy distribution $N(\epsilon) = G\epsilon^{-\Gamma}\, d\epsilon$, and the non-thermal electron distribution in the burst sources to be homogeneous. Then we obtain the volume emissivities $\eta_{1,2}(f,\theta)$ of the two polarization modes (extraordinary and ordinary waves) for $\theta \neq 90°$ as follows:

$$\eta_{1,2}(f,\theta) = \frac{G\pi e^2 f}{cs}\, \zeta_{1,2}(s,\nu) \tag{3}$$

$$\zeta_{1,2}(s,\nu) = \frac{s}{2\,|\cos\theta|} \int_{p_1}^{p_2} [a - b\,\alpha_{\pm 1,2}]^2 \, \frac{(1+p^2-1)^{-\Gamma}}{1+p^2}\, dp$$

$$a = p \sin\psi\, J_n'(x) = \frac{1}{s\cos\theta}\, [2\eta s\sqrt{1+p^2} - s^2(1+p^2\sin^2\theta) - \eta^2]^{1/2}\, J_n'(x)$$

$$b = \frac{-s\sqrt{1+p^2}\sin^2\theta}{s\cos\theta\sin\theta}\, J_n(x)$$

$$s = \frac{f}{fH} = \frac{f}{2.8H} \quad (f \text{ in MHz and } H \text{ in Gauss}) \tag{4}$$

$$\alpha_{\theta 1,2} = \frac{-2f(f^2 - f_p^2)\cos\theta}{f^2 fH \sin^2\theta \pm [f^4 fH^2 \sin^4\theta + 4f^2(f^2 - f_p^2)^2 \cos^2\theta]^{1/2}} \tag{5}$$

$$f_p(\text{MHz}) = 9 \times 10^{-3}\sqrt{N_T}, \tag{6}$$

where $p = \frac{mv}{m_o c}$ (m_o is the rest mass of an electron; mv is the mass of an electron moving with velocity v; and c is the velocity of light); Γ is the spectral index of the energy distribution; N_T (in cm^{-3}) is the number density of thermal electrons. The suffix 1 and 2 or the upper and lower signs in equation (5) correspond to the extraordinary and ordinary waves respectively; $J_n(x)$ is the Bessel function of integral order n, the prime on the Bessel function denotes differentiation with respect to its argument, G is the proportionality coefficient, f_H is the gyro-frequency of an electron in a magnetic field H,

f_p is the plasma frequency and $\alpha_{01,2}$ is called the polarization coefficients of the two characteristic waves for $\theta = 60°$. If $f >> f_p$ and $f \sim f_H$, one obtains $\alpha_{01,2} = F1$, in which $\alpha_{01} = -1$ and $\alpha_{02} = +1$ will correspond to right-handed and left-handed circularly polarized waves, respectively.

3.2 The Thermal Gyro-Absorption

The absorption coefficient of the thermal gyro-absorption has been given by several workers. Here, the formulae reduced by Zlotnik (1968) are used since these seem to be convenient for the computation.

For quasi-longitudinal propagation (for the above-mentioned cases $\theta = 60°$ and 120°), if $f \sim f_p$ and $s \geq 2$, one can obtain from Zlotnik (1968) the optical thickness of the gyro-resonance absorption layer in the plasma with inhomogeneous magnetic field as follows:

$$\tau_{js} = 2 \frac{s^{2s}}{2^s s!} \frac{f_p^2}{f} \beta_T^{2(s-1)} L_H (1 \pm |\cos\theta|)^2 (\sin\theta)^{2(s-1)} \qquad (7)$$

where $\beta_r = \frac{KT}{m_0 c^2}$, T is the electron temperature, K is Boltzmann constant, and L_H is the characteristic length reflecting the significant change of magnetic field along the line of sight. The upper and lower signs correspond to the extraordinary wave (j = 1) and ordinary wave (j = 2) respectively.

According to those mentioned above and, together with the configuration of the magnetic field in Fig. 2, the gyro-resonance absorption layer for individual harmonics is parallel to the photosphere. If $s(f/f_H)$ represents the harmonic number, then after substituting s into equation (1), we can get the height h above the photosphere for the given frequency f and harmonic number s, i.e.,

$$h = d \left(\frac{2.8 H_o}{f} s \right)^{1/3} - 1 \quad . \qquad (8)$$

Furthermore, we can also get the thickness of the emitting layer

$$\Delta h_s = \frac{d}{3} \left(\frac{2.8 H_o}{f} \right)^{1/3} s^{-2/3} \quad . \qquad (9)$$

3.3 The Spectrum of Gyro-Synchrotron Emission From the Assumed Cylindrical Radio Sources

The spectrum and polarization of the emission from the assumed cylindrical radio source (Fig. 3) can be computed from Equations (2), (3), (4), (5), (6), (7) and (9) for two modes of the wave.

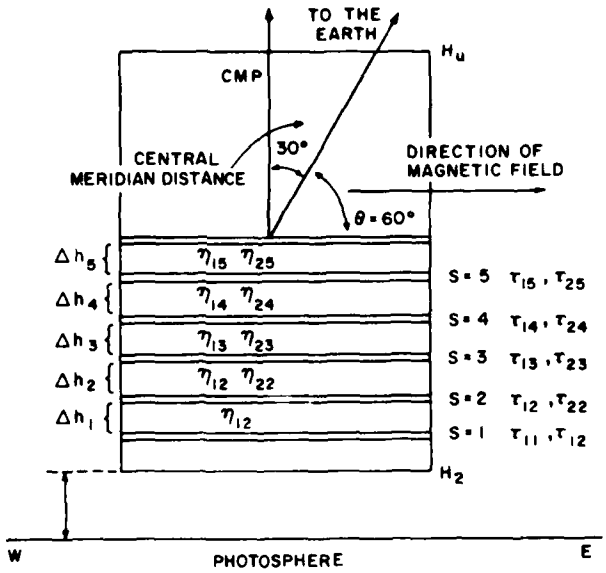

Figure 3. The distribution of gyro-resonance absorption layer and emitting layer in a cylindrical model Type IV- radio burst-source.

For the given frequency f, if η_{1s} and η_{2s} represent respectively the volume emissivity of extraordinary and ordinary waves between the gyro-resonance absorption layer of the s-th harmonic and that of the (s +1)-th harmonic, and if τ_{1s} and τ_{2s} denote the optical thickness of the gyro-resonance layer of the s-th harmonic of the extraordinary and ordinary wave correspondingly, then under the condition considered in the present model (see Table 1)

$$\tau_{js} \equiv 0, \quad \text{when} \quad s \geq 6 .$$

Hence the absorption factor $\exp(-\tau_{js})$ is necessary here only at s smaller than 5. Thus, for $s \leq 5$, the flux density received at the earth due to the emission from the corresponding volume is the summation of the contributions from two modes at wave in each emitting layer below the s = 5 absorption layer according to the radiation transfer equation (2). However, the flux density due to the volume emissivity contained from the s = 5 absorption layer to the upper boundary, $s = S_{up}$, of the radio source is determined by the corresponding integration from the boundary limits: $s = 5$ to $s = S_{up} = \frac{f}{2.8\, H_{up}}$, in which H_{up} represents the magnetic field strength at the upper boundary (Fig. 3).

Then the total flux density S(f) due to the entire radio burst-source for $\theta = 60°$ becomes

$$S(f) = S_1(f) + S_2(f) \tag{10}$$

where $S_1(f)$ and $S_2(f)$ represent the total flux density contributed by the extraordinary and ordinary waves, respectively, with

$$\begin{aligned} S_1(f) = {} & \frac{G\pi^2 e^2 \gamma_o^2}{cR^2} \; f \; \frac{1}{2} \; h_{2\,12} e^{-(\tau_{13}+\tau_{14}+\tau_{15})} \\ & + \frac{1}{3}\Delta h_3 \zeta_{13} e^{-(\tau_{14}+\tau_{15})} + \frac{1}{4}\Delta h_4 \zeta_{14} d^{-\tau_{15}} \\ & + \frac{d}{3f^{1/3}} (2.8\, H_o)^{1/3} \int_5^{S_{up}} S^{-5/3}\, \zeta_{15}\, ds \quad , \end{aligned} \tag{11}$$

$$\begin{aligned} S_2(f) = {} & \frac{G\pi^2 e^2 \gamma_o^2}{cR^2} \; f \; \Delta h_1 \zeta_{21} e^{-(\tau_{22}+\tau_{23}+\tau_{24}+\tau_{25})} \\ & + \frac{1}{2}\Delta h_2 \zeta_{22} e^{-(\tau_{23}+\tau_{24}+\tau_{25})} + \frac{1}{3}\Delta h_3 \zeta_{23} e^{-(\tau_{24}+\tau_{25})} \\ & + \frac{1}{4}\Delta h_4 \zeta_{24} e^{-\tau_{25}} + \frac{d}{3f^{1/3}} (2.8\, H_o)^{1/3} \int_5^{S_{up}} S^{-5/3} \zeta_{25}\, ds, \end{aligned} \tag{12}$$

where r_o is the linear radius of the radio burst-source observed,

$$\begin{aligned} S_{13} &= S_1(s,\ \theta = 60°) \quad \text{and} \\ S_{24} &= S_2(s,\ \theta = 60°) \end{aligned} \tag{13}$$

in equation (4).

In addition, one can obtain the number of nonthermal electrons per unit volume in the radio burst-source

$$N = G \int_{\varepsilon_{min}}^{\varepsilon_{max}} \varepsilon^{-\Gamma}\, d\varepsilon \quad , \tag{14}$$

hence the total number of non-thermal electrons is NV, and ε_{min} and ε_{max} is determined by p_1 and p_2, respectively.

From equation (5), one can obtain for $\theta = 60°$: $\zeta_{o1,2} = f_1$, in which $\zeta_{o1} = -1$ corresponds to the extraordinary wave reduced to a right-handed circularly

polarized wave, thereby the flux density may be represented by $S_1 = S_R$. The quantity $\alpha_{\theta 1,2} = +1$ corresponds to the ordinary wave reduced to a left-handed circularly polarized wave; the flux density may be represented by $S_2 = S_L$, hence the polarization degree for Type IV-b radio burst is given by

$$\pi(f) = \frac{S_1(f) - S_2(f)}{S_1(f) + S_2(f)} . \tag{15}$$

For $\theta = 120°$, $\alpha_{\theta 1,2} = \pm 1$, i.e., the sense of circular polarization is reversed from $\theta = 60°$, thus the polarization degree of Type IV-dm radio burst is given by

$$\pi(f) = \frac{S_2(f) - S_1(f)}{S_1(f) + S_2(f)} . \tag{16}$$

4. CONCLUSIONS AND ANALYSIS

As stated above, we have cited some physical quantities (see Table 1) published by Castelli et al. (1973), Sturrock (1968) and Castelli et al. (1967), to compute the U-shaped spectrum of Type IV radio bursts at 1521 UT 7 August 1972.

The computed results are listed in Table 2 and the observation date of U-shaped spectrum is plotted in Fig. 4.

Table 1. Physical Parameters of Type IVb Radio Burst-Source and Type IV-dm Radio Burst-Source

Physical Parameter	Type IVb Radio Burst	Type IV-dm Radio Burst
Photospheric field magnetic H_o (Gauss)	3×10^3	3×10^3
Angular diameter	1'.6	3'.0
Height of the lower boundary h_l (km)	1.5×10^4	1.13×10^5
Height of the upper boundary hu (km)	6×10^4	1.7×10^5
Temperature in the plasma of source	5×10^6	6×10^6
Number density of thermal electrons (cm^{-3})	10^{10}	2×10^8
Characteristic length L_H(cm)	4×10^9	4×10^{10}
Angle θ (degree)	60°	120°
Minimum momentum of non-thermal electrons p_1	0.66	0.66
Maximum momentum of non-thermal electrons p_2	4.70	4.70
Index of energy spectrum Γ	1.0(*)	1.0(*)

(*) The value of Γ is adopted from Castelli et al. (1967).

Table 2. Parameters Related to the Non-Thermal Electrons in the Radio Burst-Source

Parameters	Type IV-s Radio Burst-Source	Type IV-dm Radio Burst-Source
Number density of non-thermal electrons	$1.0 \times 10^3 (cm^{-3})$	$1.7 \times 10^3 (cm^{-3})$
Total number of non-thermal electrons in the radio source	2×10^{32}	1.4×10^{33}

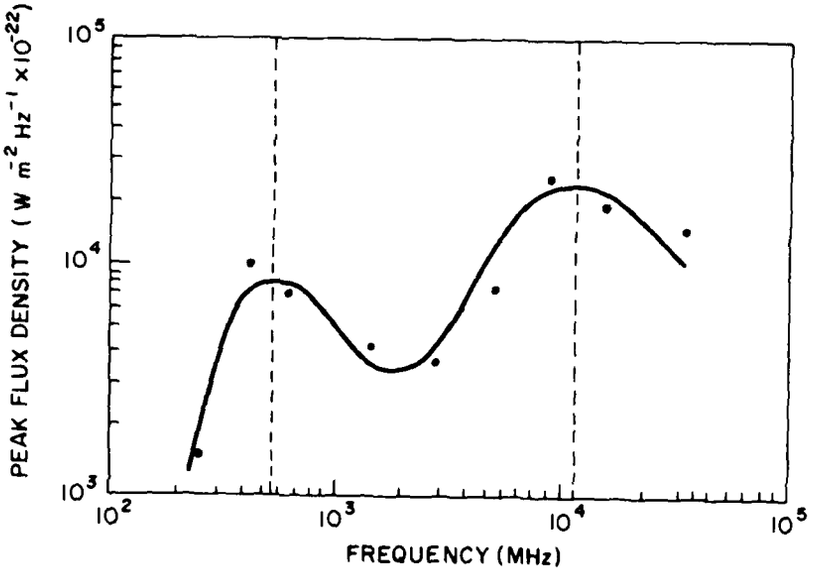

Figure 4. The comparison between the computed U-shaped spectrum (solid line) and observation (dots) depicts the valley between the Type IV-s and Type IV-dm radio sources.

Although we simply assume the volumes of Type IV-s and Type IV-dm radio sources to be cylinders in the models mentioned above, we found, nevertheless, that computed U-shaped spectrum of Type IV radio bursts is consistent with that observed. Thus, we can draw the following conclusions:

1. During the explosive phase (the second acceleration phase) of a proton flare, the effective emission mechanism generating the U-shaped spectrum of Type IV radio bursts is due to gyrosynchrotron radiation and the effective absorption mechanism is due to gyroresonance absorption, so that the data concerned in the computed model may approach the real physical parameters in the radio burst-sources for this event.

2. The peak frequencies of Type IV-s and IV-dm radio bursts are determined by the equation $f_{max} = (3\text{-}4) \times 2.8\ H_s$, in which H_s represents the magnetic field of the lower boundary of the radio sources. The valley between these two peak frequencies appears near (2000~3000) MH_z which is the frequency range between the lower frequency part of Type IV-s radio burst and the higher frequency part of Type IV-dm radio burst. The corresponding emissions in this frequency range are generated in the region between the upper boundary of Type IV-dm burst-source

and the lower boundary of Type IV-m burst-source, i.e., the flare explosive region or the annihilation region of the magnetic field during the explosive phase of the proton flare. In this region the magnetic field strength is so weak that it must lead to the conclusion that the volume emissivity of gyrosynchrotron radiation must decrease rapidly. Moreover, the lower frequencies' emissions of Type IV-m bursts are not only affected by the gyroresonance absorption but also suppressed by the background plasma itself (see Svestka, 1975, for a discussion of the Razin effect), whereas the higher frequencies' emissions of Type IV-dm burst are rapidly decreased due to the fact that their emitting volumes diminished rapidly with increasing frequencies. As a consequence of these combined effects, a valley is formed near the frequency range 2000-3000 MHz on the peak flux density spectrum of Type IV radio bursts. Occasionally, a peak emission may be observed at the same frequency range during the process of some flare-bursts. The differences between these flare-bursts and those producing the U-shaped spectrum may be explained by the ejection of considerable amount of material. Probably, the former has neither developed yet to the explosive phase nor ejected sufficient material to form the sources of Type IV-m and Type IV-dm bursts (Svestka, 1976).

3. The foregoing discussion illustrates the suggestion that the U-shaped spectrum of Type IV radio bursts constitutes radio evidence of the proton flare development to the second acceleration phase. During this phase the electrons and protons are accelerated simultaneously to high energies. Particularly, the electrons may be accelerated to high energy (MeV), but they can be accelerated only to 10-100 KeV during the flash phase (the first acceleration phase) as discussed by Sturrock (1974).

It is shown by space observations that the second acceleration phase happens about 5-10 minutes after the flash phase, and the energy of protons approaches 100 MeV even 1 BeV, as noted by Castelli and Guidice (1976). Thus, it can be seen that the occurrences of the U-shaped spectrum must clearly correlate with those of the proton events.

Castelli and Guidice (1976) pointed out that the U-shaped spectrum criteria (used for prediction of proton events) came to be identified mainly with principal PCA's; i.e., those with measured riometer absorption $\geq$ 2db at 30 MHz. However, the satellite detectors can detect numerous much weaker proton events produced by small flares. These small flares often produce neither great ejection of material nor U-shaped spectrum. Hence when the U-shaped spectrum is associated with a proton event, the probability is high; but when the proton events (including the proton events detected by the satellites) occur with the U-shaped spectrum appearing before hand, the probability is very low. The above description may account for the relation between the proton events and the U-shaped spectrum studied by Sarris (1971) with satellites Explorer 33 and 35.

From Castelli et al. (1973), we can see that U-shaped spectra associated with a proton event or ground level event were observed, without exception, on 2, 4 and 7 August 1972. These events obviously indicate that the electrons and protons accelerated simultaneously to high energies are very large in number during the explosive phase of proton flares, so that the high energy protons escaping to interplanetary space, even to earth, become larger in number.

For the event on 7 August 1972, the spectrum of Type IV-m radio bursts showed that the microwave part got harder and harder (i.e., the spectrum curve got flatter and flatter) with the lapse of time. At 1518 UT, the part of the spectrum higher than the peak frequency f_{max} arrived at its hardest level (Fig. 5); forty minutes later, a GLE occurred at 1600 UT (see Castelli et al., 1973).

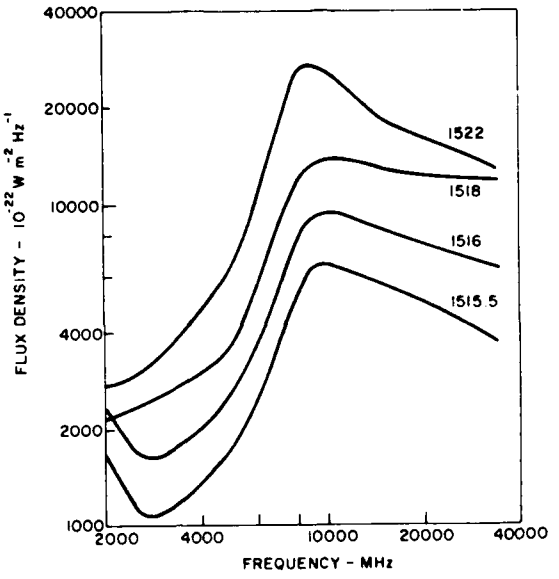

Figure 5. Flux density spectra at different times during the event of 7 August 1972. Note that spectrum above f max is hardest at 1518 UT.

This phenomenon is believed to be due to the fact that the electrons and protons are accelerated to the high energies; while the gyrosynchrotron emissions caused by the high energy electrons are strengthened, the high energy protons escaping to the interplanetary space are increased. Therefore the evolution of the microwave part of the U-shaped spectrum of Type IV radio bursts can be used for proton event forecasting.

4. Finally, the discussion in §3.4 shows that the radio emissions from Type IV-$_m$ and Type IV-dm sources are all circularly polarized waves under quasi-longitudinal propagation. The polarization degree for each radio source computed from equation (15) or (16) with the data listed in Table 1 are shown in Table 3. One can see from Table 3 that the sense of polarization reverses at the frequency 2000 or 3000 MH_z. At the higher frequencies the right-handed circular polarization is dominant, but at the lower frequencies the left-handed one is dominant. This phenomenon arises from the fact that the magnetic field lines in the Type IV-$_m$ burst-source are anti-parallel to that in the Type IV burst-source.

Since we adopt a simple cylinder as the volume of the burst-source in our computation, the computed results are not accurate enough for precise comparison with observations and should be used essentially to gain insight for the overall problem.

Table 3. Variation of the Polarization Degree with Frequency for Type IV-b and Type IV-dm Radio Sources at 1521 UT 7 August 1972.

Type IV Burst-Source (θ = 60°)		Type IV-dm Burst-Source (θ = 120°)	
f(MHz)	η(f)%	f(MHz)	η(f)%
2000	-28.6	300	-20.3
3000	+27.6	400	-25.9
5000	+31.3	500	-30.9
10000	+31.7	600	-33.4
13000	+33.2	700	-31.8
15000	+32.2	800	-30.5
20000	+29.7	900	-20.4
25000	+28.0	1000	-28.5
30000	+26.7	2000	-24.0
35000	+25.6		

Acknowledgments

We would like to express our appreciation for discussions with our colleagues Zhou Ai-hua and Jiang Shu-ying.

References

Castelli, J. P., Aarons, J., and Michael, G. A.: 1967, "Flux density measurements of radio bursts of proton-producing flares and nonproton flares", *J. Geophys. Res., 72,* 5491.

Castelli, J. P., Barron, W. R., and Badillo, V. L.: 1973, "Highlights of radio activity during disk passage of McMath plage no. 11976", in Helen E. Coffey (ed.), *Collected Data Reports on August 1972 Solar-Terrestrial Events,* Part I, (UAG-28), U. S. Department of Commerce, NOAA, Boulder, p. 183.

Castelli, J. P. and Guidice, D. A.: 1974, "Solar bursts at λ = 2 cm on July 31, 1972", *J. Geophys. Res., 79,* 889.

Castelli, J. P., Carrigan, A. L., and Ko, H. C.: 1974, "Spectral association of the 7 August 1972 solar radio burst with particle acceleration", in G. Newkirk, Jr. (ed.), *Coronal Disturbances,* IAU Symp. 57, D. Reidel, Dordrecht, p. 143.

Castelli, J. P. and Guidice, D. A.: 1976, "Impact of current solar radio patrol observations", *Vistas in Astronomy, 19,* part 14, 335.

References

Ko, H. C. and Chuang, C. W. : 1973, "The relation between the radiated and received powers due to gyrating electrons in ambient plasma", *Astrophys. Letters, 15,* 125.

Ramaty, Reuven: 1969, "Gyrosynchrotron emission and absorption in a magnetoactive plasma", *Astrophys. J., 158,* 753.

Sarris, E. T.: 1971, "Study of solar flares by the satellites Explorers 33 and 35", (AD-731686), MS thesis, University of Iowa.

Solar Geophysical Data: August 1972, edited by Academic Sinica.

Sturrock, P. A.: 1968, "A model of solar flares", in K. O. Kiepenheuer (ed.), *Structure and Development of Solar Active Regions,* IAU Symp. 35, D. Reidel, Dordrecht, p. 471.

Sturrock, P. A.: 1974, "Particle acceleration in solar flares", in G. Newkirk, Jr. (ed.), *Coronal Disturbances,* IAU Symp. 57, D. Rediel, Dordrecht, p. 437.

Svestka, Z.: 1976, *Solar Flares,* D. Reidel, Dordrecht.

Takakura, T. and Scalise, E.: 1970, "Gyrosynchrotron emission in a magnetic dipole field for the application to the center-to-limb variation of microwave impulsive bursts", *Solar Phys., 11,* 434.

Trulsen, J. and Fejer, J. A.: 1970, "Radiation from a charged particle in a magnetoplasma", *J. Plasma Phys., 4,* 825.

Zheleznyakov, V. V.: 1970, *Radio Emission of the Sun and Planets,* Pergamon Press, *Oxford.*

Zlotnik, E. Ya.: 1968, "Theory of the slowly changing component of solar radio emission. I.", *Soviet Astron., 12,* 245.

Discussion

Smart: Your model for generating the U-shaped spectral signature is very interesting and has the potential of satisfying the theorists' principal objections (i.e., that two different emission levels in the solar atmosphere are required). However, my question is directed to Professor Wu. Does your hydrodynamic model of a shock propagating through the helmet streamer configuration generate a pulse (increase) in magnetic field that would act as a reflecting barrier for electrons in the top of the streamer such that there would be an emission level there?

Wu: Yes, I believe so. For example, we show the density enhancement right behind the shock in which the emission is enhanced. Magnetic flux enhancements would also be present. Conditions appropriate for either (or both) plasma oscillations and gyro-emission are predicted by our model.

Giovanelli: On the Sun, an unstable condition leading to an explosion cannot exist with such a simple model (and of course it requires a finite conductivity). Hence in reality the field structure - and the problem to be solved - becomes much more complicated.

Dryer: I would like to comment that Dr. T. Yeh is currently looking into the reconnection model associated with such a complex magnetic topology such as that proposed years ago by Dr. Giovanelli. So I would agree that the simple sketches which usually appear in the literature are probably too simplistic and possibly topologically untenable.

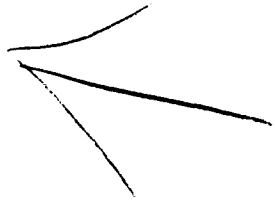

6. The Proton Flare of 1976 April 30

S. I. Avdjushin and N. K. Perejaslova
Institute of Applied Geophysics,
Hydrometeorological Service, Moscow, U.S.S.R.

V. V. Fomichev and I. M. Chertok
Solar Radio Laboratory, IZMIRAN, Moscow, U.S.S.R.

Abstract

It is possible to use solar radio data to predict the flux of protons from certain flares. The flare of 1976 April 30 gave us an opportunity to compare such predictions with the satellite measurements of particle fluxes.

1. INTRODUCTION

Rapid development of the active region McMath 14179, which began on April 29, culminated in a proton flare at 20^h47^m UT on 1976 April 30 of importance 1B at 08° S, 46° W (Solar Geophysical Data, 1976). This flare was a source of protons with a

wide range of energies (Solar Geophysical Data, 1976; Avdjushin et al., 1977). It was followed by an intense radio burst at centimetre, decimetre and metre wavelengths. In such events it is possible to use the radio data to predict the flux of subsequent protons. This particular event gave us an opportunity to compare such predictions with satellite measurements of particle fluxes.

The frequency spectrum of the maximum flux densities of the radio emission (Figure 1) was found from the data at fixed frequencies reported in Solar Geophysical Data (1976). The fluxes exceeded 1000 s.f.u.* at metre and centimetre wavelengths and had the U-shaped peak power spectral form typical of proton flares (Castelli et al., 1967).

2. METHOD

The maximum flux density of microwaves at a frequency of 3 GHz may be used to estimate the expected flux of accelerated particles. According to Akinyan et al. (1977) the maximum intensity (J) of proton flux with energy E > 10, 30 and 60 MeV recorded near the Earth and the radio flux (S) of the burst for longitudes between 20° and 80° W are empirically connected in the following way:

$$J = J(S) \cdot \phi \qquad (1)$$

where J(S) is found from:

$$\text{for } E > 10 \text{ MeV} \quad \log J = 0.0295\, S^{0.58}$$

$$\text{for } E > 30 \text{ MeV} \quad \log J = 0.055\, S^{0.5} - 1.0$$

$$\text{for } E > 60 \text{ MeV} \quad \log J = 0.243\, S^{0.338} - 2.0 \quad \text{if } S < 3000$$

$$\log J = 0.1\, S^{0.45} - 2.0 \quad \text{if } S > 3000$$

(S is given in s.f.u.) and ϕ is a parameter computed from the intensity of metre wave emission which accounts for the ease with which the accelerated particles may escape from the flare region.

In the present case the parameter S = 2000 s.f.u. (Figure 1). The intensity of the metre wavelength radiation at frequencies < 245 MHZ seems not to have exceeded the value 1000-2000 s.f.u. Observations with the Culgoora spectrograph show the radio emission at metre wavelengths included bursts of Type II and IV with intensity of importance 2. According to Akinyan et al. (1977) such an intensity is not enough to facilitate the escape of particles from the flare region. In this case they give $\phi \approx 0.7$. Using all the data above and equation (1), we obtain the following values of maximum proton flux in particles $cm^{-2}\ s^{-1}\ sr^{-1}$ near the earth: J = 170 for energies > 10 MeV, J = 21 for energies > 30 MeV and J = 9 for energies > 60 MeV.

To construct time profiles of proton flux one also needs to know the delays between the maximum of the microwave burst, and both the beginning of increase, Δt_1, and the maximum, Δt_2, of particle flux, and a parameter, τ, describing the

---

*1 s.f.u. = 10^{-22} W m^{-2} Hz^{-1}

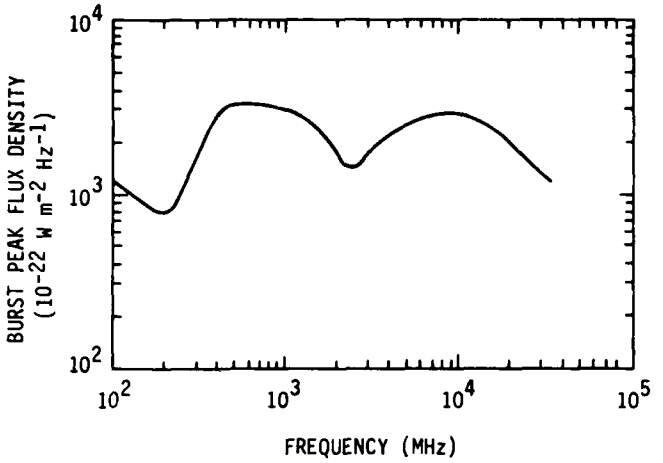

Figure 1. The spectrum of maximum flux densities of radio emission according to the data reported in Solar Geophysical Data (1976). Note the U-shaped peak power spectrum typical of proton flares.

exponential decay of the proton flux. A statistical analysis (Akinyan and Chertok, 1977) has shown that for heliographic longitudes 20° - 80° W the mean values of these parameters are: $\Delta t_1 \approx 0.5$ h for protons of all energies under consideration and $\Delta t_2 \approx 4$ h for E > 10 MeV and 3 h for E > 30 and > 60 MeV. However, for phenomena with relatively unfavorable conditions of escape, when the intensity of metre-wave radiation is <5000 s.f.u. and S > 1000 s.f.u. the mean delays increase Δt_1 up to approximately 1.9 h and Δt_2 up to approximately 9 h. The spread of these values however, is high and the values may lie anywhere in the intervals $0.4 \leq \Delta t_1 \leq 4.3$ h, and $3.3 \leq \Delta t_2 \leq 13.4$ h.

The decay of proton intensity with time follows a law which is approximately exponential, with mean time constant $\tau \approx 9$, 8 and 7.5h for E > 10, 30 and 60 MeV respectively.

3. RESULTS

The proton fluxes following the flare of 1976 April 30 were recorded in the polar region of the Earth's magnetosphere by the Soviet Meteor satellite (Avdjushin, et al., 1977). The intensity of proton fluxes with energies E > 90, 40, 25, 15 and 5 MeV were measured.

In Figure 2 filled circles show observed maximum proton fluxes in different energy ranges. Open circles show the predicted proton flux for E > 10, 30 and 60 MeV. Figure 3 compares the observed time profiles of protons (points) with the

predicted time profiles (lines). The agreement between the observed and the predicted time profiles is generally satisfactory. In particular, the most important parameter - the maximum proton flux in each energy range - differs from the observed value by less than a factor of 1.5. The predicted decay rate is also close to that observed. The time delays Δt_1 (0.5 h) and Δt_2 (2.5 to 3 h), appear to be lower than the predictions based on the comparatively weak metre wavelength emission. This reflects the real condition of escape from the corona and the interplanetary medium and the high spread already mentioned of Δt_1 and Δt_2 typical in this type of event.

4. CONCLUSION

In conclusion, the parameters of the proton flux reaching the Earth after the flare of 1976 April 30 could be satisfactorily estimated based on the information contained in the radio bursts at metre and centimetre wavelengths.

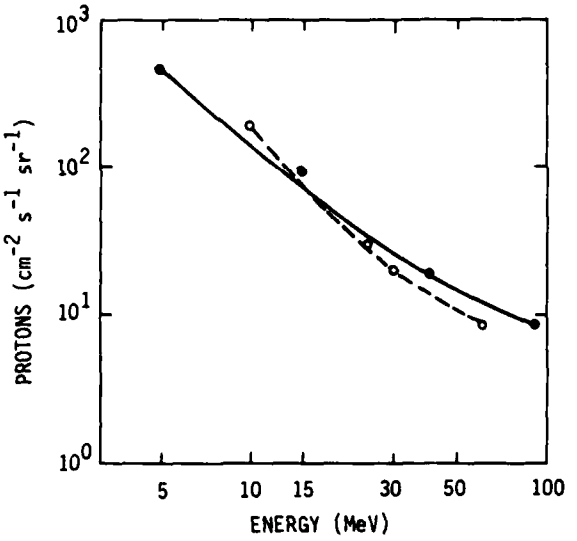

Figure 2. Proton fluxes following the proton flare 1976 April 30 recorded in the polar zone of the magnetosphere of the Earth by Meteor (Avdjushin et al., 1977). Filled circles are maximum intensities of proton fluxes with energies E >90, 40, 25, 15 and 2 MeV. Open cicles are intensities of proton fluxes with energies E > 10, 30, and 60 MeV predicted from radio observations.

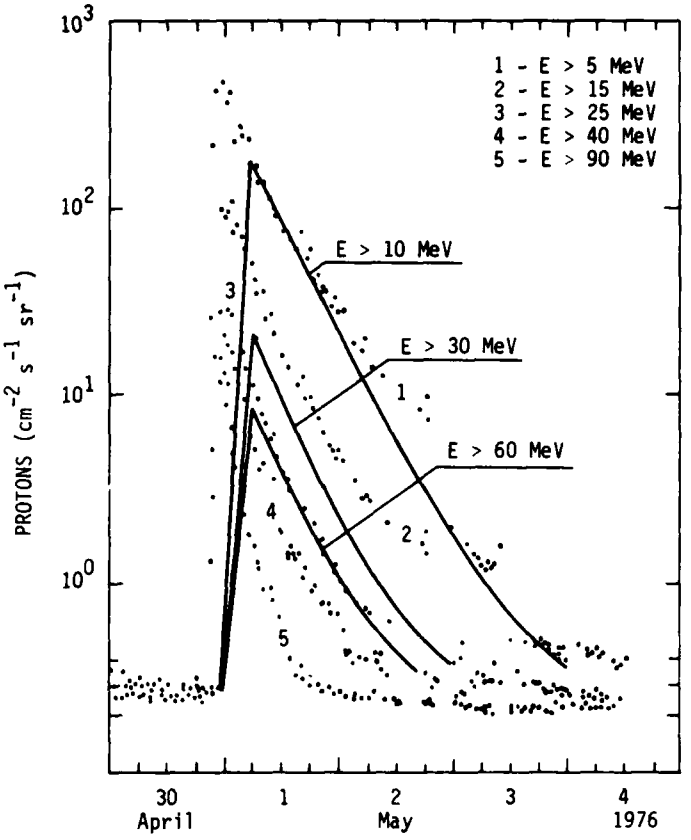

Figure 3. Time profiles of protons: points represent experimental profiles of proton data observed by the Meteor satellite; solid lines are calculated profiles based on radio data.

Acknowledgment

This work forms part of the program of the Australian-Russian Science Agreement. The authors thank R.A. Duncan for assistance with the English presentation.

References

Akin'yan, S. T. and Chertok, I. M.: 1977, "Determination of the parameters of solar protons in the vicinity of the Earth from radio bursts. III. Temporal reference functions.", *Geomagn. Aeron. (U.S.S.R.), 17,* 596. (English Translation, *Geomagn. Aeron. (U.S.A.), 17,* 407.)

Akin'yan, S. T., Formichev, V. V., and Chertok, I. M.: 1977, "Determination of the parameters of solar protons in the vicinity of the Earth from radio bursts. II. Longitudinal attenuation function.", *Geomagn. Aeron. (U.S.S.R.), 17,* 177. (English Translation, *Geomagn. Aeron. (U.S.A.), 17,* 123.)

Avdjushin, S. I., Perejaslova, N. K., Kulagin, Yu. M., Nazarova, M. N., and Petrenko, I. E.: 1977, "Observations of solar cosmic rays by 'Meteor' satellite in March - May 1976", in H. E. Coffey and J. A. McKinnon (eds.), *Collected Data Reports for STIP Interval II 20 March - 5 May 1976, (UAG-61),* U. S. Department of Commerce, NOAA, Boulder, p. 157.

Castelli, J. P., Aarons, J., and Michael, G. A.: 1967, "Flux density measurements of proton-producing flares and nonproton flares", *J. Geophys. Res., 72,* 5491.

Solar Geophysical Data: 1976, U. S. Department of Commerce, Boulder, Colorado, No. 386.

7. Relativistic Solar Particle Events During STIP Intervals II and IV

M. A. Shea and D. F. Smart
Air Force Geophysics Laboratory
Hanscom AFB
Bedford, Massachusetts 01731, U.S.A.

Abstract

Using spaceship "Earth" as a detector located at 1 AU, the relativistic solar cosmic ray events of 30 April 1976 and 22 November 1977 are compared to deduce the relativistic solar particle flux anisotropy and pitch angle characteristics in the interplanetary medium. These two ground level events occurred during STIP Interval II and IV respectively - periods of time of coordinated and cooperative scientific efforts.

1. INTRODUCTION

The concept of STIP Intervals was adopted in 1975 by the membership of the SCOSTEP Study of Travelling Interplanetary Phenomena for the purpose of concentrated study of a specific time interval and the solar-physics phenomena that may occur

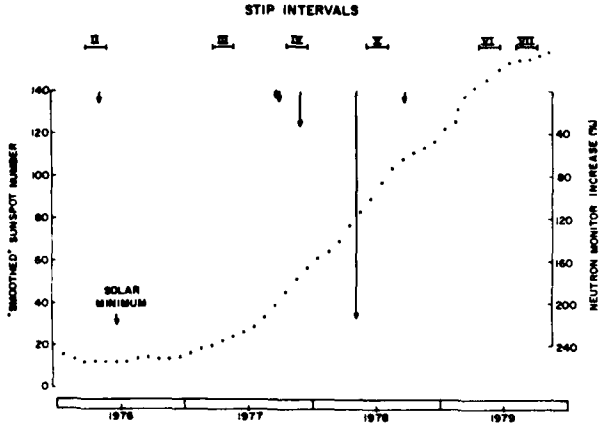

Figure 1. Smoothed sunspot number from 1976 through 1979. The STIP Intervals are indicated at the top of the figure. The occurence of ground-level events is indicated by arrows extending from the top of the figure, and the length of the arrows indicates the magnitude of the ground-level event.

during the selected period. Most intervals were selected in advance with prime consideration given to radial or magnetic connection of various spacecraft. Each interval was designated for a two month period in an effort to maximize studies of temporal and spatial phenomena without overly burdening the satellite tracking facilities.

Six STIP Intervals were designated between January 1976 and December 1979, as shown in Figure 1. This four-year time span included solar minimum in 1976 and the rising portion of the 21st solar cycle as indicated by the smoothed sunspot number also illustrated in Figure 1. There were six ground-level relativistic solar cosmic ray events during this time period, with the events producing increases on sea-level high latitude neutron monitors ranging from two percent to 214 percent. Two of these ground level events occured during STIP Intervals. One was on 30 April 1976 near solar minimum during STIP Interval II, and the other was on 22 November 1977 during STIP Interval IV. In this paper we will use the neutron monitor measurements on spaceship "Earth" to compare these two relativistic solar particle events and deduce the relativistic solar particle flux anisotropy and pitch angle characteristics in the interplanetary medium.

2. SOLAR PARTICLE PROPAGATION

Figure 2 is an artist's concept of a solar flare that is associated with the acceleration and release of high energy (E ± 1 MeV) solar protons from the sun into the interplanetary medium. Many of these particles travel along the interplanetary magnetic field lines to 1 AU (i.e. Earth's orbit) and beyond, with the maximum in particle flux usually measured along the interplanetary magnetic field line originating at the flare site. Since the large scale topology of the interplanetary magnetic field is determined by "frozen in" magnetic fields being transported out of the rotating sun by the solar wind, the earth is connected to the sun by an

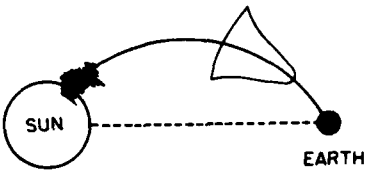

Figure 2. Conceptual illustration of the characteristics of an anisotropic solar proton flux propagating along the interplanetary magnetic field lines from the sun to the earth.

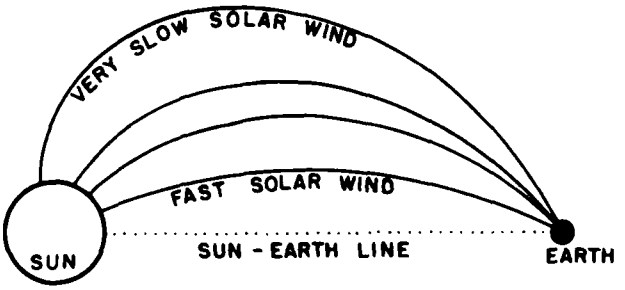

Figure 3. Conceptual illustration of an idealized "most favorable propagation path" for fast and slow solar wind speeds.

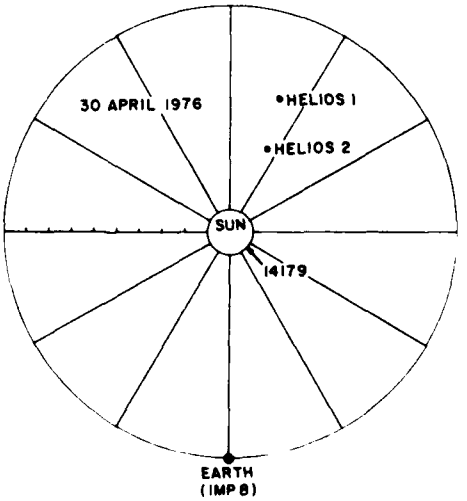

Figure 4. Position of Helios space probes relative to the sun-earth line on 30 April 1976. The flare occured in McMath plage region 14179.

interplanetary field line located at ~ 57° heliographic longitude for a solar wind velocity of 400 km/sec. If the speed of the solar wind increases the interplanetary magnetic field line connection longitude is closer to the central meridian; if the speed decreases the connection longitude is closer to the west limb of the sun. An illustration of this "most favorable propagation path" for arbitrary solar wind speeds is shown in Figure 3.

Particle detectors on spacecraft at various locations in the interplanetary medium usually record different particle intensities for the same solar particle The intensity is a function of the heliographic distance from the flare site and the radial distance from the sun as the solar particles propagate through the solar corona and out into the interplanetary medium along the magnetic field lines. A typical example is shown in Figures 4 and 5. Figure 4 gives the relative position of three spacecraft during the solar particle event at 2147 UT on 30 April 1976. Helios 1 was located at 160° W, R = 0.65 AU, Helios 2 was located at 156° W, R = 0.4 AU, and IMP 8 was located at 0° heliolongitude at 1 AU (i.e. orbiting the earth). The solar flare that was associated with the solar proton event was located at 46° W. Thus the longitudinal distance between these spacecraft and the flare location was 114°, 110°, and 46° for Helios 1, Helios 2 and IMP 8 respectively with the flare located to the east of the Helios spacecraft and to the west of the

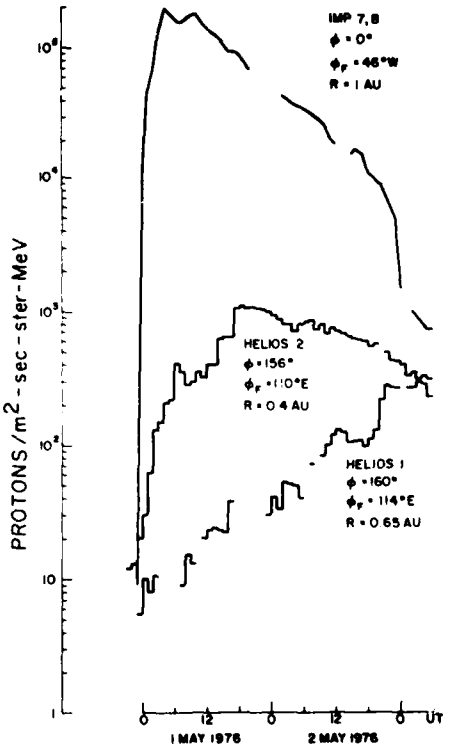

Figure 5. The 4 to 12 solar proton flux observed at three locations in space; the earth (IMP 7 and 8) and at Helios 1 and Helios 2.

IMP 8 spacecraft. Figure 5 illustrates the time-intensity profiles of the solar proton flux for this event as detected by sensors on these three spacecraft. It is clear that a significant portion of the inner heliosphere was populated with solar particles, with the detectors on IMP 8 responding to the larger flux as would be expected from its more favorable location.

3. CONCEPT OF "SPACECRAFT EARTH"

Just as a satellite can have detectors positioned at different locations on the spacecraft, the earth has ground based detectors positioned at different locations. Since the earth has a magnetic field, "spacecraft earth" can effectivly act as a satellite with its own built-in magnetic spectrometer.

Solar particles travelling through the interplanetary medium from the sun to the earth are deflected by the geomagnetic field as soon as they enter the magnetosphere. Their detection at the earth is primarily a function of particle energy and, for an anisotropic interplanetary particle distribution, a function of detector location. For detectors located above the atmosphere (i.e. balloon borne detectors or low altitude satellites) the only "shield" for these particles is the geomagnetic field. For detectors located within the atmosphere, the vertical atmospheric mass of ~ 1000 grams/cm^2 also acts as an absorber. A ground-level solar proton event implies that the solar particles must have energies greater

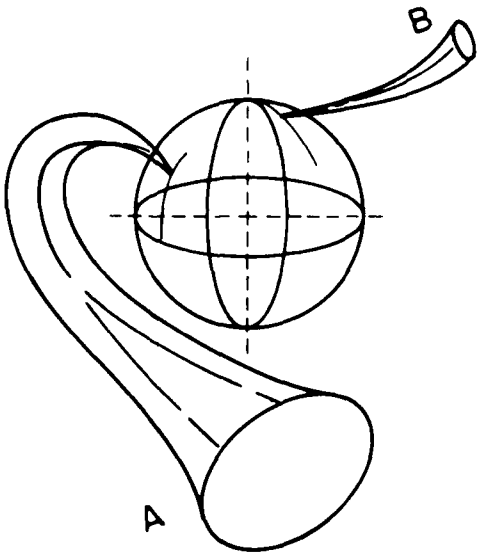

Figure 6. Conceptual illustration of restricted asymptotic cones of viewing sampling different sections of space.

than ~ 450 MeV/nucleon, the minimum energy necessary to initiate a nuclear cascade that can penetrate through the atmosphere and be recorded at sea level. Neutron monitors located at sea level in high latitude locations (> 55° geomagnetic) respond to particles greater than ~ 450 MeV; at lower latitudes the geomagnetic cutoff is the principle factor controlling particle access. At geomagnetic latitudes of ~ 45°, only particles with energies greater than ~ 3 GeV can be detected by neutron monitors. In the equatorial region, the particles must have an energy of more than ~ 13 GeV to be detected. (For this paper we are considering only particles incident in the vertical direction.)

The geomagnetic "optics" or viewing direction of a neutron monitor is extremely complicated. First introduced by Brunberg (1958) the concept was refined into asymptotic cones and directions by McCracken (1962) who advanced the technique by the use of high speed digital computers. Figure 6 illustrates two types of asymptotic cones, one for a very high latitude (i.e. polar) station which has a relatively "tight" cone viewing out of the ecliptic, and one for a moderately high latitude station with geomagnetic latitude ~ 60° having a somewhat larger cone viewing in the ecliptic plane. Stations at mid latitudes and equatorial locations have very complex cones that can cover very large ranges in longitude. Figure 7 shows the position of several asymptotic cones for high latitude stations. These cones have been calculated using the trajectory-tracing technique (McCracken, 1962) with a quiescent model of the geomagnetic field. Currents in the magnetosphere and the magnetopheric tail were not included in the field model used to determine these asymptotic cones.

Naturally, for a completely isotropic particle flux, knowledge of the geomagnetic optics, or viewing directions, of a station is not important, as the flux to be detected is limited only by the geomagnetic and/ or atmospheric cutoff. However, most relativistic solar particle events are anisotropic, and although this makes the analysis of these events more complicated, it does afford us the opportunity to deduce some of the characteristics of particle propagation in the interplanetary medium.

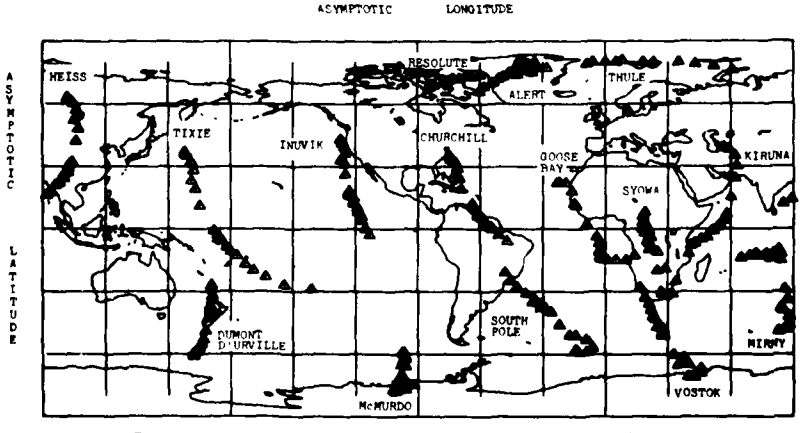

Figure 7. Illustration of the asymptotic cones of acceptance for selected high latitude neutron monitors as projected on an extended world map.

To analyze neutron monitor responses to anisotropic particle propagation, we must assume a pitch angle distribution around the interplanetary magnetic field line. From our previous work (Smart et al., 1971; Smart et al., 1979) we assume that the pitch angle distribution can be described by a Gaussian function with the width of the Gaussian curve controlling the degree of anisotropy. (See Figure 8.) A detector "viewing" into the anisotropic particle flux as illustrated by cone A in Figure 6 would record a higher increase than a detector viewing in a slightly different direction, such as illustrated by cone B. Thus the concept that the "spacecraft Earth" can be used to deduce interplanetary propagation characteristics for relativistic solar particle events.

4. NEUTRON MONITOR RESPONSE

The response of a neutron monitor to an anisotropic flux of solar particles can be calculated (see Shea et al., 1971) from the following equation:

$$I = \sum_{P_c}^{\infty} S(P_i, \chi)\, J(P_i)\, F(\alpha_i)\, A(P_i)\, \Delta P_i \qquad (1)$$

where I is the relative intensity, P is the rigidity (P_c = cutoff rigidity), $S(P, \chi)$ is the neutron monitor specific yield as a function of rigidity and

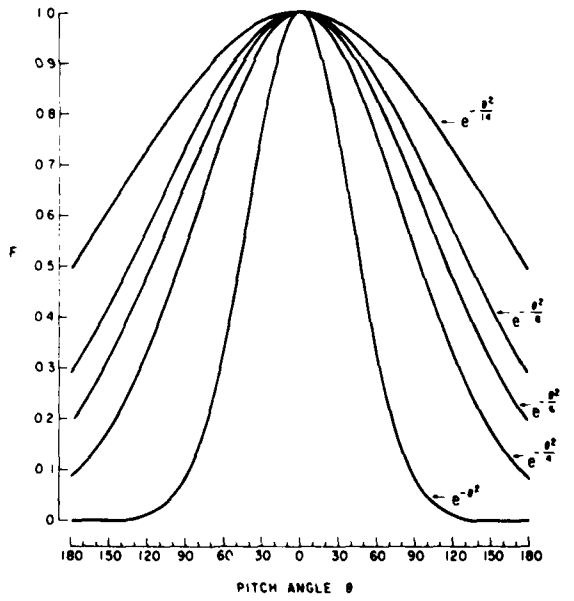

Figure 8. Illustration of various Gaussian pitch angle distributions around the interplanetary magnetic field line.

standardized depth (χ) in the atmosphere (taken at sea level for this analysis), $J(P_i)$ is the differential flux, in the interplanetary medium, of the relativistic solar protons at each specific rigidity, P_i, $F(\alpha_i)$ is a function describing the solar proton pitch angle distribution about the interplanetary magnetic field lines where α_i is the pitch angle of the "$_i$th" particle, and $A(P_i)$ is a quantized function defining if a particle with rigidity P is allowed (A = 1) or forbidden (A = 0) as determined by the trajectory calculations.

There is a unique set of values for the parameters defining the solar proton differential rigidity spectrum, anisotropy, and apparent source direction that, when transmitted through the asymptotic cone of acceptance for each neutron monitor and through the neutron monitor specific yield function, will produce the observed increase at any location on the earth. Using equation (1) the procedure is repeated several times for different stations, pitch angle distributions, spectral slopes and direction of maximum particle flux in the interplanetary medium until the "best" agreement is found for the set of stations being considered. Usually, as the event proceeds in time, the anisotropy decreases and a new expression for the Gaussian distribution must be used. In this way neutron monitor measurements provide an "instantaneous snapshot" of pitch angle distribution in the interplanet-

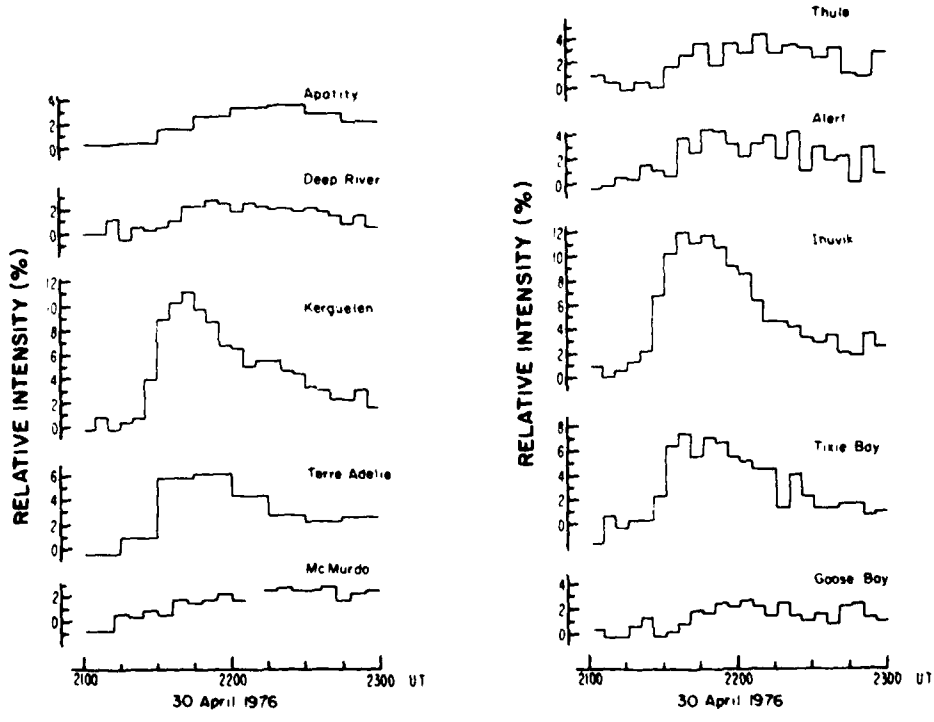

Figure 9. The 30 April 1976 ground-level solar cosmic ray event as observed by various neutron monitors.

ary medium for relativistic protons. It is emphasized that the anisotropies we are discussing in this paper are very large compared to those usually observed by spacecraft.

5. THE RELATIVISTIC SOLAR PARTICLE EVENT OF 30 APRIL 1976 DURING STIP INTERVAL II

The ground level solar particle event of 30 April 1976 was associated with a flare at 2047 UT at S 08, W 46 (Solar Geophysical Data, 1976). The flare was classified as optical importance 1B accompanied by major X-ray and radio emission. From an examination of the neutron monitor data from 10 locations, as shown in Figure 9, the earliest onset of relativistic protons appears to be between 2120 and 2125 UT at Inuvik, Canada. This station also had the largest increase of 12 percent. A comparison of the relative increases as recorded by the Inuvik and Goose Bay neutron monitors, is illustrated in Figure 10. Since both of these high latitude neutron monitors are at "atmospheric cutoff" the difference in relative intensity reflects the relativistic particle anisotropy present throughout this event.

Figure 7 shows that there is a 90° longitudinal separation between the asymptotic cone for Inuvik and the asymptotic cone for Goose Bay. Since Inuvik records the earliest onset and the highest increase, we can conclude that the Inuvik asymptotic cone of acceptance would be viewing into or close to the direction of maximum particle flux (i.e. along the interplanetary magnetic field line connecting the earth with the sun). Satellite data place the interplanetary magnetic field line at 21° N, 337° E in the GSE coordinate system (King, 1979). Translating to the earth's coordinate system shown in Figure 7, the interplanetary magnetic field would intersect the earth at ~ 20° N, 200° E longitude.

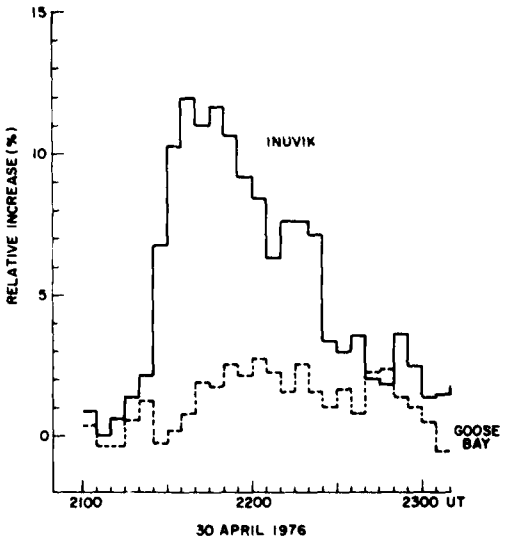

Figure 10. Relative increase observed by the Inuvik and Goose Bay neutron monitors on 30 April 1976. The difference in the observed amplitude is an indication of the observed relativistic solar proton flux anisotropy.

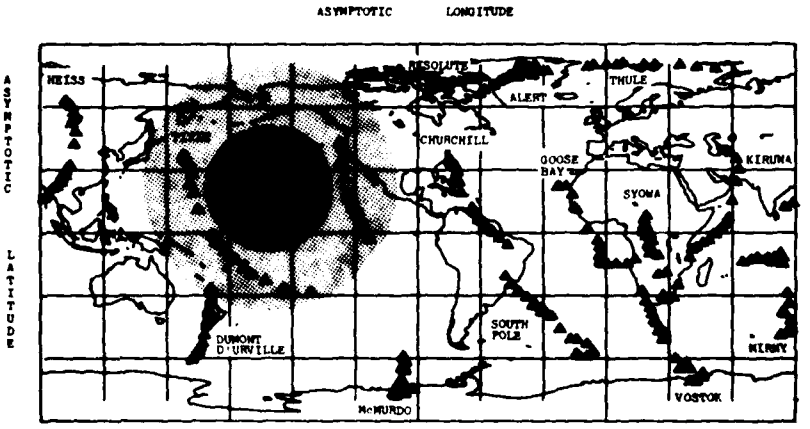

Figure 11. Illustration of the pitch angles sampled by the various narrow "asymptotic cone" neutron monitors. The maximum relativistic solar proton flux with pitch angle $< 30^{\circ}$ is indicated by the heavy shading. The light shading indicates the relativistic solar proton fluxes with pitch angles between 30° and 60°.

Using this position as the direction of maximum flux and assuming a Gaussian function of the form $e[-(\theta^2/2.5)]$ for the pitch angle distribution, we find that by using equation (1) we can obtain calculated neutron monitor increases in good agreement with the observational data. Figure 11 is similar to Figure 7 except that the shading indicates the geocentric directions in interplanetary space that contain the most intense particle fluxes. The heavy shading represents the geocentric radial direction containing particle fluxes with pitch angles 30° or less; the lighter shading represents particle fluxes with pitch angles between 30° and 60°.

In comparing this figure with the increases in Figure 9, we note that the largest increases should be recorded by the Inuvik and Tixie Bay neutron monitors, as indeed is the case. (The Kerguelen Island asymptotic cone is not illustrated in Figure 11 as it covers a wide range of longitudes. This cone, illustrated in Shea and Smart (1975), "sweeps" across this area of maximum intensity consistent with the increase shown in Figure 9.) In contrast, the Alert, Thule, Goose Bay and McMurdo asymptotic cones are far removed from the direction of maximum particle flux - in keeping with the much smaller increases recorded at these stations.

Considering stations looking in the forward direction such as Inuvik, and comparing them with stations looking in the reverse direction such as Goose Bay, we can see that the "forward to reverse" particle flux ratio is at least six to one. Determining a Gaussian distribution that when coupled with the asymptotic viewing directions and neutron monitor spectrum/yield function produces calculated increases close to the observation data results in a function of $e[-(\theta^2/2.5)]$. Since these asymptotic cones actually sample a range of pitch angles we will assume that the forward flux contains pitch angles between 0° and 60° and that the reverse flux contains pitch angles between 120°, and 180°. Evaluating our Gaussian form between these limits we find that the average "forward to reverse" flux ratio is about a factor of 10. Figure 12 illustrates the probable pitch angle distribution of the relativistic particle flux in interplanetary space and also illustrates the region of the forward flux and backward flux.

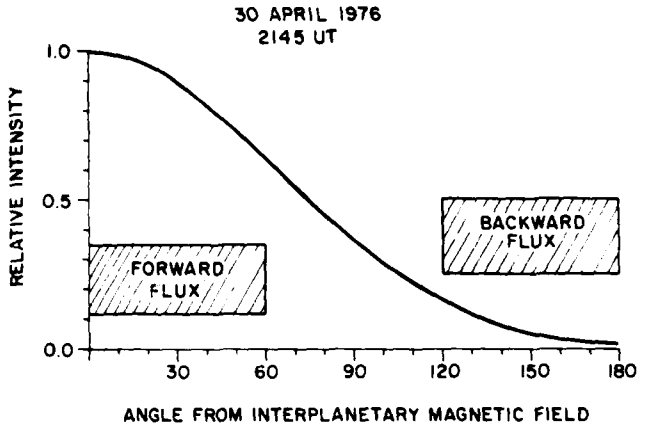

Figure 12. Derived relativistic solar proton pitch angle distribution during the maximum of the 30 April 1976 ground-level solar cosmic ray event.

6. THE RELATIVISTIC SOLAR PARTICLE EVENT OF 22 NOVEMBER 1977 DURING STIP INTERVAL IV

The relativistic solar partaicle event of 22 November 1977 was associated with a flare of importance 2B at 0945 UT. This flare was located at 24° N, 40° W (Solar Geophysical Data, 1978), again near the favorable propagation path between the sun and the earth. Since neither solar wind nor interplanetary magnetic field data are available from U.S. spacecraft, we assume a direction of maximum particle flux along an interplanetary magnetic field line intersecting the earth at a longitude of 349° (i.e. 9 AM local time) for the onset of the event and at a longitude of 330° for the time near maximum intensity.

Figure 13 illustrates the increase in cosmic ray intensity as recorded by seven neutron monitors (Komori, 1977). This was also an anisotropic particle event although the degree of anisotropy was much less than for the event on 30 April 1976. By placing the direction of maximum particle flux (longitude 330° E) on the map in Figure 7, it is evident that the Goose Bay and South Pole neutron monitors should have detected the largest increase with the Inuvik monitor, whose asymptotic cone is ~ 120° away from the longitude of the maximum particle flux, detecting a much smaller increase. We must inject a note of caution here as there is a large altitude gradient in the atmospheric secondary neutron flux and the South Pole monitor is located at an altitude of about 3000 meters. This altitude correction has not been applied to the South Pole data shown in Figure 13.

For this event we find that a particle pitch angle distribution described by a Gaussian of the form $e[-(\theta^2/8.0)]$ results in the best fit to the experimental data. Again taking the range of pitch angles between 0° and 60° for the forward flux and between 120° and 180° for the reverse flux and evaluating the Gaussian expression between these limits we find that the average "forward to reverse" flux

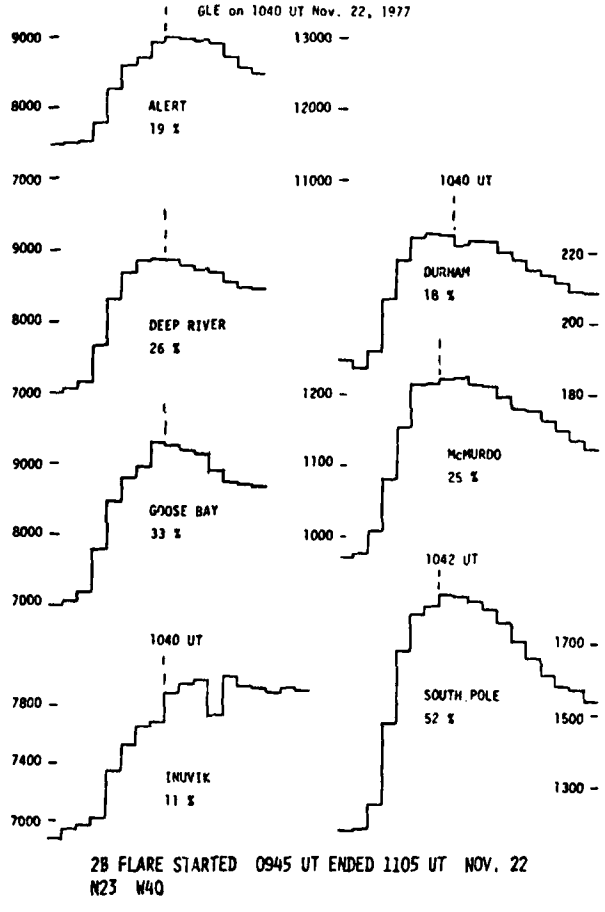

Figure 13. The 22 November 1977 ground-level solar cosmic ray event as observed by seven neutron monitors (after Komori, 1979).

ratio is about a factor of 2. An illustration of the Gaussian function for this event and the forward and backward particle flux is shown in Figure 14.

7. CONCLUSION

We have summarized the neutron monitor data for the relativistic solar particle events that occurred on 30 April 1976 and 22 November 1977. Both of the solar flares that produced these relativistic particles occurred in a location on the sun (46° W and 40° W) favorable for maximum intensity to be recorded at the earth.

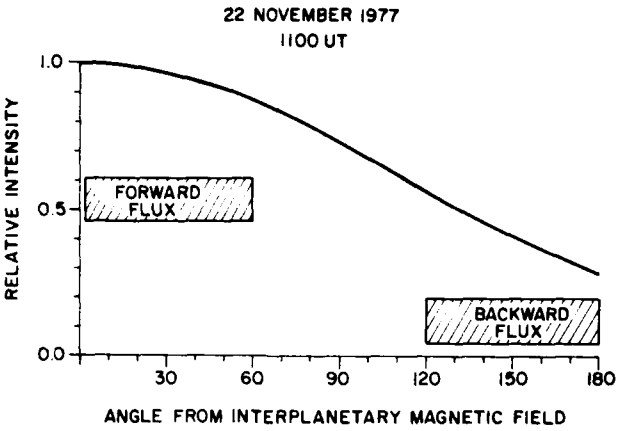

Figure 14. Derived relativistic solar proton pitch angle distribution during the maximum of the 22 November 1977 ground-level solar cosmic ray event.

From this study of these two relativistic solar particle events using the earth as a detector in space (i.e. satellite Earth) we can determine the pitch angle distribution in space throughout these events. Although there was an anisotropic particle distribution for both of these events, the degree of anisotropy was considerably different, the relativistic particle flux "forward to backward" ratio being 10 to 1 for the event of 30 April 1976 and 2 to 1 for the event of 22 November 1977.

References

Brunberg, Ernst-Ake: 1958, "The optics of cosmic ray telescopes", *Arkiv for Fysik, 14,* 195.

King, Joseph, H.: 1979, *Interplanetary Medium Data Book Supplement 1, 1975-1978,* Report No. NSSDC/WDC-A-R&S 79-08, National Aeronautics and Space Administration, Goddard Space Flight Center, Greenbelt, Md.

Komori, H.: 1979, "An analysis of relativistic cosmic ray increase on 22nd November 1977", 16th International Cosmic Ray Conference, *Conference Papers, 4,* 19.

McCracken, K.G.: 1962,"The cosmic ray flare effect. 1. Some new methods of analysis", *J. Geophys. Res., 67,* 423.

Shea, M.A., and Smart, D.F.: 1975, *"Asymptotic Directions and Vertical Cutoff Rigidities for Selected Cosmic-Ray Stations as Calculated Using the International Geomagnetic Reference Field Model Appropriate for Epoch 1975.0",* Report No. AFCRL-TR-75-0247, Air Force Cambridge Research Laboratories, Bedford, Mass.

References

Smart, D.F., Shea, M.A., Humble, J.E., and Tanskanen, P.J.: 1971, "A determination of the spectra, spatial anisotropy, and propagation characteristics of the relativistic solar cosmic-ray flux on November 18, 1968", 12th International Conference on Cosmic Rays, Hobart, *Conference Papers, 2*, 483.

Smart, D.F., Shea, M.A., Humble, J.E., and Tanskanen, P.J.: 1979, "A model of the 7 May 1978 solar cosmic ray event", 16th International Cosmic Ray Conference, *Conference Papers*, 5, 238.

Solar Geophysical Data: 1976, U.S Department of Commerce, Boulder, Colorado, No. 386.

Solar Geophysical Data: 1978, U.S. Department of Commerce, Boulder, Colorado, No. 405.

Discussion

McLean: Could the special characteristic of flares which determines whether they produce GLE, be proximity to the magnetic field line which connects to the Earth? The two examples which you gave us fit this idea.

Shea: The shape of the "time-intensity" profile of relativistic solar particle events as detected at the Earth by neutron monitors appears to be a function of the heliocentric distance between the associated flare and the most favourable propagation path, defined as the "idealized" magnetic field line connecting the Earth with the Sun. However, flares associated with ground-level events have occurred at many solar longitudes. Three ground-level events, those on 20 November 1960, 30 March 1969 and 28 January 1967, are associated with flares on the invisible part of the solar disk (i.e. $>90°$W).

Dryer: Is it possible to use the expanding shock front (temporally and spatially) as a particle modulation mechanism in the case of the different Helios 1 and 2 temporal profiles when they were both $>100°$ west of the flare site?

Shea: In our opinion it would be very difficult in view of the time associations. In interplanetary space the radially propagating shocks often act as "boundaries" between different particle populations; however, in this case you would require the equivalent of a Moreton wave to propagate very rapidly (i.e. orders of magnitude faster than the observed velocity) to 110° from the flare site and then suddenly act as a "quasi-stable" barrier between the two satellites with no further lateral propagation. The scientists with detectors on the Helios 1 and 2 space probes have reported that there appears to be a tangential discontinuity associated with a co-rotating stream between the two spacecraft and we feel this is a much more plausible explanation.

8. Thermal Cyclotron Radiation From Solar Active Regions

V. V. Zheleznyakov and E. Ya. Zlotnik
Institute of Applied Physics, Academy of Sciences,
Gorky, U.S.S.R.

Abstract

Spectra with fine structure resulting from the thermal cyclotron radio emission from solar active regions are discussed. Source conditions (distribution of magnetic field and kinetic temperature with height) are suggested which would cause the spectrum to take the form of a set of cyclotron lines and high-frequency cut-offs. Each distribution results in a characteristic spectrum and polarization. This permits one to deduce the conditions in the source through the properties of the observed microwave solar radio emission. To obtain reliable data on the fine structure and judge conditions in the sources it is necessary to study microwave solar radio emission with swept-frequency or multi-channel receivers and highly directional antennae.

1. INTRODUCTION

All the phenomena in microwave solar radio emission occur against the S-component - slowly varying radiation of the local sources above sunspots and flocculi in the active regions of the corona and chromosphere. The S-component is characterized by a smooth frequency spectrum with the maxima in the wavelength range 5-10 cm, unpolarized at longer wavelengths and polarized in the extraordinary sense at shorter wavelengths. These peculiarities were explained in terms of thermal cyclotron and free-free radiation mechanisms by Zheleznyakov (1962, 1963) and Kakinuma and Swarup (1962). Further progress in the theory of the S-component was made by analysing various models of active regions, calculating the expected characteristics of cyclotron (and free-free) radio emission in these models, and comparing these calculated characteristics with the observed ones (see Livshits et al., 1966; Zlotnik, 1968; Lantos, 1968). However, Zheleznyakov and Zlotnik (1979, 1980a,c) paid attention to the fact that thermal cyclotron radio emission in neutral current sheets of the corona causes a set of discrete cyclotron lines. If the kinetic temperature of a plasma in the sheets is sufficiently great ($T \approx 10^7$-10^8 K) these lines may be observed against the S-component mostly as radiation at the second and the third harmonics of the electron gyrofrequency $\omega_B = eB/mc$. Fine structure such as cyclotron lines should be expected in the pre-flare phases of developing active regions when the formation of hot neutral current sheets is most probable. This possibility of narrow-band features in the spectrum of microwave radio emission and of cut-offs and narrow-band features in the spectrum of radio emission of solar local sources (Kaverin et al., 1976) stimulated the present authors to consider the fine structure more thoroughly. The results of the analysis are given below.

2. REVIEW OF BASIC THEORY OF S-COMPONENT

Before discussing various forms of the fine structure in the microwave solar radio spectrum, let us recall the peculiarities of the cyclotron mechanism in the inhomogeneous magnetic fields above sunspots and the conditions of the typical S-component (see in more detail Section 13 of Zheleznyakov (1977)).

The non-relativistic electrons in a magnetic field are known to radiate and absorb the electromagnetic waves at the frequencies equal to or a multiple of the gyrofrequency $\omega \approx s\omega_B$, where $s = 1, 2, 3....$ Therefore cyclotron radiation and wave absorption at a given frequency in the inhomogeneous magnetic field occur in those gyroresonance layers where the gyrofrequency is

$$\omega_B \approx \omega/s \quad . \tag{1}$$

Under typical conditions of the solar corona and chromosphere the optical thickness of these layers τ is different for the ordinary and the extraordinary waves. For the ordinary waves the optically thick layers ($\tau \gg 1$) correspond to the harmonics $s \leqslant 2$; for the extraordinary waves such layers correspond to the values $s \leqslant 3$. In both cases the gyroresonance layers are optically thin ($\tau \ll 1$) for the higher harmonics.

A theory of the S-component is based on a model of the active region above a sunspot represented in Figure 1(a). According to Eq. (1), the gyrofrequency ω_B (in a magnetic field B) decreases monotonically with height h over the photosphere.

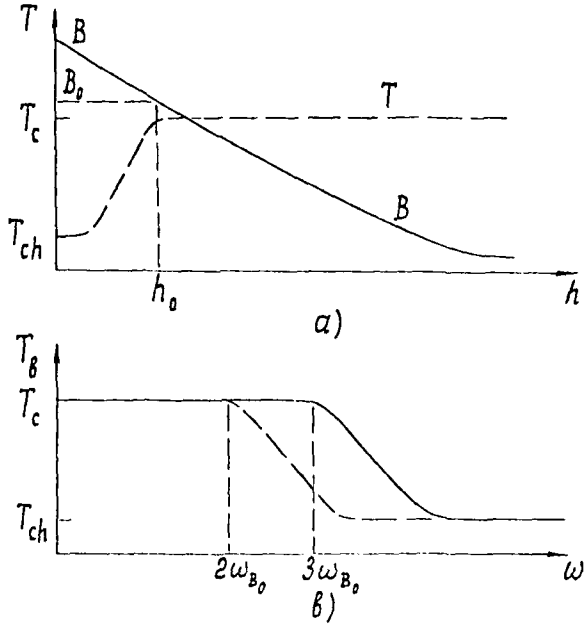

Figure 1. The model of a standard source of the S-component: a) distribution of the magnetic field B and the kinetic temperature T over the height h (h_0 is the lower edge of the corona, B_0 is the magnetic field at this level); b) the frequency spectrum of radiation; solid and dashed lines here and elsewhere correspond to extraordinary and ordinary waves.

The kinetic temperature of a plasma increases from the chromospheric values ($T_{ch} \approx 10^4$ to 3×10^4 K) to those typical of the active corona ($T_c \approx 3 \times 10^6$ K). In such magnetic fields the gyroresonance layers (Eq. 1) corresponding to the higher harmonics are situated at greater heights in the solar atmosphere (closer to the observer). This fact, along with the above values of optical thickness for the ordinary and extraordinary waves of gyroresonance layers, leads us to conclude that the second gyroresonance layer radiates the ordinary, and the third gyroresonance layer radiates the extraordinary waves. The brightness temperature of the ordinary component of radiation is

$$T_b \approx T(h_2) , \qquad (2)$$

where h_2 is the height of the second gyroresonance layer with the gyrofrequency $\omega_B = \omega/2$; the brightness temperature of the extraordinary mode is

$$T_b \approx T(h_3) , \qquad (3)$$

where h_3 is the height of the third gyroresonance layer $\omega_B = \omega/3$ (see Eq. 1). Radiation from the deeper layers is absorbed at the heights h_2 and h_3 for the ordinary and extraordinary modes respectively. The contribution of the optically thin higher harmonics is insignificant. The above argument enables us to derive the spectrum of the S-component, $T_b(\omega)$, for both waves. Such a derived spectrum is given in Figure 1(b). From this figure it is clear that for the extraordinary radiation $T_b = T_c$ at the frequencies $\omega < 3\omega_{B_0}$ corresponding to the position of the third gyroresonance level in the corona - at the heights $h > h_3$. At higher frequencies the level S = 3 sinks to the chromosphere. In the transient region T_b drops, tending to the value T_{ch}. The same is observed for the ordinary mode but the drop in T_b begins earlier - at the frequency corresponding to the moment of the transition of the level S = 2 to the heights $h < h_2$. From Figure 1(b) it follows that the thermal cyclotron radiation in a standard model of the S-component is unpolarized at the low ($\omega < 2\omega_{B_0}$) and the higher ($\omega > 3\omega_{B_0}$) frequencies and is rather strongly polarized in the range of the intermediate frequencies $2\omega_{B_0} < \omega < 3\omega_{B_0}$ for which one or both of the gyroresonance layers S = 2,3 are situated in the transition region between the chromosphere and the corona where the temperature gradient is strong.

It should be noted that in the present report all the frequency spectra are represented in terms of $I_b(\omega)$ rather than in specific intensity $I(\omega)$. To transform $I_b(\omega)$ into dependence of I on ω one should take into account that $I \sim \omega^2 T_B$. As a result the spectrum $I_c(\omega)$ has a maximum at the frequency $\omega_{max} \approx 3\omega_{B_0}$ and the spectrum of the ordinary radiation of the S-component has a maximum at the frequency $\omega_{max} \approx 2\omega_{B_0}$.

This characteristic of the frequency spectrum and polarization of the S-component is well confirmed by observations of the microwave radio emission of solar local sources over many years (Gel'freich et al., 1970). It is clear however that the model considered does not exhaust all possible conditions in the active regions. Consequently, the spectra of radio emission may be far more complicated.

3. A MODEL WITH A MAXIMUM OF MAGNETIC FIELD STRENGTH IN THE CORONA

Let us consider a spectrum of thermal cyclotron radiation in a model where the value of the magnetic field reaches its maximum at a certain height h_{max} for the previous distribution of temperature (see Figure 2(b)). For example, such a distribution of the magnetic field can be realized in a group of sunspots represented in Figure 2(a) even disregarding the electric currents in the coronal and the chromospheric plasma (Sweet, 1958). Here along the axis h passing through the neutral (zero) line of the magnetic field the maximum B is certainly present. If $h_{max} < h_1$, where h_1 is the lower edge of the corona, then the model considered is in fact reduced to the standard model. But if $h_{max} > h_1$, then the radiation spectrum changes significantly from the usual spectrum of the S-component. In fact, as implied by Figure 2(c), the brightness temperature drops towards the higher frequencies at the points $\omega = 2\omega_{B_{max}}$ (the ordinary waves) and $\omega = 3\omega_{B_{max}}$ (the extraordinary waves), since along the axis h the magnetic fields have no

AD-A130 687 PROCEEDINGS OF THE STIP (STUDY OF TRAVELLING INTERPLANETARY PHENOMENA) SY..(U) AIR FORCE GEOPHYSICS LAB HANSCOM AFB MA M A SHEA ET AL. 27 DEC 82 2/3

UNCLASSIFIED AFGL-TR-82-0390 F/G 3/2 NL

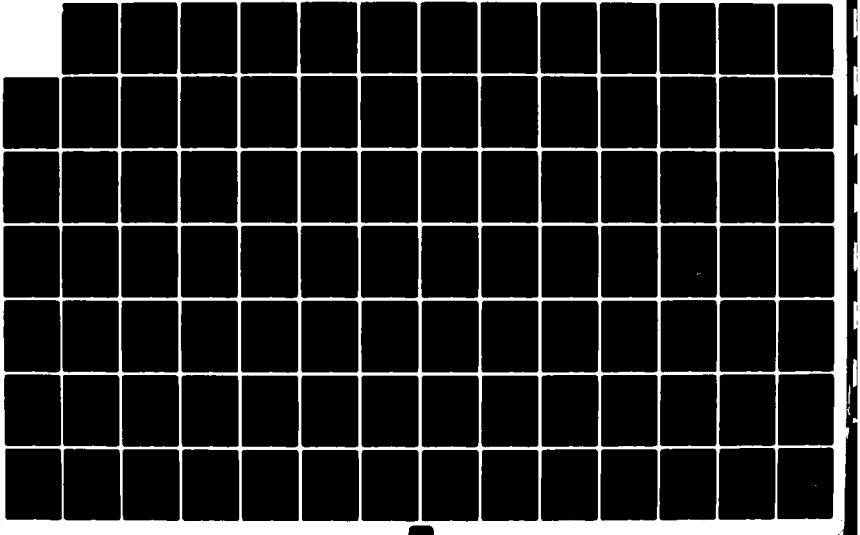

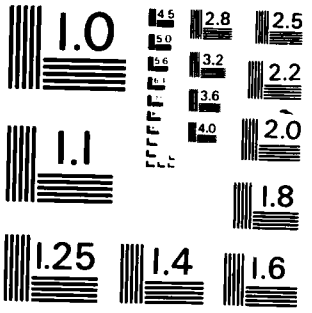

MICROCOPY RESOLUTION TEST CHART
NATIONAL BUREAU OF STANDARDS - 1963 - A

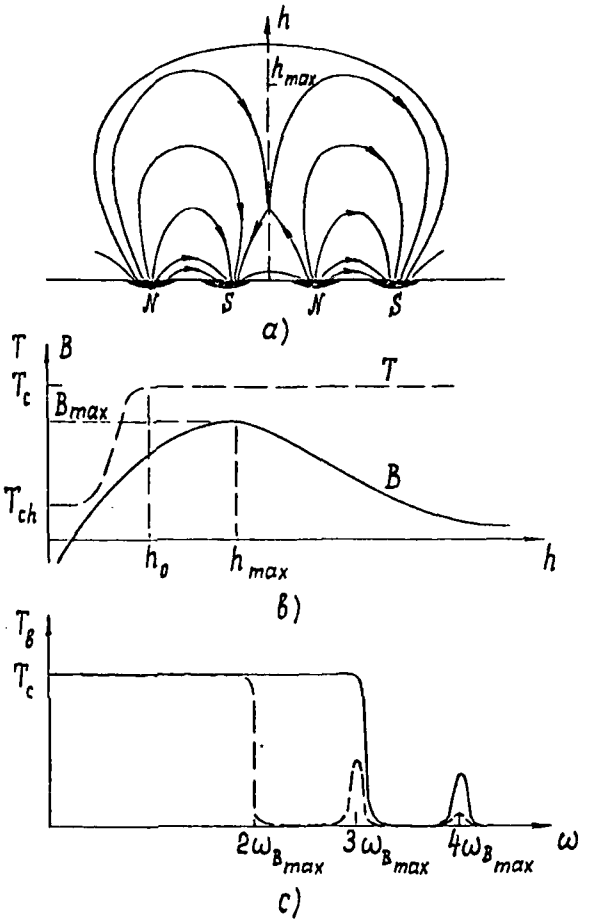

Figure 2. The model of a source with the maximum of the magnetic field over height: a) magnetic lines of force above a group of sunspots (h_{max} is the height at which the magnetic field has its maximum value); b) distribution of the magnetic field and kinetic temperature over the height; c) the frequency spectrum of radiation.

values exceeding B_{max}. Note that such values may exist at small heights in the chromosphere below the neutral point. In this case however the kinetic temperature is low; thus the contribution of these regions to radiation is neglected. In the frequency range $2\omega_{B_{max}} < \omega < 3\omega_{B_{max}}$ the radio emission is strongly polarized (with an excess of the extraordinary wave). The degree of polarization approximates 100%. Moreover, it is important to note that at the frequencies $3\omega_{B_{max}}$, $4\omega_{B_{max}}$,.... the cyclotron lines emerge because of the significant increase of optical thickness of gyroresonance layers caused by a small change in the magnetic field

at the heights $h \approx h_{max}$. For the optically thin gyroresonance layers the increase of optical thickness leads to a corresponding increase in the brightness temperature at the frequencies $\omega \approx s\omega_{B_{max}}$. The radiation in the line $\omega \approx 3\omega_{B_{max}}$ consists only of the ordinary waves. The lines at the higher harmonics are partly polarized with an excess of the extraordinary waves.

The distinctive feature of the model in Figure 2(b) with the magnetic field maximum at a certain height in the corona is the fact that the fine structure in the spectrum (a set of cyclotron lines and high-frequency cut-offs) appear under the condition where sharp gradients of the magnetic field and electron density are absent in the corona and chromosphere.

The calculated profiles of the cyclotron lines and high-frequency cut-offs are represented in Figure 3 (for the parabolic approximation of the dependence B(h) near the maximum of the magnetic field).

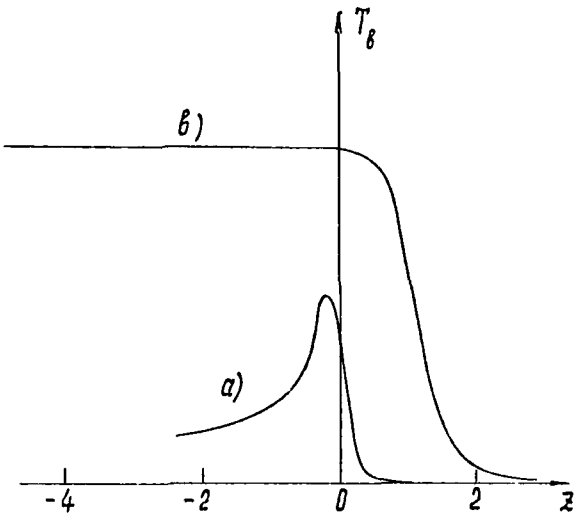

Figure 3. The calculated dependence of T_b in the cyclotron line a) and in the high-frequency cut-off b) on the parameter $z = (\omega - s\omega_{B_{max}})/\sqrt{2}\,\omega\,\beta_T \cos\alpha$ in the model with the maximum of the magnetic field (Figure 2(a)).

At the harmonics s for which the optical thickness is small at the frequency $\omega = 3\omega_{B_{max}}$, we obtain a line the form of which is represented by the curve a) in Figure 3. The halfwidth of the line $\Delta\omega$ is determined by the Doppler effect

$$\frac{\Delta\omega}{\omega} \approx \sqrt{2}\,\beta_T \cos\alpha\,, \qquad (4)$$

where $\beta_T = v_T/c$, v_T is the thermal electron velocity, α is the angle between the magnetic lines of force and the line of sight.

In the case where the optical thickness at these frequencies is well above unity, the frequency spectrum takes the form of a high-frequency cut-off given by the curve b) in Figure 3. The characteristic width of the cut-off $\Delta\omega$ is as previously determined by relation (4).

4. RADIATION FROM A THIN MAGNETIC TUBE, FILLED WITH HOT ELECTRONS

Judging from the X-ray emission data (Cheng, 1977) it is possible for the force tube of a bipolar magnetic field above a sunspot to be filled by hot electrons (Figure 4(a)). These electrons may, in principle, fill the whole of the tube or be present as an admixture to the electron component at normal coronal temperature.

As an example we treat the case where a relatively thin force tube is filled by hot electrons (with $T \gg T_c$). Let us also assume that their pressure is small compared with the magnetic pressure and that therefore the pressure of hot electrons does not markedly change the value of a magnetic field in the tube. The assumed distribution of T and B along the axis h is shown in Figure 4(b).

It is easy to see that in the framework of this model the frequency spectrum of cyclotron radiation escaping the corona along the axis h will represent a superposition of the usual spectrum of the S-component (Figure 1(b)) and cyclotron lines at frequencies which are multiples of ω_{B_t} (ω_{B_t} is the gyrofrequency in a force tube at the height h_t). This spectrum is given in Figure 5(b). Analysis shows that the force tube can radiate only the cyclotron lines $\omega \approx 2\omega_{B_t}$, $3\omega_{B_t}$,..... The second line is totally polarized in the sense of the ordinary wave. The lines beginning with the third are partly polarized, with an excess of the extraordinary wave.

5. RADIATION FROM A HOT NEUTRAL SHEET

It has been mentioned at the beginning of the report that the fine structure of a spectrum may be due to the cyclotron radiation of hot neutral current sheets (Zheleznyakov and Zlotnik, 1979, 1980c). Probably these appear in the lower corona or in the upper chromosphere during the pre-flare phase of solar activity. Thus detection of the spectral fine structure associated with neutral current sheets may prove to be an important method of predicting and recognizing such sheets.

The distribution of the magnetic field and temperature in the corona along the line of sight passing through a neutral current sheet is given in Figure 5(a). It is assumed here that the plasma has an enhanced temperature only within the limits of the neutral current sheet, including the edge regions with a magnetic field $B < B_0$.

The frequency spectrum of thermal cyclotron radiation from a neutral current sheet approaching the point h_0 is seen in Figure 5(b). It represents a set of rather broad lines at the harmonics of the gyrofrequency $\omega = s\omega_{B_0}$. The calculation

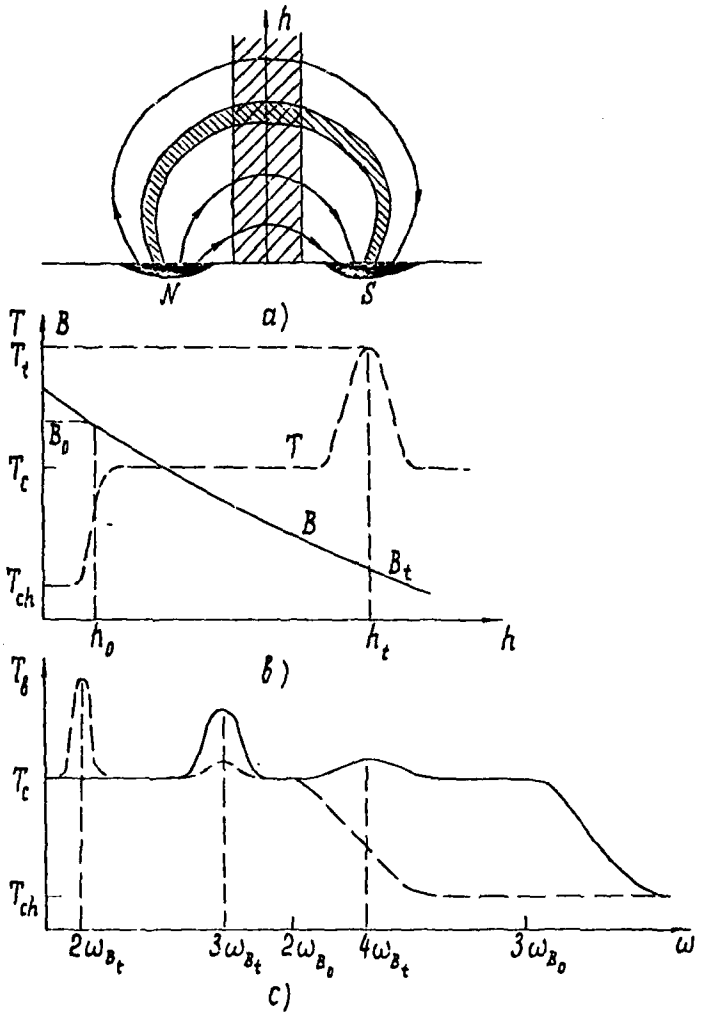

Figure 4. The model of a source with hot electrons filling the magnetic field force tube: a) magnetic lines of force with hot electrons (close hatching) and those crossed by the antenna pattern (wide hatching); b) distribution of the magnetic field and temperature over the height (B_t is the magnetic field at the level h_t of the force tube); c) the frequency spectrum of radiation.

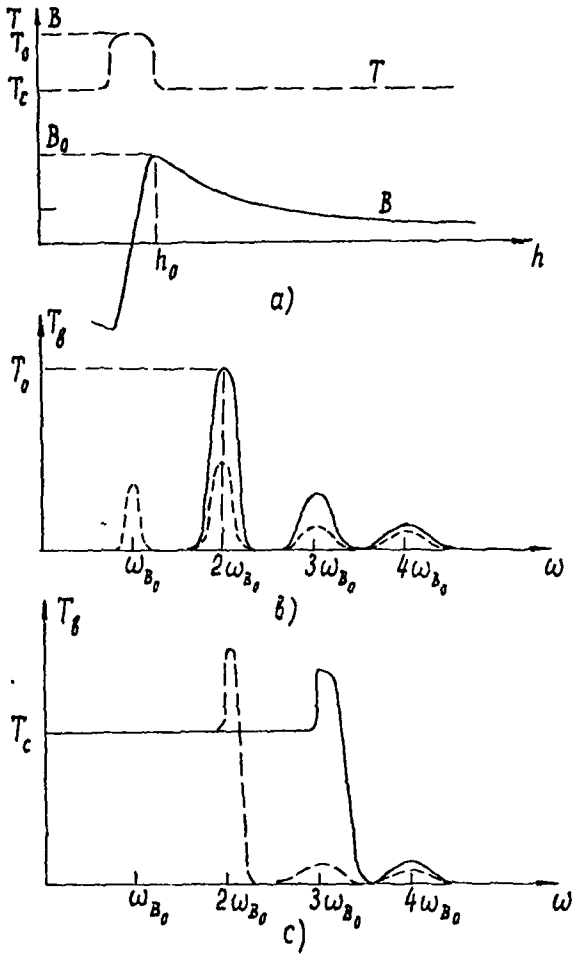

Figure 5. The model of a source with a neutral current sheet and a monotonically vanishing magnetic field: a) distribution of the magnetic field and kinetic temperature over the height (h_0 is the conventional edge of the neutral current sheet); b) the frequency spectrum of the proper radiation of the neutral current sheet; c) the frequency spectrum with allowance for absorption and radiation in the corona.

of such a spectrum has been discussed in ample detail by Zheleznyakov and Zlotnik (1980a) so it is omitted here. Note only that the appearance of discrete cyclotron lines is due to the generation of radiation in the region of a quasi-uniform magnetic field B_0 at the edge of the neutral sheet. The source is restricted from below by the level at which the plasma frequency ω_p is equal to the harmonic frequency. It should be readily apparent that the given level in the non-relativistic plasma must be situated far from the middle (i.e. at the edge) of the sheet. In fact, from the condition of static equilibrium of a plasma in the magnetic field of a neutral sheet $B_0^2/8\pi = 2N_0 \kappa T$ it follows that $\omega_{p_0} = \omega_{B_0}/2\beta_T$ (N_0 and ω_{p_0} are the density and the plasma frequency in the middle of the sheet). Since the parameter $\beta_T \ll 1$, the last equality implies that $\omega_{p_0} \gg \omega_{B_0}$. At low harmonics of the gyrofrequency $\omega = s\omega_B$ this inequality ensures the validity of the condition $\omega_{p_0} \gg \omega$. Hence it is evident that the plasma level $\omega_p = \omega$ for the emitted frequencies is located far from the middle of the sheet in the region where the magnetic field is close to B_0.

When escaping a neutral current sheet the cyclotron radiation does not contain the extraordinary mode at the frequency $\omega = \omega_{B_0}$, since $n_e^2 < 0$ in the sheet. The lines $\omega = 2\omega_{B_0}$, $3\omega_{B_0}$,..... are unpolarized or partly polarized with an excess of the extraordinary wave depending on whether the source is optically thick or optically thin. The spectrum and the polarization of radiation escaping the corona certainly differ from those in Figure 5(b) owing to absorption of the neutral current radiation in the upper regions of the corona and of the proper cyclotron radiation of these regions. For example, the line $\omega = \omega_{B_0}$ in the ordinary radiation and the extraordinary mode in the line $\omega = 2\omega_{B_0}$ will vanish owing to absorption in the corona (the first will vanish at the gyroresonance layers $\omega = 2\omega_B$, and the second at the level $\omega = 3\omega_B$). In general the observed spectrum takes the form presented schematically in Figure 5(c). The high-frequency cut-offs at the frequencies $\omega = 2\omega_{B_0}$ and $\omega = 3\omega_{B_0}$ are associated with the limiting from below of the source of the "S-component" in the corona: the radiation from the deeper regions of the corona below the neutral current sheet does not penetrate through the sheet at the frequencies $\omega < \omega_p$ (on the emission propagating through neutral current sheets in the solar corona see Zheleznyakov and Zlotnik (1980b)).

Let us stress once again that thermal cyclotron radiation is produced in the neutral current sheet by only the external regions of the sheet. The behaviour of the magnetic field toward the deeper layers (drop to zero and reversal of sign or reducing to a certain limiting value followed again by increasing) does not affect the formation of the frequency spectrum as a set of resolved cyclotron lines. Therefore the radiation with the characteristics shown in Figure 5(c) may, in principle, be generated by hot electrons trapped by the local minimum of the magnetic field in a force tube. This minimum may occur in a force tube if the energy density of hot electrons is comparable with that of the magnetic field.

6. COMPARISON OF MODELS

All our models of magnetic field and electron density distribution with height give results differing from the standard model of the S-component. They result in frequency spectra with fine structure in the form of cyclotron lines and high-frequency cut-offs. Every model however has its own characteristic spectrum and polarization of thermal cyclotron radiation. This circumstance permits us to deduce the distributions N(h) and T(h) from the observed spectrum and the polarization of microwave radiation of solar active regions. From the above it is clear that for the detection of cyclotron lines and the study of fine structure,

simultaneous spectral and polarization measurements in the wide frequency range (covering at least a factor of three in frequency) and with the adequate resolution $\Delta\omega/\omega \leqslant 0.05$ are necessary. The spectrographs should be combined with the antenna systems with as much directivity as possible: beamwidth must be less than a sunspot or the distance between sunspots in a group. Antennae similar to the RATAN-600 or the 100-m Bonn radio telescope are preferable, otherwise when receiving the radiation from the whole active region the fine structure is smoothed and one can hardly detect with confidence the cyclotron lines and cut-offs; their identification and interpretation then become doubtful. An example of this smoothing is given by the radiation from a magnetic force tube (see Figure 4). If the trapped hot electrons are distributed along the tube over the region where the magnetic field varies greatly ($\Delta B/B \gtrsim 1$), then in the total radiation the cyclotron lines will diffuse and the spectrum will be smoothed. Conversely, if the receiving is performed by the antenna with narrow knife or pencil directivity pattern (the cross-section of this pattern is represented in Figure 4(a)), then the frequency spectrum of the observed cyclotron radiation will contain discrete cyclotron lines.

A detailed discussion of the problems tackled in the present report is offered in papers by Zheleznyakov and Zlotnik (1979, 1980a,c).

7. CONCLUSION

For many years solar microwave flux and polarization have been measured at a few discrete well-spaced frequencies. The present study suggests that if observations could be made with wide-band spectrographs and spectropolarimeters using highly directional antennae, then valuable information on cyclotron lines and spectral cut-offs would be obtained. These in turn would give valuable information on the magnetic fields and temperatures in solar active regions.

References

Cheng, C.-C.: 1977, "Evolution of the high-temperature plasma in the 15 June 1973 flare", Solar Phys., 55, 413.

Gel'freich, G.B., Akchmedov, Sh.B., Borovik, V.N., Gol'nev, B.Ya., Korzhavin, A.N., Nagnibeda, B.G., and Peterova, N.G.: 1970, "A study of local sources of the slowly-varying component of solar radio emission in the cm-wavelengths range", Izv. Glavonoya Astron. Obs., No. 185, 167.

Kakinuma, T., and Swarup, G.: 1962, "A model for the sources of the slowly varying component of microwave solar radiation", Astrophys. J., 136, 975.

Kaverin, N.S., Kobrin, M.M., Korshunov, A.I., Tikhomirov, V.A., and Tikhomirov, Yu.V.: 1976, "Fine structure in the spectrum of the S component of solar radio emission at 4.5-7 GHz", Pis'ma Astron. Zh., 2, 577; Engl. transl., Sov. Astron. Lett., 2, 229 (1976).

Lantos, P.: 1968, "A model for thermal gyromagnetic radio emission from solar active regions", Ann. Astrophys., 31, 105.

References

Livshits, M.A., Obridko, B.H., and Pikel'ner, S.B.: 1966, "Radio emission and atmospheric structure above sunspots", Astron. Zh., 43, 1135; Engl. transl., Sov. Astron. AJ, 10, 909 (1967).

Sweet, P.A.: 1958, "The neutral point theory of solar flares", in Electromagnetic Phenomena in Cosmical Physics (ed. B. Lehnert) (Proc. IAU Symp. No. 6), p. 123 (Cambridge Univ. Press).

Zheleznyakov, V.V.: 1962, "The origin of the slowly varying component of solar radio emission", Astron. Zh., 39, 5; Engl. transl., Sov. Astron. AJ, 6, 3 (1962).

Zheleznyakov, V.V.: 1963, "The frequency spectrum of the slowly varying component of solar radio emission", Astron. Zh., 40, 829; Engl. transl., Sov. Astron. AJ, 7, 630 (1964).

Zheleznyakov, V.V.: 1977, Electromagnetic Waves in Cosmic Plasma, Nauka, Moscow.

Zheleznyakov, V.V., and Zlotnik, E.Ya.: 1979, "Diagnostics of neutral current layers under space conditions", Usp. Fiz. Nauk., 128, 725; Engl. transl., Sov. Phys. Usp., 22(8), 665 (1979).

Zheleznyakov, V.V., and Zlotnik, E.Ya.: 1980a, "Thermal cyclotron radio emission of neutral current sheets in the solar corona", Solar Phys., 68, 317.

Zheleznyakov, V.V., and Zlotnik, E.Ya.: 1980b, "Fine structure of microwave solar radio emission from solar activity centers", Astron. Zh., 57, 778; Engl. transl., Sov. Astron., 24(4), 448.

Zheleznyakov, V.V., and Zlotnik, E.Ya.: 1980c, "Influence of neutral current sheets in the cosmic plasma on the frequency spectrum of transmitted radio emission", Astron. Zh., 57, 1038; Engl. transl., Sov. Astron., 24(5), 595.

Zlotnik, E.Ya.: 1968, "Theory of the slowly changing component of solar radio emission. I, II", Astron. Zh., 45, 310, 585; Engl. transl., Sov. Astron. AJ, 12, 245, 464 (1968).

Discussion

Alurkar: What's the width of the line emission you are expecting?

Zlotnik: The width of the line is determined by the Doppler effect and so must be of the order of β_T - the ratio of the electron thermal velocity to the light velocity. If the kinetic temperature is of the order of 10^8 K, then $\Delta\omega/\omega \sim 0.1$. The line may be more narrow for lower temperatures.

Schwenn: Is there any relation between your results and Dr. Alurkar's measurements shown this morning?

Zlotnik: I'm not sure, because my results are for centimeter-decimeter wavelengths rather than decametric wavelengths which Dr. Alurkar is concerned with.

9. Observations of the Quiet Sun at Decametre and Metre Wavelengths

A. A. Abranin and L. L. Bazeljan
Institute of Radiophysics and Electronics,
Academy of Science, Ukrainian S.S.R., Kharkhov, U.S.S.R.

R. A. Duncan
Division of Radiophysics, CSIRO,
P.O. Box 76, Epping, N.S.W. 2121, Australia

Abstract

During the STIP interval, April 1976, the very low level of sporadic radio emission of the Sun at decametre and metre wavelengths presented us with a good opportunity to observe the radio emission of the quiet Sun.

1. DECAMETRIC OBSERVATIONS

Decametric investigations of the radio emission of the quiet Sun are difficult because of the weakness of the radiation and the high brightness temperature of the cosmic background. These difficulties are increased by the ionosphere and by strong interference from radio stations. The ionosphere produces undesirable attenuation and fluctuations of signal because of ionospheric inhomogeneities. As a result even the flux density of the quiet Sun for frequencies <30 MHz is hardly known (Cronyn and Erickson, 1965; Bazelyan et al., 1970; Aubier et al., 1971). Of the structure of the <30 MHz quiet Sun nothing is known.

In April 1976 this kind of measurement was attempted at 25 MHz at Kharkov. The period was one of very low radio emission activity. As well as two-dimensional maps of the Sun obtained with a large radio telescope, observations of the partial solar eclipse of April 29 were made. Because of interference however only the first part of the eclipse was successfully observed. We present here a short description of the equipment and some of the observational results.

The observations were made using the radio telescope UTR-2, which has five simultaneous beams separated in declination by 24' arc (Braude et al., 1971). Each beam has a half-power width of 28' arc in right ascension and 35' arc in declination. Phase-modulated radiometers were used as receivers. The bandwidth of the i.f. amplifiers was 5 kHz, and the time constant was 15 s. To reduce the effect of interference two independent receiving channels were used, separated in frequency by 50-100 kHz. Observations of the Sun were made daily at ±2 h from local noon. They consisted of several series of records, each series consisting of three scans, although, in principle, one scan is enough. The declination of the central beam for the three scans was $\delta_\odot$ -0°.2, $\delta_\odot$ and $\delta_\odot$ +0°.2. The duration of each scan was 10 min.

The first step in processing was scaling the scans using the calibration signal of the radiometers and the parameters of the radio telescope. Then the records of the two independent channels were averaged and smoothed over an interval of 2 min. This interval corresponds approximately to the half-power width of the beam. From these smoothed scans radio maps of the Sun were constructed.

The resultant maps of the brightness distribution of the quiet Sun for particular times are given in Figures 1a, 1b. One is for one hour before local noon and the other for one hour after local noon (8^h25^m and 10^h25^m UT). The optical disk of the Sun and its active regions (Solar Geophysical Data, 1976a), and the corona at 5303 Å (Braude et al., 1971) are also shown. The coordinates are declination in degrees and "right ascension" in minutes of time measured from the centre of the Sun.

During the period of observation and the preceding days, solar activity was limited to the McMath regions 14179 and 14185. It was mainly weak chromospheric flares and subflares (Solar Geophysical Data, 1976a). Two centres of activity were observed in the radio wavelength range 8.5 mm to 2 cm also (Solar Geophysical Data, 1976a), but at decametre wavelengths these two regions are indistinguishable because of either low intensity or small separation.

Figure 1 shows a very large shift of the radio image of the Sun from its optical position. As the shift of the radio image is in the same direction for two practically symmetrical observations either side of noon, interpretation in terms of ionospheric refraction is unlikely. Furthermore, on the preceding day, 1976 April 29 (Figure 2a) the maximum of radio brightness coincided closely with the centre of the optical disk, although the position of the Sun in the sky during the observation was the same. Hence the displacement observed on April 30 seems not to have been associated with refraction or scattering in the solar corona.

As one can see both the displacement of the maximum radio brightness from the centre of the optical disk and the intensity of radio emission were significantly higher on April 30 (Figure 1) than on April 29 (Figure 2a). On April 30 there was also a significant variation of brightness distribution, between 0825 and 1025 UT. Such fast variations may be due to abrupt increases of activity at decametre wavelengths from one or more active regions. This would be in accordance with an observed growth of solar activity at both optical and high-frequency radio wavelengths (Solar Geophysical Data, 1976a,b). This increase in activity was however observed in McMath region 14179, and if the same region gave increased emission at decametre wavelengths one should have expected the shift of emission to be in the opposite direction to that observed.

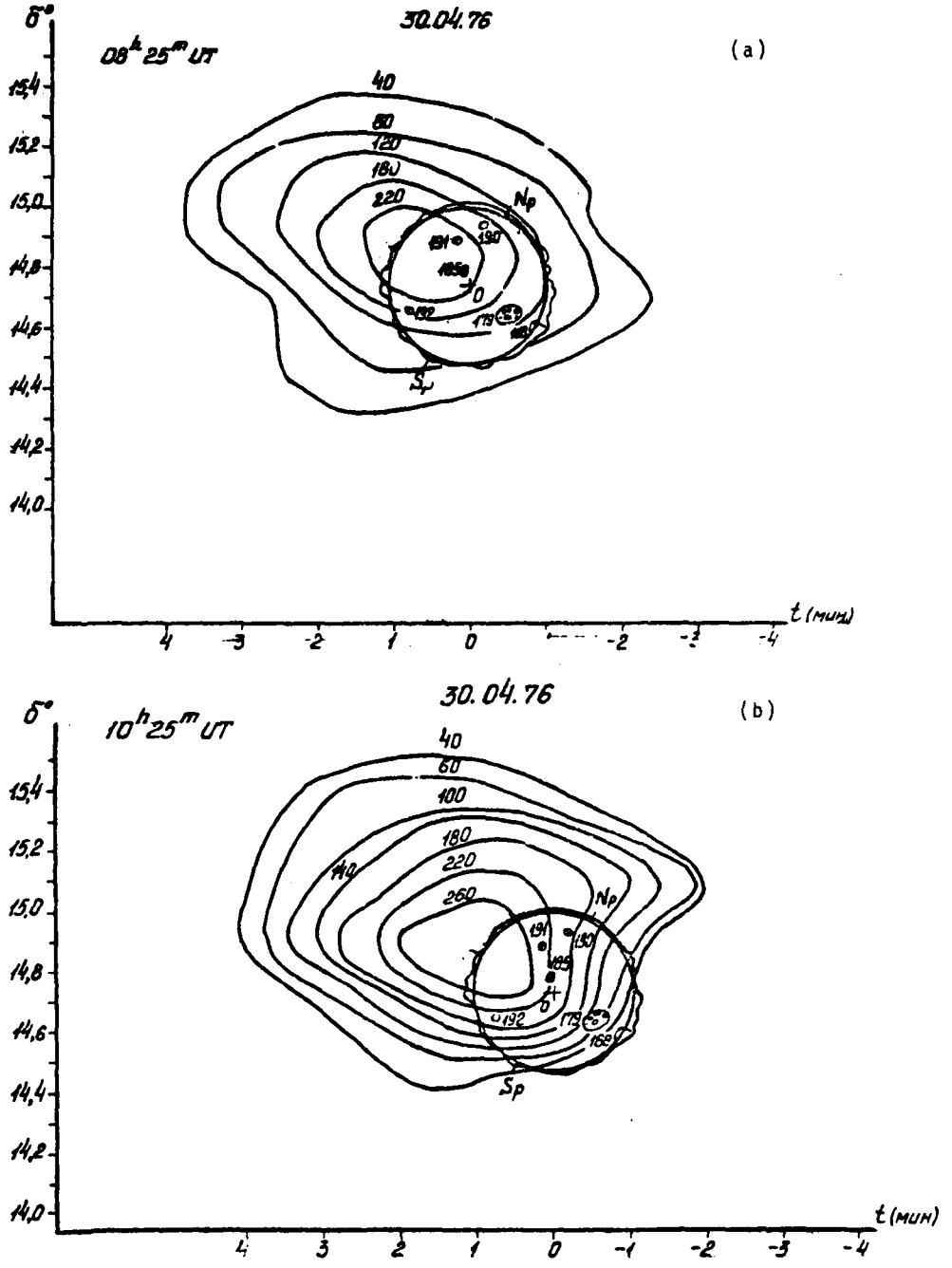

Figure 1. Brightness distribution over the quiet Sun, as observed with the radio telescope UTR-2 at 25 MHz on 1976 April 30.

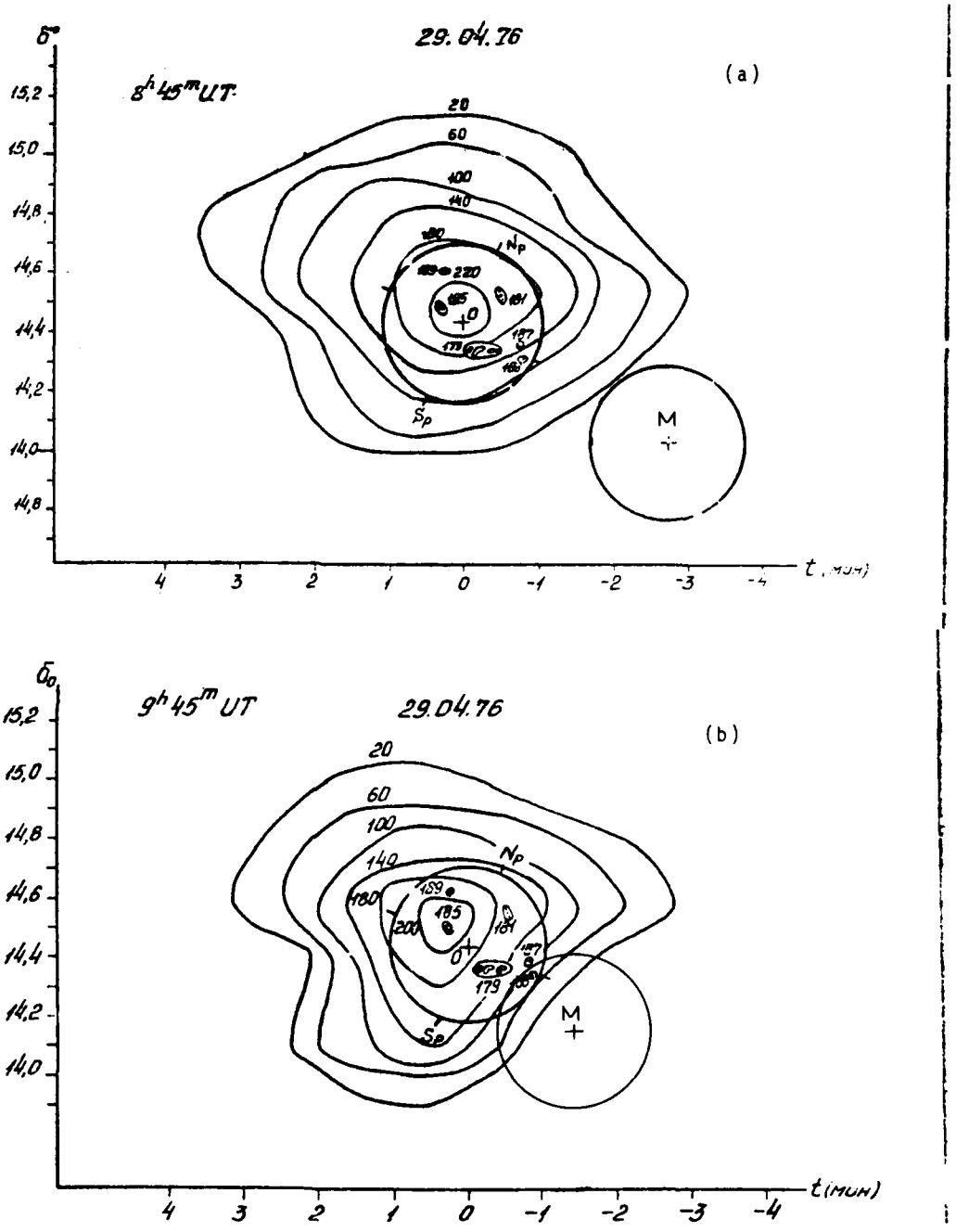

Figure 2. Brightness distribution as in Figure 1, but for the day of the eclipse, 1976 April 29. The circle with centre M shows the position of the Moon.
(a) 08^h45^m; (b) 09^h45^m.

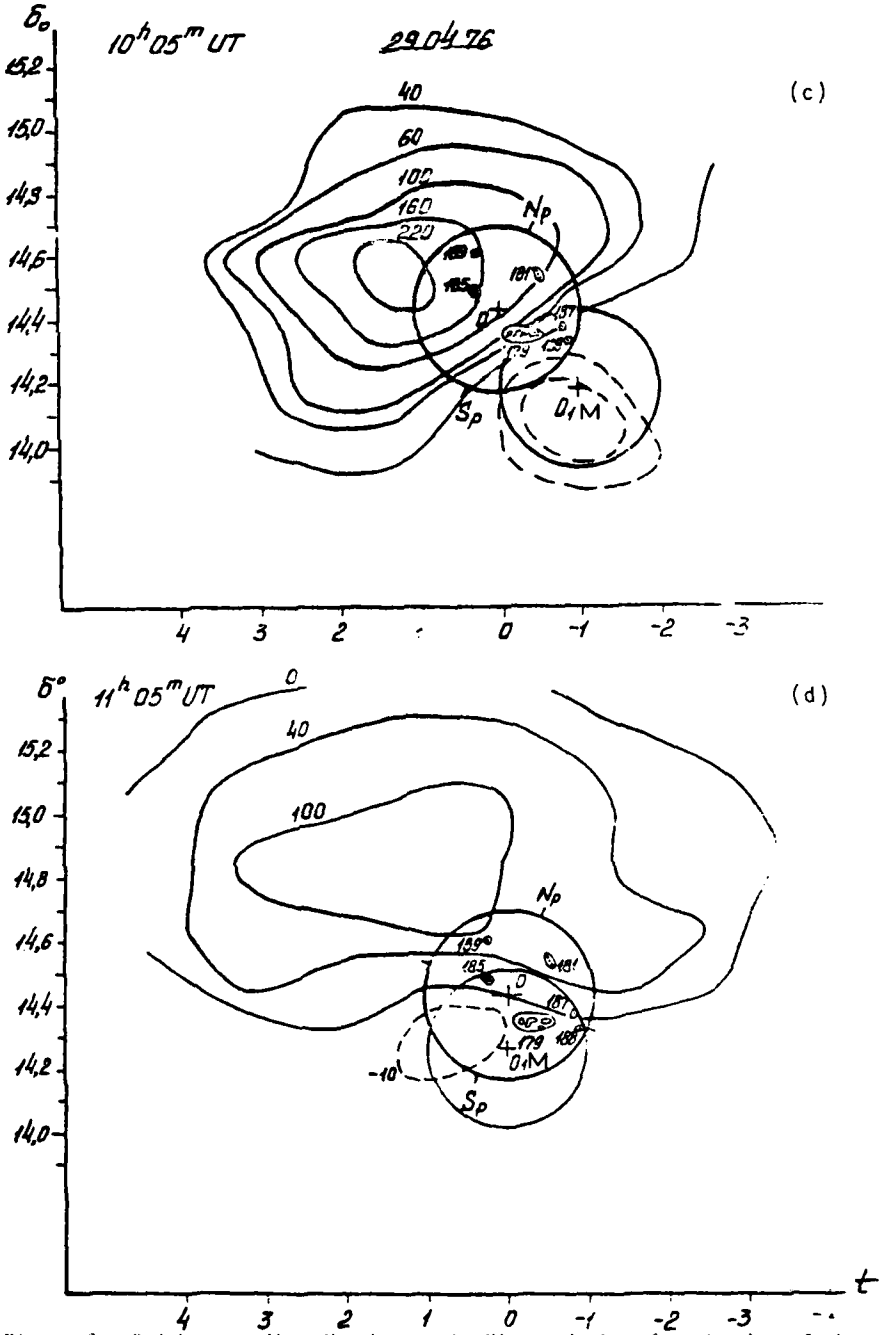

Figure 2. Brightness distribution as in Figure 1, but for the day of the eclipse, 1976 April 29. The circle with centre M shows the position of the Moon. (c) 10^h05^m; (d) 11^h05^m.

We conclude that the S-component at decametre wavelengths is significant and results in disturbance to the form of the radio corona. Thus any estimate of the equatorial and polar dimensions of the radio corona should take into account radio emission from local sources. It is possible however that the intensity of decametric emission from local sources changes very slowly, as is the case at centimetre wavelengths. If so the data above are atypical and are instead related to the fast growth of solar activity.

Figure 2 shows radio maps of the Sun obtained during the partial solar eclipse 1976 April 29. The centres of the Moon (M) and of the Sun (O) and their disks are shown. The centres of solar activity are also shown.

Figure 2a is a pre-eclipse map, taken at a time when the Moon was too far from the Sun to affect the apparent brightness distribution.

Figure 2b refers to the first contact. Here the Moon screens a part of the solar corona and thus causes a displacement of the centre of the brightness distribution.

Figure 2c shows a more advanced stage of the eclipse. Now not only the corona but also part of the solar disk, including part of the active region McMath 14179, is occulted. Against the background of the solar corona, the Moon appears as a source in absorption (isolines with "negative" apparent fluxes). This absorption region is distinctly displaced from the optical position of the Moon. The absorption image seems to be shifted away from the region of maximum gradient of radio brightness (difference of the solar corona and lunar brightness).

Finally, Figure 2d shows the brightness distribution at the maximum phase of the occultation (0.66). At this moment the Moon has covered both active regions on the solar disk. This has caused a marked drop in apparent brightness.

2. METRIC OBSERVATIONS

The Culgoora radioheliograph (Wild, 1967; Sheridan et al., 1973) routinely maps the Sun at 80 and 160 MHz. Each map is derived from observations integrated over about 1 min. For a source at the zenith the beamwidth is 3'.8 at 80 MHz and 1'.9 at 160 MHz. However, in mapping extended sources such as the quiet Sun confusion from sidelobes causes the major loss of definition.

Maps taken close to local noon for April 29 and 30 are shown in Figures 3 and 4 respectively. The main feature seen at 80 MHz is an elongation of the contours along a line within about 15° of the equatorial plane of the Sun. We believe (Sheridan, 1978) that this shape portrays the shape of the corona during sunspot minimum. The polar flattening reflects the polar coronal holes as seen, during sunspot minimum, in the white-light corona; likewise the equatorial bulge reflects the equatorial streamers. In addition we see a suggestion of finer structure - two maxima separated by a shallow valley - on the disk. Such minor maxima are common and probably indicate streamers (Dulk and Sheridan, 1974).

At 160 MHz the radio corona is similar in shape but smaller than at 80 MHz (Wild, 1973). This is because most of the thermal bremsstrahlung is emitted from just above the plasma level, and this is of course closer to the photosphere at 160 than at 80 MHz. As is usual (Sheridan and Smerd, 1977), disk structure is more pronounced at 160 than at 80 MHz.

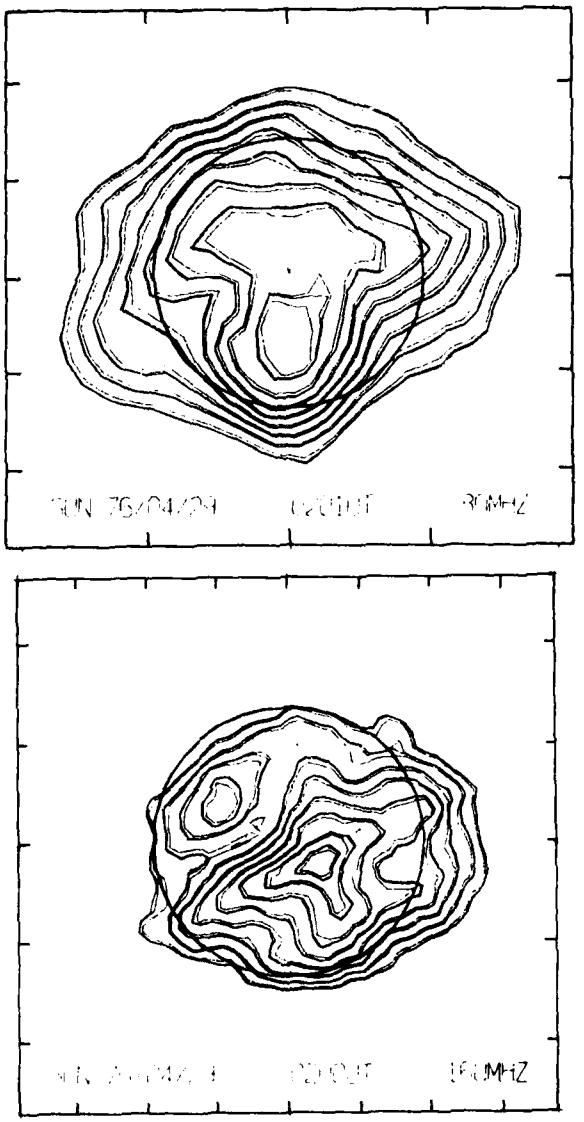

Figure 3. Brightness distribution over the Sun, as observed at Culgoora at 80 and 160 MHz on 1976 April 29. (a) Highest contour 7.8 x 10^5 K; contour intervals 8.6 x 10^4 K. (b) Highest contour 2.2 x 10^5 K; contour intervals 2.4 x 10^4 K.

These 80 and 160 MHz maps show little displacement of the radio from the optical disk. Thus, from this Culgoora evidence, we cannot exclude the possibility that the displacement seen at 25 MHz arose through ionospheric refraction.

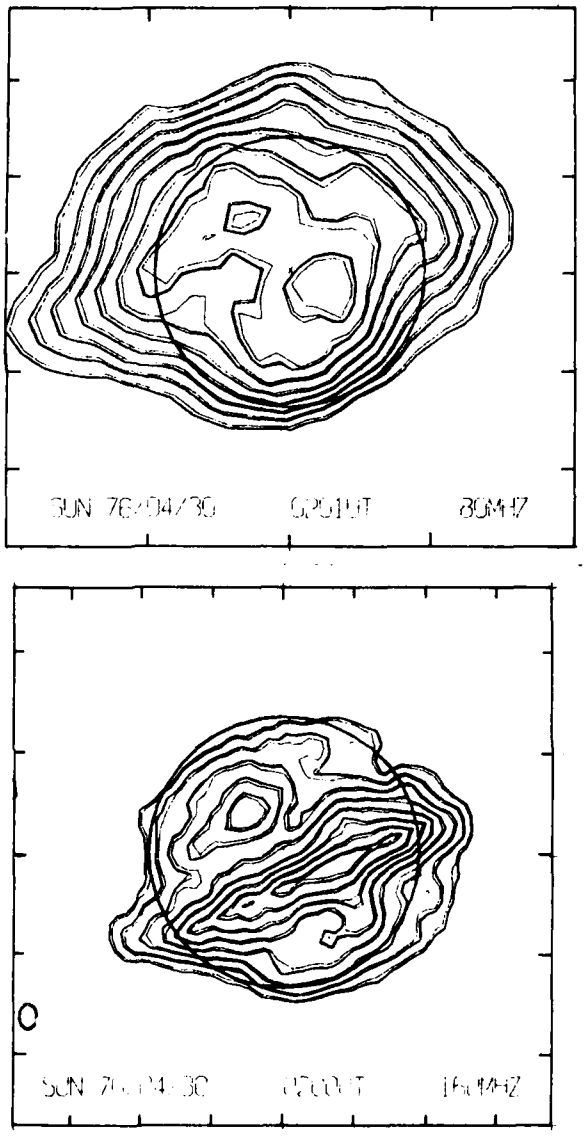

Figure 4. Brightness distribution over the Sun, as observed at Culgoora at 80 and 160 MHz on 1976 April 30. (a) Highest contour 6.9 x 10^5 K; contour intervals 7.6 x 10^4 K. (b) Highest contour 2.0 x 10^5 K; contour intervals 2.2 x 10^4 K.

References

Aubier, M., Leblanc, Y., and Boischot, A.: 1971, "Observations of the quiet sun at decameter wavelengths - effects of scattering on the brightness distrbution", *Astron. Astrophys., 12,* 435.

Bazelyan, L. L., Braude, S. Ya., and Men', A. V.: 1970, "Scattering of the decameter radio emission of the crab nebula by the solar corona", *Astron. Zh., 47,* 188, (*Soviet Astron., 14,* 153).

Braude, S. Ya., Bruk, Yu. M., Mel'janovskiy, P. A., Men', A. V., Sodin, L. D., and Sharykin, N. K.: 1971, IRE Acad. Sci., Ukr.S.S.R. (Kharkov), Preprint No. 7.

Cronyn, W. M. and Erickson, W. C.: 1965, "The flux and brightness of the sun at 26.3 mc/sec.", *Astron. J., 70,* 672.

Dulk, G. A. and Sheridan, K. V.: 1974, "The structure of the middle corona from observations at 80 and 160 Mhz", *Solar Phys., 36,* 191.

Sheridan, K. V.: 1978, "Some recent explorations of the solar corona from the Culgoora solar radio observatory", *Proc. Astron. Soc. Aust., 3,* 185.

Sheridan, K. V., Labrum, N. R., and Payten, W. J.: 1973, "Three-frequency operation of the Culgoora radioheliograph", *Proc. Inst. Elec. Electron. Engrs., 61,* 1312.

Sheridan, K. V. and Smerd, S. F.: 1977, "Radio and euv studies of coronal holes", *Izv. Vyssh. Uchebn. Zaved. Radiofiz., XX,* 1331, (*Soviet Radiophysics and Quantum Electronics", 20,* 917).

Solar Geophysical Data: 1976a, U. S. Department of Commerce, Boulder, Colorado, No. 382.

Solar Geophysical Data: 1976b, U. S. Department of Commerce, Boulder, Colorado, No. 387.

Wild, J. P.: 1967, "The Culgoora radioheliograph", *Proc. Inst. Radio Electron. Eng. Aust., 28,* 277.

Wild, J. P.: 1973, "The Sun - close up of a star", in H. Messel and S. T. Butler (eds.), *Focus on the Stars,* Shakespeare Head Press, Sydney, p. 73.

10. The Rise, Decline, and Possible Relationship Between Two Proton Flare Producing Regions Including Details of the Activity Patterns of Their Known Antecedent and Descendant Plages

Susan McKenna-Lawlor
Physics Department
St. Patrick's College
Maynooth, Co. Kildare
Ireland

Abstract

An account of solar circumstances (X-ray, optical, radio and magnetic) characterizing the disk transit proton-flare-producing regions McMath 15031 and 15266 is presented, together with corresponding details concerning their identifiable antecedent and descendant plages. Differences and similarities between these proton producing centers are discussed, and they are individually suggested to have constituted responses to instabilities associated with the presence beneath the photosphere of an anomalous region capable of causing strong magnetic flux to appear episodically within the confines of an identifiable solar zone.

1. INTRODUCTION

It is the purpose of the present paper to describe in detail the solar history of two plages which gave rise respectively to (a) the major GLE proton flare of November 22, 1977, relevant to STIP Interval IV and (b) the well known sequence of outstanding proton producing flares occurring in April-May, 1978. In the former case, the energetic flare occurred during the first disk transit of an active center that first developed on the invisible hemisphere. By its next appearance at the east limb, this region was of negligible solar importance. For details see Section 3. Plage 15266, progenitor of the April-May sequence was, on the other hand, associated with the emergence of new flux within and close to an active area that had already shown as many as five transits and the magnetically metamorphosed region thus produced thereafter went on to transit a total of five times. Section 4 presents not only an account of solar circumstances attending the transit of Plage 15266, but also those of its various known antecendents and descendants. In Section 5, differences and similarities between the two proton producing centers are described, and in Section 6 they are individually suggested to have constituted responses to instabilities associated with the presence beneath the photosphere of an anomalous region, capable of causing strong magnetic flux to appear episodically within the confines of an identifiable solar zone.

It may be noted that "returns" to the visible disk of individual plages could be recognized with reasonable confidence by giving due cognizance (a) to the effects of differential solar rotation and (b) to evolutionary changes associated with the growth and decay of underlying spot field deduced, from white light records, to have taken place while individual regions were transiting the invisible hemisphere.

In order to summarize the waxing and waning of activity within transition plages rotation by rotation, an "activity profile" was prepared for each transit described which shows, in tabular form, the day by day evolution, as monitored in calcium light, of the plage concerned, as well as information concerning variations in the field strength, area, spot count and magnetic classification of its underlying spot group. The frequency, with respect to class, of any observed flares is also given and the numbers of Sudden Ionospheric Disturbances, X-ray bursts and single frequency and dynamic radio events attending the flares mentioned are listed.

For convenience, those anomalous locations within the solar atmosphere in which the proton flares of November 1977 and April-May 1978 developed will hereafter be referred to as Active Regions I and II.

2. SOURCES AND KINDS OF SOLAR DATA ANALYZED

The experimental data used were taken primarily from the monthly publicaton Solar Geophysical Data (SGD) compiled by the National Geophysical and Solar-Terrestrial Data Center, Boulder, Colorado, U.S.A. Errata or revisions to primary data sets which appear in these publications from time to time are incorporated without comment into the material presented.

Flare data were taken from SGD "Comprehensive Reports". Flare importance is generally deemed to be that assigned in the associated summary "Group Reports" but, in individual cases where no importance rating was originally ascribed, a suggested importance, based on such flare parameters as were available, is here supplied with an added question mark to indicate special uncertainty.

Through the kindness of the staff of McMath-Hulbert Observatory, center line as well as on and off band Hα pictures of the April-May flares were available for study. Data concerning calcium plage regions were taken directly from the daily SGD reports of the McMath-Hulbert and Catania Observatories. Sunspot data used includes the Mt. Wilson and NOAA (Boulder, Ramey, Manila) SGD reports. Original drawings of the individual groups made at Mt. Wilson (and supplied by World Data Center A, NOAA, Boulder, Colorado, U.S.A.) were also consulted and used where necessary to correct the SGD classification listings.

Information concerning the X-ray variability of individual solar regions was taken from SGD "quick-look" OSO-8 maps. These displays, some of which are reproduced in Figure 1 were constructed from coverage obtained during a representative thirty minute period (neither the most quiet nor the most active).

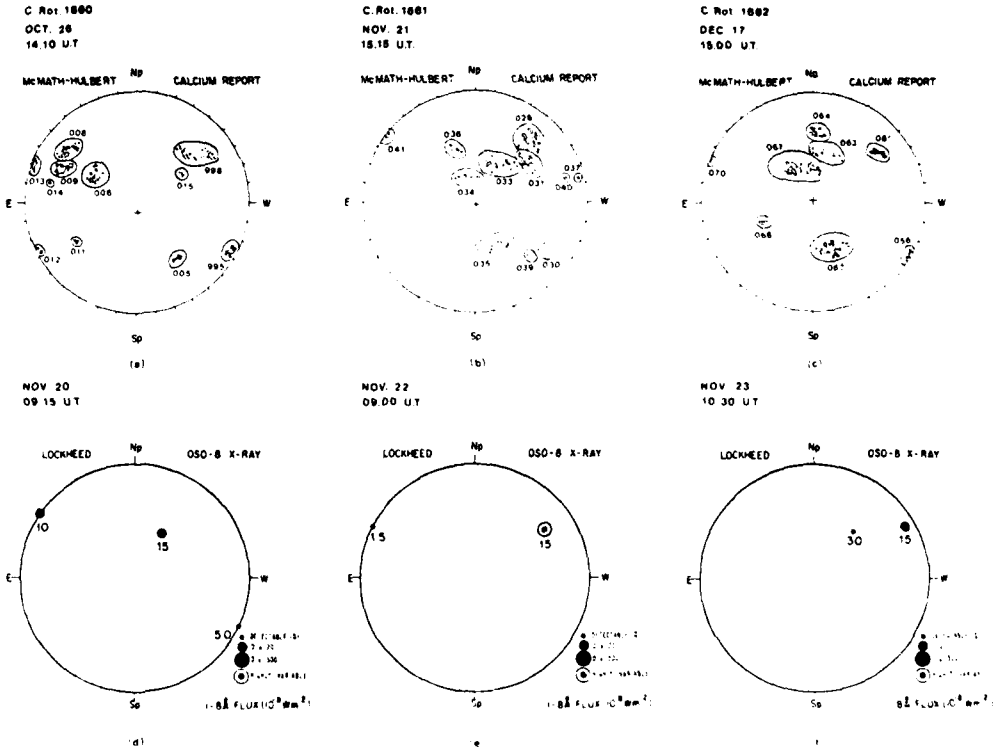

Figure 1. Top: Calcium plage reports of the McMath-Hulbert Observatory showing the same general region of the solar atmosphere during Carrington rotations 1660, 1661 and 1662. Plage 15031 (cf. 1b), which returned to the disk as plage 15063 in December, was associated on November 22, 1977 with the occurrence of an important proton event. Bottom: OSO-8 X-ray maps taken before, on the day of and following the proton event. The relative-intensity of a region is here indicated by dots of different sizes where "detectable", (D), nominally corresponds to 5X times the background value. The three dot sizes employed represent D-20D, 20D-500D and > 500D. If the source varied by more than an order of magnitude over a time period of < 2 hours, a "highly variable" indicator, consisting of a dot surrounded by a circle, is used rather than a "typical" intensity.

Satellite data concerning X-ray bursts and world-wide reports of SID's were taken from composite SGD lists. Suggestions contained in these compilations as to the possible association of individual events with flares are altered without comment in the text when updated information rendered this necessary. Similar corrective treatment is accorded to SGD lists of "flare-related" radio bursts recorded at fixed and swept frequencies.

Data concerning solar proton events were taken from SGD "provisional" lists.

3. DEVELOPMENTAL HISTORY OF ACTIVE REGION I

Active region I was first identified during Carrington Rotation 1661, when it was designated McMath Plage 15031. Only adjacent Plage 15033 had previously crossed the solar disk, i.e. once as Plage 15015 (see Figure 1), and this latter feature was already in an advanced state of decline and showed no special activity during the November transit. Structures 15028, 15034, 15036, 15037, and 15040 had, on the other hand, all developed since the previous rotation so that Plage 15031, which first rotated over the east limb on November 12, 1977, developed at a previously "quiet" location during a period characterized by ambient rising flux.

3.1 Plage 15031

OSO-8 observations indicate that Plage 15031 constituted a weak X-ray source up until November 18, by which time it displayed a moderate intensity enhancement. After an ensuing decline it became "highly variable" on November 22 (the day of the proton flare), returning to a steady condition by the succeeding day. (Compare maps (e) and (f) of Figure 1.) These events were complimented by a rising level of sub-flaring in the plage previous to November 22, an effect apparent, (see Table 1) despite significant gaps in the flare patrol record over the days concerned. This waxing solar activity culminated on November 22 in the production at 0945 UT, of an importance 2B flare accompanied by an importance 2 Sudden Ionospheric Disturbance (SID) of Widespread Index 5 and broad band single as well as swept frequency radiation, (see Table 2). An associated X-ray burst was also recorded. These related occurrences were climaxed, in less than an hour, by the onset of a ground-level particle event.

It is noted that three of the flares occurring on November 22 prior to the importance 2B event, were associated with the generation of minor centimeter burst radiation as detailed in Table 2. The closest recorded event to the major flare was additionally associated with the production of an importance 1 Sudden Phase Anomaly (SPA) of Widespread Index 1. The first flare to be associated with an ionospheric disturbance previous to this was an importance sf event at 1132 UT on November 20 (accompanied by an importance 1 Sudden Enhancement of Atmospherics (SEA) of Widespread Index 1). After the major flare of November 22 no further activity other than an importance sf event on November 24 was reported in region 15031 prior to its limb transit.

Examination of the original Mt. Wilson drawings reveals that by 1645 UT on November 17, a $\beta(\delta)$ configuration was present in the underlying spot group. (Compare Figures 2a and 2b.)

TABLE 1.

The evolution, as monitored in calcium light, of those plages in which the proton flares of November 1977 and April-May 1978 developed (cf. Tables 1 and 10, respectively) together with corresponding details concerning their antecedent and descendent plages. The sources of these data together with complimentary information concerning plage related magnetic features, flare activity, SID's, X-ray bursts and single frequency and dynamic radio events, are described in Section 2. The conventions of presentation adopted are generally similar to those contained in Solar Geophysical Data (Supplement, No. 390, 1977. The number of flares identified within a particular plage, however, having an importance class with the range sf to 4b is indicated according to the scheme {number of flares identified (reported flare importance)} In cases where no importance rating was assigned in the source material to a particular flare, a suggested importance, based on such parameters as are available, is assigned by the author and the event listed according to the scheme 1? (i.e. suggested flare importance). The areas are measured in millionths of the solar hemisphere.

I DEVELOPMENTAL HISTORY AND ACTIVITY PROFILE OF McMATH PLAGE 15031

McMATH PLAGE NO.	DATA 1977	E (1): NOV. 12	13	14	15	16	17	18	19	20	21	22	23	24			W (1): NOV.
15031	PLAGE AREA #	200	400		200	600	1200		1800		1500			1800			
	INTENSITY	1.0	1.0		2.0	3.0	3.5		3.5		3.0			3.5			
MT.WILSON NUMBER 19894	MT. W. CLASS				(B)	(BF)	B(D)	(B)		BF(D)	(BF)		(BF)	(AF)			
	FIELD STRENGTH				3	4	5	4		5	4		4	2			
	AREA#				10	10	110	440	420	230	180		120				
	SPOT COUNT				2	1	15	21	0	16	4		9				
	NOAA CLASS				Axx	Axx	CRI	DAL	Xx	DAI	DAC		DRI				
H ALPHA ACTIVITY	REPT. FLARES				1(sn)		2(sn)	3(sf)	3(sf)	4(sf)	4(sf)	2(sn)		1(sf)			
										1(sn)		1(1f)					
												1(2b)					
X-RAY ACTIVITY	NO. OF SIDs									1		2					
	NO. X-RAY BTS.						1					1					
SF BST. ACTIVITY	NO. OF cm BTS.											3					
	NO. cm-dm BTS.																
	NO. cm-m BTS.											1					
DYNAMIC RADIO EVENTS	NO. TYPE II																
	NO. TYPE IV											1					

TABLE 2.

Ionizing and Fixed Frequency Radiation Accompanying Flaring in Plage 15031, During Carrington Rotation 1661

Date	OPTICAL FLARE					SUDDEN IONOSPHERIC DISTURBANCES						FIXED FREQUENCY CM. RADIATION				
Nov. 1977	Beg. UT	Max. UT	End. UT	Imp. Class	Cor Area SqDeg.	Beg. UT	Max. UT	End UT	Imp.	W.sp. Index	Type	Beg. UT	Max. UT	End. UT	Flux* Den. Mean	Freq. MHz.
15	1255	1255	1300D	-N	0.9											
17	1100	1106	1145D	-N	-											
17	1215	1215	1230	-N	1.1											
18	0433	0442U	0510	-F	0.4											
18	0826	0829	0845	-F	-											
18	1726F	-	1732D	-F	0.2											
19	0857	-	1044	-F	-											
19	1036	1036	1055	-F	-											
19	1424	-	1424D	-F	-											
20	0852	0858	0906	-F	-											
20	1132	1135	1143	-F	-	1132U	1207	1220	1-	1	SEA					
20	1235	-	1248	-F	-											
20	1308	1318	1334	-F	-											
20	1416	1419	1426D	-N	-											
21	0014	0020	0036	-F	0.3											
21	0141	0210	0254	-F	-											
21	1048	-	1057	-F	-											
21	2312	2326	2337	-F	0.2											
22	0217	0227	0304	-N	-							0215	0216.4	0222	1.2	3750
22	0330	0334	0400	1F	2.6							0331	0333.2	0351	1.0	3750
22	0424	0428	0505	-N	0.8	0423	0428	0500	1-	1	SPA	0424.	0425.8	0440	4.0	3750
22	0945	1005	1108	2B	6.3	0948	1010	1152	2-	5	SWT, SEA (SPA, SES.	0948.8	1007.	1102.9	479.0	2695**
24	0907	0909	0920D	-F	-											

* Units 10^{-22} W^{-2} Hz^{-1}

** Accompanying Type IV and Type III events.

The next available record, made at 1610 UT on November 20, shows that, by this time, the following spots had become dominant. No magnetic observations were made on the day of the major flare. Thereafter, the spot group was seen to be in rapid decline, reaching class α f by November 24. A report from Boulder indicates that the largest spot in the group had an asymmetric or complex penumbra on the day before the major flare and a rudimentary penumbra on the succeeding day. (See Table 1 for details.)

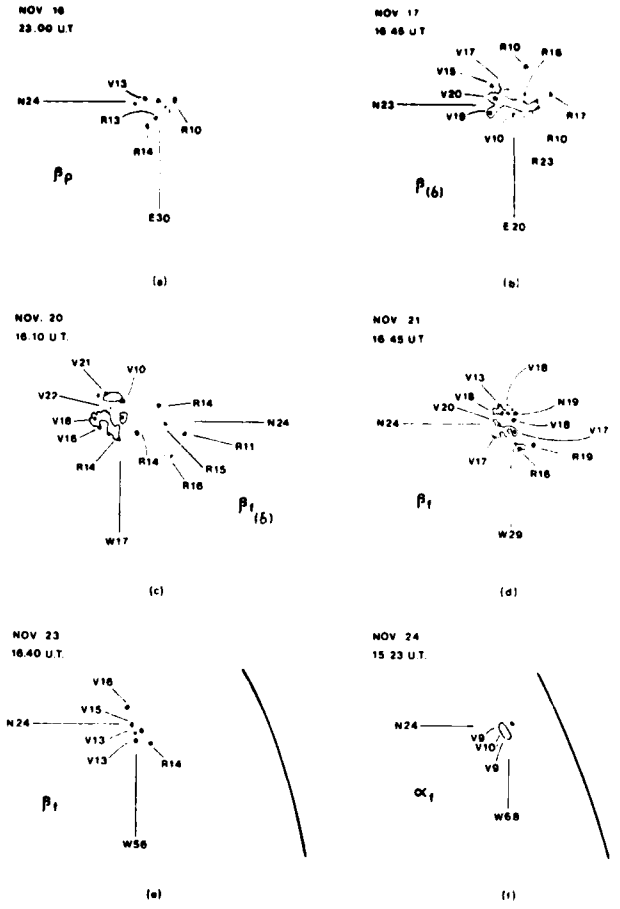

Figure 2. Reproduction of drawings of spot group Mt. Wilson 19894, originally made at the Mt. Wilson Observatory during Carrington rotation 1661. The north is at the top of each drawing; the west is to the right.

3.2 Plage 15063

On its next disk transit, when it was re-numbered McMath Plage 15063, the region which had previously been the source of the proton flare was so substantially reduced in area and brightness as to be of negligible significance, (see Table 3). No observed flaring occurred during the course of its transit, and the Mt. Wilson observers reported no spots in the underlying magnetic field.

4. DEVELOPMENTAL HISTORY OF ACTIVE REGION II

Plage 15266, which gave rise to a spectacular series of proton flares in April-May 1978, occurred in a part of the solar atmosphere that had been highly disturbed since the preceding January. As shown in Figure 3, which traces the

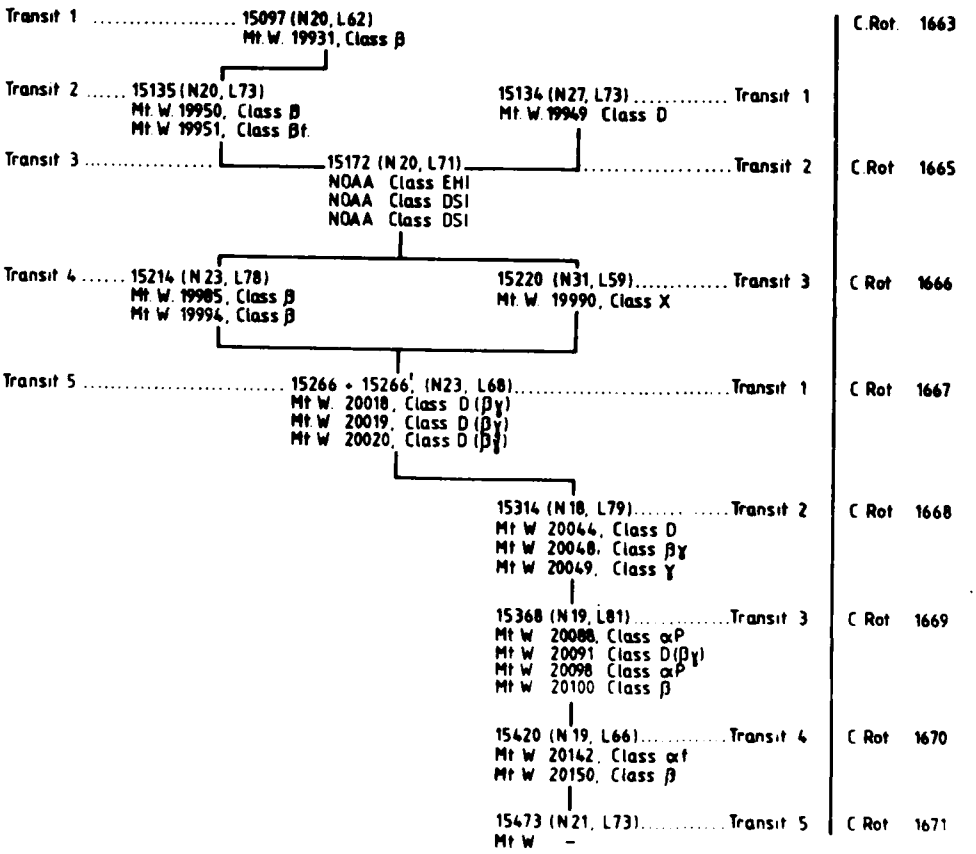

Figure 3. The development and decline of that active solar centre which, in Carrington rotation 1667, gave rise to the spectacular series of proton flares of April-May, 1978.

TABLE 3.

The evolution, as monitored in calcium light, of those plages in which the proton flares of November 1977 and April-May 1978 developed (cf. Tables 1 and 10, respectively) together with corresponding details concerning their antecedent and descendent plages. The sources of these data together with complimentary information concerning plage related magnetic features, flare activity, SID's, X-ray bursts and single frequency and dynamic radio events, are described in Section 2. The conventions of presentation adopted are generally similar to those contained in Solar Geophysical Data (Supplement, No. 390, 1977. The number of flares identified within a particular plage, however, having an importance class with the range sf to 4b is indicated according to the scheme (number of flares identified (reported flare importance)) In cases where no importance rating was assigned in the source material to a particular flare, a suggested importance, based on such parameters as are available, is assigned by the author and the event listed according to the scheme 1? (i.e. suggested flare importance). The areas are measured in millionths of the solar hemisphere.

3 DEVELOPMENTAL HISTORY AND ACTIVITY PROFILE OF McMATH PLAGE 15063

McMATH PLAGE NO.	DATA 1977	E (1) DEC. 10	11	12	13	14	15	16	17	18	W (1) DEC.
15063	PLAGE AREA @	300	600					700	700	900	
	INTENSITY	1.0	1.0					1.5	1.5	1.0	
	MT. W. CLASS										
MT.WILSON NUMBER	FIELD STRENGTH										
-----	AREA@										
	SPOT COUNT										
	NOAA CLASS										
X-RAY ACTIVITY	NO. OF SIDs										
	NO. X-RAY BTS.										
SF BST. ACTIVITY	NO. OF cm BTS.										
	NO. cm-im BTS.										
	NO. cm m BTS.										
DYNAMIC RADIO	NO. TYPE II										
EVENTS	NO. TYPE IV										

development and decline of this anomalous region, the antecedents of this structure included a sequence of four reappearances of Plage 15097. Another sequence of three reappearances of Plage 15134 occurred so spatially close to the first set mentioned that, in Carrington Rotation 1665, contributions from these two sources were jointly given the number Plage 15172. During the next transit, the individual elements of the two adjacent plage streams were again separately distinguished.

By Carrington Rotation 1667, the underlying magnetic situation had again become highly complex. New flux, which had in particular emerged within the ambience of previously existing magnetic fields, had indeed so fundamentally altered the character of the overlying plage that, while vestiges of its previous structure (designated in Figure 3 by the number 15266') survived, the overall character of the region was so modified that it was deemed appropriate to consider it to constitute a "new" feature (15266 + 15266'). This "new" plage made four further appearances before subsiding into the ambient background.

4.1 Plage 15097

The first member plage of that series preceding the April-May transit rotated over the east limb on January 7, 1978 during Carrington Rotation 1663, when it was accorded the designation Plage 15097. Its passage was characterized on days 11-14 by a moderate level of sub-flaring (probably incompletely reported due to extensive gaps in the H-alpha patrol observations), falling off thereafter to cease on January 18, (see Table 4). Associated electromagnetic accompaniments were minor. A cm-dm burst of maximum measured mean flux density 9.2 solar flux units (sfu) at 2695 MHz, accompanied an importance sn flare at ~ 2240 UT on January 11. A low level of X-ray activity was reported by OSO-8 observers in the plage on the morning of January 11, declining on suceeding days. However, a "highly variable" X-ray condition was reported to be present close to the time of an importance (SF-?) flare in the region at 1005 UT on January 16. Associated Mt. Wilson group 19931 rose in complexity from NOAA Class BXO on January 9 to Class DSI by at least January 13.

4.2 Plage 15135

Plage 15135 constituted, on February 1, the first return on Plage 15097. The general enhancement in area and intensity attained during this passage was a consequence of the emergence at this location of new magnetic flux since Mt. Wilson group 19931 of Class AXX which transited the west limb on January 18-19 had by this time re-emerged to the east as developing group Mt. Wilson 19950, accompanied by developing group Mt. Wilson 19951, (see Table 5). OSO-8 observations indicate that, from late on February 2 through February 3, the plage was "highly variable" in X-rays, declining on the succeeding days to a steady but moderate level of activity. February 3 was also the most flare active day of the transit. Three of the minor flares then occurring were collectivly associated with the production of 3 SID's, 2 X-ray bursts and 2 cm-dm bursts. These latter events had durations of only 0.4 minute and 4.8 minutes with corresponding mean peak flux densities of 10.1 sfu and 3.3 sfu, at 2695 and 2800 MHz respectively. These flares occurred during an interval when the underlying group was waxing from NOAA Class HSX to Class CHO.

TABLE 4.

The evolution, as monitored in calcium light, of those plages in which the proton flares of November 1977 and April-May 1978 developed (cf. Tables 1 and 10, respectively) together with corresponding details concerning their antecedent and descendent plages. The sources of these data together with complimentary information concerning plage related magnetic features, flare activity, SID's, X-ray bursts and single frequency and dynamic radio events, are described in Section 2. The conventions of presentation adopted are generally similar to those contained in Solar Geophysical Data (Supplement, No. 390, 1977. The number of flares identified within a particular plage, however, having an importance class with the range sf to 4b is indicated according to the scheme {number of flares identified (reported flare importance)} In cases where no importance rating was assigned in the source material to a particular flare, a suggested importance, based on such parameters as are available, is assigned by the author and the event listed according to the scheme 1? (i.e. suggested flare importance). The areas are measured in millionths of the solar hemisphere.

A DEVELOPMENTAL HISTORY AND ACTIVITY PROFILE OF McMATH PLAGE 15097

McMATH PLAGE NO.	DATA 1978	E (1) JAN. 7	8	9	10	11	12	13	14	15	16	17	18	19			W (1) JAN.
15097	PLAGE AREA #			500	800	1100	1000		1500	2000			2000				
	INTENSITY			2.0	2.5	3.0	3.0		3.0	3.0			2.5				
MT.WILSON NUMBER: 19931	MT. W. CLASS							(B)					AF				
	FIELD STRENGTH							4					2				
	AREA#			30	100			80		80	80	60	40				
	SPOT COUNT			6	10			12		8	2	3	3				
	NOAA CLASS			BXO	XX			DSI		CRO	CSO	CSO	AXX				
H ALPHA ACTIVITY:	REPT. FLARES					3(sf)	2(sf)	1(sf)	4(sf)	1(sf)	1(sf)		2(sf)				
						3(sn)		3(sn)	1?1f		1?1f						
X-RAY ACTIVITY	NO. OF SIDs																
	NO. X-RAY BTS.																
SF BST. ACTIVITY:	NO. OF cm BTS.																
	NO. cm-dm BTS.					1											
	NO. cm-m BTS.																
DYNAMIC RADIO EVENTS	NO. TYPE II																
	NO. TYPE IV																

TABLE 5.

The evolution, as monitored in calcium light, of those plages in which the proton flares of November 1977 and April–May 1978 developed (cf. Tables 1 and 10, respectively) together with corresponding details concerning their antecedent and descendent plages. The sources of these data together with complimentary information concerning plage related magnetic features, flare activity, SID's, X-ray bursts and single frequency and dynamic radio events, are described in Section 2.

5 DEVELOPMENTAL HISTORY AND ACTIVITY PROFILE OF McMATH PLAGE 15135

McMATH PLAGE NO.	DATA 1978	E (1) FEB. 1	2	3	4	5	6	7	8	9	10	11	12	13	14	W (1) FEB.
15135	PLAGE AREA #	400	1700	2800	3500	3200	3500	3500	3100	3100	3400	3400	3500		1600	
	INTENSITY	2.0	3.5	3.5	3.5	3.5	3.0	3.5	3.5	3.5	3.5	2.5	3.5		3.5	
MT.WILSON NUMBER 19950	MT. W. CLASS		(B)	(B)					(AP)							
	FIELD STRENGTH		3	4					3							
	AREA&		130		240	60	70	40	130							
	SPOT COUNT		4		13	4	9	4	11							
	NUAA CLASS		CAO		ESI	DSI	CAO	CSO	DSO							
MT.WILSON NUMBER 19951	MT. W. CLASS		(AP)	(BF)					(BF)							
	FIELD STRENGTH		3	4					4							
	AREA&		130	130	210	120	190	110						80	60	
	SPOT COUNT		1	1	6	4	24	15						2	1	
	NUAA CLASS		HSX	HSX	CHO	DHO	DAI	DSO						CSO	HSX	
H ALPHA ACTIVITY	REPT. FLARES	1(sf)	2(sf)	4(sf)	2(sf)	7(sf)	1(sf)	3(sf)	5(sf)	4(sf)		1(sf)	1(sf)		1(sn)	
			3(sn)	6(sn)		3(sn)		1(sn)		4(sn)						
				1(sb)		1(sb)										
				1(1n)												
				1(1b)												
X-RAY ACTIVITY	NO. OF SIDs			3		1										
	NO. X-RAY BTS.			2		1										
SF BST. ACTIVITY	NO. OF cm BTS.															
	NO. cm-dm BTS.			2												
	NO. cm-m BTS.															
DYNAMIC RADIO EVENTS	NO. TYPE II															
	NO. TYPE IV															

Thereafter, with the exception of an X-ray burst and an importance 1 SPA of Widespread Index 1 recorded on February 5 in association with the occurrence at 0014 UT of an importance sf flare, no other event recorded during the transit displayed associated activity.

4.3 Plage 15134

New adjacent Plage 15134, which came around the east limb on February 1, was associated with developing bi-polar group Mt. Wilson 19949. From approximately mid-transit, its characteristic of constituting a "highly variable" X-ray source was complimented by the corresponding close association between rather minor flaring in the plage and the production of time associated X-ray bursts and SID's, (see Table 6). Sometimes also, centimeter or centimeter-decimeter bursts of low mean peak flux density occurred in association with the observed flaring.

Examination of the original Mt. Wilson drawings reveals that, on February 8, when Plage 15134 was showing particular variability in X-rays and the region was especially flare active, a $\beta\delta$ configuration was present in the underlying spot group. No later spot drawings of the group are available, but NOAA reported a decline from Class ESO on February 8 to Class DSO by February 13.

An importance 1+ SID of Widespread Index 5, accompanied by an X-ray burst, broad band cm-dm radiation and Type II and Type IV events, which began on February 10 at 2103 UT during a gap in the optical observations, may also have been associated with unobserved flaring in this region-particularly since OSO-8 observers recorded a very dramatic peak in the level of X-radiation produced by the plage at 0100 UT on February 11. No other active center on the disk showed a corresponding level of X-ray activity.

4.4 Plage 15172

Plages 15134 and 15135 were deemed on their return during Carrington Rotation 1665, to form a single composite structure designated McMath Plage 15172, (see Table 7). Observers at Boulder recognized three spot groups as associated with this region at approximate mean latitudes N14°, N20°, and N27°. The level of X-ray activity as observed by OSO-8, as well as the frequency of X-ray burst and SID associated flaring within particular parts of the plage, appeared as could be deduced from those magnetic reports available from March 5 to depend intimately on the level of complexity of the immediately underlying spot group.

The most important flare to occur during this transit, a 2B event on March 6 at 1125 UT accompanied by an X-ray burst, an SID of importance 2 with Widespread Index 5, a broad band radio burst with mean peak flux density 50 sfu at 2650 MHz and a Type II event, occurred above that group located at N27° during an interval when it was waxing from NOAA Class HSX to Class CSO. Although this latter group had declined to Class HAX by March 9, it revived to reach Class DSI by March 10. The most energetic overlying flare to occur during this interval was an importance sn event at 0823 UT on March 9, accompanied by a broad band radio burst of mean peak flux density 4 sfu and duration 10 minutes at 3100 MHz.

TABLE 6.

The evolution, as monitored in calcium light, of those plages in which the proton flares of November 1977 and April-May 1978 developed (cf. Tables 1 and 10, respectively) together with corresponding details concerning their antecedent and descendent plages. The sources of these data together with complimentary information concerning plage related magnetic features, flare activity, SID's, X-ray bursts and single frequency and dynamic radio events, are described in Section 2. The conventions of presentation adopted are generally similar to those contained in Solar Geophysical Data (Supplement, No. 390, 1977. The number of flares identified within a particular plage, however, having an importance class with the range sf to 4b is indicated according to the scheme {number of flares identified (reported flare importance)} In cases where no importance rating was assigned in the source material to a particular flare, a suggested importance, based on such parameters as are available, is assigned by the author and the event listed according to the scheme 1? (i.e. suggested flare importance). The areas are measured in millionths of the solar hemisphere.

6 DEVELOPMENTAL HISTORY AND ACTIVITY PROFILE OF McMATH PLAGE 15134

McMATH PLAGE NO.	DATA 1978	E (1) FEB. 1	2	3	4	5	6	7	8	9	10	11	12	13	14	15	W (1) FEB.
15134	PLAGE AREA #	300	500	700	900	1100	1200	1400	1500	2100	2400	2400	2400		1800	500	
	INTENSITY	1.0	3.5	3.5	3.0	3.0	3.0	3.0	3.5	3.5	3.5	3.5	3.5		3.0	1.0	
MT.WILSON NUMBER 19949	MT. W. CLASS		(AP)	(B)					(D)								
	FIELD STRENGTH	2	3						4								
	AREA#	30	50	30	10	100	70	180						120	60		
	SPOT COUNT	2	2	3	2	16	13	15						2	1		
	NOAA CLASS	BXO	BXO	BXO	BXO	DKI	DAO	ESO						DSO	HSX		
H ALPHA ACTIVITY	REPT. FLARES		1(sf)	3(sf)	1(sf)		4(sf)	4(sf)	2(sf)	1(sf)	3(sf)	4(sf)	4(sf)		1(sn)		
				2(sn)				1(sn)	3(sn)	3(sn)		1(sn)	2(sn)				
				2(sb)					1(1n)	2(sb)		1(1f)	1(1n)				
				1(1n)						1(1n)							
										1?1n							
X-RAY ACTIVITY	NO. OF SIDs			1				1	3	3		1	1				
	NO. X RAY BTS.						2	3	3	1	2	3					
SP RST. ACTIVITY	NO. OF cm BTS.						1				1						
	NO. cm-dm BTS.							1	1								
	NO. cm-m BTS.																
DYNAMIC RADIO EVENTS	NO. TYPE II																
	NO. TYPE IV																

TABLE 7.

The evolution, as monitored in calcium light, of those plages in which the proton flares of November 1977 and April-May 1978 developed (cf. Tables 1 and 10, respectively) together with corresponding details concerning their antecedent and descendent plages. The sources of these data together with complimentary information concerning plage related magnetic features, flare activity, SID's, X-ray bursts and single frequency and dynamic radio events, are described in Section 2. The conventions of presentation adopted are generally similar to those contained in Solar Geophysical Data (Supplement, No. 390, 1977. The number of flares identified within a particular plage, however, having an importance class with the range sf to 4b 's indicated according to the scheme {number of flares identified (reported flare importance)}. In cases where no importance rating was assigned in the source material to a particular flare, a suggested importance, based on such parameters as are available, is assigned by the author and the event listed according to the scheme 1? (i.e. suggested flare importance). The areas are measured in millionths of the solar hemisphere.

DEVELOPMENTAL HISTORY AND ACTIVITY PROFILE OF McMATH PLAGE 15172

McMATH PLAGE NO.	DATA 1978	E (1) FEB. 28	1	2	3	4	5	6	7	8	9	10	11	12	13	14	W (1) MAR.
15172	PLAGE AREA @	800	3000	6000	7400	7400	7000	7000	7000	8000	8000	7800		7500	3200	1100	
	INTENSITY	1.0	4.0	3.5	3.5	3.5	3.5	4.5	3.5	3.5	3.0	3.5		3.0	2.0	1.0	
	MT. W. CLASS																
MT.WILSON NUMBER (N20)	FIELD STRENGTH: AREA@						380	380	320	380	240	340	340	160			
	SPOT COUNT						10	21	27	14	2	14	12	1			
	NOAA CLASS						EHI	EHO	EHI	EHI	EHO	CHI	CHO	HAX			
	MT. W. CLASS																
MT.WILSON NUMBER (N14)	FIELD STRENGTH AREA@						20	40	60	100	20	10	30				
	SPOT COUNT						1	14	15	16	3	2	3				
	NOAA CLASS						HSX	DSI	DSO	DAI	DSO	BXO	BXO				
	MT. W. CLASS																
MT.WILSON NUMBER (N27)	FIELD STRENGTH AREA@						50	50	40	40	40	50	50	50			
	SPOT COUNT						1	1	3	4	2	11	10	2			
	NOAA CLASS						HSX	HSX	CSO	CSO	HAX	DSI	DRO	CRO			
H ALPHA ACTIVITY	REPT. FLARES	1(sf); 4(sf); 1(1f); 2(sf)			2(sf)	2(sf)	2(sf)	4(sf); 1(sn)		2(sf); 1(sn)		2(sf); 1(sf)		2(sn); 1(sf)		1(sf); 1(sf)	
			1(sn);		2(sn);	1(sn)	3(sn);	1(sn);	1(sb);	1(sn);		2(sn);	4(sn);	1(sb);	2(sn);	1(1f);	
					1(1f);	3(1n);	1(sb);	1(2b);				1(sb);	1(1n);		2(sb);	1(1n);	
															1?sb;		
															1(1n);		
															1?1n;		
X RAY ACTIVITY	NO. OF SIDs			1	1	4	1	2		1					3		
	NO. X RAY BTS.					3	2	2		1					2		
SF RST. ACTIVITY	NO. OF cm BTS.					1											
	NO. cm-dm BTS.					1											
	NO. cm-m BTS.							1			1						
DYNAMIC RADIO EVENTS	NO. TYPE II				1			1									
	NO. TYPE IV																

4.5 Plage 15214

The inherent twin elements of composite Plage 15172 of the previous passage, were assigned numbers 15214 (rotation 4) and 15220 (rotation 3) during their March-April transit, (see Tables 8 and 9). Plage 15214, which had shown some X-ray variability during its previous passage, was again seen from OSO-8 to be variable during Carrington Rotation 1666. Observations were somewhat limited at both X-ray and optical wavelengths but, at least from April 7-9, a fairly high level of minor flaring, accompanied in particular on April 9 by X-ray burst and SID activity, was recorded in association with this region. A centimeter wave length burst of duration 4.3 minutes and mean flux density 8.1 sfu at 4995 MHz, was additionally associated with an importance sn flare at 0215 UT on April 9.

Underlying bipolar groups Mt. Wilson 19985 and 19994 appeared, from the available measurements, to have been of low field strength. Also, the plage was in a state of general decline as regards its area, and probably also its brightness, as it transited the west limb.

4.6 Plage 15220

Plage 15220 was in rapid decline as regards area and brightness during its March-April disk passage, (see Table 9). It produced several sub-flares while it was close to the east limb but no accompanying electromagnetic effects were reported.

4.7 Plage 15266

It might reasonably have been expected when Plages 15214 and 15220 transited the west limb during Carrington rotation 1666, that the overall trend of decay exhibited at these locations would be maintained. However, the emergence while the disturbed region was on the invisible hemisphere of new magnetic flux, particulary within the ambience of previously existing fields, so radically transformed the character of those plage elements present that, as already noted, the resultant structure may be deemed to have constituted a new feature (15266, incorporating but vestiges (15266') of previously recognizable plage components. See the overall "Activity Profile" presented in Table 10. Spot Groups Mt. Wilson 20018 and 20019 transiting beneath the "new" plage appeared to be returns of Group 19985 and 19994 of the previous rotation, although the birth of new flux had imparted to these previously decayed fields a greatly enhanced complexity. Mt. Wilson 20020 on the other hand was located in a previously undisturbed solar region to the east of the other groups.

Examination of center line and off band H-alpha pictures of the famous series of proton associated flares occurring in the plage on days April 28, 29, 30. and May 1 respectively, reveals that the events of April 28 and 30 avoided the large leading spots of Mt. Wilson 20018 and showed a preferred association with Group 20019, which displayed a $\delta(\beta\gamma)$ configuration on April 28. The flares of April 29 and May 1 on the other hand were associated with (δ) Mt. Wilson Group 20018. See the summary of

TABLE 8.

The evolution, as monitored in calcium light, of those plages in which the proton flares of November 1977 and April–May 1978 developed (cf. Tables 1 and 10, respectively) together with corresponding details concerning their antecedent and descendent plages. The sources of these data together with complimentary information concerning plage related magnetic features, flare activity, SID's, X-ray bursts and single frequency and dynamic radio events, are described in Section 2.

8 DEVELOPMENTAL HISTORY AND ACTIVITY PROFILE OF MCMATH PLAGE 15214

MCMATH PLAGE NO.	DATA	E (1) MAR. 28	29	30	31	1	2	3	4	5	6	7	8	9	10	11	W (1) APR.
15214	PLAGE AREA #:	1000	2400	3400	3500	3500	3000		2800	3000		2800	2500	1800	1300		
	INTENSITY	2.5	2.5	2.5	2.5	2.5	2.5		2.5	2.5		2.5	3.0	3.0	1.5		
	MT. W. CLASS	(B)															
MT.WILSON NUMBER	FIELD STRENGTH:	3															
17985	AREA#	10															
	SPOT COUNT	2															
	NOAA CLASS	BAO															
	MT. W. CLASS									B)				B)			
MT.WILSON NUMBER	FIELD STRENGTH:									1				3			
19994	AREA#																
	SPOT COUNT																
	NOAA CLASS																
H ALPHA ALTIVITY	REPT. FLARES		1(sn)				3(sf)			1(sf)	1(sf)	1(sf)	3(sb)		1(1n)		
										1(sn)	4(sn)	1(sn)					
											2(sn)	1(1n)					
X-RAY ALTIVITY	NO. OF SIDs											1	4		1		
	NO. X-RAY BTS.												2				
SF RDI. ALTIVITY	NO. OF cm BTS.												1				
	NO. cm da BTS.																
	NO. cm a BTS.																
DYNAMIC RADIO	NO. TYPE II EV:																
	NO. TYPE IV EV:																

TABLE 9.

The evolution, as monitored in calcium light, of those plages in which the proton flares of November 1977 and April-May 1978 developed (cf. Tables 1 and 10, respectively) together with corresponding details concerning their antecedent and descendent plages. The sources of these data together with complimentary information concerning plage related magnetic features, flare activity, SID's, X-ray bursts and single frequency and dynamic radio events, are described in Section 2. The conventions of presentation adopted are generally similar to those contained in Solar Geophysical Data (Supplement, No. 390, 1977. The number of flares identified within a particular plage, however, having an importance class with the range sf to 4b is indicated according to the scheme {number of flares identified (reported flare importance)} In cases where no importance rating was assigned in the source material to a particular flare, a suggested importance, based on such parameters as are available, is assigned by the author and the event listed according to the scheme 1? (i.e. suggested flare importance). The areas are measured in millionths of the solar hemisphere.

9 DEVELOPMENTAL HISTORY AND ACTIVITY PROFILE OF McMATH PLAGE 15220

McMATH PLAGE NO.		MAY 1978	E (1) MAR. 30	31	1	2	3	4	5	6	7	8	9	10				W (1) APR.
15220	PLAGE AREA #		700	800	1400	1600		1500	1500		1600	1400	1100	1000				
	INTENSITY		2.5	3.0	2.5	2.5		2.5	2.5		2.0	1.5	1.0	1.0				
MT.WILSON NUMBER 19990	MT. W. CLASS				X													
	FIELD STRENGTH				1													
	AREA#			30														
	SPOT COUNT			3														
	NOAA CLASS			BXO														
H ALPHA ACTIVITY	REPT. FLARES	1(sf)				1(sf)												
		1(sn)																
		1(sb)																
X-RAY ACTIVITY	FREQ. OF SIDs																	
	X RAY BTS.(FF)																	
SF RST. ACTIVITY	NO. OF cm BTS.																	
	NO. cm om BTS.																	
	NO. cm-m BTS.																	
DYNAMIC RADIO EVENTS	NO. TYPE II EV.																	
	NO. TYPE IV EV.																	

TABLE 10.

The evolution, as monitored in calcium light, of those plages in which the proton flares of November 1977 and April-May 1978 developed (cf. Tables 1 and 10, respectively) together with corresponding details concerning their antecedent and descendent plages. The sources of these data together with complimentary information concerning plage related magnetic features, flare activity, SID's, X-ray bursts and single frequency and dynamic radio events, are described in Section 2. The conventions of presentation adopted are generally similar to those contained in Solar Geophysical Data (Supplement, No. 390, 1977. The number of flares identified within a particular plage, however, having an importance class with the range sf to 4b is indicated according to the scheme {number of flares identified (reported flare importance)}. In cases where no importance rating was assigned in the source material to a particular flare, a suggested importance, based on such parameters as are available, is assigned by the author and the event listed according to the scheme 1? (i.e. suggested flare importance). The areas are measured in millionths of the solar hemisphere.

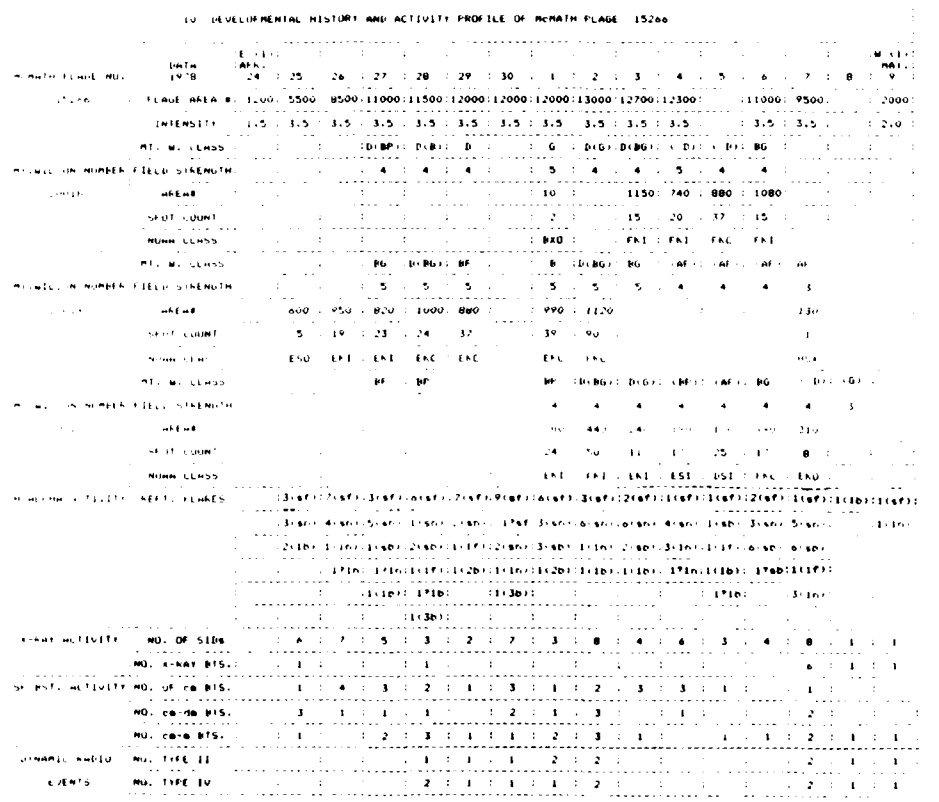

10 DEVELOPMENTAL HISTORY AND ACTIVITY PROFILE OF McMATH PLAGE 15266

		DATE 1978	APR. 24	25	26	27	28	29	30	MAY 1	2	3	4	5	6	7	8	MAY 9
McMATH PLAGE NO.																		
	PLAGE AREA @		1200	5500	8500	11000	11500	12000	12000	12000	13000	12700	12300		11000	9500		2000
	INTENSITY		1.5	3.5	3.5	3.5	3.5	3.5	3.5	3.5	3.5	3.5	3.5		3.5	3.5		2.0
	MT. WIL. CLASS					D(BP)	D(BG)	D		G	D(G)	D(BG)	D		D	BG		
MAGNETIC IN	NUMBER FIELD STRENGTH					4	4	4		5	4	4	5	4	4			
	AREA@									10		1150	740	880	1080			
	SPOT COUNT									2		15	20	37	15			
	NUMB CLASS									BXO		FKI	FKI	FKC	FKI			
	MT. WIL. CLASS					BG	D(BG)	BF		B	D(BG)	BG		AF	AF	AF		
MAGNETIC IN	NUMBER FIELD STRENGTH					5	5	5		5	5	5	4	4	4	5		
	AREA@		600	950	820	1000	880			990	1120					130		
	SPOT COUNT		5	19	23	24	37			39	90					1		
	NUMB CLASS		EAO	EAI	EKI	EKC	EKC			EKC	EKC					HSX		
	MT. WIL. CLASS				BF	BF				BF	D(BG)	D(G)	BF	AF	BG	D	G	
MAGNETIC IN	NUMBER FIELD STRENGTH									4	4	4	4	4	4	4	5	
	AREA@									90	440	240	190	110	190	210		
	SPOT COUNT									24	50	11	1	25	17	8		
	NUMB CLASS									EKI	EKI	EKI	ESI	DSI	EKC	EKO		
H-ALPHA FLARES			3(sf)	2(sf)	3(sf)	4(sf)	7(sf)	9(sf)	6(sf)	3(sf)	2(sf)	1(sf)	1(sf)	2(sf)	1(sf)	1(1b)	1(sf)	
			3(1n)	4(sn)	5(sn)	1(sn)	1(sn)	1*sf	3(sn)	6(sn)	6(sn)	4(sn)	1(sn)	3(sn)	5(sn)			1(1n)
			2(1b)	1(1n)	1(sn)	2(sn)	1(1f)	2(sn)	3(sn)	1(1n)	2(sn)	3(1n)	1(1f)	6(sn)	6(sn)			
				1*1n	1*1n	1(1f)	1(2b)	1(1n)	1(2b)	1(1b)	1(1n)	1*1n	1(1b)	1*1b	1(1f)			
					1(1b)	1*1b		1(3b)					1*1b	3(1n)				
						1(3b)												
X-RAY ACTIVITY	NO. OF SIDs		4	7	5	3	2	7	3	8	4	6	3	4	8	1	1	
	NO. X-RAY BTS.		1			1									6	1	1	
2F RAD. ACTIVITY	NO. OF cm BTS.		1	4	3	2	1	3	1	1	2	3	3	1	1			
	NO. cm-dm BTS.		3	1	1	1		2	1	3		1			2			
	NO. cm-m BTS.		1		2	3	1	1	2	3	1		1	1	2	1	1	
DYNAMIC RADIO EVENTS	NO. TYPE II					1	1	1	2	2					2	1	1	
	NO. TYPE IV					2	1	1	1	2					2	1	1	

information concerning these various events contained in Table 11.*

An importance sb flare at 0010 UT on April 28, accompanied by an importance 1 SID of Widespread Index 5, broad band radio radiation with maximum mean flux density 167 sfu at 2695 MHz and a Type IV event, also appears to have been associated with Group 20019.

On May 1, a broad band radio burst with maximum mean flux density 3.4 sfu at 2695 MHz and an accompanying Type II burst, occurred in association with an importance sn flare at 0538 UT above Mt. Wilson Group 20020. This latter group was waxing from Class β p to $\delta(\beta\gamma)$ configuration on this day and, thereafter, until Plage 15266 transited the west limb on May 9. All of the energetic flaring associated with this region (see the summary list in Table 10) occurred directly above the aforementioned group. OSO-8 observations indicate that the overlying active part of the plage, while constituting a variable X-ray source on the days previous to transit, became outstandingly variable by at least 0315 UT on May 7, that is prior to an importance 1n flare at 0327 UT accompanied by an importance 3 SID, and X-ray burst, broad band radio radiation with maximum mean flux density 250 sfu at 2695 MHz and Type II and Type IV events.

4.8 Plage 15314

Plage 15314 was a return of Plage 15266. During this transit, in Carrington Rotation 1668, it was associated with underlying Mt. Wilson spot groups 20044, 20048, and 20049, (see Table 12). Of the groups concerned, Mt. Wilson 20048 attained a $\beta\gamma$ configuration on May 27, declining thereafter in complexity to a bipolar state. Group 20049 showed more variability, first attaining a γ configuration on May 27 and after a general decline reverting again briefly to Class γ between May 31 and June 1. These variations were complimented by corresponding changes in the level of (localized) overlying flaring accompanied by X-ray bursts and/or SIDs, and in the ability of part of the supernatent plage to function as a "highly variable" source of X-rays. In some cases minor radio bursts accompanied the flaring, and in particular on May 28, a broad band burst with mean maximum flux density 5 sfu at 2695 MHz accompanied an importance 1b event at 1310 UT.

Mt. Wilson 20044 had attained a delta configuration by at least May 25 and retained a high level of complexity until June 1. Again, special periods of X-ray variability in the overlying plage, as detected by OSO-8, were complimented by corresponding variations in the level of X-ray burst and SID associated flaring produced at this location. Broad band radio bursts of low peak flux density additionally accompanied "ionizing" flares at 0630 UT and 1523 UT on May 30. The most energetic event to occur during this transit was an importance 3b flare at 1006 UT on May 31, accompanied by an SID of importance Class 2+ and Widespread Index 5, and an X-ray burst. Its accompanying broad band single frequency radiation achieved a mean maximum flux density of 49.2 sfu at 2695 MHz and associated Type II and Type IV bursts were produced.

Examination of underlying Group 20044 reveals that, between May 31 and June 1, its internal magnetic gradient decreased significantly. A further importance 1b flare above this location at 2113 UT on June 1, was reported in addition to ionizing and very minor broad band radio radiation, to be accompanied by a Type II burst. By

*A forthcoming paper (in preparation) will suggest that these were not in fact four independent flares but rather two complex flares each with two phases and two maxima.

TABLE 11

Data Relating to the Major Proton Associated Flares of April - May 1978.

Date 1978	Beg. UT	Max UT	End UT	Imp.	Underlying Spots Mt. Wilson Group	Mean Flux Density sfu.	Assoc.Dynamic Spectrum Events
			H Alpha Flare				
April 28	1306	1355	2232	3B	20019		
April 29	2036	-	2211D	2B	20018		
April 30	1420	1455	1859D	3B	20019		
May 01	1910	-	2230	2B	20018		
			Sudden Phase Anomaly				
April 28	1306	1332	1500	3+			
April 29	1854	1922	2126D	3			
April 30	1443	1457	1630	3			
May 01	1916	2008	2258	2+			
			Single Frequency Events at 2695 MHz.				
April 28	1303.4	1334.2	1639.2			5495	I,II,III,IV,V.
April 29	1852.3	1914.2	2046.8			1776	I,II,III,IV.
April 30	1419.5L	1459.5	1704.0			505	I,II,III,IV.
May 01	1917L	1929.5	2110D			643	I,II,III,IV.

TABLE 12.

The evolution, as monitored in calcium light, of those plages in which the proton flares of November 1977 and April-May 1978 developed (cf. Tables 1 and 10, respectively) together with corresponding details concerning their antecedent and descendent plages. The sources of these data together with complimentary information concerning plage related magnetic features, flare activity, SID's, X-ray bursts and single frequency and dynamic radio events, are described in Section 2. The conventions of presentation adopted are generally similar to those contained in Solar Geophysical Data (Supplement, No. 390, 1977. The number of flares identified within a particular plage, however, having an importance class with the range sf to 4b is indicated according to the scheme {number of flares identified (reported flare importance)}. In cases where no importance rating was assigned in the source material to a particular flare, a suggested importance, based on such parameters as are available, is assigned by the author and the event listed according to the scheme 1? (i.e. suggested flare importance). The areas are measured in millionths of the solar hemisphere.

12 DEVELOPMENTAL HISTORY AND ACTIVITY PROFILE OF MCMATH PLAGE 15314

MCMATH PLAGE NO.	DATA 1978	E (1/) MAY. 21	22	23	24	25	26	27	28	29	30	31	1	2	3	W (1/) JUN.
15314	PLAGE AREA @	1500	5100	8200	10000	11000	11300	12000	10700	10300	11500	11400	12000	1100	900	
	INTENSITY	3.5	3.5	3.5	3.5	3.5	3.5	3.5	3.5	3.5	3.5	3.0	3.5	3.0	3.0	
	MT. WL. CLASS	(BF)	(BP)			(D)	(D)	(D)	(D)	(D)	(G)	(G)	(G)	(BF)		
MT.WILSON NUMBER	FIELD STRENGTH	3	4			5	5	5	5	5	5	5	5	3		
20044	AREA@	70	480	70	640	760	650	580	480	500	550	360	260	260		
	SPOT COUNT	2	5	1	37	57	52	50	40	35	45	24	12	4		
	NUMA CLASS	CSO	DAC	CSO	FAC	FAC	FAI	FAI	FAI	FAI	FAC	FAI	D	H		
	MT. WL. CLASS					(AF)	(B)	(BG)	(BG)	(B)	(B)	(B)	(B)			
MT.WILSON NUMBER	FIELD STRENGTH					2	3	4	4	4	4	4	4			
20048	AREA@						20	70	100	220	150	110				
	SPOT COUNT						1	21	19	16	7	7				
	NUMA CLASS						DAI	DAI	DAI	DAI	DAO	DAO				
	MT. WL. CLASS					(AF)	(AF)	(G)	(BF	(BF)	(BF)	(AF)	(G)	(BF	(AF)	
MT.WILSON NUMBER	FIELD STRENGTH					5	5	5	6	5	5	5	5	5	4	
20049	AREA@				120	100	100	10	80	80	130	90				
	SPOT COUNT				1	3	5	9	8	7	2	1				
	NUMA CLASS			HSX	CSO	CSO	CSO	CSO	CSO	CSO	HSX					
H ALPHA ACTIVITY	REPT. FLARES	2(sf)	2(sf)	1(sf)	2(sn)	1(sf)	4(sf)	2(sf)	2(sn)	2(sf)	6(sf)	3(sn)	1(sf)	3(sn)	1(sn)	
		3(sn)	1(sn)	2(sn)	1(1b)	5(sn)	3(sn)	5(sn)	2(sn)	1(sb)	6(sn)	1(sb)	4(sn)	1(sb)	1(sn)	
		1(sbR		1(sb)	1?1b	2(sb)			1(1b)	1(1b)	1(sb)	1(3b)	1(1b)			
		1(1?)		1(1b)					2(1b)	1(1b)	1(1b)					
											1(2b)					
											1(2b)					
X-RAY ACTIVITY	NO. OF SIDs	1	1	1	1		3	1	4	4	7	2	1	2	1	
	NO. X-RAY BTS.	1	2		1		1	2	6	3	5	3	1	3	1	
SF RDF. ACTIVITY	NO. OF CB BTS.		1	1			1	1		3	6	1	1			
	NO. CB IB BTS.		1	1	2	1	2	3	3	3	3		1			
	NO. CB B BTS.								1		2	1		1		
DYNAMIC RADIO	NO. TYPE II											1	1			
EVENTS	NO. TYPE IV											1				

June 2, Group 20044 had declined to magnetic Class 2 p and no further energetic flares were seen to be associated with this region. A Forbush decrease of 5% which occurred near mid-day on June 2, might have been associated with the activity described in the previous paragraphs.

4.9 Plage 15368

Plage 15368 was a return of Plage 15314 in Carrington Rotation 1669 and was associated during this traverse with Mt. Wilson Group 20088, 20091, 20098, and 20100, (see Table 13). Of these, the bipolar Group 20100 marked the position of emergence of new flux while Groups 20091, 20088, and 20098 corresponded with previously transiting Groups 20049, 20044, and 20048.

The flare patrol was very incomplete during much of the relevant period, particularly on June 16 and from June 22-27 inclusive. On June 22 the largest recorded flare of the transit, an importance 2b event at 1643 UT occurred, accompanied by an importance 2+ SID of Widespread Index 5, broad band radio radiation with maximum peak flux density 51.6 sfu at 2695 MHz and associated dynamic events of Type II and IV. SID related flaring with some acompanying minor radio burst activity was also detected on June 20.

Examination of the Mt. Wilson drawings reveals that the immediately underlying spot group Mt. Wilson 20091, achieved a $\delta(\beta\gamma)$ configuration between June 19 and 20, declining to a β configuration by June 22. There was a revival in magnetic complexity between June 25 and 26 when a γ configuration was again attained. The available records indicate the complimentary presence of moderate flare activity, accompanied by low energy ionizing and/or radio radiation, from June 27 to June 30. Also, OSO-8 observations show that the relevant part of the active plage, while sustainedly constituting an X-ray source during its June transit, became "highly variable" between at least 1930 UT on June 28 and 0115 UT on June 29. The underlying spot group again decayed from configuration $\beta\gamma$ to configuration β p between June 28 and 29.

4.10 Plage 15420

Plage 15420 was a return of Plage 15368 in Carrington Rotation 1670. It was, however, so reduced in brightness and in area as to be a minor solar feature, (see Table 14) while associated Mt. Wilson Groups 20142 and 20150 were but vestiges of the corresponding main groups of the previous passage. Only one faint sub-flare was reported in the region during this transit and no associated X-ray activity was recorded.

4.11 Plage 15473

Plage 15473 was a scarcely perceptible return of Plage 15420 during Carrington Rotation 1671, (see Table 15). No flare of magnetic activity was reported in this region.

TABLE 13.

The evolution, as monitored in calcium light, of those plages in which the proton flares of November 1977 and April-May 1978 developed (cf. Tables 1 and 10, respectively) together with corresponding details concerning their antecedent and descendent plages. The sources of these data together with complimentary information concerning plage related magnetic features, flare activity, SID's, X-ray bursts and single frequency and dynamic radio events, are described in Section 2. The conventions of presentation adopted are generally similar to those contained in Solar Geophysical Data (Supplement, No. 390, 1977. The number of flares identified within a particular plage, however, having an importance class with the range sf to 4b is indicated according to the scheme {number of flares identified (reported flare importance)}. In cases where no importance rating was assigned in the source material to a particular flare, a suggested importance, based on such parameters as are available, is assigned by the author and the event listed according to the scheme 1? (i.e. suggested flare importance). The areas are measured in millionths of the solar hemisphere.

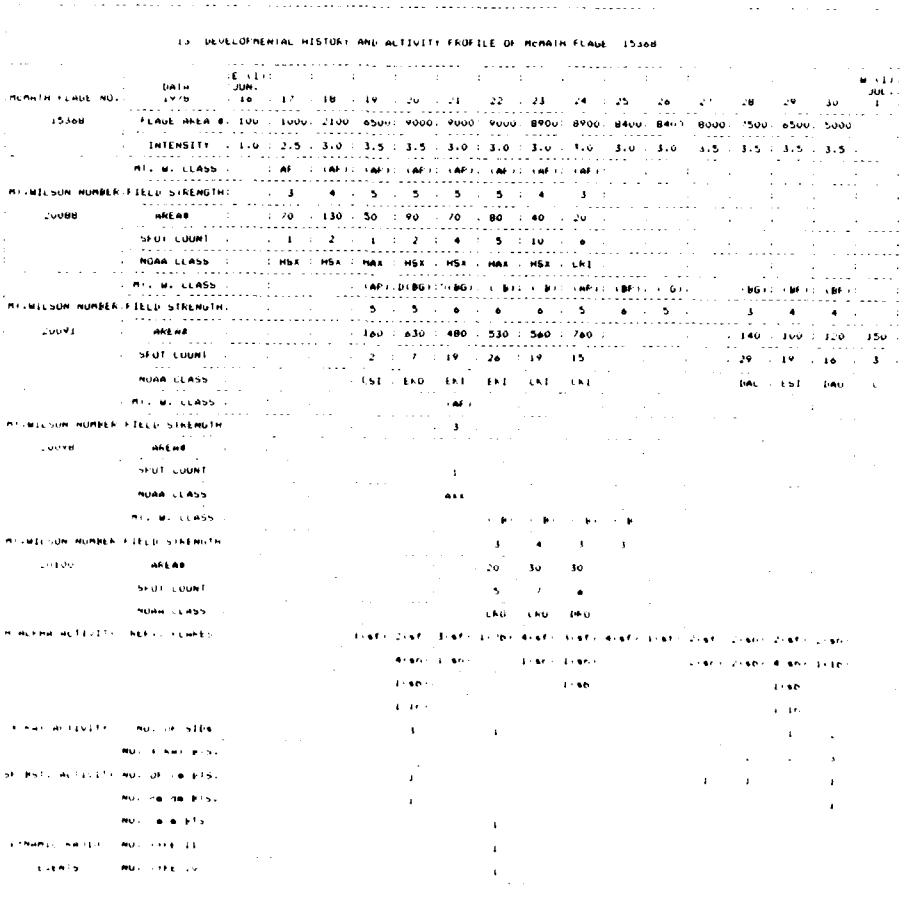

TABLE 14.

The evolution, as monitored in calcium light, of those plages in which the proton flares of November 1977 and April–May 1978 developed (cf. Tables 1 and 10, respectively) together with corresponding details concerning their antecedent and descendent plages. The sources of these data together with complimentary information concerning plage related magnetic features, flare activity, SID's, X-ray bursts and single frequency and dynamic radio events, are described in Section 2. The conventions of presentation adopted are generally similar to those contained in Solar Geophysical Data (Supplement, No. 390, 1977. The number of flares identified within a particular plage, however, having an importance class with the range sf to 4b is indicated according to the scheme {number of flares identified (reported flare importance)} .

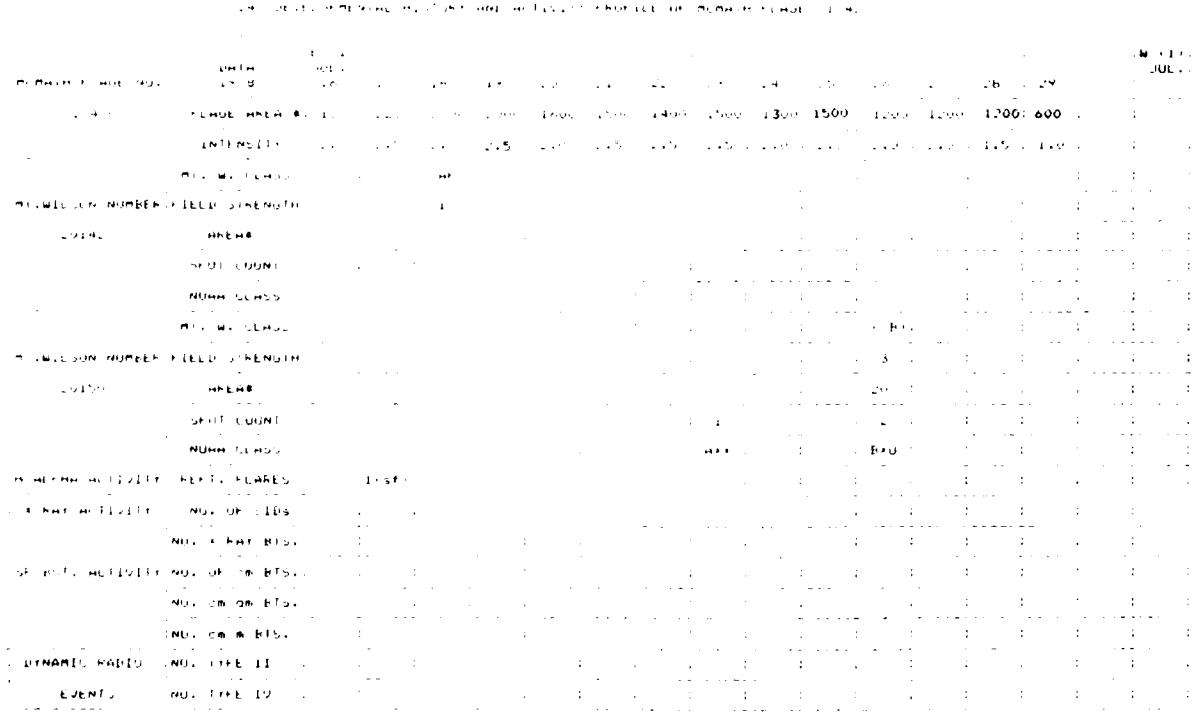

TABLE 15.

The evolution, as monitored in calcium light, of those plages in which the proton flares of November 1977 and April-May 1978 developed (cf. Tables 1 and 10, respectively) together with corresponding details concerning their antecedent and descendent plages. The sources of these data together with complimentary information concerning plage related magnetic features, flare activity, SID's, X-ray bursts and single frequency and dynamic radio events, are described in Section 2. The conventions of presentation adopted are generally similar to those contained in Solar Geophysical Data (Supplement, No. 390, 1977. The number of flares identified within a particular plage, however, having an importance class with the range sf to 4b is indicated according to the scheme {number of flares identified (reported flare importance)} In cases where no importance rating was assigned in the source material to a particular flare, a suggested importance, based on such parameters as are available, is assigned by the author and the event listed according to the scheme 1? (i.e. suggested flare importance). The areas are measured in millionths of the solar hemisphere.

15 DEVELOPMENTAL HISTORY AND ACTIVITY PROFILE OF MCMATH PLAGE 154?:

MCMATH PLAGE NO.:	DATA 1978	E 12 AUG. 13	14	15	16	17	18	19	20	21	22	23	24	W (1) AUG.
154?3	PLAGE AREA #.	100	200	200	100	200	300	300	300	200	200	200	200	
	INTENSITY	1.0	1.0	1.5	1.0	1.0	1.0	1.5	1.5	1.5	2.0	1.0	1.5	
	MT. W. CLASS													
MT.WILSON NUMBER	FIELD STRENGTH													
----	AREA#													
	SPOT COUNT													
	NOAA CLASS													
H ALPHA ACTIVITY	REPT. FLARES													
X-RAY ACTIVITY	NO. OF SIDs													
	NO. X-RAY BTS.													
SF RST. ACTIVITY	NO. OF 3m BTS.													
	NO. 3m-9m BTS.													
	NO. 9m-# BTS.													
DYNAMIC RADIO	NO. TYPE II													
EVENTS	NO. TYPE IV													

5. DIFFERENCES AND SIMILARITIES BETWEEN THE PROTON PRODUCING REGIONS

Plage 15031, parent to the November 22 proton event, which was born in a previously "quiet" solar region, remained identifiable during only two solar rotations and constituted a feature of negligible solar importance during its second traverse. Plage 15266 on the other hand, parent to the April-May series. was born among the remanents of a previously existing active region and continued to retain its new identity over five full rotations.

In both instances, an anomalous magnetic situation characterized that part of the photosphere directly underlying the active plage. No white light pictures were available on November 22 but delta configuration and reversed polarities were reported to be present in associated Mt. Wilson Group 19894 on preceeding days. In the case of the April-May events, the birth of new flux inside the boundaries of an already existing, but greatly decayed, magnetic region, resulted in the build up of an especially complex magnetic situation, and associated Mt. Wilson Groups 20018 and 20019, both displayed a delta configuration by (at least) April 28, (the day of the first major proton flare).

An impression is given by the records that the occurrence of the November 22 flare may have been associated with an accelerated decay of underlying Group Mt. Wilson 19894 which had declined to an α f configuration by November 24. In the case of Groups 20018 and 20019, the intermittent emergence, within and close to the same general location, of further flux over a period encompassing several subsequent rotations, counteracted any incipient general tendency towards magnetic decline after the major flare series.*

6. POSSIBLE COMMON RELATIONSHIP OF THE ACTIVE REGIONS TO A LONG LIVED SUB-PHOTOSPHERIC SOURCE OF MAGNETIC FLUX

The history of the rise and decline of Plage 15031 and 15266 given in Sections 3 and 4, forms part of a larger study made by the author of the waxings and wanings of all active regions with a zone of northern solar hemisphere extending between heliographic Carrington longitudes L25° and L85°, over the periods of their visibility from Earth during Carrington Rotation 1659-1672 (i.e. within the bridging interval of a terrestrial year from September 1977 to September 1978).

Against this background, which involved the study of 30 independent plages, some 8 of which executed three or more traversals of the solar disk, it was noted that the ability of a particular plage to survive depended directly on the level of complexity of its underlying magnetic field. Within the atmospheric zone considered, strong fields surfaced only within a narrow band extending roughly from mean latitudes N16° - N26°. To the north and south of this domain, the fields that emerged were markedly weaker with no recorded births to the north of mean latitude N39° and to the south of mean N13°. Since the level of flaring observed within a particular plage was itself a close function of the level of complexity of the underlying magnetic field, the locations at which energetically important flares were triggered

* Compare with the recovery of the magnetic field strength exhibited on two occasions by that part of Mt. Wilson Group 14284 directly underlying the trigger point of a sequence of three homologous proton flares in McMath Plage 5265, (McKenna-Lawlor, 1980).

showed the same latitude dependency as that exhibited by long-lived plages and complex magnetic fields.

Those plage sequences producing the various proton flares considered (and many other energetically significant events as monitored by their electromagnetic accompaniments), were further spatially associated with a persistent, although somewhat intermittently yielding "well-spring" of magnetic flux, situated between heliographic longitudes L52° - L79°*. Specifically, Mt. Wilson Group 19984, underlying "November" Plage 15031, was reported on emergence** to be located at mean latitude N23° and mean heliographic longitude L61°.

Mt. Wilson Groups 20018 and 20019, underlying that western part of Plage 15266 associated with the production of the April-May proton flare, (see Section 4) were, on the other hand, reported on emergence to extend between mean latitudes N19°-N25° and mean heliographic longitudes L71°-L79°. A temporally and spatially related group which developed at mean latitude N25° and mean heliographic longitude L52° was especially associated with energetic flaring showing a different morphology to that of the homologous proton events but present in the eastern part of the same plage.

These spatial relationships suggest that while their component plage structures and precise positions were different, the important proton flares of November 22, 1977 and April-May 1978 may have constituted responses to instabilities associated with the presence beneath the photosphere of an anomalous region capable of causing the episodic emergence over an extended time period of strong magnetic flux within the confines of a solar zone lying roughly between latitudes N16° - 26° and mean heliographic longitudes L52° - L79°.

Compare this finding with the assertion by Svestka (1968) that "proton flare activity regions are not randomly distributed on the solar disk but tend to occur in complexes of activity which stay on the solar surface for many months and even years". See also Dodson and Hedeman (1968) and a general discussion of related work by Svestka (1976).

Acknowledgments

My best thanks are due to E. Ruth Hedeman of the McMath-Hulbert Obseratory for valuable discussions and for the gift of on and off-band McMath H-alpha spectroheliograms of the proton flares of April 28 - May 1, 1978.

* Another "well-spring" of flux, associated with the production, in other plage sequences, of energetically significant flares between September 1977 and September 1978, were located, within the same latitude limits, between heliographic longtitudes L29° and L32°.

** A systematic change with time of solar longitudes in a direction opposite to that of solar rotation was exhibited by all of the plages studied.

References

Dodson, H.W., and Hedeman, E.R.: 1968, "Some patterns in the development of centres of solar activity, 1962-1968", in K.O. Kiepenheuer (ed.), *Structure and Development of Solar Active Regions*, Proc. IAU Symp. No. 35, D. Reidel Publ. Co., Dordrecht, p. 56.

McKenna-Lawlor, S.M.P.: 1980, "Short-term prediction of the potential of an active region to produce recurrent proton flares", in R.F. Donnelly (ed.), *Solar-Terrestrial Prediction Proceedings*, Vol. *III*, U.S. Department of Commerce, NOAA, ERL, Boulder, Colorado, p. C-12.

Svestka, Z.: 1968, "Loop prominence systems and proton-flare active regions", in K.O. Kiepenheuer (ed.), *Structure and Development of Solar Active Regions*, Proc. IAU Symp. No. 35, D. Reidel Publ. Co., Dordrecht, p. 287.

Svestka, Z.: 1976, *Solar Flares*, Geophysics and Astrophysics Monograms Vol. 8, D. Reidel Publ. Co., Dordrecht.

Discussion

Dryer: Concerning the two pairs of flares (28, 29, 30 April 1978 and 1 May 1978), would you think that a repetitive twist-flare-relaxation, followed by a repetition of this pattern (such as the ideas of Tanaka and Nakagawa) could have taken place here?

McKenna-Lawlor: That is very interesting suggestion. It is certainly feasible and I would like to explore the possibility further.

11. Theoretical MHD Simulations of Coronal Transients and Interplanetary Observations

M. Dryer
Space Environment Laboratory, NOAA/ERL
Boulder, Colorado 80303, U.S.A.

R. S. Steinolfson
The University of Alabama in Huntsville
Huntsville, Alabama 35899, U.S.A.

Z. K. Smith
Space Environment Laboratory, NOAA/ERL
Boulder, Colorado 80303, U.S.A.

Abstract

A major long-range goal of theoretical simulations of solar-generated disturbances (transients, coronal holes, etc.) is the realistic modeling of a propagating disturbance from the sun into and throughout interplanetary space. Simulations of this kind, using MHD fluid theory, must always be confronted with observations in order to assess the degree to which one or the other is inadequate. We describe some of this on-going work which is concerned with both one- and two-dimensional, time-dependent MHD simulations.

The first example of such work begins with the simulation of a flare-produced coronal transient. In this case, a sudden current pulse is assumed to produce emerging magnetic flux. This "magnetic pulse" is sufficient to drive a weak shock wave into the solar wind by virtue of an outwardly-directed Lorentz force. Explicitly the pulse is assumed to consist of a linearly-increasing (with time) magnetic field of 0.72 G at the base of a closed magnetic topology (initially in hydrostatic equilibrium) to a value ten times larger over a 10-minute period. The shock achieves a velocity of 230 km s^{-1} (which would be superimposed upon the existing solar wind).

A second example is concerned with a series of corotating interaction regions which were observed during a 60-day period by Pioneers 10 and 11 in 1973 prior to, during, and subsequent to the former spacecraft's flyby of Jupiter. An opportunity for a stringent test of our one-dimensional model was made possible by the nearly radial alignment of these two spacecraft. By using the upstream spacecraft data as input into the time-dependent MHD model, we obtained a simulation of the solar wind characteristics at Jupiter that compared very well to the actual solar wind plasma and magnetic field data that were measured by Pioneer 10 at that planet.

These examples dramatically illustrate the need for extensive observational information at the inner boundary in order to assess the validity of any comprehensive, self-consistent theoretical model. The second example dramatically illustrates the desirability of using actual data for both input and downstream comparison in order to assess the validity of a relatively straight-forward, yet comprehensive, self-consistent theoretical model. On the other hand, the first example has not been tested with actual data as yet, although remote observations of white-light density enhancements and type II shock velocities offer guidance for post-flare diagnostics. In the absence of additional data close to the sun (such as densities, velocities, temperatures and magnetic fields), we suggest that there is, at this time, no alternative to resorting to certain assumptions (such as the current pulse used herein) concerning the forcing function for initiation of multi-dimensional MHD simulation models of cause-and-effect.

I. INTRODUCTION

It has become abundantly clear to observers and theoreticians alike that the field of solar-terrestrial physics will progress only through coordinated, interdisciplinary observations suggested by the title of this symposium and their direct confrontation with theoretical models and simulations. The ambitious plans outlined for the spacecraft partners in the observational phase in the 1980s and 1990s by Bohlin and Chipman (1980) should be complemented by a strong theoretical program.

It is our contention that dynamic MHD models and simulations should play a major role in such an international program. Non-self-consistent phenomenological models (often referred to as "cartoons" in the magnetospheric physics community) are no longer adequate or satisfactory as noted by the U.S. Space Science Board (1978). Kuperus (1980) notes that numerical fluid calculations give promising results, notwithstanding the restrictions the theoretician is forced to make. He notes, further, that these calculations ought to be made in three dimensions using kinetic theory instead of the fluid approximation in order "to give full credit to all possible wave modes and interactions." Indeed, the philosophy and strategy for the temporal three-dimensional approach, taking the solar surface and the boundary of the heliosphere (as the inner and outer boundaries, respectively) into account, have been outlined by Wu (1980) and Yeh (1980). Also, Nakagawa, Wu and Han (1980) have described a quasi-three-dimensional MHD model (often referred to as the 2 1/2-dimensional model in fusion research). In addition, both Wu (1980) and Cuperman (1980) have noted the relative merits and limitations of the fluid vis-à-vis kinetic approach and the need for more physical insight via a "hybrid" treatment. This latter approach has met with some success in pioneering simulations for laboratory fusion processes (Liewer and Krall, 1973). Cuperman (1980)

recommends a three-pronged strategy in this regard: (i) development and use of higher-order moments (fluid) equations as well as more realistic closure conditions and transport coefficients for the macroscopic description of the solar wind; (ii) use of computer simulation experiments on the nonlinear collective relaxation process through particle-wave-particle interaction due to plasma electromagnetic instabilities; and (iii) the hybrid strategy wherein collective interactions in the evaluation of transport coefficients, as deduced from quasi-linear theory and computer simulation experiments, are incorporated into the higher order moment equations.

The reader will recognize that an ambitious plan, such as that outlined above, should advance in an orderly fashion from the present state-of-art. The present models contain the basic physics necessary to study the large-scale, gross observations but do not contain the mathematical and physical elegance noted above. Such elegance, we believe, is required for study of the finer details of the bulk flows and are not necessary for our present purposes in the discussion which follows below. This paper will direct attention to several examples representative of present dynamical, MHD, fluid models. We have chosen the following examples:

(i) Two-dimensional, time-dependent, planar MHD model for coronal mass motion as a result of an emerging magnetic flux through the photosphere; and

(ii) One-dimensional, time-dependent, MHD model for solar wind dynamics as a result of interaction among multiple, coronal-hole-generated, corotating structures which were measured by Pioneers 10 and 11 during two solar rotations when these spacecraft were essentially co-linear with the sun.

The strategy adopted in the first example has been reviewed most recently by Wu (1980) and extended by Steinolfson and Wu (1980.) It has been recognized by some observers (c.f., Anzer, 1980; Sheridan, 1980, Gergely and Kundu, 1980; and Maxwell and Dryer, 1980) as a viable model for providing insight to the phenomenon of coronal transients (c.f., Michels et al., 1980). It is important to note that this approach does not consider the original flash phase of a flare or triggering mechanism for an eruptive prominence. This primary phase is associated with current sheet disruptions (Syrovatskii and Somov, 1980; Somov and Syrovatskii, 1980; and Sermulina et al., 1980) and rapid conversion of the magnetic energy stored within force-free magnetic topologies into thermal and kinetic energetic forms. The subsequent phase does not consider these initial physical processes; instead, their consequences may be considered as producing a thermal or magnetic pulse with a certain magnitude as well as temporal and spatial extent. During this secondary phase (coronal mass motion which moves, generally preceded by an MHD shock if the pulse is sufficiently large, into interplanetary space), the relative degree of wave propagation and mass motion is determined by dynamical interplay between plasma motion, plasma forces, and magnetic forces as characterized by the plasma β (ratio of thermal to magnetic pressure). "Magnetic control", then, is actually one of modulation of this secondary phase. That is, as $\beta \to 0$, there will be minor plasma mass motion, but there will be rapid MHD wave motion which will steepen into a weak fast-mode shock. Alternatively as β increases to, say, 0.1 or greater, substantial mass motion (supplied from the chromospheric layer), accompanied by nonlinear MHD waves' steepening into a shock wave, most definitely will take place and will be detected as a type II radio burst. Additional diagnostics will include type IV radio emission due, presumably, to gyrosynchrotron radiation (or even plasma oscillations as suggested for very bright events by Duncan, Stewart and Nelson, 1980) and white light coronal transients. The case discussed here is the simulation of the coronal response to a magnetic pulse. It will be shown that β (r, θ, t: where r is radial distance, θ is the solar latitude, and t is time after the pulse is initiated)

exhibits values over a wide range, both $\gtrless 1$. Thus, the degree of magnetic modulation ("magnetic control," if you will) must be examined to discern its dependence on the relative contribution of inertial, thermal, gravitational, and magnetic forces.

The strategy adopted in the second example noted above is to consider the extension to 5 AU of a series of high speed streams during a 60-day period in late 1973. Coronal-hole-generated high speed streams, rather than flares, are assumed to be responsible for these observations by Pioneers 10 and 11. The basic physics of the "secondary phase" must be the same as for that following flares, even though the coronal hole's solar surface boundary conditions and their initial values are different - and undoubtedly milder - than those for the flare so that the ensuing mass motion and wave propagation are also milder. However, it is well-known that the longer-lasting energy and momentum addition to the solar wind will also produce MHD shock waves at large distances (sometimes even within 1 AU). It is now known that these convective pressure pulses, sometimes bounded by forward and reverse MHD shock waves, buffet the planetary magnetospheres of Earth and Jupiter and produce substantial, albeit temporary, deformation of their bow shock waves and magnetopauses. The shocks themselves also produce local acceleration of solar wind protons to near-MeV energies as well as a chopper-like modulation of energetic Jovian electrons.

It is our intention, then, to present two examples of dynamic MHD modeling - one close to the sun, the second far from the sun - to demonstrate the necessity for modeling which considers the region of space from the sun outward, in a continuous fashion, to the distant reaches of the heliosphere.

2. RESULTS AND DISCUSSION

We now discuss the two examples which were outlined in the Introduction.

2.1 Two-Dimensional, Time-Dependent, Planar MHD Model Near the Sun

The basic equations and assumptions made in the development of this model have been described by Steinolfson et al., (1978) and will not be repeated here. Although thermal pressure pulses have mainly been considered (Steinolfson et al., 1978; Dryer et al., 1979; Dryer and Maxwell, 1979) the present example assumes that the pulse at the coronal base is produced by emerging magnetic flux due to a hypothesized sub-photospheric current pulse. This work, described by Steinolfson et al. (1979), assumes the pre-pulse, steady-state, coronal atmosphere to be permeated by a force free closed magnetic topology. We repeat some of the features described by this latter paper.

We consider a model in which the driving force (the solar event) is created when new magnetic flux due to photospheric currents emerges through the solar surface and interacts with the pre-existing field. There is a growing body of observational data which supports this possibility for some forms of solar activity. This emerging flux model has been speculated on for some time from a

theoretical viewpoint as well (see, e.g., Tur and Priest, 1978, and Syrovatskii and Somov, 1980). The driving force created by the emerging flux consists of an increase in the magnetic pressure producing an outwardly directed Lorentz force. The thermal pressure also increases in the simulated solar event, but it increases as a result of the emerging flux rather than independently as in previous studies.

The model we use is applicable to a meridional plane and is similar to that used by Steinolfson et al. (1978). We assume that the solar atmosphere can be treated as a single fluid with negligible dissipative effects. The necessary time-dependent equations are given there and will not be repeated here.

The atmosphere is assumed initially to be in hydrostatic equilibrium and to obey a polytropic law with a polytropic index, γ, of 1.1. The initial thermodynamic conditions at the base of the atmosphere (1.0 $r_\odot$) are temperature $T = 2.5 \times 10^6$K and number density $n = 3 \times 10^8$ cm^{-3}. The initial magnetic field is assumed to be force free and is calculated as discussed by Steinolfson et al. (1978, Paper I). A schematic of the initial field is shown in Figure 1. The magnetic field configuration at time $t = 0$ in this Figure is referred to as a "closed-field" configuration in Paper I since simulated solar events at the solar surface near the equator produce transients which must propagate across the field lines in order to reach the outer corona. The magnitude of the initial magnetic field B is taken to be such that B = 0.72 G at the solar base at the equator.

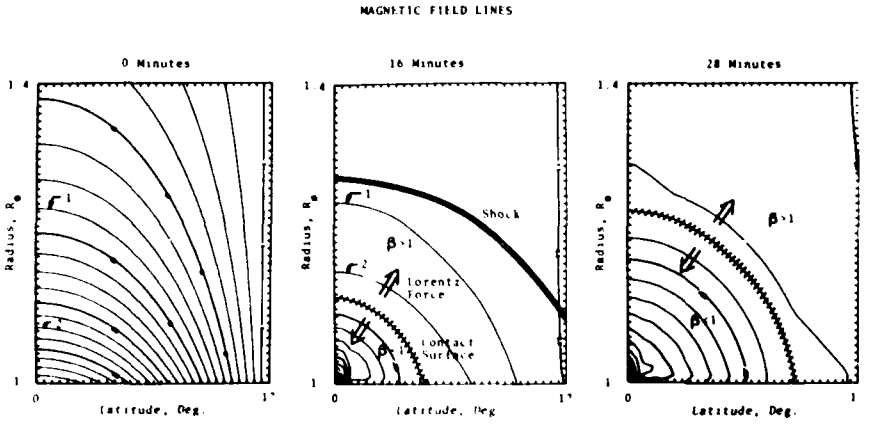

Figure 1. The magnetic field lines initially and after 16 and 28 minutes. The equator is at the left-hand edge on each plot and the solar surface at the base. The magnetic field is in the clockwise direction. Several representatives field lines, labeled 1 and 2 at t = 0 min., are also shown at t = 16 min.

The emerging magnetic flux is assumed to be due to a photospheric line current flowing into the plane of the paper in Figure 1 at the equator and 7000 km

below the solar surface. This current produces an emerging field in the same direction as the initial field so the Lorentz force created when they interact is directed outward. The photospheric current is increased linearly over a 10-minute period, and its final magnitude enhances the magnetic field at the solar surface at the equator by a factor of 10 over its initial value.

The time-dependent coronal response to the emerging flux is calculated by numerically solving the time-dependent equations in Paper I. The solution is symmetric about the equator. Thus, the computations are performed, and the results are presented, only for the region shown in Figure 1.

The magnetic field lines, initially and after 16 and 28 minutes of physical time, are shown in Figure 1. The outward motion of the field lines is indicated by the displacement of the field lines labeled 1 and 2. Since the electrical conductivity is infinite in this study, fluid particles remain attached to the field lines. As a result, the field line initially at the solar surface represents the contact surface at later times and separates initial coronal material from new material flowing upward through the coronal base. The contact surface is indicated by the field line with the short hatched lines across it in Figure 1.

A shock is formed ahead of the coronal disturbance as a natural consequence of the non-linear MHD. Once the shock is formed it moves outward without regard to the emerging flux. The shock has propagated beyond the region shown in Figure 1 for t = 28 minutes. The initial coronal material between the shock and the contact surface has been heated, compressed and accelerated by the shock, while the new material behind the contact surface has been heated and compressed by the emerging flux. The Lorentz force is directed outward between the shock and the contact surface and is directed inward below the contact surface. The plasma beta (β) is greater than unity above the contact surface and less than unity below it indicating the relative importance of the magnetic and thermal forces in the two regions.

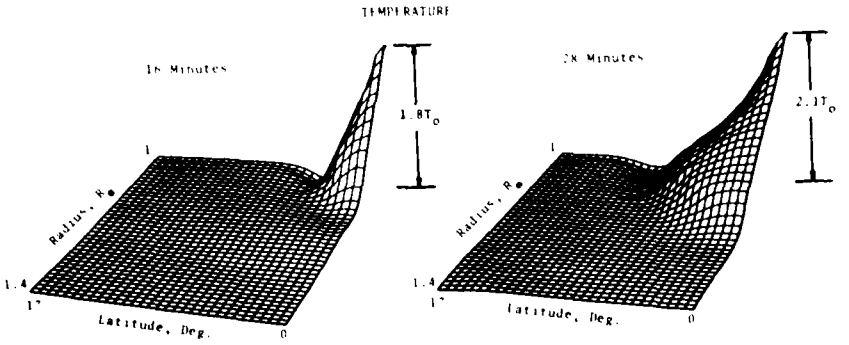

Figure 2. The temperature after 16 and 28 minutes referenced to the initial temperature at each point. The equator is at the right-hand edge and the solar surface at the top.

The major difference between the present results for emerging magnetic flux and the results obtained for a thermal pressure perturbation (as in Steinolfson et

al., 1978; and Dryer et al., 1979) is the presence of the inward directed Lorentz force below the contact surface. The Lorentz force tends to retard the outward motion of the new material, but the resulting increase in magnetic and thermal pressure drives the material outward. The tendency for the Lorentz force to trap the material behind the contact surface causes the emerging field to heat and compress it as shown on the next two figures which show carpet plots of the temperature and density, respectively, after 16 and 28 minutes. The values plotted in the figures are the physical quantities normalized by the initial values at each point. As shown in the figures, the temperature increases by a factor of about 2 at most, and the density by a factor of about 4. The contact surface is just ahead of the temperature maximum in Figure 2 and just ahead of the density minimum in Figure 3. This hot, dense region near the solar surface may be responsible for producing the X-rays often seen in solar events. For all simulations using a thermal pressure perturbation, the temperature and density below the contact surface are anti-correlated thereby reducing the possibility of producing X-rays.

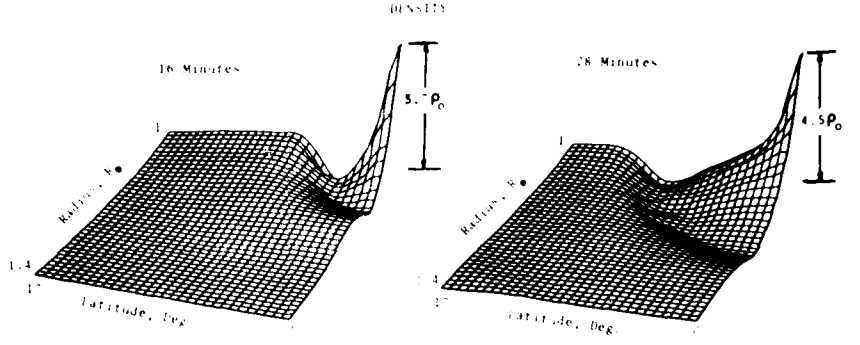

Figure 3. The density after 16 and 28 minutes referenced to the initial density at each point. Orientation is the same as for Figure 2.

There is only a slight increase in the thermodynamic quantities across the shock wave since the shock is weak and γ is small. There is a relatively large increase in the plasma velocity across the shock, however, as indicated in Figure 4 which shows the plasma velocity vectors.

It is apparent that emerging magnetic flux will produce an interplanetary disturbance. This is more obvious in Figure 5 which shows the shock and contact surface trajectories along the equator. Although we have only followed the disturbance for 30 minutes, both the shock and the contact surface have reached constant velocities and will presumably continue on outward into the interplanetary medium. For the thermal pressure perturbation used in the closed-field configuration by Steinolfson et al. (1978), none of the material below the contact

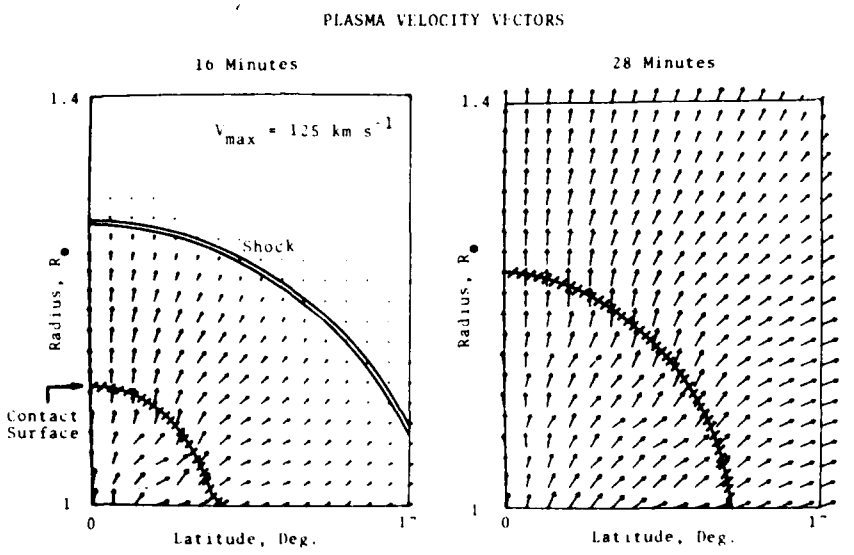

Figure 4. The plasma velocity vectors after 16 and 28 minutes. Orientation is the same as for Figure 1. Each vector points in the direction of the velocity and has a length proportional to the velocity at its base. As noted in the box for t = 16 min., the largest velocity at this time is 125 km s^{-1}.

surface reached the outer corona. Note that the shock velocity is quite low, much less than the values of 1000 km/sec, or even greater, detected by type II radio emission (Stewart, 1980). We have not investigated this example further to determine the behavior of such a simple emerging flux assumption on a longer time scale or by using large current pulse magnitudes. It might even be appropriate to suggest that flares with flash phases (e.g., Somov and Syrovatskii 1980; Sermulina et al., 1980) associated with current sheet disruptions (not considered here) may well be shown, with such a model, to have large thermal pulses as well, as suggested by Dryer and Maxwell (1979) and Maxwell and Dryer (1980). It is of particular importance that cause-and-effect (the former as just discussed; the latter as measured in the interplanetary medium) be studied with synoptic spacecraft measurements. A limited amount of research in this regard has been performed by Gosling et al. (1975) and Wu et al. (1976) who make phenomenological associations of coronal transients, as observed via Skylab and OSO-7 white-light observations, with Pioneer 9 and 10 (respectively) *in situ* plasma observations of the shock waves and disturbed solar wind which followed these shock precursors.

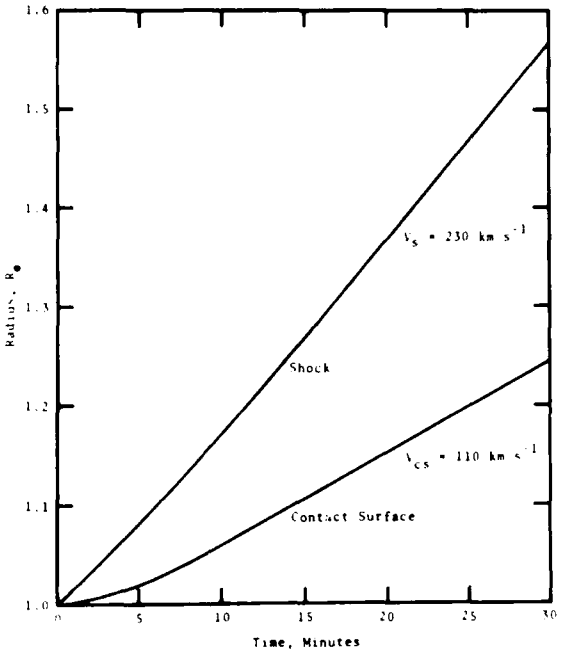

Figure 5. Trajectories of the shock and the contact surface along the equator.

2.2 One-Dimensional, Time-Dependent MHD Model Far From the Sun: Direct Comparison with Pioneer 10/11 Observations

The radial alignment of Pioneers 11 and 10 (at ~ 2.8 and 5.0 AU, respectively) with the sun provided an excellent opportunity to test a one-dimensional MHD model (Steinolfson, Dryer and Nakagawa, 1975) via a direct confrontation with plasma and magnetic field observations. The present study is an extension of that already published by Dryer et al. (1978). It is an extension in time to demonstrate the simulated corotating interaction regions (CIRs) which buffeted Jupiter before, during, and after the Pioneer 10 encounter with the Jovian magnetosphere as discussed by Smith, Fillius, and Wolfe (1978).

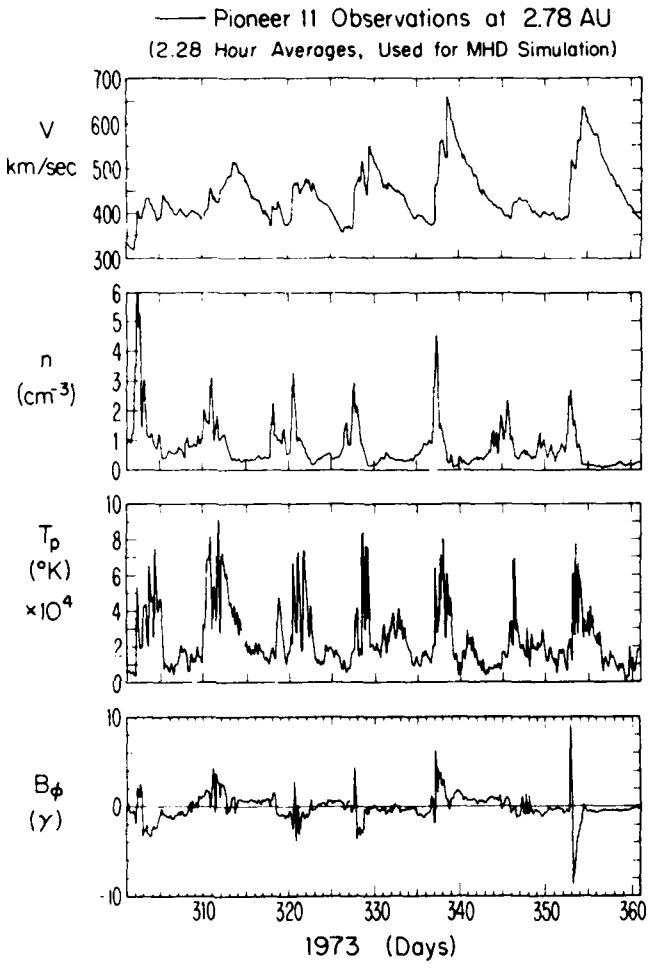

Figure 6. Pioneer 11 observations at 2.78 AU. These parameters are used as input for the MHD modeling.

Figure 6 shows the solar wind velocity, density, proton temperature, and azimuthal magnetic field measured from Day 301 to Day 361, 1973, by Pioneer 11. This spacecraft was initially located at ~ 2.78 AU and was aligned with Pioneer 10 which (during this epoch) approached Jupiter, flew past this planet within its magnetosphere, and continued beyond Jupiter in the solar wind. The data shown in Figure 6 were used as a 60-day "forcing function" for the one-dimensional model

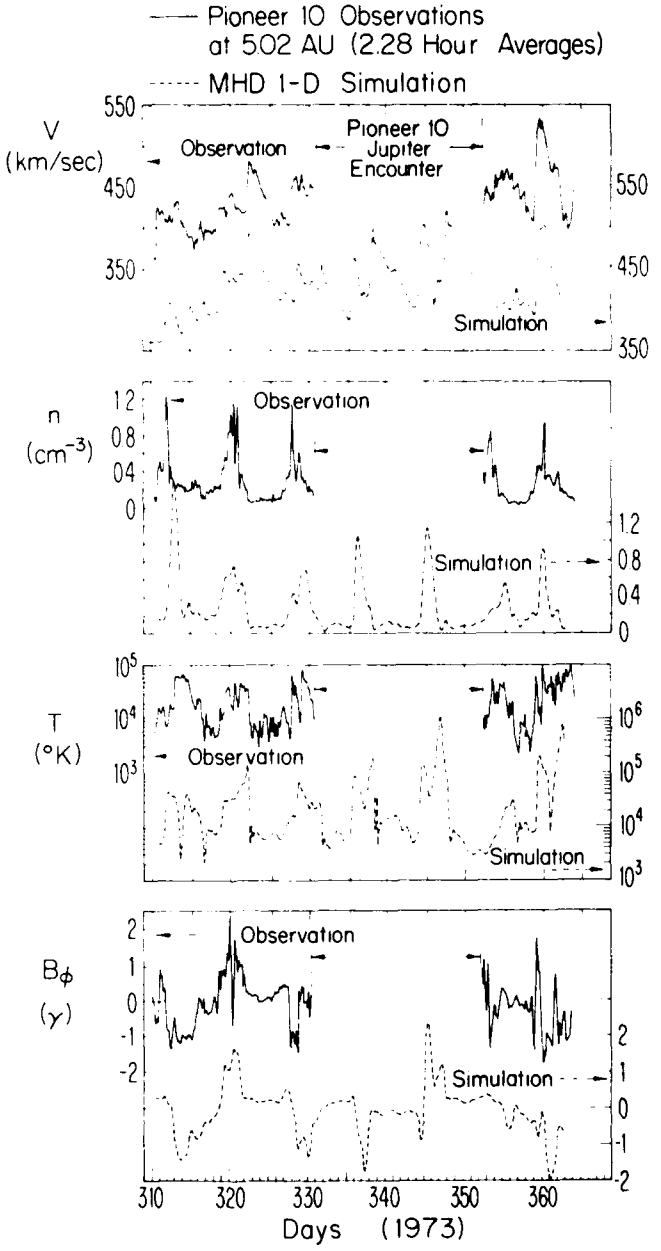

Figure 7. Pioneer 10 observations and the MHD model simulations at 5 AU.

noted above. The time-dependent simulation provided temporal and spatial computations for the ensuing response which was tracked beyond 5 AU. The time scale of the simulation obtained at Jupiter, at 5.02 AU, was corrected for the variations caused by the changing spacecraft separation during the 60-day observation period. Also, the spacecraft velocities were taken into account. This procedure made it possible to "pull out" the simulated parameters as "observed" by hypothetical instruments in front of the planet's bow shock wave. It was, therefore, possible to make a direct comparison with Pioneer 10's actual observations before and after its penetration of the Jovian magnetosphere. It was also possible to predict the varying solar wind's pressure impingement upon the Jovian magnetosphere during the time of the encounter.

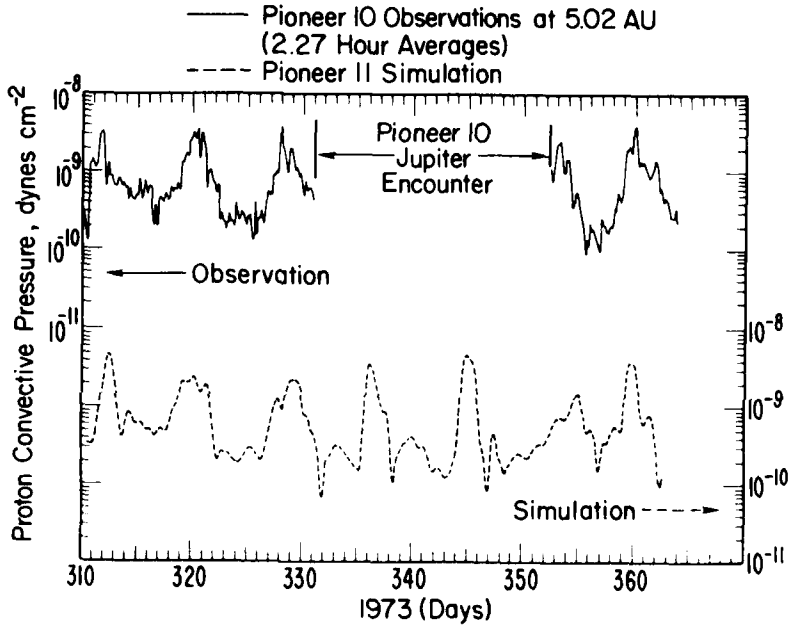

Figure 8. Corotating interaction regions at 5 AU as defined by the convective pressure.

This comparison is shown in Figure 7. It is clear that comparison of the phasing and magnitudes of the individual parameters is satisfactory. The CIRs, themselves, are more clearly discerned in Figure 8 which shows the convective pressure, dyn cm^{-2}. The simulated and observed pressure pulses agree to within 3 hours with two exceptions: the first pulse and the partial pulse which were observed as the spacecraft emerged from the Jovian magnetosphere. We conclude that the MHD fluid approximation, even confined to one-dimension (the radial one) and one-fluid, is highly satisfactory for demonstrating the essential physics of dynamic solar wind streams.

Acknowledgments

The work performed by RSS was supported through NOAA Grant No. NA80RAD00012. We wish to thank Dr. T. Yeh for his suggestions during the preparation of this report.

References

Anzer, U.: 1980, "MHD aspects of coronal transients," in M. Dryer and E. Tandberg-Hanssen (eds.), *Solar and Interplanetary Dynamics*, Proc. IAU Symposium No. 91, D. Reidel Publ. Co., Dordrecht-Holland, p. 263.

Bohlin, J. D. and Chipman, E. G.: 1980, "A program for the observations of the sun and heliosphere from space 1980-1995," in M. Dryer and E. Tandberg-Hanssen (eds.), *Solar and Interplanetary Dynamics*, Proc. IAU Symposium No. 91, D. Reidel Publ. Co., Dordrecht-Holland, p. 523.

Cuperman, S.: 1980, "Physical processes and models of interplanetary responses: suggested theoretical studies," in M. Dryer and E. Tandberg-Hanssen (eds.), *Solar and Interplanetary Dynamics*, Proc. IAU Symposium No. 91, D. Reidel Publ. Co., Dordrecht-Holland, p. 459.

Dryer, M. and Maxwell, A.: 1979, "Radio data and a theoretical model for the fast-mode MHD shock wave generated by the solar flare of 1973 September 5, 18:26 UT," *Astrophys. J., 231,* 945-959.

Dryer, M., Smith, Z. K., Smith, E. J., Mihalov, J. D., Wolfe, J. H., Steinolfson, R. S., and Wu, S. T.: 1978, "Dynamic MHD modeling of solar wind corotating stream interaction regions observed by Pioneer 10 and 11," *J. Geophys. Res., 83,* 4347-4352.

Dryer, M., Wu, S. T., Steinolfson, R. S. and Wilson, R. M.: 1979, "Magnetohydrodynamic models of coronal transients in the meridional plane. II. Simulation of the coronal transient of 1973 August 21," *Astrophys. J., 227,* 1059-1071.

Duncan, R. A., Stewart, R. T., and Nelson, G. J.: 1980, "Recent very bright type IV solar metrewave radio emissions," in M. Dryer and E. Tandberg-Hanssen (eds.), *Solar and Interplanetary Dynamics*, Proc. IAU Symposium No. 91, D. Reidel Publ. Co., Dordrecht-Holland, p. 381.

Gergely, T. E. and Kundu, M. R.: 1980, "Decameter radio and white light observations of the 21 August 1973 coronal transient," in M. Dryer and E. Tandberg-Hanssen (eds.), *Solar and Interplanetary Dynamics*, Proc. IAU Symposium No. 91, D. Reidel Publ. Co., Dordrecht-Holland, p. 245.

References

Gosling, J. T., Hildner, E., MacQueen, R. M., Munro, R. H., Poland, A. I., and Ross, C. L.: 1975, "Direct observations of a flare related coronal and solar wind disturbance," *Solar Phys., 40,* 439-448.

Kuperus, M.: 1980, "Symposium summary," in M. Dryer and E. Tandberg-Hanssen (eds.), *Solar and Interplanetary Dynamics*, Proc. IAU Symposium No. 91, D. Reidel Publ. Co., Dordrecht-Holland, p. 547.

Liewer, P. C. and Krall, N. A.: 1973, "Self-consistent approach to anomalous resistivity applied to theta pinch experiments," *Phys. Fluids, 16,* 1953-1963.

Maxwell, A. and Dryer, M.: 1980, "Radio data and computer simulations generated by solar flares," in M. Dryer and E. Tandberg-Hanssen (eds.), *Solar and Interplanetary Dynamics*, Proc. IAU Symposium No. 91, D. Reidel Publ. Co., Dordrecht-Holland, p. 251.

Michels, D. J., Howard, R. A., Koomen, M. J., Sheeley, N. R., Jr., and Rompolt, B.: 1980, "The solar mass ejection of 8 May 1979," in M. Dryer and E. Tandberg-Hanssen (eds.), *Solar and Interplanetary Dynamics*, Proc. IAU Symposium No. 91, D. Reidel Publ. Co., Dordrecht-Holland, p. 387.

Nakagawa, Y., Wu, S. T. and Han, S. M.: 1980, "Dynamics of coronal transients: two-dimensional non-plane MHD models," in M. Dryer and E. Tandberg-Hanssen (eds.), *Solar and Interplanetary Dynamics*, Proc. IAU Symposium No. 91, D. Reidel Publ. Co., Dordrecht-Holland, p. 495.

Sermulina, B. J., Somov, B. V., Spektor, A. R. and Syrovatskii, S. I.: 1980, "Gasdynamics of impulsive heated solar plasma," in M. Dryer and E. Tandberg-Hanssen (eds.), *Solar and Interplanetary Dynamics*, Proc. IAU Symposium No. 91, D. Reidel Publ. Co., Dordrecht-Holland, p. 491.

Sheridan, K. V.: 1980, "Evidence for open field lines from active regions: short communication," in M. Dryer and E. Tandberg-Hanssen (eds.), *Solar and Interplanetary Dynamics*, Proc. IAU Symposium No. 91, D. Reidel Publ. Co., Dordrecht-Holland, p. 261.

Smith, E. J., Fillius, R. W. and Wolfe, J. H.: 1978, "Compression of Jupiter's magnetosphere by the solar wind," *J. Geophys. Res., 83,* 4733-4742.

Somov, B. V. and Syrovatskii, S. I.: 1980, "Magnetically driven motions in solar corona," in M. Dryer and E. Tandberg-Hanssen (eds.), *Solar and Interplanetary Dynamics*, Proc. IAU Symposium No. 91, D. Reidel Publ. Co., Dordrecht-Holland, p. 487.

Space Science Board: 1978, *"Space Plasma Physics: The Study of Solar System Plasmas, 1978, - Colgate Report,"* Vol. I., National Academy of Sciences/National Research Council, Washington, D.C., pp. 12-13.

Steinolfson, R. S., Dryer, M., and Nakagawa, Y.: 1975, "Numerical MHD simulation of interplanetary shock pairs," *J. Geophys. Res., 80,* 1223-1231.

Steinolfson, R. S. and Wu, S. T.: 1980, "Evolution of coronal magnetic structures," in M. Dryer and E. Tandberg-Hanssen (eds.), *Solar and Interplanetary Dynamics*, Proc. IAU Symposium No. 91, D. Reidel Publ. Co., Dordrecht-Holland, p. 483.

References

Steinolfson, R. S., Wu. S. T., Dryer, M. and Tandberg-Hanssen, E.: 1978, "Magnetohydrodynamic models of coronal transients in the meridional plane. I. The effect of the magnetic field," *Astrophys. J., 219,* 324-335.

Steinolfson, R. S., Wu, S. T., Dryer, M. and Tandberg-Hanssen, E.: 1979, "Effects of emerging magnetic flux on the solar corona," in H. Rosenbauer (ed.), *Proc. Solar Wind IV Conference*, Springer-Verlag, Heidelburg, in press.

Stewart, R. T.: 1980, "Transient disturbances of the outer corona," in M. Dryer and E. Tandberg-Hanssen (eds.), *Solar and Interplanetary Dynamics*, Proc. IAU Symposium No. 91, D. Reidel Publ. Co., Dordrecht-Holland, p. 333.

Syrovatskii, S. I. and Somov, B. V.: 1980, "Physical driving forces and models of coronal responses," in M. Dryer and E. Tandberg-Hanssen (eds.), *Solar and Interplanetary Dynamics*, Proc. IAU Symposium No. 91, D. Reidel Publ. Co., Dordrecht-Holland, p. 425.

Tur, T. J., and Priest, E. R.,: 1978, "A trigger mechanism for the emerging flux model of solar flares," *Solar Phys., 58*, 181-200.

Wu, S. T.: 1980, "Theoretical interpretation of travelling interplanetary phenomena and their solar origins," in M. Dryer and E. Tandberg-Hanssen (eds.), *Solar and Interplanetary Dynamics*, Proc. IAU Symposium No. 91, D. Reidel Publ. Co., Dordrecht-Holland, p. 443.

Wu, S. T., Dryer, M., and Han, S. M.: 1976, "Interplanetary disturbances in the solar wind produced by density, temperature, or velocity pulses at 0.08 AU," *Solar Phys., 49*, 187-204.

Yeh, T.: 1980, "Global modeling of disturbances in the corona-interplanetary space," in M. Dryer and E. Tandberg-Hanssen (eds.), *Solar and Interplanetary Dynamics*, Proc. IAU Symposium No. 91, D. Reidel Publ. Co., Dordrecht-Holland, p. 503.

12. Three-Dimensional Distribution of the Solar Wind Velocity Deduced From IPS Observations

T. Kakinuma, H. Washimi, and M. Kojima
The Research Institute of Atmospherics
Nagoya University
Nagoya, Japan

Abstract

The IPS observations of the high-latitude radio source 3C48 are used to derive the distribution of the solar wind velocity in lonitude and latitude for periods of several rotations during 1974-1979, by model calculations. The observations during 1974-1978 show the existence of the north polar high-speed (800 km/sec) region. This region extended from the pole down to $45^\circ \sim 50^\circ$ latitude for most of 1974-1977, while the region contracted up to 80° in 1978 and was hardly observed in early 1979.

I. INTRODUCTION

One of the important subjects in the observation of the interplanetary scintillation (IPS) of radio sources is to derive a three-dimensional picture of the solar wind. Dennison and Hewish (1967) first made three-station observations of IPS

and found that the solar wind at high latitudes was faster than at low latitudes. Watanabe et al. (1974) investigated the relation between the solar wind velocity and EUV brightness of the corona. They found an inverse correlation between them at high latitudes. This explains the negative results obtained for the latitude dependence of wind velocity, observed by Hewish and Symonds (1969) and also by Vitkevitch and Vlasov (1972), and suggests the change of wind velocity at high latitudes is due to solar activity. Coles and Rickett (1976) showed that the average solar wind speed increased away from the equatorial plane with an average average gradient of 2.1 km/sec per degree of latitude during 1971-1975, and recently they reported a solar cycle change of the high-latitude solar wind (Rickett and Coles, 1979). Kakinuma (1977) derived the latitudinal distribution of the solar wind velocity in 1974 by a model calculation and showed that the solar wind velocity was 800 km/sec at latitudes above 45°.

In order to derive the velocity distribution in longitude and latitude, it is necessary to observe, simultaneously, many radio sources in different directions. The number of radio sources which are now observed is not sufficient to cover all solar coordinates at one time. However, when the corona is stable during several solar rotations, we can infer the large-scale three-dimensional structure of the solar wind from observations of a small number of radio sources, even from observations of one high-latitude source. Sime and Rickett (1978) derived the velocity distribution in longitude and latitude for each year from 1973 to 1977 by assuming that the solar wind speed at the point of closest approach of the line of sight to the sun was measured by the IPS method and by averaging together IPS observations of several radio sources over several rotations. Kakinuma et al. (1979) also derived the latitude and longitude distribution of the solar wind speed in 1974 by model calculations using the observations of 3C48. In this paper, we discuss the velocity distribution from 1974 through 1979.

2. MODEL CALCULATION

IPS observations at Nagoya University are being carried out at three stations: Toyokawa, Fuji, and Sugadaira. The observing frequency is 69 MHz. Details of our receiving system have been described by Kojima et al. (1979). The velocity of the diffraction pattern drifting across the earth is derived by cross-correlation analysis (Kakinuma et al., 1973). We calculate three cross-correlation functions of intensities between pairs of stations and then calculate the velocity from the time lags of the cross-correlation functions under the assumption of a radial flow and a frozen pattern. We take into account the anisotropy of the pattern in the calculation.

Hansen et al. (1976) have shown that the coronal structure remains stable over periods of several months during the declining and the minimum phases of solar activity. In such a case, we can infer the distribution of the solar wind velocity in longitude and latitude from IPS observations of a high-latitude source. The IPS pattern speed is a weighted average of the transverse components of the solar wind velocity along the line of sight to the radio source. The heliographic coordinates of sources of the solar wind crossing the line of sight change every day with the movement of the radio source relative to the sun and to the solar rotation. Thus observations of the pattern speed during several rotations may be considered to include information about the velocity distribution over a wide range of longitude and latitude. We have attempted to derive the velocity distribution of the solar wind by model calculations using the observations of 3C48 from which we can obtain a high signal-to-noise ratio.

Our model consists of two distributions: one for the "background solar wind" which corresponds to the lower envelope of the daily plots of IPS pattern speed, and the other for localized high-speed streams which correspond to enhancements above the lower envelope. The observations of 3C48 in 1974, for example, show that this model is reasonable (Kakinuma, 1977). In the calculation, we used the weak scattering and weak scintillation approximation. We assumed a power-law spectrum (power-law index = -3) of electron density fluctuation (Δn_e) the inverse square dependence on the radial distance of electron density fluctuation, and a Gaussian brightness distribution of the radio source. We used the values given by Readhead and Hewish (1974) for source size. The proton flux is commonly Hewish (1974) for source size. The proton flux is commonly assumed to be nearly constant; thus $\Delta n_e \propto V^{-1}$, if $\Delta n_e \propto n_p$. However, if we assume $\Delta n_e \propto V^{-1}$, a velocity more than 1000 km/sec will be required at the pole to predict the lower envelope of the observations in 1974. A comparison of spacecraft and IPS measurements of the solar wind (Coles et al., 1978) also shows that Δn_e is not proportional to n_p. Thus we assumed $(\Delta n_e)^2 \propto V^{-1}$, except for the region of stream-stream interaction at the leading edge of the stream. The stream model used in the calculation is shown in Figure 1. In this model, Δn_e at the leading edge, is 2 times higher than the ambient level at a distance of 1 AU from the sun in the equatorial plane, and decreases with increasing latitude and with decreasing radial distance. We used Carrington's synodic rotation rate for all latitudes, and also assumed that there was no radial distance dependence of the solar wind velocity.

Using the same method as used in the daily analysis of observations, crosspower spectrum from 0.1 Hz to 1 Hz, and then the intensity cross-correlation function by the Fourier transformation, the pattern speed was calculated from the time lag of the cross-correlation function. First we determined the distribution fit to the lower envelope of daily plots of pattern speed and then included the enhancements due to localized high-speed streams.

3. VELOCITY DISTRIBUTION

A comparison of the observed and the predicted IPS pattern speeds for February-July 1974 is shown in Figure 2. There are some differences between them, as we have neglected the temporal variations of velocity distribution, but this figure shows that our model is a good approximation. In our model, in the northern Hemisphere (above -7° latitude), the speed of the "background solar wind" increases with latitude, and can be given by 300 + 500 x $\sin^2$(2 x latitude) km/sec up to 45°, and 800 km/sec at latitudes above 45° as shown in Figure 1. During the time period February-July 1974, there were two corotating high-speed streams. One was centered on 250° Carrington longitude and was an equatorward extension of the north polar high-speed region. The other, centered on 90° Carrington longitude, was an extension over the equator of the southern high-speed streams, which was most likely an equatorward extension of the south polar high speed region. The existence of the high-speed stream associated with an equatorward extension of the solar coronal hole has been pointed out by many authors. This distributon is consistent with the observation of the K-corona (Hansen et al., 1976) and the averaged distribution derived by Sime and Rickett (1978). This distribution also shows that there is no localized high-speed stream at latitudes above 45°, agreeing with Houminer's result. He has found by scintillation index measurements that there is no stream-stream interaction at latitudes above 40° (Houminer, 1977). The enhancements in pattern speed in high-latitude observations are due to high-speed streams crossing the line of sight at latitudes below 45° (Kakinuma, 1977); speed enhancements in high-latitude observations do not always mean the existance of high-speed streams at high latitudes.

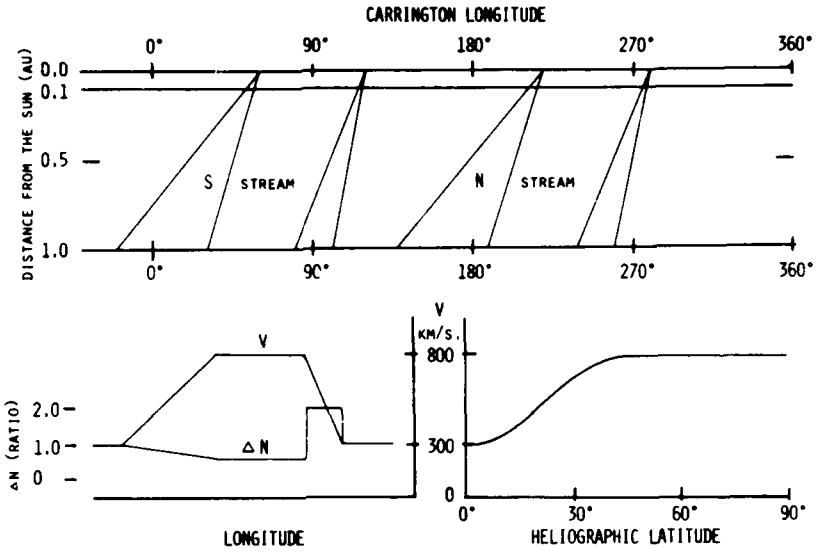

Figure 1. The stream model and the model of latitudinal distribution of the solar wind velocity for 1974.

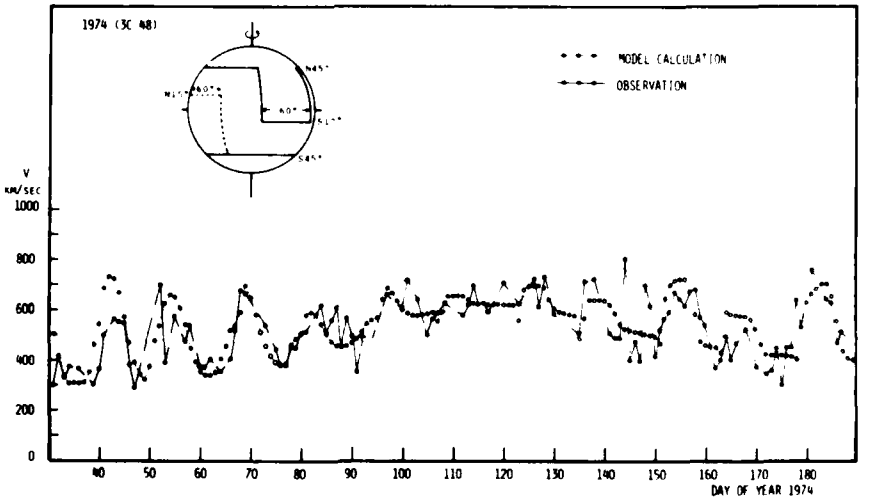

Figure 2. Observed and calculated IPS pattern speeds and the model calculations (using an 800 km/sec source region) for 1974. The IPS source is 3C48.

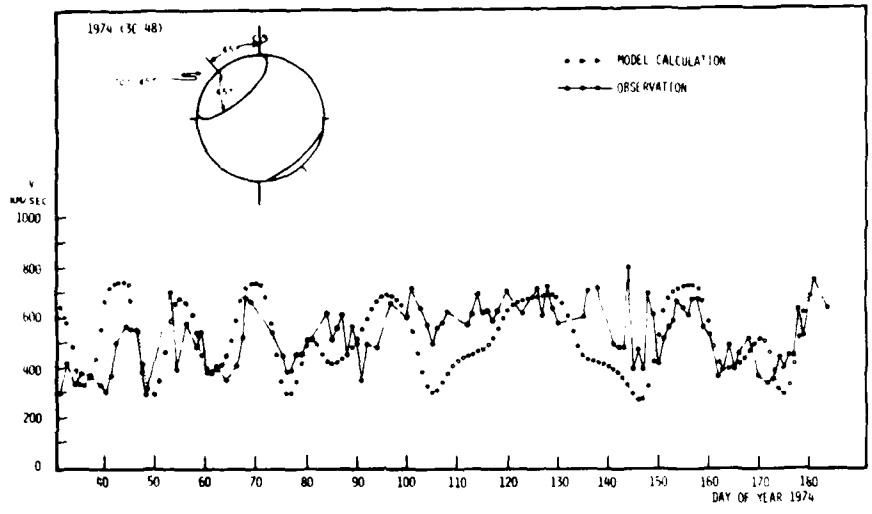

Figure 3. Observed and calculated IPS pattern speeds and the model calculations (using an 800 km/sec tilted polar high-speed source region) for 1974. The IPS source is 3C48.

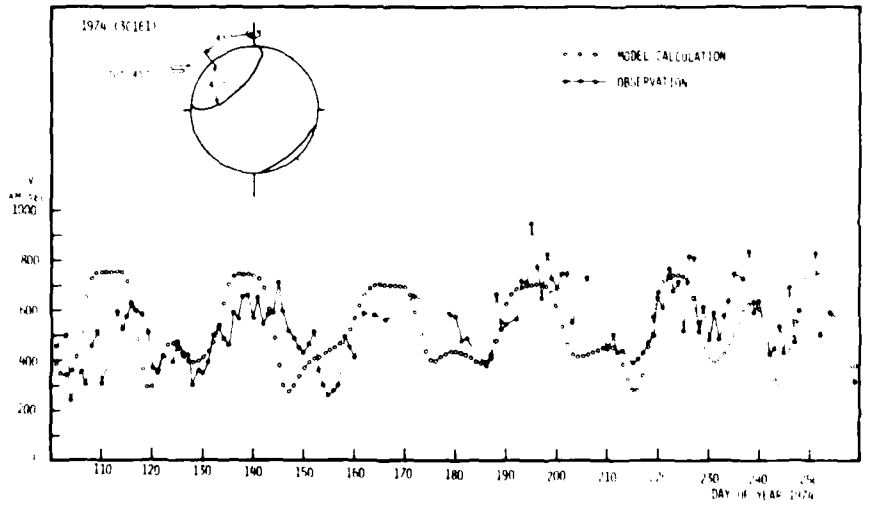

Figure 4. Observed and calculated IPS pattern speeds and the model calculations (using an 800 km/sec tilted polar high-speed source region) for 1974. The IPS source is 3C161 (UCDS observations).

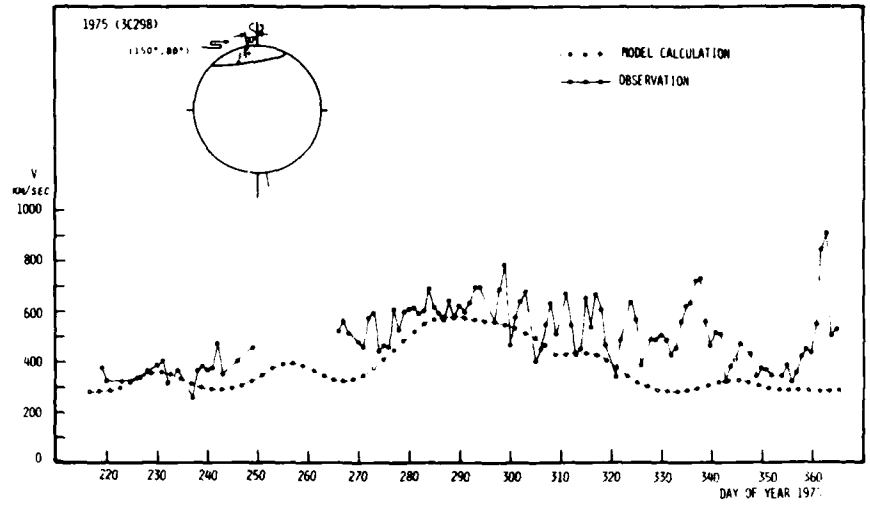

Figure 5. Observed and calculated IPS pattern speeds and the model calculations (using an 800 km/sec source region) for 1975. The IPS source is 3C298.

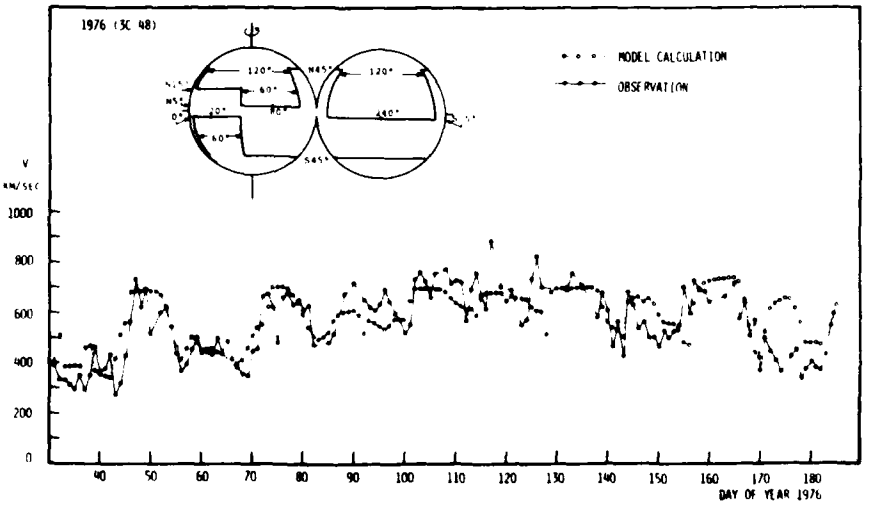

Figure 6. Observed and calculated IPS pattern speeds and the model calculations (using an 800 km/sec source region) for 1976. The IPS source is 3C48.

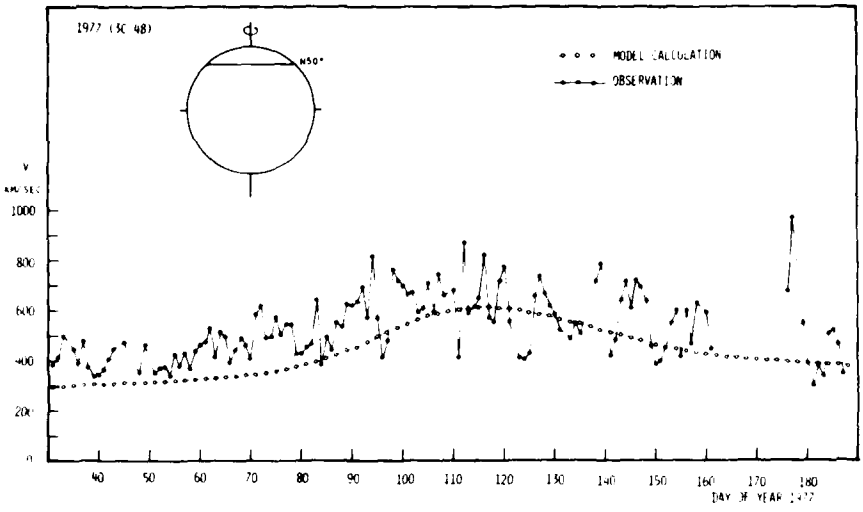

Figure 7. Observed and calculated IPS pattern speeds and the model calculations (using an 800 km/sec source region) for 1977. The IPS source is 3C48.

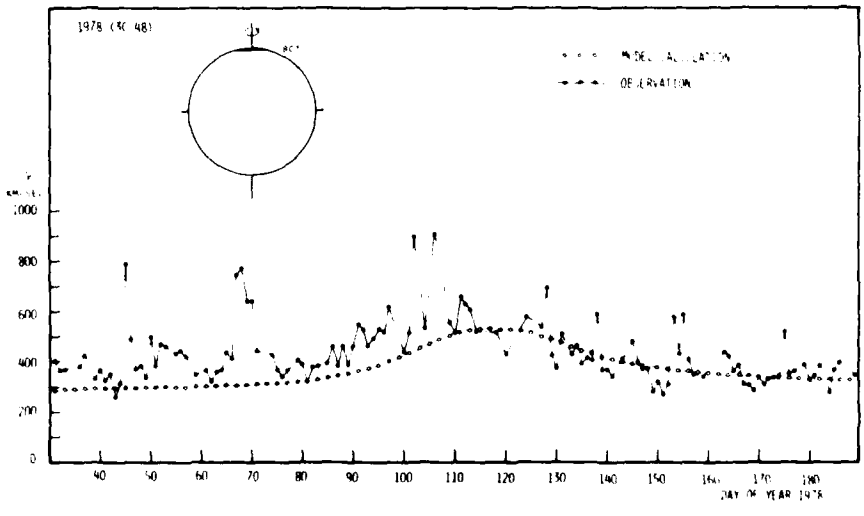

Figure 8. Observed and calculated IPS pattern speeds and the model calculations (using an 800 km/sec source region) for 1978. The IPS source is 3C48.

Sime and Rickett (1978) have concluded, from the averaged velocity distribution, that the polar high-speed regions were not symmetric about the spin axis, but were centered more than 30° from the rotation axis during 1973-1975. As shown in Figure 3, the tilted polar high-speed regions seem to be a good approximation, but the distribution shown in Figure 2 is much better for the northern hemisphere in in 1974. UCSD observations for 3C161 (southern high latitude source) in 1974, however, are well approximated by the polar high-speed regions tilted by 45°, as shown in Figure 4. K-coronameter observations (Hansen et al., 1976) also show that the north polar hole extended from the pole to 45° latitude and was symmetric about the rotation axis in 1974, while the south polar hole was displaced from the pole during from the pole during April-September 1974.

The calculations for 1976 (Figure 6) show that there were two corotating high-speed streams in the northern hemisphere which were equatorward extensions of the polar high-speed region: one centered on 240° Carrington longitude, was a stable wide stream and the other, centered on 50° Carrington longitude developed from February to April and decayed afterwards. The former was observed by the earth-orbiting spacecraft IMP 8 (Solar Geophysical Data, NOAA, 1976), but was hardly detected by the IPS observations of 3C144 (ecliptic latitude = -1.4°). This shows that the edge of the stream was very sharp in latitude, as pointed out by Sime and Rickett (1978).

In 1977 and 1978, many active regions appeared at mid-latitudes and no stable recurrent stream was noticed. Therefore, we have calculated the velocity distributions fit to the lower envelope of the observations of pattern speed. The north polar high-speed stream of 800 km/sec extended down to 50° latitude in 1977, while it extended only to 80° in 1978 (Figures 7 and 8). For these years, the lower envelope seems to be slightly asymmetical with respect to the day when the radio source was closest to the sun. This is accounted for if we assume that the polar high-speed region was displaced by a few degrees from the pole, or that it was gradually shrinking. It is interesting to note that the recurrent depression of the pattern speed was observed in 1977. This may have been caused by a slow-speed stream at mid-latitudes associated with an active region.

4. SUMMARY AND CONCLUSION

We have derived the distributions of the solar wind velocity for 1974-1978 using the 3C48 observations, and have shown the existance of the polar high-speed (800 km/sec) source region and its extension to the equatorial plane. As shown in Figure 9, the north polar high speed region extended from the pole down to 45° ~ 50° latitude for most of 1974-1977 (we used 3C298 observations for 1975, as shown in Figure 5, because we did not make observations in January-June 1975), while the boundary of the region moved up to 80° in 1978. The observations in 1979 show that this region almost disappeared. The shrinking of the polar stream (faster than 500 km/sec), coinciding with a corresponding contraction of the polar coronal hole, has also been found by Rickett and Coles (1979). It is well known that the solar magnetic dipole field reverses near the solar maximum. Our results show that the polar high-speed region shrunk without tilting from the rotation axis. This suggests that the dipole field does not rotate to reverse, but is apparently vanishing. The behavior of the polar coronal hole is interesting, and it is important to continue monitoring the polar high-speed stream for the coming years.

In this paper, we have used the observations of only one source. If we add the observations from two other sources, an ecliptic source and a southern high-latitude source, we will be able to derive a more detailed distribution for both

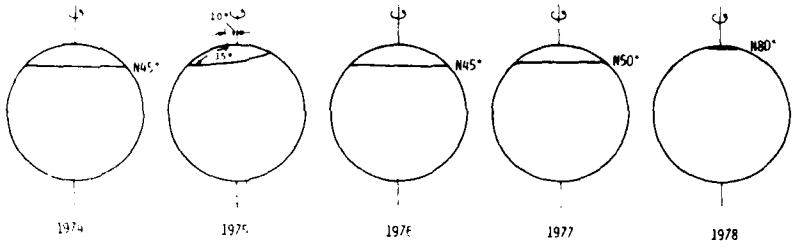

Figure 9. Variations of the north polar high-speed region during 1974-1978.

hemispheres. We are interested in north-south asymmetry of the distribution suggested by the UCSD observations for 3C161 in 1974, and we are planning to study this phenomena.

Acknowledgment

We are grateful to Professor W.A. Coles for providing IPS data at UCSD.

References

Coles, W.A., and Rickett, B.J.: 1976, "IPS observations of the solar wind speed out of the ecliptic", *J. Geophys. Res., 81,* 4797.

Coles, W.A., Harmon, J.K., Lazarus, A.J., and Sullivan, J.D.: 1978, "Comparison of 74 MHz interplanetary scintillation and IMP 7 observations of the solar wind during 1973", *J. Geophys. Res., 83,* 3337.

Dennison, P.A., and Hewish, A.: 1967, "The solar wind outside the plane of the ecliptic", *Nature, 213,* 343.

Hewish, A., and Symonds, M.D.: 1969, "Radio investigation of the solar plasma", *Planetary Space Sci., 17,* 313.

Hansen, R.T., Hansen S.F., and Sawyer, C.: 1976, "Long lived coronal structures and recurrent geomagnetic patterns in 1974", *Planetary Space Sci., 24,* 381.

Houminer, Z.: 1977, "Scintillation observations of the interplanetary plasma", in M.A. Shea, D.F. Smart and S.T. Wu (eds.), Study of Travelling Interplanetary Phenomena/ 1977, D. Reidel, Dordrecht, p. 119.

Kakinuma, T., Washimi, H., and Kojima, M.: 1973, "On the analysis of the observations interplanetary scintillations obtained with three spaced receivers", *Publ. Astron. Soc. Japan, 25,* 271.

References

Kakinuma, T.: 1977, "Observations of interplanetary scintillation: solar wind velocity measurements", in M.A. Shea, D.F. Smart and S.T. Wu (eds.), Study of Interplanetary Phenomena/ 1977, D. Reidel, Dordrecht, p. 101.

Kakinuma, T., Washimi, H., and Kojima, M.: 1979, "IPS observations of the solar wind", paper presented at the International Workshop on Selected Topics of Magnetospheric Physics, Tokyo, March 1979.

Kojima, M., Watanabe, T., Ishida, I., Maruyama, K., and Kakinuma, T.: 1979, "A full-automatic system for the observation of interplanetary scintillation", *Proc. Res. Inst. Atmosph. Nagoya Univ., 26,* 95.

Readhead, A.C.S., and Hewish, A.: 1974, "Fine structure in radio sources at 81.5 MHz-III", *Mem. Roy. Astron. Soc., 78,* 1.

Rickett, B.J., and Coles, W.A.: 1979, "Solar cycle changes in high latitude solar wind", paper presented at the NASA Symposium to Study the Solar Cycle and Dynamics Mission, Wellesley, Massachusetts, June 1979.

Sime, D.G., and Rickett, B.J.: 1978, "The latitude and longitude structure of the solar wind speed from IPS observations", *J. Geophys. Res., 79,* 3841.

Vitkevitch, V.V., and Vlasov, I.V.: 1972, "Characteristics of interplanetary electron irregularities according to observations in 1967-1969", *Soviet Astron., 16,* 480.

Watanabe, T., Shibasaki, K., and Kakinuma, T.: 1974, "Latitudinal distribution of solar wind velocity and its relation to solar EUV corona", *J. Geophys. Res. 79,* 3841.

Discussion

Schwenn: In the STIP-77 Proceedings we showed in situ measurements from both Helios solar probes during early 1976. There is clear evidence for the occurrence of a sharp latitudinal boundary confirming your model assumption. Did you try to include real stream profile measurements into your model calculations?

Kakinuma: Our model is very simple. We should include a real stream profile to obtain a more detailed velocity distribution.

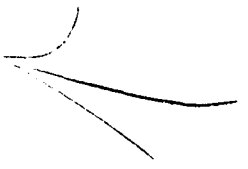

13. Interplanetary Scintillations at 103 MHz

S. K. Alurkar and R. V. Bhonsle
Physical Research Laboratory
Ahmedabad-380009, India

Abstract

With a view to studying the structure and dynamics of the interplanetary medium, a three-station interplanetary scintillation (IPS) observatory is being developed in India. Operating with only half the aperture (~2500 m^2) at a frequency of 103 MHz, the first IPS telescope at Thaltej near Ahmedabad is making daily observations of 8-10 radio sources. Parameters of the intensity pattern, such as scintillation index, autocorrelation, temporal power spectrum, moments of intensity etc., are computed. With a two-parameter curve-fitting method it is found that the IPS power spectra are best matched with an exponential law.

1. INTRODUCTION

Observations of the interplanetary scintillation of compact ($\leqslant 1''$) radio sources have been successfully used to delineate the microscale ($\sim$100 km) structure and dynamics of the interplanetary medium in the ecliptic plane as well as outside it. Such observations are also useful for deriving the structure of very compact radio sources, particularly at low frequencies, where the VLBI technique is impracticable (Hewish et al., 1964; Cohen et al., 1967; Armstrong and Coles, 1972; Kakinuma and Watanabe, 1976). In this note we present preliminary IPS observations made at Thaltej near Ahmedabad.

2. OBSERVATIONS AND ANALYSIS

The radio telescope used for these observations comprises a filled-aperture dipole antenna array having an aperture of $\sim$5000 m^2 at 103 MHz. (Only half the aperture was used for the present observations.) The r.f. signals, after being amplified through low-noise preamplifiers, are combined in a beam-forming matrix yielding a 32-beam pattern. The size of each beam is 8° E-W × 2° N-S. A selected beam is connected to a total-power receiver with a bandwidth of 2 MHz. An analogue recording of intensity fluctuations of a radio source is made with a time constant of 0.1 s. After A/D conversion at a sampling frequency of 20 Hz the data are recorded on a digital magnetic tape and then processed on an IBM 360/44 computer. Normally about 20 min of useful data per day per source is available. So far observations on 3C 48, 3C 144, 3C 147, 3C 161, 3C 196, 3C 237, 3C 273, 3C 298 and 3C 459 have been made.

Autocorrelation and intensity power spectra were computed using an FFT algorithm from successive 50-s segments of data. After editing, the selected spectra were summed to get an average spectrum. Usually each source was observed for about 30 min, followed by an off-source recording of about 5 min.

In Figure 1 are shown typical IPS power spectra for five scintillators. Off-source spectra were taken into account in choosing the high-frequency cut-off of the on-source spectra ($\sim$3 Hz and $\sim$2 Hz for strong and weak scintillators respectively). The spectra were best described by an exponential law in the frequency range 0.3–3 Hz for strong and 0.3–1.5 Hz for weak scintillating sources, with indices of 2.6 for 31° elongation and about 4.0 for elongations exceeding 40°.

The indices are plotted versus elongation in Figure 2 for four sources. At elongations around 20°, 3C 48 has an average index of 2–3, which increases to about 4 at higher elongations beyond about 20° and is scattered around an average of 4.

The first and (square-root) second moments (f_1 and f_2) of the intensity spectra were computed using the relations

$$f_1 = \int_0^{f_c} f\,P(f)\,df \Big/ \int_0^{f_c} P(f)\,df$$

and $$f_2^2 = \int_0^{f_c} f^2\,P(f)\,df \Big/ \int_0^{f_c} P(f)\,df \quad ,$$

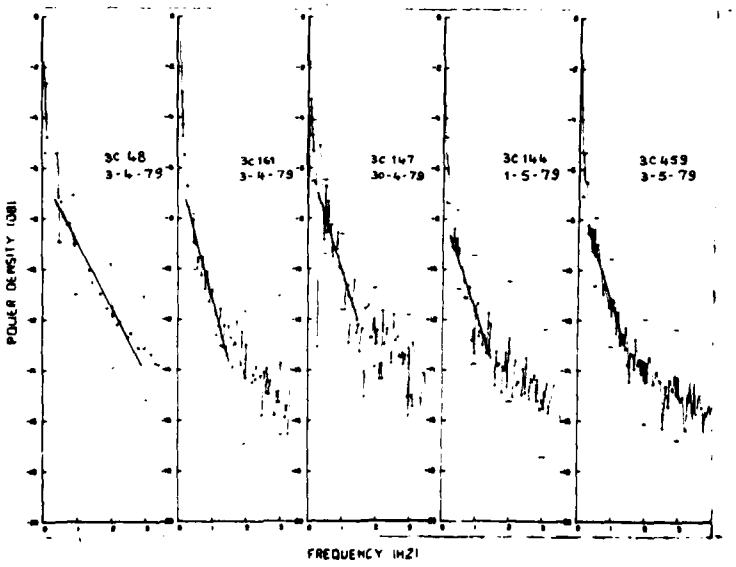

Figure 1. IPS spectra for five sources. The thick solid line is an exponential fit for 3C 48 data over 0.3-3 Hz and for other sources over 0.3-1.5 Hz.

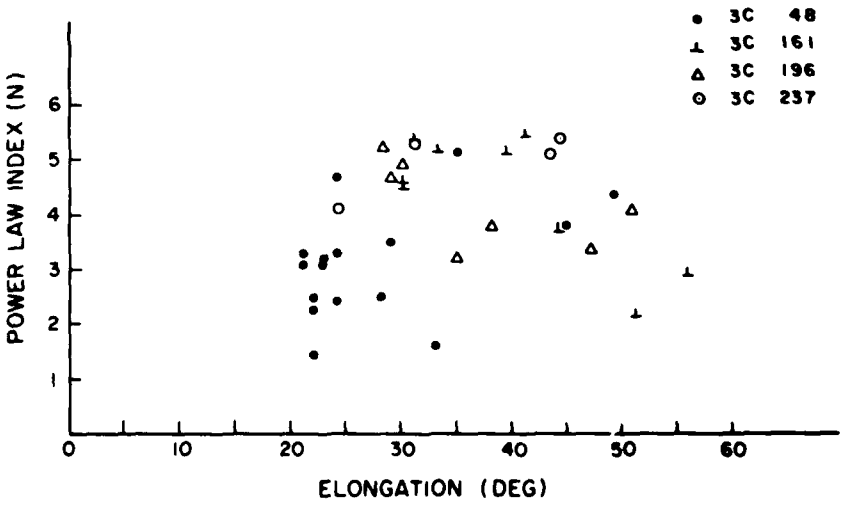

Figure 2. Indices of exponential fit vs. elongation.

where P(f) is the power spectrum estimated up to the cut-off frequency f_c at which the spectrum meets the off-source noise spectrum; f_1 and f_2 are measures of the width of the spectrum, the former being less affected than the latter by the noise in the tail of the spectrum. Further, f_1 gives more weight to large-scale components and is therefore more accurate because of the increased signal-to-noise ratio (Readhead et al., 1978). For the IPS data taken at Ahmedabad f_1 and f_2 were around 0.8 and 0.9 Hz, and these values remained nearly constant for elongations higher than 30°. The quality of the data can be judged from the ratio f_2/f_1 (~1.13), which in the case of a noise-free exponential spectrum is equal to $\sqrt{2}$.

3. DISCUSSION

For the 103 MHz IPS data taken at Ahmedabad for solar elongations higher than 20° the power spectrum index is 2-4 for strong and about 4 for weak scintillators, the former being comparable with the results of Milne (1976). More precise determination of the background noise spectrum is necessary for accurately fixing the cut-off frequency of the scintillation spectra.

Acknowledgments

We express our sincere thanks to Professors D. Lal and S.P. Pandya for showing keen interest in this work. We are grateful to all our colleagues in the IPS group for their dedicated efforts in developing the IPS station and also for providing computer programs for data analysis. Financial support for this project came from the Departments of Space and Science and Technology, Government of India.

References

Armstrong, J.W., and Coles, W.A.: 1972, "Analysis of three-station interplanetary scintillation", J. Geophys. Res., 77, 4602.

Cohen, M.H., Gundermann, E.J., Hardebeck, H.E., and Sharp, L.E.: 1967, "Interplanetary scintillations. II. Observations", Astrophys. J., 147, 449.

Hewish, A., Scott, P.F., and Wills, D.: 1964, "Interplanetary scintillation of small diameter radio sources", Nature, 203, 1214.

Kakinuma, T., and Watanabe, T.: 1976, "Interplanetary scintillation of radio sources during August 1972", Space Sci. Rev., 19, 611.

Milne, R.G.: 1976, "Interplanetary scintillation power spectra", Aust. J. Phys., 29, 201.

Readhead, A.C.S., Kemp, M.C., and Hewish, A.: 1978, "The spectrum of small-scale density fluctuations in the solar wind", Mon. Not. R. Astron. Soc., 185, 207.

14. Analysis of IPS Data Using A Periodic Phase Screen Model for the Solar Wind

A. Basu and S. K. Alurkar
Physical Research Laboratory
Ahmedabad-380009, India

Abstract

The intensity pattern obtained by diffraction from a periodic phase screen of finite dimensions has two distinct length scales: the width of the diffraction maxima and their interpeak distance. These can be uniquely related to two length scales in the screen, namely the lateral extent of the screen and the phase period.

In the weak scattering limit the autocorrelation and the Fourier transform of such a pattern are dominated by terms depending on the total size of the screen. We justify our assertion that the interplanetary medium (IPM) acts like a screen of finite lateral extent, and show that in this case the second moment of the power spectrum does not yield the desired information on irregularity sizes in the solar wind. This must be extracted from high-order terms, in particular from the dips in the power spectrum.

The results of the present model and Salpeter's (1967) random phase screen model are compared with observations. The validity of the model as an idealization

of the IPM is also examined.

The values of irregularity size calculated from observations taken at Ahmedabad are a few hundred kilometres on the basis of this model.

1. INTRODUCTION

Radio waves from astronomical sources reach the observer on Earth after diffraction through a translating screen of varying refractive index formed by the solar wind. In the weak scattering limit the scale of fluctuations in the medium is usually determined from

(i) the spatial auto-correlation length of the intensity pattern, given the solar wind velocity, or

(ii) q^{-1}, where q is the first moment (Readhead et al., 1978) or square root of the second moment of the power spectrum.

The power spectrum or inverse Fourier transform of the intensity $F^{-}(I)$ gives the power distribution in the fluctuations over a range of wave numbers (Salpeter, 1967).

We will show that if the medium is finite in lateral extent, the major contribution to the above quantities comes from L, the screen size, rather than ℓ, the scale of irregularities in the medium, assuming the screen to be phase periodic with Φ, the amplitude of phase variations, about unity.

The necessity of considering a finite screen arises because the effective size of the screen is always limited by several factors.

(i) For very weak scattering $L = L_S = 2z\theta_S$, where θ_S is the angle of scattering.

(ii) If the source is not monochromatic, the temporal coherence of the source, or finite bandwidth of the receiver, sets a limit to L beyond which coherence is destroyed. We assume that the bandwidth can be made sufficiently small so that this limit need not be considered.

(iii) For an incoherent source (e.g. a star) the lateral extent of coherence of the wavefront at a distance z from the source is (Champeney, 1973)

$$L_c = 1.22\lambda z/D = 1.22\lambda/\alpha \quad ,$$

where α is the angular size of the source and D is the diameter of the source. If α is sufficiently small so that $L_c \geq L_S$, the source scintillates. Large sources are non-scintillating, since incoherent contributions destroy scintillation when $L_S \sim L_c$.

If L becomes comparable to ℓ, then the assumption of a "random" distribution of irregularities is open to question because it is valid only in the presence of a large number of irregularities within the diffracting region, i.e. when $\ell \ll L$.

If the spectrum of ℓ is truncated by L, and in addition the power hierarchy of the irregularities is such that the largest sizes contain the maximum power, then the number of irregularities having the highest power within the scattering region

may be very small. In such a case the periodic phase approximation may be closer to the actual situation than the random phase approximation.

In the following we calculate the effects of diffraction by a periodic screen. Only the Fraunhofer results are presented (although this imposes the rather stringent condition $L^2/4z \lesssim \lambda/20$ (or $L \approx 3 \times 10^2$ km for $z \approx 1$ A.U., $\lambda \approx 3$ m) because of the extremely simple linear relations that emerge between pattern scales and characteristic scales in the medium.

2. DIFFRACTION FROM A THIN ONE-DIMENSIONAL SCREEN

When a plane wave of unit amplitude is diffracted by the infinite screen $f(x,0)$, the complex amplitude is (Champeney, 1973)

$$f(X,z) = \frac{1-i}{\sqrt{2\lambda z}} e^{i2\pi\sqrt{z^2+X^2}/\lambda} \int_{-\infty}^{\infty} e^{-i2\pi(X/\lambda z)x} f(x,0)dx \qquad (1)$$

and intensity

$$I(X,z) = 1/\lambda z \left| F_{x/\lambda z}[f(z,0)] \right|^2 , \qquad (2)$$

where λ = wavelength of diffracted radiation,
z = distance of observer from the screen,
x,X = coordinates at the screen and observer respectively,
F,F^- = direct and inverse Fourier transforms,
$X/\lambda z$ = Fourier conjugate of x.

The inverse Fourier transform of $I(X,z)$ is

$$F_S^-(I) = 1/\lambda z \int_{-\infty}^{\infty} e^{2\pi i SX} \left| F_{X/\lambda z}[f(x,0)] \right|^2 dX$$

or

$$F_{r/\lambda z}^-(I) = \int_{-\infty}^{\infty} e^{2\pi i r(X/\lambda z)} \left| F_{X/\lambda z}[f(x,0)] \right|^2 d(X/\lambda z) , \qquad (3)$$

where λzS has been replaced by r. By the autocorrelation theorem (Bracewell, 1965) the right-hand side of Eq. (3) is the autocorrelation of $f(x,0)$.

$$F_{r/\lambda z}^-[I(X,z)] = A_{f(x,0)}(r)$$

$$= \langle f(x,0) f(x+r,0) \rangle . \qquad (4)$$

Equation (4) suggests an easy way to determine the autocorrelation of an arbitrary infinite screen if the spatial intensity distribution in the Fraunhofer region is known.

If the screen is of finite lateral extent, the new screen function $f'(x,0) = f(x,0)W(x/L)$, where $W(x/L)$ is an envelope function of width L that tends to zero for large values of x. The intensity is the convolution

$$I(X,z) = 1/\lambda z \left| F_{X/\lambda z}[f(x,0)] * F_{X/\lambda z}[W(x/L)] \right|^2 \tag{5}$$

and

$$F^{-}_{r/\lambda z}[I(X,z)] = A_{f'(x,0)}(r)$$

$$= \langle f(x,0)W(x/L)f(x+r,0)W(x+r/L)\rangle \quad . \tag{6}$$

It can be seen from Eq. (5) that the intensity pattern is the convolution of two independent functions with different scales. Since the scale of a function is inversely related to that of its Fourier transform, the first term on the right-hand side of Eq. (5) gives a pattern scale proportional to $\lambda z/\xi$ and the second term a pattern scale $\lambda z/L$. In other words, if there are two independent scales in the intensity pattern, the shorter is inversely proportional to the overall size of the screen while the longer is inversely proportional to the irregularity scale of the screen.

2.1 Diffraction by a Thin One-Dimensional Periodic Phase Screen

$$\text{If } f(x,0) = e^{i\psi\cos(2\pi x/\xi)} \text{ and}$$

$$\begin{aligned} W(x/L) &= 1 \qquad |x| \leq \tfrac{1}{2}L \quad , \\ &= 0 \qquad |x| > \tfrac{1}{2}L \quad , \end{aligned} \tag{7}$$

the explicit form of the intensity is determined by Ratcliffe (1956) for an infinite screen. For finite L,

$$I(X,z) = \sum_{n=-\infty}^{\infty} L^2 J_n^2(\psi) \operatorname{sinc}^2 \frac{L}{\lambda z}\left(X - \frac{n\lambda z}{\xi}\right) \quad . \tag{8}$$

As shown in Figure 1, this intensity exhibits a series of diffraction maxima of width $2\lambda z/L$ and separation $\lambda z/\xi$. $J_n(\psi)$ goes rapidly to zero for $n > \psi$ and this sets a limit to the order of diffraction maxima actually seen.

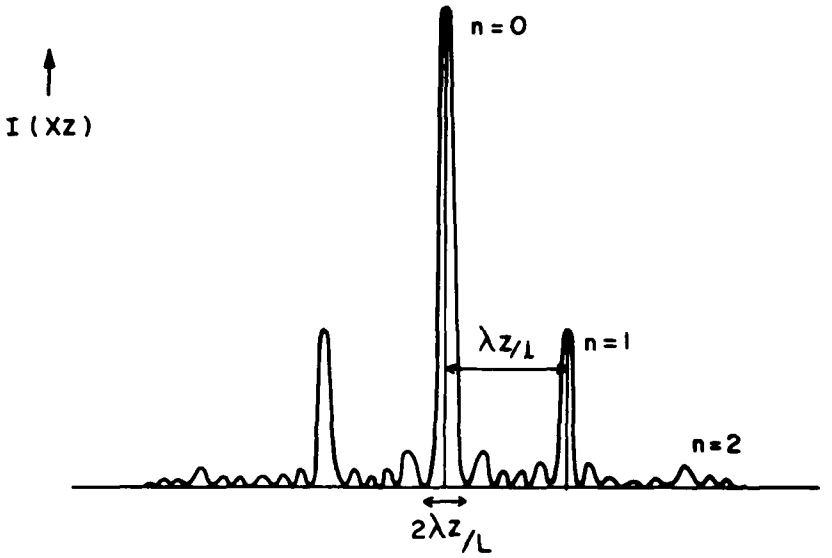

Figure 1. Diffracted intensity I(x,z) at a distance z from a phase screen $f(x,0) = e^{i\phi \cos 2\pi x/\ell}$ truncated at $x = \pm\frac{1}{2}L$, for $\zeta = 1$.

2.2 The Inverse Fourier Transform of I and the Second Moment of $F^{-}(I)$ for a Periodic Phase Screen

From Eq. (8):

$$F_S^-(I) = L \sum_{n=-\infty}^{\infty} J_n^2(\phi) \Lambda(\lambda z S/\ell)\, e^{2\pi i (n\lambda z S/\ell)}$$

or

$$F_{r/\lambda z}^-(I) = L \sum_{n=-\infty}^{\infty} J_n^2(\phi) \Lambda(r/\ell)\, e^{2\pi i (nr/\ell)} \quad , \tag{9}$$

where $\Lambda(r/L) = 1 - |r|/L \qquad |r| \leq L \ ,$

$\qquad\qquad = 0 \qquad\qquad\quad |r| > L \ .$

$\Lambda(r/L)$ is nothing but the autocorrelation of W(x/L) as expected from Eq. (6).

For $\zeta \approx 1$,

$$\mathrm{Re}\, F_{r/\lambda z}^-(I) \approx \left[J_0^2(\phi) + 2J_1^2(\phi) \cos \frac{2\pi r}{\ell}\right] L\Lambda\left(\frac{r}{L}\right) \tag{10}$$

(see Figure 2), and the normalized second moment of $F_S^-(1)$

$$S = \frac{1}{6}\left(\frac{L}{\lambda z}\right) + O\left(\frac{J_1^2(\zeta)}{J_0^2(\zeta)}\right) \quad . \tag{11}$$

From Eqs. (10) and (11) it can be seen that the dominant contributions to $F^-(1)$ and S_2 come from terms independent of ζ for $\zeta \approx 1$.

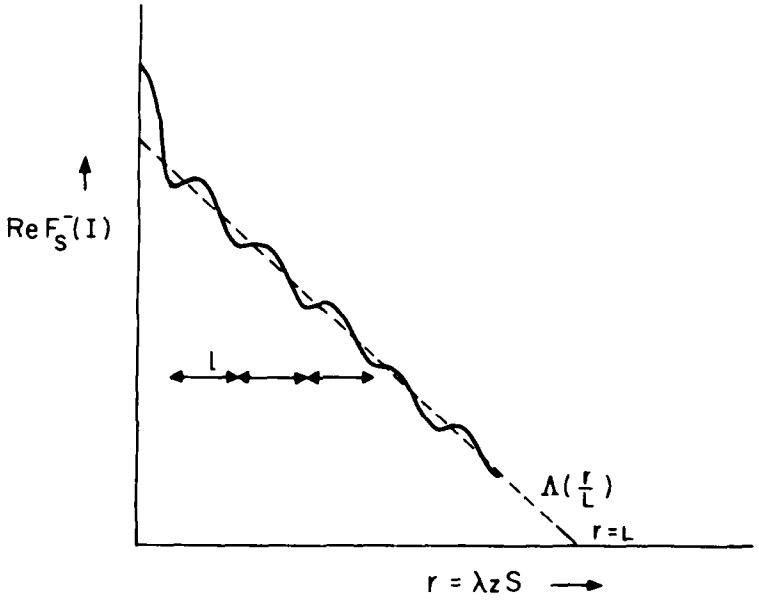

Figure 2. Fourier transform of I(X,z) for $\zeta \approx 1$.

$$\frac{F_S^-(1)|_{r=r'}}{F_S^-(1)|_{r=0}} = \left[1 - \frac{2J_1^2(\zeta)}{J_0^2(\zeta)}\right]\left[1 - \frac{|r'|}{L}\right] .$$

2.3 The Autocorrelation Function of Intensity for a Periodic Screen

Similarly we find

$$A_I(R) = \frac{\langle I(X,z)\, I(X+R,z)\rangle}{\langle I^2(X,z)\rangle}$$

$$= \frac{\sum_{n_1,n_2=-\infty}^{\infty} J_{n_1}^2(\phi)\, J_{n_2}^2(\phi) \int \frac{\sin^2 X'}{X'^2} \frac{\sin^2(X'+\Delta)}{(X'+\Delta)^2}\, dX'}{\sum_{n_1,n_2=-\infty}^{\infty} J_{n_1}^2(\xi)\, J_{n_2}^2(\xi) \int \frac{\sin^2 X'}{X'^2} \frac{\sin^2(X'+\Delta')}{(X'+\Delta')^2}\, dX'} \quad , \tag{12}$$

where $X' = \pi L\left(\frac{X}{\lambda z} - \frac{n_1}{\xi}\right)$,

$\Delta = \pi L\left(\frac{n_1 - n_2}{\xi} - \frac{R}{\lambda z}\right)$,

$\Delta' = L\left(\frac{n_1 - n_2}{\xi}\right)$.

It can be shown that

$$\int_{-\infty}^{\infty} \frac{\sin^2 X}{X^2} \frac{\sin^2(X+\Delta)}{(X+\Delta)^2}\, dX = \frac{\pi}{\Delta^2}\left(1 - \frac{\sin 2\Delta}{2\Delta}\right) \quad , \tag{13}$$

$$A_I(R) = \frac{\sum_{n_1,n_2=-\infty}^{\infty} J_{n_1}^2(\xi)\, J_{n_2}^2(\xi) \frac{\pi}{\Delta^2}\left(1 - \frac{\sin 2\Delta}{2\Delta}\right)}{\sum_{n_1,n_2=-\infty}^{\infty} J_{n_1}^2(\xi)\, J_{n_2}^2(\xi) \frac{\pi}{\Delta'^2}\left(1 - \frac{\sin 2\Delta'}{2\Delta'}\right)} \quad . \tag{14}$$

Again, the largest term A_0 corresponding to $n_1 = n_2 = 0$ is independent of z.

$$A_I(R) = \frac{\frac{\pi}{2\Delta_0^2}\left(1 - \frac{\sin 2\Delta_0}{2\Delta_0}\right)}{\frac{\pi}{2\Delta_0'^2}\left(1 - \frac{\sin 2\Delta_0'}{2\Delta_0'}\right)} \quad ,$$

$$\Delta_0 = \frac{\pi LR}{\lambda z} \quad . \tag{15}$$

This corresponds to the central lobe of the autocorrelation function and has oscillations on a scale $\lambda z/L$. At the first minimum, $\Delta_0 = \frac{1}{4}\pi$ and $L = \lambda z/R$. This relation is used to determine L from $A_I(R)$.

Taking terms up to the next order for $\xi \approx 1$,

$$A_I(R) \approx \frac{\frac{1}{\Delta_0^2}\left(1 - \frac{\sin 2\Delta_0}{2\Delta_0}\right) + \frac{2J_1^2(\Phi)}{J_0^2(\Phi)}\frac{1}{\Delta_1^2}\left(1 - \frac{\sin 2\Delta_1}{2\Delta_1}\right)}{\frac{2}{3} + \frac{2J_1^2(\Phi)}{J_0^2(\Phi)}\frac{1}{\Delta_1^2}\left(1 - \frac{\sin 2\Delta_1}{2\Delta_1}\right)} \quad , \tag{16}$$

where $\Delta_0 = \frac{\pi L}{\lambda}$; $\Delta_1 = \pi L\left(\frac{1}{\lambda} - \frac{R}{\lambda z}\right)$.

A_I has a secondary maximum when $\Delta_1 = 0$ at $R = \lambda z/L$ (Figure 3).

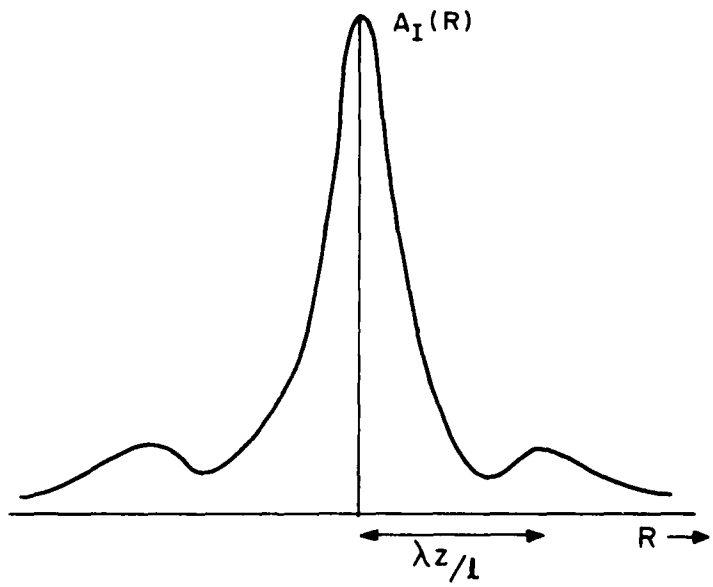

Figure 3. Autocorrelation of intensity $\langle I(X,z)I(X+R,z)\rangle$.

$$A_I\left(R = \frac{\lambda z}{L}\right) = \left[\frac{P + \frac{4}{3}\frac{J_1(\Phi)}{J_0(\Phi)}}{\frac{2}{3} + \frac{2J_1^2(\Phi)}{J_0^2(\Phi)}P}\right] \quad , \tag{17}$$

where $P = \frac{1}{\Delta_1^2}\left(1 - \frac{\sin 2\Delta_1}{2\Delta_1}\right)$.

3. DETERMINATION OF PARAMETERS OF THE SCATTERING SCREEN FROM THE OBSERVATIONS

3.1 Determination of ℓ and ϕ for a Periodic Screen

From Eq. (10) it can be seen that the minima in Re $\Gamma_{r/\lambda z}(I)$ are situated at

$$\frac{r}{\lambda z} = \frac{\ell}{2\lambda z}, \frac{3\ell}{2\lambda z}, \frac{5\ell}{2\lambda z} \ldots \text{etc.} \tag{18}$$

That is, the distance between the dips in $\Gamma(I)$ gives a direct measure of ℓ, provided $\phi \approx 1$. If $\phi \gg 1$, additional dips are obtained at intervals $\Delta r = \ell/n$, which would make the determination of ℓ difficult ($n \approx \phi - 1$; $2 < \phi < 10$). ϕ can be obtained from a set of relations for each dip in $\Gamma(I)$.

$$\frac{\Gamma_{r/\lambda z}(I)\big|_{r = k\ell/2}}{\Gamma_{r/\lambda z}(I)\big|_{r=0}} = \left\{1 - \frac{2J_1^2(\phi)}{J_0^2(\phi)}\right\}\left\{1 - \frac{k\ell}{2L}\right\} \qquad k = 1, 3, 5 \ldots \tag{19}$$

The width of $\Gamma_{r/\lambda z}(I)$ corresponds to L.

In the autocorrelation function the distance to the first sidelobe is $\lambda z/\ell$. Although ϕ can be determined from $A_I(R)$ in principle, this method is likely to be unsatisfactory because the autocorrelation is normalized by its value at R = 0, which has a large contribution from random noise.

3.2 Distribution of Power in Different Scales for an Aperiodic Screen

The distribution of scale sizes ℓ is estimated from the frequency distribution of the spacing between successive peaks in the scintillation pattern. If the time lag between peaks is τ, and $N(\tau)$ the frequency distribution of τ, the power $\Phi^2(q)$ in the phase fluctuations as a function of wave number is proportional to $N^2(\tau)$, where $q = 2\pi v\tau/\lambda z$. Figure 4(a) shows a sample histogram of $N(\tau)$ vs. τ and Figure 4(b) gives log $N^2(\tau)$ as a function of log τ. The steep fall in the distribution for low values of τ is due to the finite size of the screen, which filters out irregularities larger than L.

4. COMPARISON OF QUALITATIVE FEATURES OF THE MODEL WITH OBSERVED FEATURES OF IPS

The model for the solar wind is

$$f(x,0) = e^{i\psi(x)\cos(2\pi x/\ell)} .$$

It is assumed that $\phi(\ell)$ is an increasing function of ℓ for $\ell \leq L$. The specific form of $\phi(q = 2\pi/\ell)$ can be determined experimentally from $N(\tau)$ vs. τ (Figure 4).

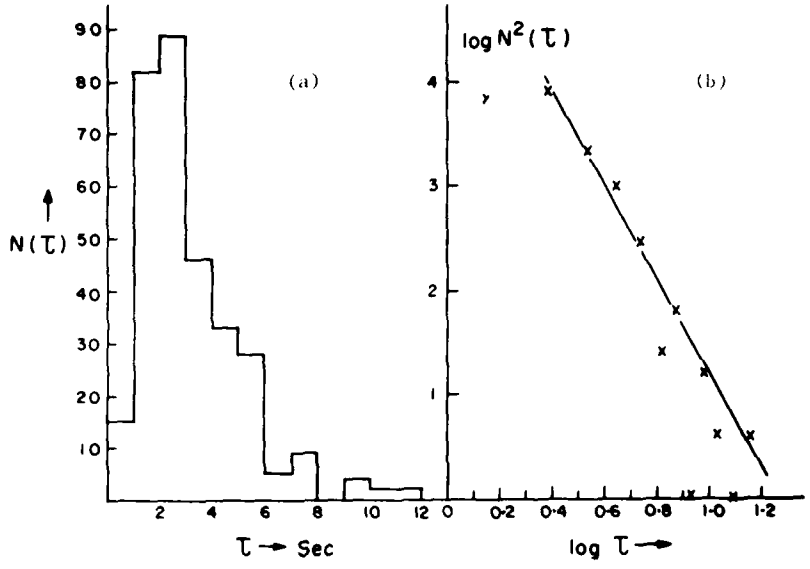

Figure 4. (a) Histogram of $N(\tau)$ vs. τ. The wave number q equals $2\pi v\tau/\lambda z$. (b) Log $N^2(\tau)$ vs. log τ. The corresponding range of q is 1.4×10^{-2} km^{-1} to 8.7×10^{-2} km^{-1}.

The size of the screen $L = L_s = 2z\theta_s$, where

$\theta_s = \frac{1}{2}\left(\frac{D}{\ell}\right)^{\frac{1}{2}} r_e \Delta n_e \lambda^2$ (Scheuer, 1968),

r_e = classical electron radius,

Δn_e = density fluctuation of electrons,

D = depth of scattering region.

The largest irregularity within the scattering region is $\ell \approx L_s$, and since $\phi(\ell)$ increases with ℓ, it is also the dominant scale.

4.1 Observed Features of IPS

(i) From the model we find that the depth of fading varies proportionally with the inverse of the width of the diffraction peaks, and thus it varies proportionally to λ. We also find that the scintillation rate is proportional to the inverse of

the distance between peaks, which is proportional to

$$\ell/\lambda z \approx L_s/\lambda z \propto \lambda \quad ,$$

as observed in the case of scintillation.

(ii) Again from the model we can predict the variation of scintillation index m with elongation ϵ. We expect that with decreasing elongation θ_s would increase, and consequently m also would increase (Eq. 8) until $L_s = L_c$. Beyond this, any further increase in L_s would cause m to decrease owing to incoherent contributions from the edges of the wavefront.

This is in qualitative agreement with the variation of m with ϵ as seen in Figure 5.

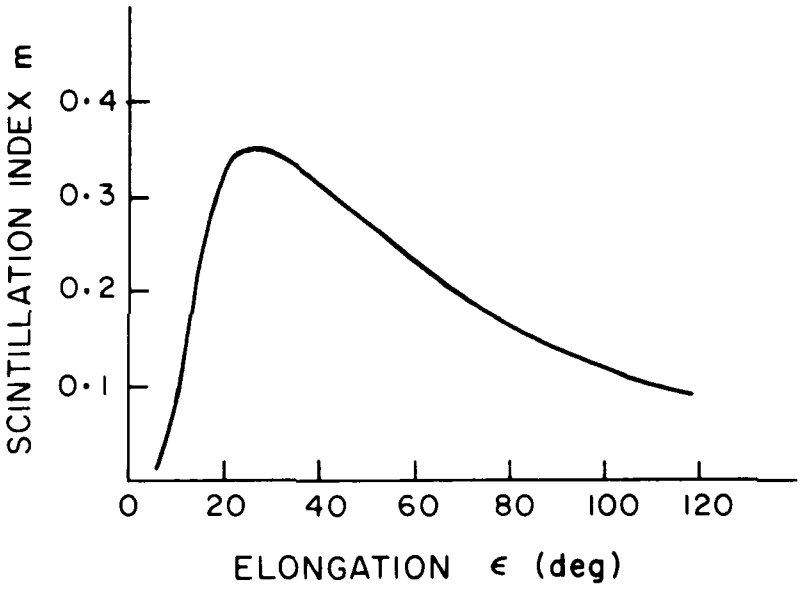

Figure 5. Variation of scintillation index with solar elongation ϵ.

The source size α can be determined from the point at which $m = m_{max}$. The width of the peaks is equal to $\lambda z/L_c$, which is approximately equal to $z\lambda/1.22$. In terms of the cut-off frequency $f_c = v/L_c$

$$\alpha = \frac{1.22v}{zf_c} \quad \text{at } m = m_{max} \quad .$$

This is in agreement with Cohen et al. (1966) except that according to our arguments the source size can be obtained only from the point $m = m_{max}$. Elsewhere the cut-off frequency is determined by L_s and is unrelated to the size of the source.

(iii) The maximum of m vs. ε occurs at smaller elongations for shorter wavelengths and smaller source size (Figure 5). At $m = m_{max}$,

$$L_s = 1.22\lambda/\alpha = z(D/\ell)^{\frac{1}{2}} r_e \Delta n_e \lambda^2 \quad .$$

If α is assumed constant, then a shorter λ requires a higher Δn_e, which means that the maximum of the m vs. ε curve shifts toward smaller ε for decreases in λ. If α increases, $m = m_{max}$ shifts towards larger elongations. It remains to be seen whether quantitative agreement can also be obtained with observations.

(iv) According to Salpeter (1967) the dips in the power spectrum are due to a $\sin q^2$ factor (the Fresnel filter). The spacing between the dips is then expected to decrease with increasing q. In the Fraunhofer region the dips are expected to be equally spaced, as we generally observe. Buckley (1975) and Lovelace et al. (1970) also mention that the dips in the power spectrum do not agree with the theoretical values from Salpeter. This may be due to the finite size of the screen, which makes the Fraunhofer approximation adequate except at very large elongations.

5. RESULTS

Some sample values of ℓ and L calculated from IPS observations taken at UCSD using the results of our model are shown in Table 1.

Table 1

ϕ	ℓ (km)	ℓ (km)	$\ell L/\lambda$ (km)	z (km)
20-30*	1.8×10^2	3.4×10^3	1.53×10^7	1.36×10^8
40	1.33×10^2	8.85×10^2	2.94×10^6	1.15×10^6
60	1.31×10^2	9.17×10^2	3.00×10^6	6.90×10^7
70	1.3×10^2	4.17×10^2	1.36×10^6	5.57×10^7
96†	1.5×10^2	7.8×10^1	2.93×10^5	1.5×10^7

*The true irregularity scale is $\sim(\phi-1)\ell$ if $2 \leq \phi \leq 10$.
†Fraunhofer approximation and localized thin-screen approximation not expected to hold.

At small elongations, if $\phi \gg 1$, then the true irregularity scale is $\sim(\phi-1)\ell$. Taking this into account we see that the largest irregularities that are observed are of the order of hundreds of kilometres.

In Figure 4(a) the histogram ($\varepsilon \approx 40°$), prepared from IPS observations taken at Ahmedabad, gives the distribution of $\Phi(\ell)$ over values of ℓ ranging from ~10 to 500 km. There is very little power left in irregularities below ~100 km. The peak power is at 400 km, above which truncation effects set in.

After the completion of this paper an earlier work (Briggs, 1961) was brought to our attention. The conclusion of Briggs was that the scale measured from the pattern autocorrelation is either ℓ or L, depending on whether we have $z \ll \ell L/\lambda$ or $z \gg \ell L/\lambda$. Since our calculations are in the Fraunhofer region they appear to be in agreement with Briggs.

Using this criterion we see in Table 1 that for IPS we are usually in the "far" region as defined by Briggs. Our results may therefore be of relevance to IPS observations, even though Fraunhofer conditions may not hold strictly.

6. SUMMARY

(i) The auto-correlation function of a diffracting screen and its limiting envelope can be obtained from the relation

$$A_{f(x,0)W(x/L)}(r) = F^{-}_{r/\lambda z}(I) \quad .$$

(ii) In the Fraunhofer region, pattern scales are inversely proportional to the scales in the medium. The shorter scale is proportional to L^{-1} and the longer scale to ℓ^{-1}. To determine ℓ, the longer scale must be selected.

(iii) Since the autocorrelation function and second moment of power spectrum preferentially pick out the smaller scale L^{-1}, they may give erroneous estimates of ℓ.

(iv) Source sizes can be determined from the point $m = m_{max}$.

$$\text{Angular diameter } \alpha = \frac{1.22}{z} \times (\text{width of diffraction peaks}) \quad ,$$

$$= \frac{1.22v}{f_c} \quad ,$$

where f_c is the frequency cut-off in $F^{-}(I)$.

(v) From $F^{-}_{r/\lambda z}(I)$, the value of ϕ can be determined by taking the ratio of $F^{-}(I)$ at each minimum with its value at r = 0, if $0 < \phi < 2$, and using the relation

$$\frac{F^{-}_{r/\lambda z}(I)\Big|_{r = k\ell/2}}{F^{-}_{r/\lambda z}(I)\Big|_{r = 0}} = \left\{1 - \frac{2J_1^2(\phi)}{J_0^2(\phi)}\right\}\left\{1 - \frac{k^2}{2L}\right\} \quad . \qquad k = 1, 3, 5\ldots$$

(vi) If $\phi \gg 1$, the dominant J_n occurs at $n = \phi - 1$ for $\phi \lesssim 5$ and for $\phi = 10$, $J_{\phi-1}$ and $J_{\phi-2}$ are comparable.

For $\phi < 10$, the true irregularity scale will be $\sim(\phi-1)\ell$, where ℓ is measured from $F^{-}(1)$.

(vii) The model cannot be used if the power in several scale sizes is comparable.

Acknowledgments

We are grateful to Professor W.A. Coles for the use of some IPS data taken at UCSD, and to Dr. B.H. Briggs for comments and for directing our attention to his paper.

References

Bracewell, R.N.: 1965, The Fourier Transform and its Applications, McGraw Hill, New York.

Briggs, B.H.: 1961, "Diffraction by an irregular screen of limited extent", Proc. Phys. Soc., LXXVII, 305.

Buckley, R.: 1975, "Diffraction by a random phase-changing screen: A numerical experiment", J. Atmos. Terr. Phys., 37, 1431.

Champeney, D.C.: 1973, Fourier Transforms and their Physical Applications, Academic Press, London.

Cohen, M.H., Gundermann, E.J., Hardebeck, H.E., Harris, D.E., Salpeter, E.E., and Sharp, L.E.: 1966, "Radio sources: Angular size from scintillation studies", Science, 153, 745.

Lovelace, R.E., Salpeter, E.E., Sharp, L.E., and Harris, D.E.: 1970, "Analysis of observations of interplanetary scintillations", Astrophys. J., 159, 1047.

Ratcliffe, J.A.: 1956, "Some aspects of diffraction theory and their application to the ionosphere", Rep. Prog. Phys., 19, 188.

Readhead, A.C.S., Kemp, M.C., and Hewish, A.: 1978, "The spectrum of small-scale density fluctuations in the solar wind", Mon. Not. R. Astron. Soc., 185, 207.

Salpeter, E.E.: 1967, "Interplanetary scintillations. I. Theory", Astrophys. J., 147, 433.

Scheuer, P.A.G.: 1968, "Amplitude variations in pulsed radio sources", Nature, 218, 920.

Discussion

Zlotnik: Could you say anything about the shape of irregularities? Are they iostropic or elongated? What about the scale sizes of irregularities?
Alurkar: They are elongated, with typical ellipiticity ratio of around 1.8. IPS determines scale sizes in the range 10 to 1000 km.

15. STIP VII Observations of the Northern Solar Corona - A First Report on the Scope of Data and the Early Results

Thomas A. Croft
SRI International
Menlo Park, California 94025, U.S.A.

Abstract

During late August and early September, 1979, four interplanetary spacecraft passed through superior conjunction. Within a short time their radio signals all passed through the northern corona of the sun on the way to earth. Because this event was foreseen, the months of August and September had been declared to be STIP Interval VII so that observers, using earth-bound instruments and instruments aboard other spacecraft, could acquire data to be correlated with measurements derived from the four interplanetary spacecraft signals. These conjunctions offered an excellent opportunity to observe the plasma within a few radii of the sun, at latitudes between 20^{o} N and the Pole.

In this first report on STIP Interval VII, we stress the type and extent of the measurements that were obtained from the spacecraft. Four types of signal processing will yield different types of information about the solar plasma through its influence on the passing radio signals. These types of processing and their resulting data are described. A severe limitation on

the schedule was the high percentage of available tracking time devoted to Pioneer 11 as it passed Saturn on September 1, 1979. For this purpose, as the highest priority, observing time was assigned to NASA's limited number of receivers. Coverage of the other three spacecraft was achieved through the hard work and enthusiasm of personnel associated with NASA's Deep Space Network (DSN) of receiving stations.

In this report it is not possible to include many of the experimental results because the processing is only partially completed. We do provide a comprehensive guide to the expected results so that the scientific community may have a schedule of our observations.

1. BACKGROUND

As a radio wave travels in interplanetary space, its velocity is affected by the number density of the free electrons. Because the solar wind is mostly ionized hydrogen, it follows that plasma density is almost equal to the electron number density. (A correction can be made for helium to increase the accuracy by a few percent.) The solar wind and corona influence passing radio waves in a variety of measurable ways, most of which are manifestations of changes in the phase velocity, i.e., the speed of the wave fronts.

With American spacecraft, the signals to earth are S-band (2295 MHz) or X-band (8415 MHz). At these frequencies the waves travel slightly faster than the speed of light by an amount that is, for all practical purposes, proportional to the electron number density. Signals that are impressed upon the radio waves by some form of modulation must travel at less than the speed of light, i.e., at the group velocity. Both phase and group velocities depend upon the frequency of the radio wave; plasma effects are much larger at the lower frequencies. Other radio propagation phenomena, such as absorption and scattering, play no part in the program of measurement and analysis we are undertaking.

1.1 Observable Effects

In order to determine interplanetary group velocity, we can impress the same modulation simultaneously on X-band and S-band transmissions from the spacecraft and then measure their relative arrival times at earth. The delay difference shows how much greater the effect was at S-band than at X-band. The delay difference between the two bands is attributable to plasma. Because the group velocity is decreased below the speed of light by a small quantity, which is again proportional to the electron number density, the delay difference can be converted into a measurement of the electron content along the line of sight. (The delay is an integral of delays all along the path. From this we derive an integral of electron number density all along the path,

which is the electron content.)

The measurement of differential group velocity is disadvantageous in two ways: (1) It requires the provision of expensive special equipment on the spacecraft that is often not used for any other purpose, and (2) it is inaccurate in comparison to the corresponding measurement of differential phase delay. Unfortunately, it is not possible to measure the phase delay; we cannot measure the relative time of arrival of waves at the two frequencies because any distinguishing characteristic imparted to a wave that makes up the signal must travel at the group velocity, by definition. Instead we must measure the frequencies of the two signals, that is, the rate of arrival of wave fronts. If the electron content increases, then the frequencies will change accordingly. From frequency measurements we can determine the time rate of change of electron content along the path. This can be integrated with respect to time, yielding the electron content, but the constant of integration can never be determined except by independent measurement of the group delay.

The differential phase delay offers advantages of equipment simplicity and greater accuracy. The best results are achieved when both systems are implemented, as has been done in a solar-wind experiment flown aboard Pioneers 6 through 9 (Croft, 1979).

Small-scale turbulence and irregularity in the corona (or solar wind) causes correspondingly small-scale distortion in the wave fronts that traverse the medium. The resulting interplanetary scintillation (IPS) is most often measured by the signals from radio stars, but spacecraft signals provide a more readily interpreted result because the source of the signal is known to be vanishingly small (in areal extent) and temporally stable.

1.2 Closed-Loop and Open-Loop Records

During the reception of spacecraft signals by the DSN, controllable radio parameters are optimized for the detection of signal characteristics that maximize the likelihood of telemetry success. A fairly crude measurement of scintillation may be obtained from the "closed-loop" records. (This name refers to the fact that the phase-lock loop is fully operational at the time of signal detection.) Such noise data may be available during all the hours that the receiver operates. The great virtue of such records is that they can be obtained for long, uninterrupted intervals at modest cost.

At times of high priority, special recordings are made by highly linear receiving apparatus in which no effort is made to detect the signal. Instead, the signal plus all the noise in predetermined bandwidth is carefully filtered and the resulting noisy waveform is then converted to digits and recorded digitally. By this means, the scientist can gain access to almost any parameter associated with the radio signal with almost no degradation. The best scintillation data are obtained in this manner, which is called "open-loop" recording because there is no phase-lock loop in action at the time of reception. The practical limitation lies in the time and expense of programming and operating a computer to simulate the action of a radio receiver, detect the signal and process it to extract the parameter of interest.

In this report we call the latter type of data a "linear" recording and designate it with symbol L. Those recordings of the detected signal made at the time of actual reception by closed-loop receivers are given the symbol D.

1.3 The Mean and Variance of Plasma Density

In another, broader, view the spacecraft measurements are seen to fall into two classes: (1) Some of the measurements relate to the degree of local irregularity in the plasma; therefore, we consider that these measurements provide information about the variance of the density. (2) In a like manner of thinking, the differential phase and group delay observations provide evidence about the mean value of the density.

2. SPACECRAFT ALIGNMENTS IN AUGUST AND SEPTEMBER

The usefulness of these spacecraft lies in the fact that their radio path to earth passes near the sun. As is suggested by the conceptual sketch in Figure 1, the signals depicted are sensitive to the solar plasma. Their greatest sensitivity by far is in the vicinity of the sun. The tendency for the plasma density to vary roughly as the inverse square of the distance from the sun creates a natural weighting of the sun's plasma influence toward the raypath perihelion. As a consequence, one of the most important experimental parameters is the perihelion distance, perhaps easily visualized in terms of the Sun-Earth-Probe (SEP) angle or the apparent distance of the spacecraft from the sun as they both appear in the sky to the imaginative observer. A useful graphical presentation is then the view of the spacecraft as seen from earth, drawn in a cross section perpendicular to the line of sight and containing the sun. We will use such a drawing, exemplified by Figure 2, which illustrates the closest approach from among the four paths. In this picture, the spacecraft appears to move from left to right with the passage of time, but the motion is only relative to the sun. If the picture were drawn in an inertial frame, then the Voyager would move slowly to the left, but the sun would move more rapidly to the left. These motions are caused by the combined movement of the Voyager and of the observer on earth; because the angular rate of motion of the earth exceeds that of the Voyager, the latter appears to move to the right relative to the sun. The same holds true to Pioneer 11 and Voyager 1, but Pioneer Venus is nearer the sun and thus has a higher angular rate than earth. It appears to move to the left. These actions are diagrammed in Figure 3, which depicts the four trajectories for almost three months. The positions of Helios 1 and 2 are shown in Frame (e) of the figure. In the last frame is shown the relative position of all six spacecraft on one particular day at about the midpoint of the interval of interest. It is important to visualize that each of these spacecraft is in motion at a different rate in a different direction; all the directions are nearly east-west.

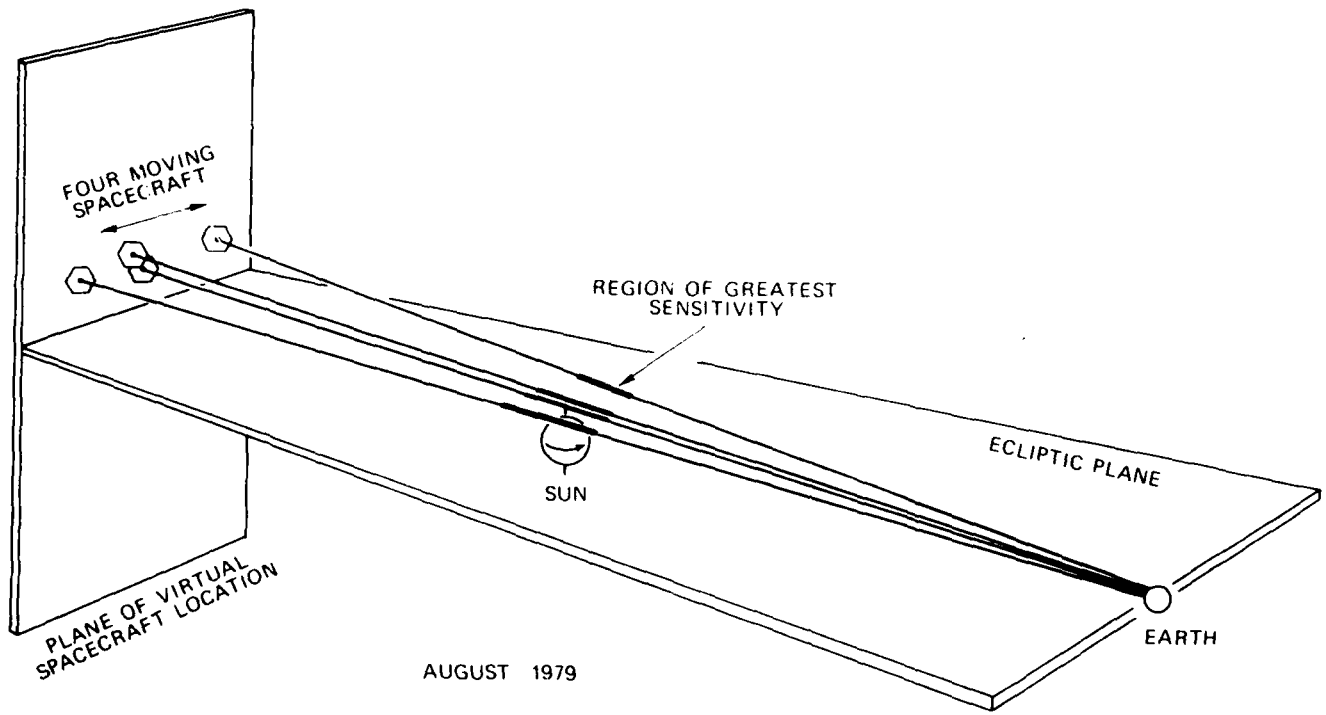

Figure 1. An illustration of the concept that long-path interplanetary signals may be useful for remote sensing in the corona.

Figure 2. The close approach of a signal to the sun is evident in scale drawings of the view from Earth (example provided by D. P. Holmes).

AD-A130 687 PROCEEDINGS OF THE STIP (STUDY OF TRAVELLING INTERPLANETARY PHENOMENA) SY..(U) AIR FORCE GEOPHYSICS LAB HANSCOM AFB MA M A SHEA ET AL. 27 DEC 82 3/3

UNCLASSIFIED AFGL-TR-82-0390 F/G 3/2 NL

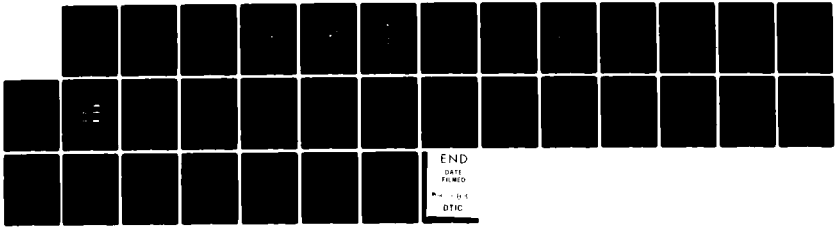

END

DATE FILMED

DTIC

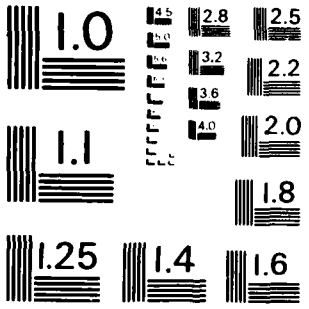

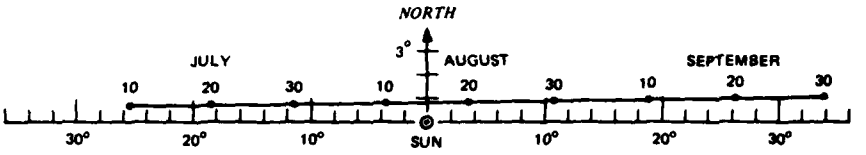

(a) VOYAGER 2 ON TRAJECTORY JSX — MEASURES S- AND X-BAND SCINTILLATION, AND ELECTRON CONTENT

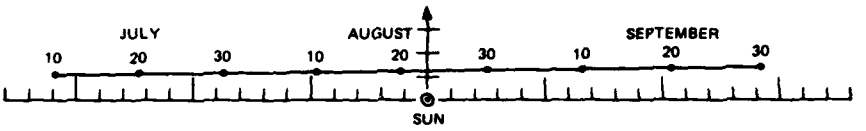

(b) VOYAGER 1 ON TRAJECTORY JST — MEASURES S- AND X-BAND SCINTILLATION, AND ELECTRON CONTENT

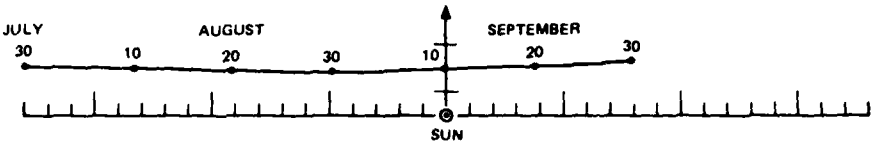

(c) PIONEER 11, PASSING NEAR SATURN ON SEPTEMBER 1 — MEASURES S-BAND SCINTILLATION

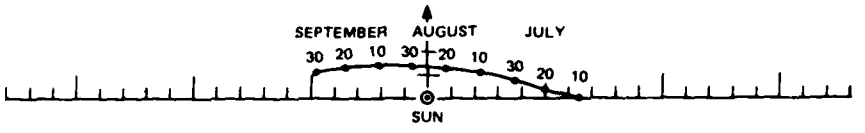

(d) PIONEER VENUS, ORBITING VENUS — MEASURES S- AND X-BAND SCINTILLATION. MIGHT MEASURE RATE OF CHANGE OF CONTENT.

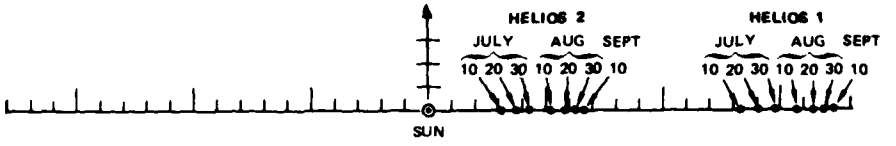

(e) HELIOS 1 AND 2 — MEASURE S-BAND SCINTILLATION

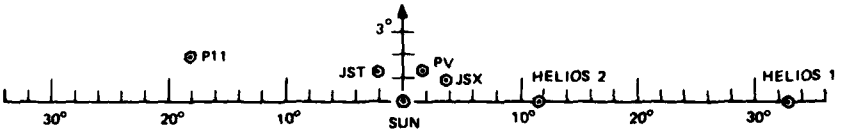

(f) AN EXAMPLE — ALL SPACECRAFT ON AUGUST 20, 1979

Figure 3. Positions of six spacecraft relative to the sun as seen from Earth.

2.1 Encounters Between Spacecraft Along Heliocentric Radials

Because three spacecraft moved right and one moved left, there were three occasions on which two spacecraft radio paths lay along the same radial line from the sun. Figure 4 illustrates the first of these occasions which, in a somewhat humorous vein, have been termed "close encounters". (EOS, 1978.) In this figure we see that the radio paths from Pioneer Venus and from Voyager 2 were in the plane that contained the center of the sun. The plane was tilted 28.4° N of the ecliptic plane. The plasma which traveled through these radio signal paths is assumed to be traveling radially outward from the sun at a solar latitude of about 28°. The important point is that this same plasma passes through both radio paths in turn. To my knowledge, no such encounter has been observed previously.

The value of an encounter is twofold: Firstly, it offers a means for studying the comparative scintillation on the two paths; therefore it is an avenue for determining the evolution of turbulence in the corona while the plasma makes its transit through this important region. Secondly, we hope to find some characteristic delay between the two records that will indicate the time of travel for the plasma to make the 3.2 $R_{\odot}$ trip between the two paths. If this is possible, then we will have an independent measurement of the plasma velocity that can be compared to the same velocity inferred from the scintillation by an established approach. The derivation of a velocity value with high confidence would itself be of value; however, the most useful purpose served would, perhaps, be the calibration of the scintillation approach for deriving velocities.

2.2 The Exceptional Pairing

The closest encounter of all three was that between Voyager 1 and Pioneer Venus depicted in Figure 5. The plasma transit between paths on this day may have occurred in only 10 or 20 minutes. The switch in DSN recording between spacecraft had to be rapid, far faster than the one hour that is conventionally set aside for this task! I travelled to the Goldstone Tracking Station on August 22, 1979 to describe this quick-change objective. With the help of the enthusiastic staff of the station, a series of short cuts were devised so that the transfer was made in only 50 seconds. Considering the complexity of the electronics and the enormous mass of the 64-meter dish that had to be steered in such a short interval, the 50-second switchover is a record that may stand for some time to come. It was only possible through the skill and innovative approach of the operators.

2.3 The Pioneer Pairing

Another, more distant encounter, which is depicted in Figure 6, involved the two Pioneer spacecraft. This and the August 23, 1979 encounter suffered from a weak Pioneer Venus signal. Its high-gain antenna had been disabled intentionally from August 20, 1979 onward so that the Pioneer operators could devote their full attention to the Saturn Encounter. We look forward with considerable interest to the processing of these signals; we hope that they will prove strong enough to provide useful data.

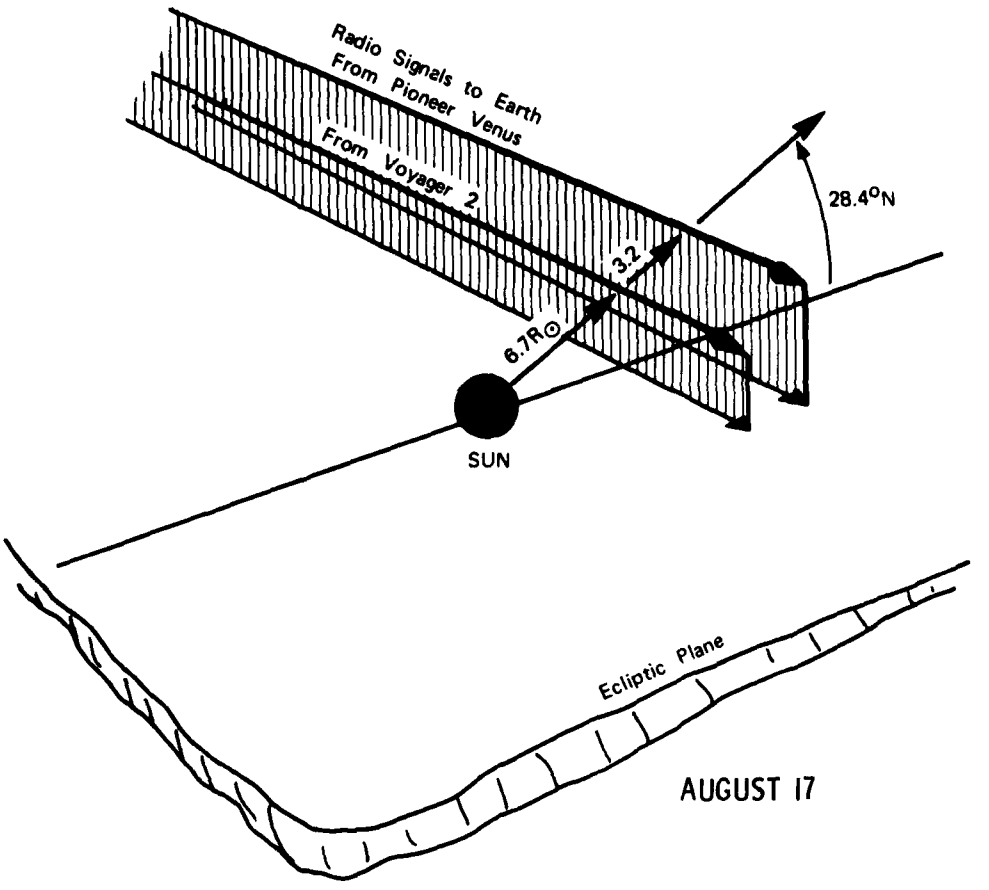

Figure 4. The radial alignment of two signal paths on August 17, 1979.

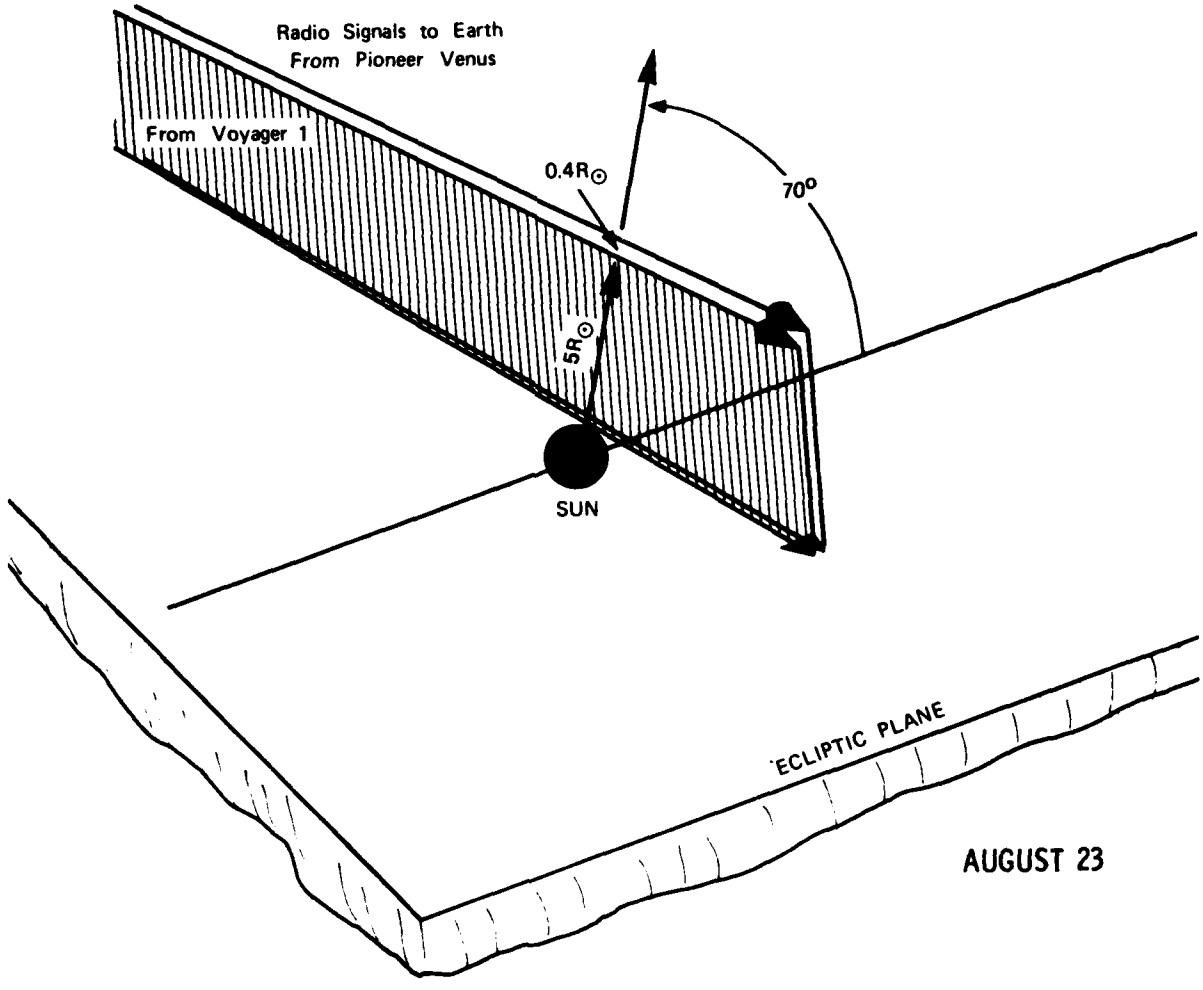

Figure 5. The second radial alignment; the closest encounter of the three.

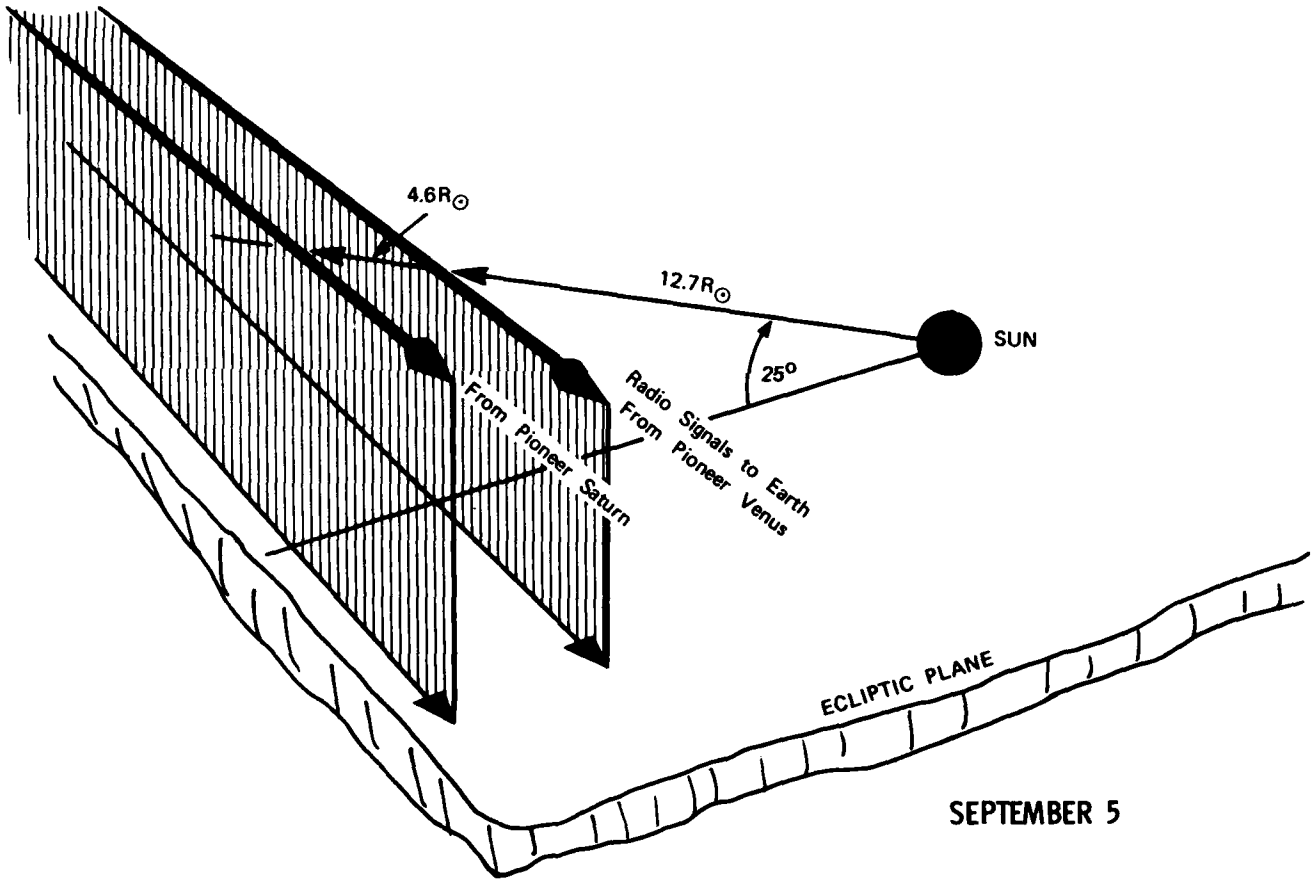

Figure 6. The third and last radial alignment was much like the first except the signals were much weaker.

2.4 A Useful Guide

A summary of the spacecraft positioning during the key parts of STIP VII is shown in Figure 7. This is drawn to scale, as it would appear to an observer on earth if the spacecraft were visible and were photographed each day at 00 UT. Those readers who are contemplating correlative data analysis will find that this figure, together with the tables of the time coverage which are given later, gives a summary of the spacecraft records.

One objective of collaboration will surely be the tracking of solar active regions wherein these spacecraft records offer evidence of the ejection of high speed, turbulent, or dense plasma. The emphasis must be placed upon those active regions at latitudes north of about 20^{o}. With this limitation, the Voyagers and Pioneers show much promise.

3. ILLUSTRATION OF THE FORMS OF OBSERVATION DERIVED

From fluctuations in the frequency of the arriving signal, detected by the closed-loop receivers, the DSN can calculate and record on magnetic tape the "Doppler noise." Information about this parameter is given by a series of articles in the bimonthly "Deep Space Network Progress Report*," which is published by the Jet Propulsion Laboratory of Pasadena, California. An example of the data obtained by Pioneer 11 on September 4, 1979 is presented in Figure 8. The lowest record shows Doppler noise with a sample averaging time of 0.1 second. For the successively higher records these averaging times are 1 second, 10 seconds, and 100 seconds. From a comparison of these, one can derive the spectral index by a method illustrated by Berman and Conteas (1978). These Doppler noise records offer both a means of determining the general level of scintillation and a means of determining the index. In the search for evidence of streams of plasma from the sun, these should serve as primary data because they will be available for many more hours than any other data form. Records such as Figure 8 should be available whenever the direct recordings exist. As we will shortly illustrate via tabulation, these are relatively plentiful.

*Now entitled "The Telecommunications and Data Acquisition Progress Report."

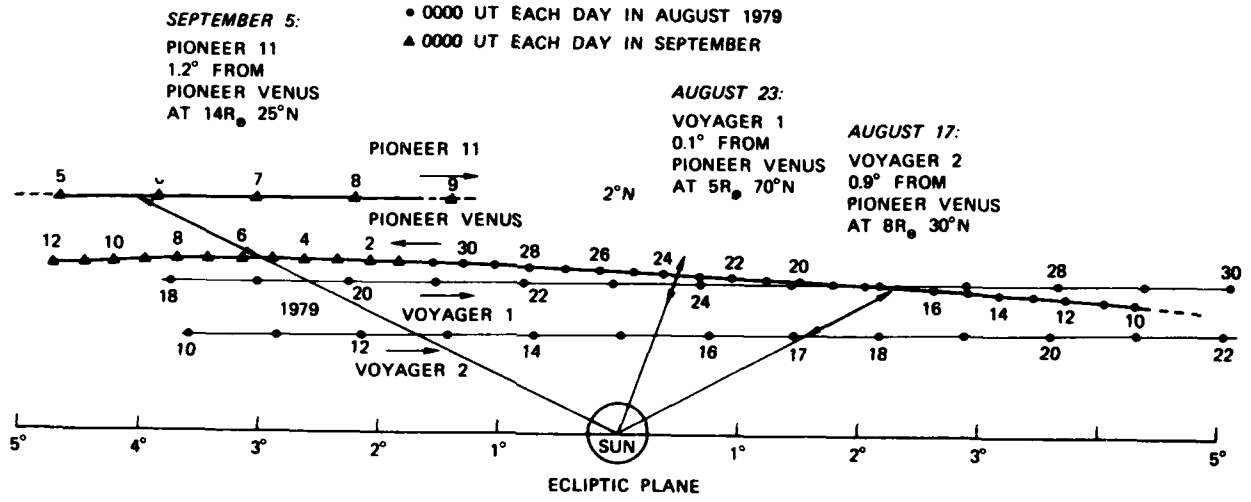

Figure 7. A useful chart which summarizes the geometrical and timing relationships. (The view from earth is drawn to scale.)

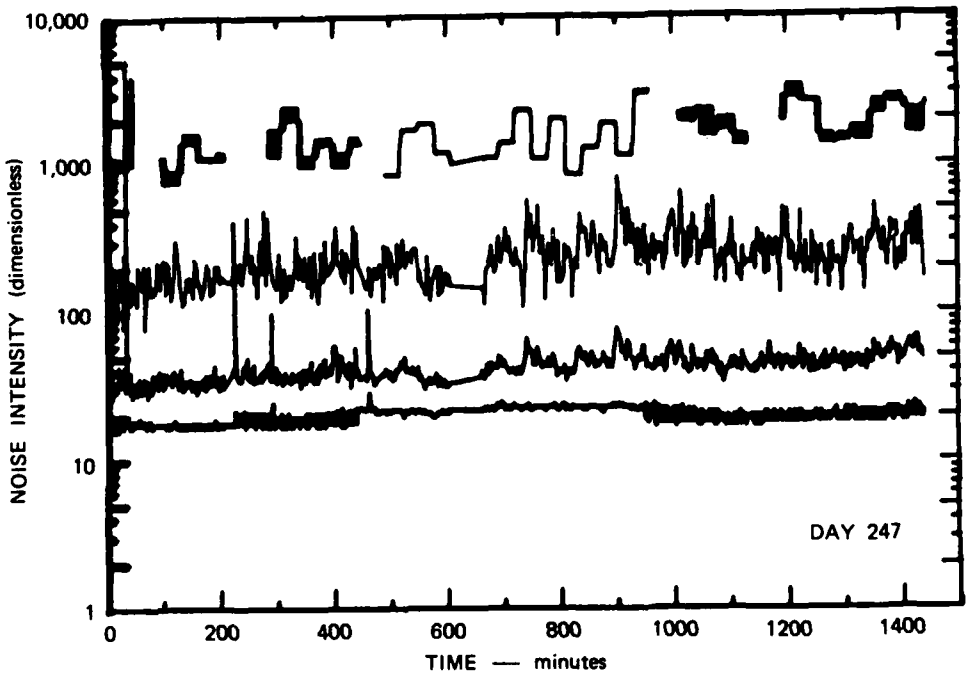

Figure 8. An example of one day's "Doppler noise" records from Pioneer 11, three days after its Saturn encounter. The curves were derived from the same parameter, but averaged over 0.1, 1, 10 or 100 seconds.

3.1 Doppler Noise vs Electron Content

Figure 9 is provided by A. L. Berman (Private Communication) as an illustration that the Doppler noise varies roughly in proportion to the electron content; that is, to the average plasma density along the signal path. In this record, the electron content was derived along the path to Mars using the dual-frequency signals from Viking. The differential group delay approach was used and so the total content could be determined. From the coordinated variation between the Doppler noise and the content, plotted together here, one can see that there is indeed a strong correlation between the two. They are not completely coupled, however. The Doppler noise is, in this respect, much like the scintillation index in that a high value represents a combination of the prevalence of high speed, high density, or high turbulence in some unknown combination. From the standpoint of physics, the observation provides a measurement of the inhomogeneity of the refractive index distribution; this inhomogeneity can be brought about either by a dense region of relatively small turbulence or a diffuse region of intense turbulence.

When direct recordings are available, it is often possible to determine the differential phase delay. The differential phase delay cannot be determined from the Pioneer Saturn direct recordings, because it only uses a single frequency. The Voyagers have a capability to modulate both the S- and X-band signals providing the information necessary to calculate differential group delay. Putting these facts together, we see that direct recordings from Pioneer Venus provide differential phase delay capability and direct recordings from Voyagers provide both differential group and differential phase delay capability. None of these data have yet been processed. Because of intense scintillation we expect that the closed-loop receivers often have detected signals that are too unstable to support these differential delay calculations. Until we have had an opportunity to attempt the processing, we cannot ascertain how much of the electron content measurement can be obtained by these direct means.

3.2 An Example of Past Interplanetary Correlations with Content

To illustrate the value of electron content, and to stress the importance of correlative analysis, Figures 10 and 11 show a series of events that were observed in early 1969. The relative positions of the earth and of the three participating spacecraft are sketched in Figure 10 from which it can be inferred that the solar wind disturbances causing the correlated periods of activity must have spanned many tens of millions of kilometers. The spirals shown in Figure 10 depict the steady-state flow pattern from the sun based upon the Carrington rotation rate and an assumption that the solar wind speed was 400 kilometers per second. One dot is shown for each one hour of travel. The path from earth to Pioneer 8 is shaded to emphasize that the dual-frequency system measured the average solar wind density along the path. (This was a Stanford University-Stanford Research Institute* experiment on four Pioneers.) The density is the electron content divided by the length of the path. As shown on the top plot in Figure 11, the electron content underwent about six discrete increases, which correlated one-to-one with clearly recognizable

*Now SRI International

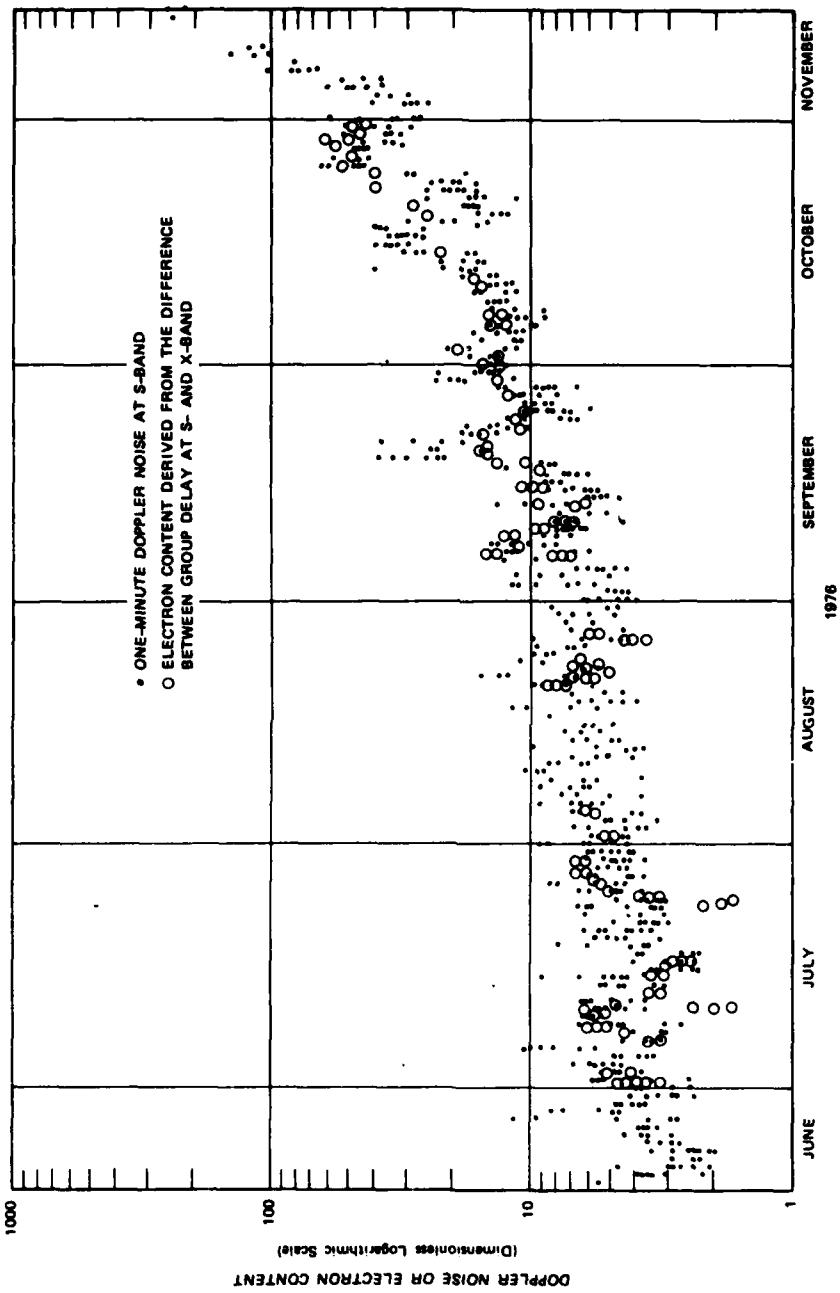

Figure 9. An illustration of the correlation between Doppler noise and electron content (example provided by A. L. Berman, private communication).

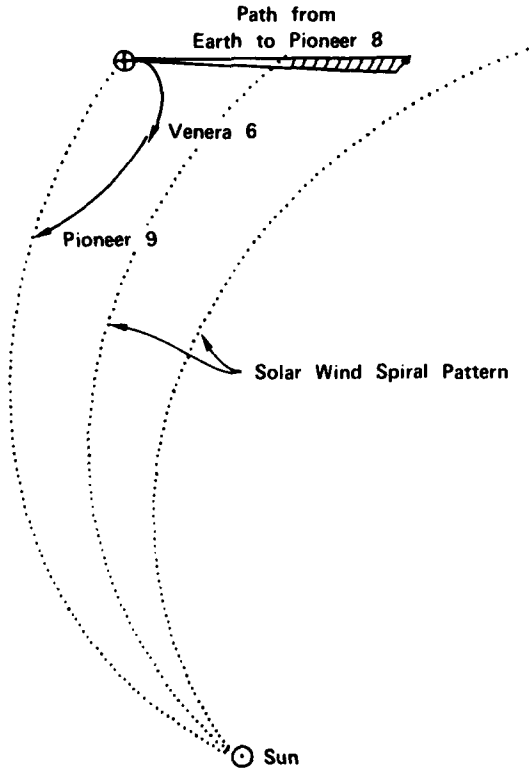

Figure 10. Positions of Earth and of three interplanetary spacecraft during the interval depicted in the next figure.

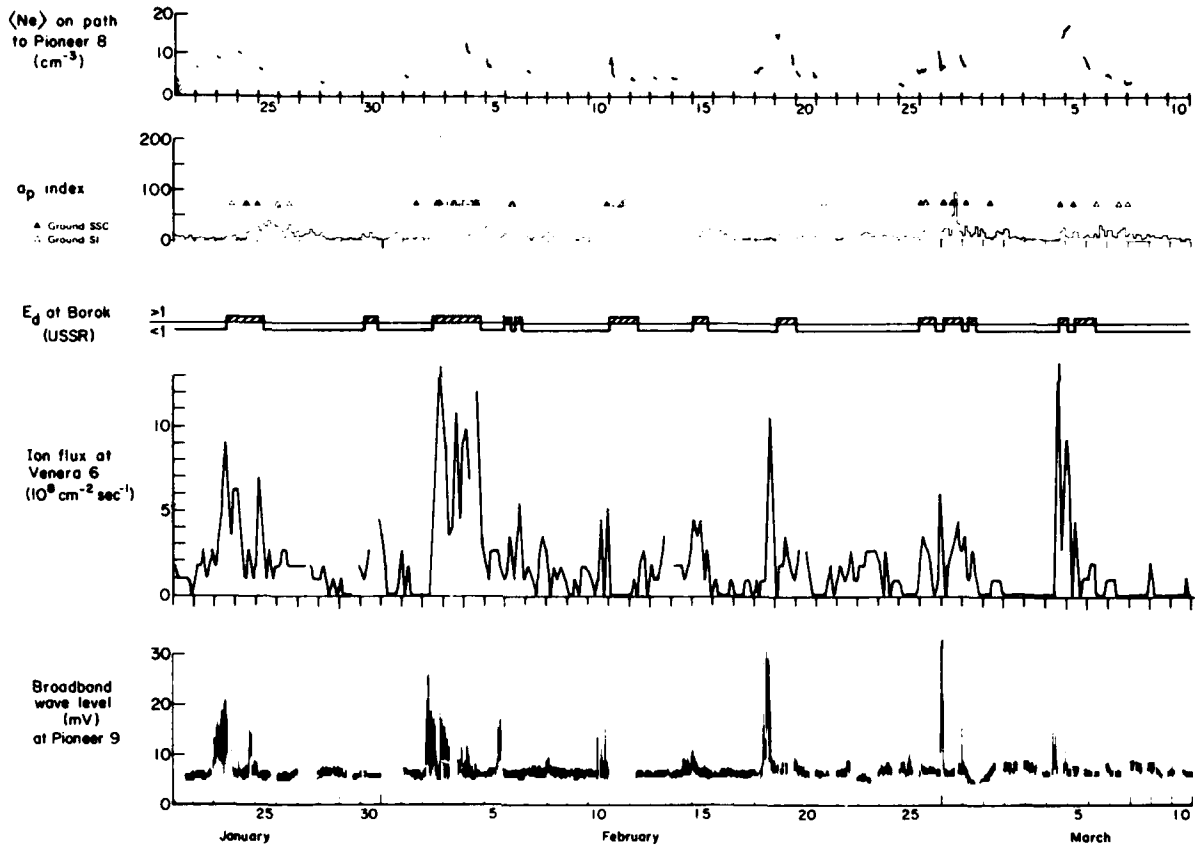

Figure 11. Five forms of data from four regions in space, illustrating the data correlation over tens of millions of kilometers between disparate measurements.

events at earth, at Venera 6, and at Pioneer 9.

The Soviet data, comprising the Venera flux and the earth current index, E_d, from Borok, USSR were obtained from Gringauz et al. (1970). The Pioneer 9 record of broadband wave level is that of Scarf and Siscoe (1971). Scarf and Wolfe (1974) have shown that these wave levels correlate with the solar wind density in the vicinity of the spacecraft. The events shown in Figure 11, interpreted in the light of the geometry of Figure 10, are intended to illustrate that the content observations may yield valuable information if they are correlated with other measurements. The likelihood of correlation is reasonably high, as is shown by the reliable appearance of the same six regions of activity at roughly the same time intervals at the four widely separated interplanetary locations.

3.3 Linear Recordings

Processing of linear recordings by a conventional digital computer would be prohibitively expensive; fortunately, we have an "array processor," which is a specially wired computer adapted for the Fast Fourier Transform. At the time of this writing we have working programs that have produced sample data for the Narrabri meeting, but results of scientific value are not expected until 1980. Figure 12, kindly supplied by the Jet Propulsion Laboratory (Holmes, Private Communication, 1979), shows spectra like those that are presently being derived by our software from the available tapes.

By programming the computer to simulate a phase-lock-loop receiver, it is possible to carry out processes that are unattainable by means of electronics. The signal is detected and its radio frequency phase is recorded for subsequent statistical manipulation. Most of the useful information relating to scintillation is derived from this phase, although for some purposes the strength of the signal (which also scintillates) provides a useful data source. For the moment, we can report only that the linear recordings exist in adequate quantity and their quality seems to be excellent. The processing is just beginning and steady progress is anticipated.

3.4 Other Participating Groups

In addition to the study of these linear recordings by array processor conducted by our group at SRI International, another group at nearby Stanford University, under the direction of Professors V. R. Eshleman and G. L. Tyler, is engaged in a more extensive study of the Voyager linear recordings. Additionally, Drs. R. T. Woo and J. W. Armstrong, at the Jet Propulsion Laboratory, are studying the linear recordings from Pioneer Venus and Pioneer Saturn. The Stanford and Jet Propulsion Laboratory groups are also utilizing the closed-loop records (D) as an adjunct to their studies.

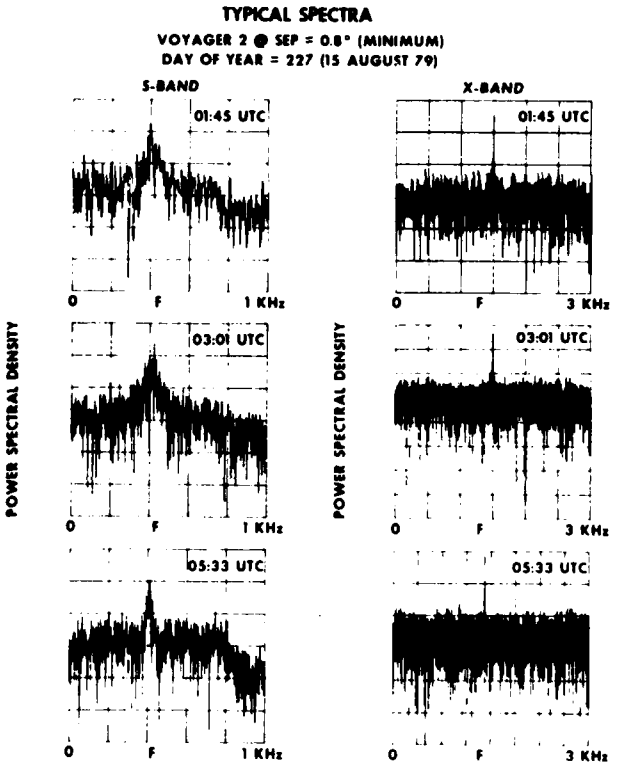

Figure 12. An intermediate data product: Spectra at S-band (2295 MHz) and at X-band (8415 MHz) derived from linear recordings of the Voyager 2 signals (D. P. Holmes, private communication, 1979).

4. SCHEDULE OF DATA AVAILABILITY

Most of the information about the Pioneer data is now available, but the Voyager picture is still incomplete. In any case, the Voyager records will contain more of the closed-loop data (D) than is shown in the following tables.

In Tables 1 through 8, we have included a computerized status report that summarizes the extent of the data. In the coming months, as the picture emerges and more details become clear, we will make successive corrections to this computer file and periodically issue a corrected set of tables to any scientist who expresses an interest.

In addition to the part of the tables that describes the availability of data, we plan to add comments about the activity, evident in those data. There was (fortunately) a great deal of solar activity during STIP Interval VII. For the moment we have not attempted to incorporate measures of solar activity although it would be a natural extension of the record to include such information.

To read these tables correctly, please note that an entry of D means that the direct recordings are available for some part of the one hour interval beginning at the time shown in the heading. Similarly, L means linear recordings exist. Typically, recordings are continuous for several hours. A continuous string of Ds extending over five consecutive hourly periods might mean that the record lasted as much as five or as little as three hours: that it began in the first hour and extended into the fifth hour. Those investigators who find the first and last hours of timing critical should contact us for greater detail. The inner hours in any such group of letters can be considered as fully covered.

5. SUMMARY

During the passage of the four spacecraft through conjunction, we obtained extensive records of radio signals that travelled the solar corona about 1° to 2° N of the sun. Four types of derived data are starting to appear as the processing gets underway, but few experimentally significant results are ready to be presented. With the exception of the Voyager closed-loop (D) recordings, we provide a summary of the schedule of data that will become available. Those who have relevant observations of the sun or of the solar wind are encouraged to collaborate in the study of these data.

Acknowledgments

This work was sponsored by the Air Force Geophysics Laboratory and by the National Aeronautics and Space Administration.

References

Berman, A. L., and Conteas, A. D.: 1978, "Radial and solar cycle variations in the solar wind phase fluctuation spectral index as determined from Voyager 1978 solar conjunction data", The Deep Space Network Progress Report 42-48, p. 58.

Croft, Thomas A.: 1979, "A graphical summary of solar wind electron content observations by Pioneer 6, 8, and 9", J. Geophys. Res., 84, 439.

EOS: 1978, "Solar wind study", EOS Transactions, 59, 906.

Gringauz, K. I., Troitskaya, V. A., Solomatina, E. K., and Shchepetnov, R. V.: 1970, "Variations of solar wind fluxes observed on board Venera-5 and Venera-6 from January 21 to March 21 1969 and pulsations of the earth's electromagnetic field caused by these variations", in V. Manno and D. E. Page, (eds.), Intercorrelated Satellite Observations Related to Solar Events, D. Reidel, Dordrecht, p. 130.

Scarf, F. L., and Siscoe, G. L.: 1971, "The Pioneer 9 electric field experiment: Part 2, Observations between 0.75 and 1.0 AU", Cosmic Electrodynamics, 2, 44.

Scarf, F. L., and Wolfe, J. H.: 1974, "Pioneer 9 plasma wave and solar plasma measurements for the August 1972 storm period", J. Geophys. Res., 79, 4179.

TABLE 1. THE WEEK BEGINNING AUGUST 03, 1979

```
                    UNIVERSAL TIME OF DAY
S/C                      AM                        PM
    M | | | | | | | | | N | | | | | | | | | | | M
    0   2   4   6   8  10  NOON  2   4   6   8  10  12

AUGUST 3 - DAY 215
PV
PS
V1  D D D D D D D D   D D   D D D D D D D D
V2

AUGUST 4 - DAY 216
PV
PS
V1      D D D D D D   D D D D D D D D D D D
V2

AUGUST 5 - DAY 217
PV
PS
V1  D D D   D D D D   D D D D D D D D D D D
V2

AUGUST 6 - DAY 218
PV
PS
V1              D D   D D D D D D D D   D D
V2

AUGUST 7 - DAY 219
PV
PS
V1          D D D D   D D D D D D D D D D D
V2

AUGUST 8 - DAY 220
PV
PS
V1  D D D D D D D D
V2  D D D D   D D D                 D   D D

AUGUST 9 - DAY 221
PV
PS
V1  D D D D D D D D D                       D D     D
V2    D D   D D
```

TABLE 2. THE WEEK BEGINNING AUGUST 10, 1979

```
                    UNIVERSAL TIME OF DAY
S/C                      AM                        PM
    M | | | | | | | | | N | | | | | | | | | | | M
    0   2   4   6   8  10  NOON  2   4   6   8  10  12

AUGUST 10 - DAY 222
PV  D D D D D D D D D D D D D D D D D D D D D D D DLD D
PS
V1  D D D D D D D D
V2    D DLDLDLDLDL                  DLDLDLDLDL

AUGUST 11 - DAY 223
PV  D D D D D D D D D D D D D D D D D D D D D D D DLD D
PS
V1  D D D D D D D D
V2    DLDLDLDLDL                    DLDLDLDLDL

AUGUST 12 - DAY 224
PV  D D D D D D D D D D D D D D D D D D D D D D D DLD D
PS
V1  D D D D D D D D
V2    DLDLDLDLDL                    DLDLDLDLDL

AUGUST 13 - DAY 225
PV  D D D D D D D D D D D D D D D D D D D D D D D DLD D
PS
V1  D D D D D D D D
V2    DLDLDLDLDL                    DLDLDLDLDL

AUGUST 14 - DAY 226
PV  D D D D D D D D D D D D D D D D D D D D D D D DLDLD
PS
V1  D D   D D D D D
V2    DLDLDLDLDL                    DLDLDLDLDL

AUGUST 15 - DAY 227
PV  D D D D D D D D D D D D D D D D D D D D D D D DLDLD
PS
V1  D D D D D D D D                                 D D
V2    DLDLDLDLDL                    DLDLDLDLDL

AUGUST 16 - DAY 228
PV  D D D D D D D D D D D D D D D D D D D D D D D D D D
PS
V1
V2    DLDLDLDLDL                                DLDLD
```

(PV = Pioneer Venus, PS = Pioneer 11 = Pioneer Saturn, V1 = Voyager 1 and V2 = Voyager 2)

TABLE 3. THE WEEK BEGINNING AUGUST 17, 1979

UNIVERSAL TIME OF DAY

```
S/C   M  |  |  |  |  |  |  |  |  |  |  |  N  |  |  |  |  |  |  |  |  |  |  |  M
      0  |  2  |  4  |  6  |  8  |  10 |  AM |  NOON  2  |  4  |  6  |  8  |  10 |  PM 12
```

AUGUST 17 - DAY 229
PV D D D D D D D D D D D D D D D D D D D D DLDLD
PS
V1
V2 DLDLDLDLDL

AUGUST 18 - DAY 230
PV D D D D D
PS
V1 DLDLDLDL
V2

AUGUST 19 - DAY 231
PV D D D D D
PS
V1 DLDLDLDLDL
V2

AUGUST 20 - DAY 232
PV D D D D D
PS
V1 DLDLDLDLDL
V2

AUGUST 21 - DAY 233
PV D D D
PS
V1 DLDLDLDLDL
V2

AUGUST 22 - DAY 234
PV D D D
PS
V1 DLDLDLDLDL
V2

AUGUST 23 - DAY 235
PV DLDL
PS L
V1 DLDLDLDL
V2 D D D

TABLE 4. THE WEEK BEGINNING AUGUST 24, 1979

UNIVERSAL TIME OF DAY

```
S/C   M  |  |  |  |  |  |  |  |  |  |  |  N  |  |  |  |  |  |  |  |  |  |  |  M
      0  |  2  |  4  |  6  |  8  |  10 |  AM |  NOON  2  |  4  |  6  |  8  |  10 |  PM 12
```

AUGUST 24 - DAY 236
PV D
PS
V1 DLDLDLDLDL
V2 D D D D

AUGUST 25 - DAY 237
PV D D
PS
V1 DLDLDLDL
V2 D D D D D D D D D D

AUGUST 26 - DAY 238
PV D
PS
V1 DLD DLDLDLDL
V2 D D D D D D D D D D

AUGUST 27 - DAY 239
PV D D
PS
V1 DL
V2 D D D

AUGUST 28 - DAY 240
PV D
PS
V1
V2 D D

AUGUST 29 - DAY 241
PV D
PS
V1
V2 D D D D D D D D D D D

AUGUST 30 - DAY 242
PV D D D D
PS
V1 D D D D
V2 D D D D DLDLDLDLDLD

TABLE 5. THE WEEK BEGINNING AUGUST 31, 1979

UNIVERSAL TIME OF DAY

```
S/C          AM                                  PM
    M | | | | | | | | | N | | | | | | | | | | | M
    0   2   4   6   8  10 NOON 2   4   6   8  10  12

AUGUST 31 - DAY 243
PV                                                 D D
PS
V1  D                                                 D D
V2  DL                                  D D D D D DLDLDLDLDL

SEPTEMBER 1 - DAY 244
PV                                                    D D
PS                      D D D D D D D D D D D D D D    D D
V1  D D D D D D D                                     D D
V2  D                                   D

SEPTEMBER 2 - DAY 245
PV  D
PS  D D D D D D D D D D D D D D D D D D D D D D D D D D
V1  D D D D D D                                       D D
V2  DL                                  D D D D D D D D D D

SEPTEMBER 3 - DAY 246
PV                                          D
PS  D D D D D D D D D D D D D D D D D D D D D D D D D D
V1  D D D D D D D                                     D D
V2  D                                     D D D D D D D D D

SEPTEMBER 4 - DAY 247
PV                                        D D       D D D
PS  D D D D D D D D D D D D D D D D D D D D D D D D D D
V1  D D D D D D D   D D D D D D D D D D D D
V2                                      D D D D D D D D D D

SEPTEMBER 5 - DAY 248
PV                                        DLDLDL  D   D
PS  D D D D D D D DLDLDLDLDLDLDLDLDLDLDLDLD D D D D D
V1  D D D D D D D                                     D
V2  D                                   D D D D D D D D D D

SEPTEMBER 6 - DAY 249
PV                                                  D D D
PS  DLDLDLDLDLDLDLD D D DLDLDLDLDLDLDLDLDLDLDLDLD D
V1    D D D D D D                                     D D
V2  D                                   D D D D D D D D D D
```

TABLE 6. THE WEEK BEGINNING SEPTEMBER 7, 1979

UNIVERSAL TIME OF DAY

```
S/C          AM                                  PM
    M | | | | | | | | | N | | | | | | | | | | | M
    0   2   4   6   8  10 NOON 2   4   6   8  10  12

SEPTEMBER 7 - DAY 250
PV                                        D D       D D
PS  D D D D D D D D D D D D D D DLD D D D D D D D D D
V1  D D D D D D D                                     D D
V2  D                                     D D

SEPTEMBER 8 - DAY 251
PV                                          D       D D
PS  D D D D D D D D D D D D D D DLDLDLDLDLDLDLDLDLDLDL
V1  D D D D D D D                                     D D
V2

SEPTEMBER 9 - DAY 252
PV                                        D D D D
PS  DLD D D D D D D D D D D D D D D D D D D D D D D D D
V1  D D D D D D D                         D D D D D D D D D D
V2

SEPTEMBER 10 - DAY 253
PV                                  D D D D D       D D
PS  D D D D D                                 L L L L L
V1  D D           D D D                   D D D D D D D D D
V2                                                    D D D

SEPTEMBER 11 - DAY 254
PV
PS
V1  D                                       D D D D D D D D D D
V2  D D D D D         D D D   D D D                   D D D

SEPTEMBER 12 - DAY 255
PV
PS
V1  D               D D D D D D D D D D D       D
V2  D D                               D D D   D D D D D D

SEPTEMBER 13 - DAY 256
PV
PS
V1  D D D D D D D
V2  D                       D D D D D D D             D D D
```

TABLE 7. THE WEEK BEGINNING SEPTEMBER 14, 1979

```
                    UNIVERSAL TIME OF DAY
S/C                      AM                        PM
    M | | | | | | | | | | N | | | | | | | | | | M
    0   2   4   6   8  10 NOON 2   4   6   8  10  12

SEPTEMBER 14 - DAY 257
PV
PS
V1
V2  D D   D D     D D D D D D D D D

SEPTEMBER 15 - DAY 258
PV
PS
V1
V2

SEPTEMBER 16 - DAY 259
PV
PS
V1
V2

SEPTEMBER 17 - DAY 260
PV
PS
V1
V2                                                  D D D D

SEPTEMBER 18 - DAY 261
PV
PS
V1
V2  D D D D D D   D D D D D D D D D D D           D D D

SEPTEMBER 19 - DAY 262
PV
PS
V1
V2  D D D D D   D D D D D D D D D D D           D D D

SEPTEMBER 20 - DAY 263
PV
PS
V1
V2  D D D D D D                 D D D D D D D D D D
```

TABLE 8. THE WEEK BEGINNING SEPTEMBER 21, 1979

```
                    UNIVERSAL TIME OF DAY
S/C                      AM                        PM
    M | | | | | | | | | | N | | | | | | | | | | M
    0   2   4   6   8  10 NOON 2   4   6   8  10  12

SEPTEMBER 21 - DAY 264
PV
PS
V1
V2              D D D D D D D D D D D           D D D

SEPTEMBER 22 - DAY 265
PV
PS
V1
V2  D D D D D

SEPTEMBER 23 - DAY 266
PV
PS
V1
V2

SEPTEMBER 24 - DAY 267
PV
PS
V1
V2                                          D D D

SEPTEMBER 25 - DAY 268
PV
PS
V1
V2              D D D D D D D D D D D         D D D D

SEPTEMBER 26 - DAY 269
PV
PS
V1
V2  D D D D D D D D D D D D D D D D D D D D D D

SEPTEMBER 27 - DAY 270
PV
PS
V1
V2            D D D D D D D D D D D         D D D D
```

16. Unusually Intense Jovian Decametric Emission Observed on 1979 March 7, 1920 - 2040 UT

K. Bullough and W. Gibbons
Department of Physics,
University of Sheffield,
Sheffield, S37 RH. U.K.

Abstract

On 1979 March 7 in the period 1920-2040 UT extremely intense Jovian decametric emissions were recorded at Bradfield (53°26' N., 1°35' W.) near Sheffield. The emission was first detected after dusk at 1920 UT, when radio and communication interference fell to a low level. The initial signal intensity lay in the range 10^{-17} to 10^{-16} W m^{-2} Hz^{-1}, rising to 10^{-15} W m^{-2} Hz^{-1} in the period 2011-2027 UT and finally attaining a remarkable 10^{-14} W m^{-2} Hz^{-1} at 2032-2040 UT. The emission ceased at 2041 UT. The Jovian SIII longitude and Io phase at the beginning and end of the period were 210°.5/61°.2 and 248°.8/72°.5 respectively, corresponding to a non-Io-related source of emission.

A detailed analysis of the scintillation spectrum and indices has made it possible to identify contributions from the ionosphere and interplanetary medium and in the latter case to distinguish clearly between scattering from power-law and Cambridge small-scale irregularities. Immediately following an abrupt increase in

signal intensity at 2011 UT the ionospheric Faraday scintillation virtually disappeared, leaving only the interplanetary scintillation component (IPS). This indicated (i) that the source signal was almost perfectly circularly polarized and (ii) that the contribution to the scintillation from the Jupiter ionosphere was negligible. The scintillation data indicated a "point source" at this time with diameter <2000 km and a possible diameter during the most intense emission of up to 30,000 km.

It appears that this event was initiated by the same solar wind sector and particles that 12-14 days previously had initiated a great magnetic storm at the Earth. This dependence on magnetic disturbance is similar to that of auroral kilometric radiation on Earth.

An extremely efficient mechanism for particle-to-wave energy conversion and highly beamed emission are required. We suggest that the emission may have originated in cyclotron solitons (*Cole and Pokhotelov*, 1980) on a northern field line where the local gyrofrequency was greater than but close to 9 MHz, and whose direction at the source was towards the Earth. Such an event would be detectable at stellar distances.

1. INTRODUCTION

Decametric radio emission has been studied systematically for more than 20 years; for reviews see Warwick (1967), Gehrels (1976) and recent information from the Voyager programme (see June 1979 issue of Science). These studies have established such features as: (i) the identification of L-bursts and S-bursts; (ii) the signal polarization (usually RH elliptically polarized, especially at frequencies >20 MHz, and with the major axis close to perpendicular to the axis of rotation of Jupiter; (iii) the effect of propagation through the interplanetary medium and ionosphere on signal scintillation and fading; (iv) the dependence of signal occurrence on the Jupiter SIII longitude and Io phase. In particular the influence of Jovian SIII longitude, Io phase, and earth declination, D_E, on the reception of decametric emission has been shown to imply a very highly beamed ($\lesssim 6^\circ$ cone) signal.

It has been suggested that the main source of emission, centred on SIII longitude 240°, is associated with energetic particle precipitation into the magnetic anomaly in the northern hemisphere centred on SIII longitude 270°. The most common polarization (RH) for simple cyclotron emission is consistent with a source near the North Pole. Cole and Pokhotelov (1980) have recently proposed a cyclotron soliton mechanism for generation of the auroral kilometric radiation observed in the Earth's magnetosphere. This process is extremely efficient for particle-to-wave energy conversion. The radiation is beamed, at the source, along the field line (RH circularly polarized in the north) and has a frequency approximately twice the local gyrofrequency. It appears to be the only model which can account simultaneously for the signal power, polarization and lack of Faraday rotation and scintillation in the fraction of the propagation path lying in the Jupiter ionosphere and magnetosphere.

The observations described here were made during a project for third-year astronomy students which included, besides the recording of Jovian decametric emission, the measurement of galactic noise and a study of the diurnal behaviour of the ionosphere and its effect on radio reception. A more detailed paper is being prepared (*Bullough et al.*, 1979).

2. EQUIPMENT AND DATA ANALYSIS

The equipment (Figure 1) consisted of a three-element Yagi mounted at a height of 0.534 λ above the ground at Bradfield (53°26' N., 1°35' W.) near Sheffield.

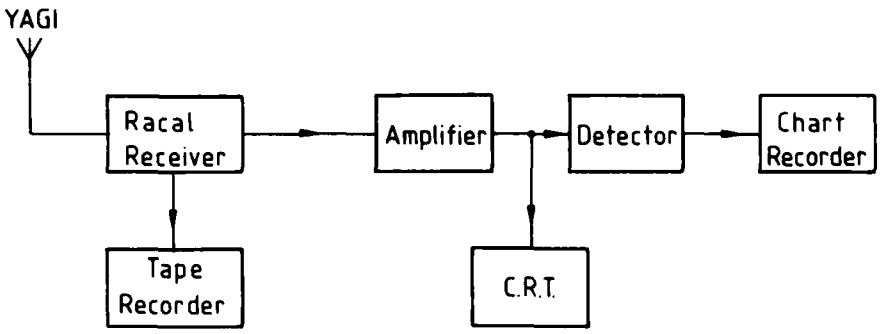

Figure 1. A block diagram of the equipment.

The beam direction was mostly maintained at a bearing 155° east of north. During the period of observation the azimuth and elevation of Jupiter increased from 135° to 166° E. of N. and 51° to 57° respectively. The influence of the F-region on radio interference, which allowed us to recognize the Jupiter signal at 1920 UT - and relatively unperturbed from 1940 UT onwards - is shown in Figure 2. The strong signal drove the receiver into a non-linear region of its response and a gain adjustment was made at 2015 UT. The original record was digitized at 2.4-s intervals, and after careful calibration a graph of the corrected signal strength (dB) was obtained (Figure 3). We also analysed selected 2-min periods which were photographically enlarged (10 times) before digitization at intervals of 0.24 s. The effective frequency response for the chart-recorded signal was 35 Hz (to -3 dB) and 70 Hz (to -6 dB) with corresponding response time, $\Delta t \approx (\pi\Delta f)^{-1}$, of 0.01 s and 0.005 s respectively. The low time resolution was appropriate to a study of the ionospheric contribution to signal fluctuation (~10 s) and also fluctuation in the source. The high time resolution made it possible to study the IPS component. A detailed spectral analysis was made and the scintillation indices S_2, S_4 obtained (Briggs and Parkin, 1963; Rufenach, 1972, 1975).

3. BACKGROUND TO THE OBSERVATIONS

The observations were made during the ascending phase of sunspot cycle 21. However, the overall sunspot activity was far higher than predicted. Zurich sunspot numbers for January, February and March were 166, 138 and 137, that for

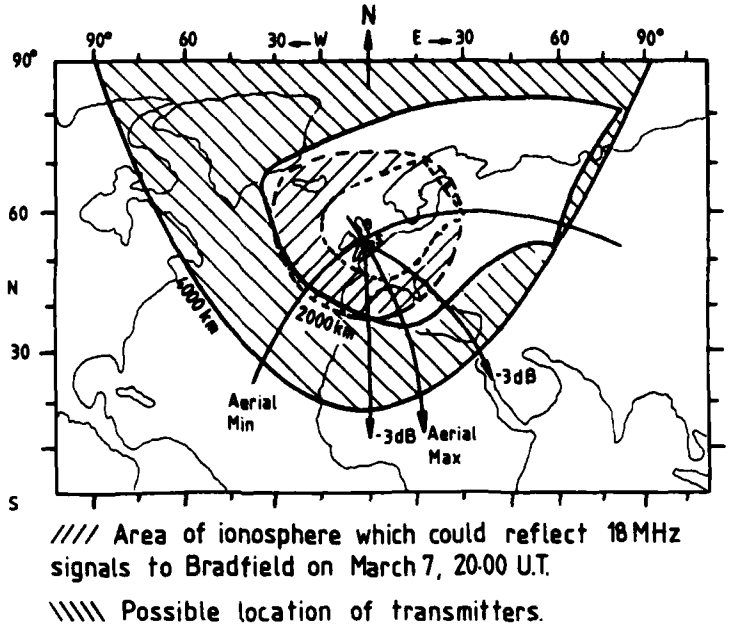

Figure 2. A map to show the area of the F-region which could have supported 18 MHz transmission to Bradfield on 1979 March 7 at 2000 UT, and the geographical location of possible transmitters, assuming a single-hop transmission.

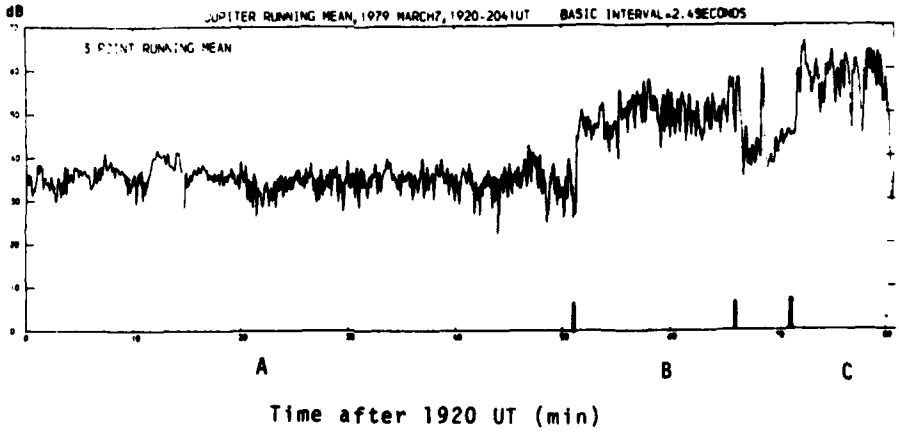

Figure 3. The Jupiter signal (1920-2041 UT), intensity (dB) vs time, digitized at 2.4-s intervals and corrected for receiver response. A three-point running mean has been applied. At 1920 UT: 0 dB = 0.72×10^{-20} W m^{-2} Hz^{-1}. At 2040 UT: 0 dB = 2.03×10^{-20} W m^{-2} Hz^{-1}.

January being the highest recorded since August 1959. The sector of solar wind which gave rise to the March 7 event is the same as that which gave rise to the geomagnetic storm of February 21/22, in agreement with the work of Barrow (1979). The dependence of Jupiter emission on solar wind parameters (velocity, interplanetary field strength and orientation) may therefore be similar to that for substorm activity in the Earth's magnetosphere (Akasofu, 1979).

Jupiter was situated at a distance of 4.57 AU from the Earth at a solar elongation of 133° E. Thus the Jupiter ray propagated closely parallel to the interplanetary field in the vicinity of the Earth. The declination, D_E, of the Earth, was +0°.64. Assuming a mean height of 350 km we see that the ray intersected the F-layer close to Slough (47°35' N., 9°41' E.), as listed in Table 1.

Table 1.

Intersection of the Jupiter ray with the F-layer

Time UT	Bradfield Azim.	Bradfield Elev.	Bradfield Long.	Bradfield Lat.	Angle of incidence to F-layer	Ray/geomagnetic field angle	Distance from Bradfield to layer (km)
1920	135°.0	50°.9	1°.1 E.	51°.7 N.	36°.7	42°.1	444
2000	149°.3	55°.5	0°.1 E.	51°.6 N.	33°.4	39°.0	424
2041	165°.5	56°.9	0°.8 W.	51°.6 N.	31°.2	40°.8	413

The Slough ionosonde and the Kp indices for March 7 indicated a normal F-layer with no Spread F (Kp = 3-, 3, 1+, 0+, 0+, 1, 2-, 2) (f_0F_2 (MHz) = 11.9, 9.2 and 7.6 at 1900, 2000 and 2100 UT respectively). These f_0F_2 values and the Ionospheric Prediction Service MUF graphs (published by U.S. Department of Commerce Publ. OT/TRER 13 Vol. 1.4) were used to construct Figure 2.

4. THE SIGNAL SCINTILLATION

From Fremouw and Rino (1973) and Briggs and Parkin (1963) we obtain a predicted scintillation index S_4 = 0.04, much lower than that observed for the low-frequency end of the scintillation spectrum (Figure 4). It was found possible to attribute the low-frequency component to Faraday rotation as the F-layer faded and differential Faraday rotation as the F-region irregularities moved through the first Fresnel zone. This deduction is confirmed, in remarkable fashion, by the variation in source signal polarization. When the signal became almost perfectly circularly polarized at 2011 UT, the ionospheric contribution to the scintillation disappeared (Figures 4 and 5).

Following the method of Readhead (1971) we calculated the scattering power of the IPS irregularities as a function of distance from the Earth to Jupiter and

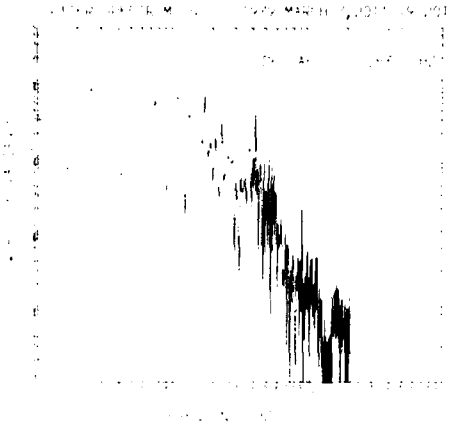

Figure 4. The power spectrum immediately after the sudden increase in signal intensity at 2011 UT.

hence, by numerical integration, S_4 as a function of source angular diameter (Figure 6). From Figure 6(a) it is clear that the scattering occurs close to the Earth, and assuming a point source, Gaussian irregularities and weak scattering, we obtain a maximum value of $S_4 = 0.53$. In Figure 5(a) S_4 (total) falls dramatically, at the moment of signal increase, to 0.61. This is close to the value 0.63 which we obtain, by extrapolation, from the Cambridge 81.5 MHz observations, and somewhat above our calculated value of 0.53. Afterwards the index recovered steadily to unity, later falling to ~0.8 during the period of most intense emission. The only possible explanation for the minimum value, $S_4 = 0.61$, is that the signal became almost perfectly circularly polarized, thereby eliminating the ionospheric contribution and demonstrating, fairly conclusively, that Faraday rotation and differential rotation are responsible. We may also conclude that Faraday rotation and scintillation in the Jupiter ionosphere/magnetosphere are both very small, indicating that the source is located some distance above that height in the ionosphere where the plasma frequency, ω_p, equals ω, the signal frequency. An important feature of Figure 4 is that, because of the enormous signal power available, we observe and can identify the IPS contribution from both the power-law irregularities (~0.1 to 1.4 Hz) and also the Cambridge small-scale irregularities ($\nu > 1.4$ Hz). The best estimate of solar wind speed in this part of the solar cycle is 400 km s^{-1} (see Gosling et al., 1976). For distance $z \approx 0.2$ AU and solar elongation 133° this yields a Fresnel cut-off frequency ν_f of 0.23 Hz (Rufenach, 1974) close to that observed. For the small-scale irregularities which are possibly elongated along the interplanetary magnetic field (Cronyn, 1972) we obtain $1.17 < \nu < 2.11$ Hz for scale sizes in the range 250 to 139 km, in excellent agreement with Figure 4. From the slope (rather ill-defined) we obtain a power-law spectrum for the irregularities: $P(k) \approx k^{-\alpha}$ where k is the wavenumber and $\alpha = 4.6$ (somewhat higher than usual).

There are three independent features at 2011 UT which indicate a very localized source:

(i) an extremely rapid rise of 11 dB in <0.01 s ($\therefore c\Delta t \approx 3{,}000$ km);

(ii) a cohesive source giving rise to a circularly polarized signal;

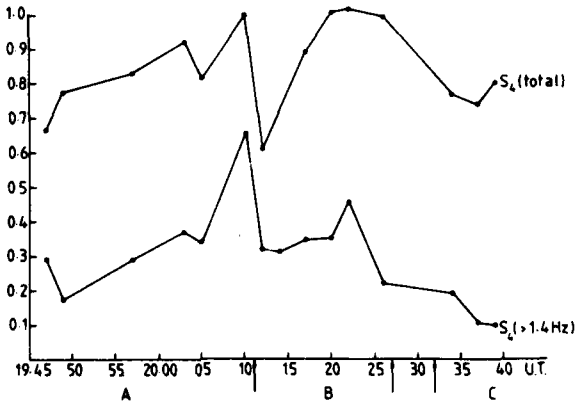

Figure 5(a). The variation in the scintillation index S_4 in the period 1945-2040 UT. (i) All frequencies, S_4 (total). (ii) Contribution from the Cambridge small-scale irregularities (S_4 > 1.4 Hz).

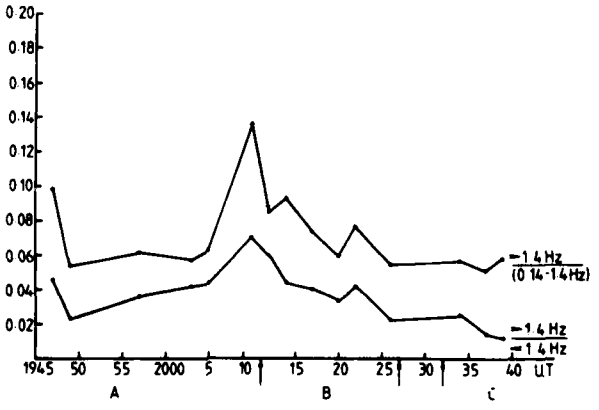

Figure 5(b). The temporal variation in the S_4 ratios:
(i) $\frac{S_4(>1.4\text{ Hz})}{S_4(<1.4\text{ Hz})}$; (ii) $\frac{S_4(>1.4\text{ Hz})}{S_4(0.14 < \nu < 1.4\text{ Hz})}$

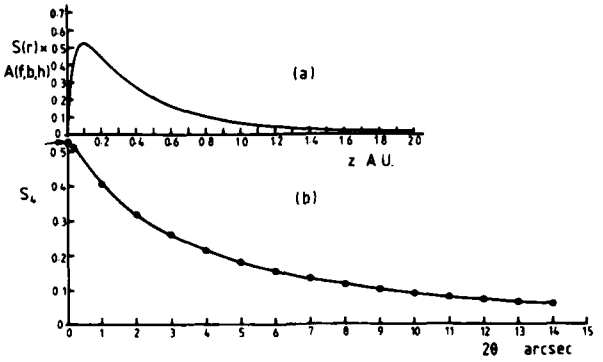

Figure 6. (a) The scattering power, S(r), multiplied by the correction factor, A(f,b,h) of Budden and Uscinski (1970) as a function of the distance, z, to Jupiter.
(b) The scintillation index S_4 vs. source angular diameter.

(iii) the scattering from the small-scale irregularities which attained a maximum value at 2011. This implies a minimum source size at that time (Figure 6b).

Gotwols et al. (1978) have pointed out that the effect of a finite-diameter source is to apply a low-pass filter to the power spectrum of the equivalent point source. For a source of Gaussian brightness distribution the temporal source cut-off frequency, ν_s, equals $u/\pi\theta_0 z$, where $u = v_s \sin\varepsilon$. In a preliminary estimate we obtain a source semi-angle, $\theta_0 \leq 0''.3$ arc at 2011-2013 UT and 1" to 1".5 arc in period A and up to 5" arc in period C. Corresponding source diameters are <2000 km at 2011-2013 UT, increasing up to possibly 30,000 km in period C (see Figure 3).

5. THE SOURCE ON JUPITER

In the previous sections we have ascertained that Jupiter had three relatively sustained levels of emission (periods A,B,C) with a maximum sustained emission in period C of $\sim 2 \times 10^{-14}$ W m^{-2} Hz^{-1}. From the scintillation data it appears that the source became strongly circularly polarized and had linear dimensions $\leq$2000 km during the sudden increase at 2011 UT, and perhaps up to 30,000 km in period C. We have also found that the solar-wind co-rotating magnetic sector that encountered Jupiter in this period was the same as that responsible for the great magnetic storm (Kp = 6+) which occurred on Earth some 12-14 days previously. This was a non-Io-related emission, and the maximum emission occurred very close to the SIII longitude (251°), corresponding to the occurrence probability maximum for 18 MHz (see Figure 2 of Thiemann and Smith, 1978).

The flux, S, of decametric radiation received on Earth, is given by

$$S = \frac{P}{\Delta f} \times \frac{1}{\gamma R^2} , \qquad (1)$$

where S (W m^{-2} Hz^{-1}) is the flux received at the Earth,
P (W) is the transmitter power,
Δf (Hz) is the bandwidth of the transmission,
γ (sr) is the solid angle over which the radiation is beamed, and
R (m) is the distance of the transmitter.

For the maximum sustained power in period C ($S = 2 \times 10^{14}$ W m^{-2} Hz^{-1} and distance R = 4.5736 AU = 6.8335×10^{11} m) we obtain

$$P = 9.3393 \times 10^{9} \Delta f \gamma W . \qquad (2)$$

For a cone of small semi-angle θ

$$P = 7.1113 \times 10^{6} \Delta f \theta^2 . \qquad (3)$$

Jupiter rotates through 1° in 1.65 min;

$\therefore$ for period C: $\theta \leq 2.42°$, which yields

$$P \leq 4.18 \times 10^{7} \Delta f W .$$

Now Δf, from previous work, is greater than 10^5 Hz and usually $\lesssim 1$ MHz

$$\therefore 4.2 \times 10^{12} < P < 4.2 \times 10^{13} W.$$

The flux observed from Jupiter is normally

$$10^{-22} < S < 10^{-20} W m^{-2} Hz^{-1}$$

(and may attain 10^{-18} W m^{-2} Hz^{-1} for S-bursts). Therefore the observed flux is $\sim 10^6$ times that normally observed. A flux so high has never been observed before. There are two main controlling factors which might explain this anomaly.

(i) Decametric emission occurrence is very sensitive to the value of D_E, even though the range (±3°.3) of the latter is smaller than the displacement of the magnetic North Pole from the geographic North Pole (Figure 7). The phase of the Jupiter period (11.86 yr) relative to the solar cycle (11.2 yr) is such as to yield negative D_E and suppress the effect of enhanced solar activity until this present cycle (21).

(ii) There was a correlation with solar wind parameters which initiated a great magnetic storm on Earth.

Furthermore, conditions for Jupiter observation are, at any time, limited to a particular area (Figure 2) on the Earth and hampered by radio interference, particularly in the evening. Perhaps neglect of the non-Io-related emission in favour of the supposedly stronger Io-related emission has caused these events to be missed.

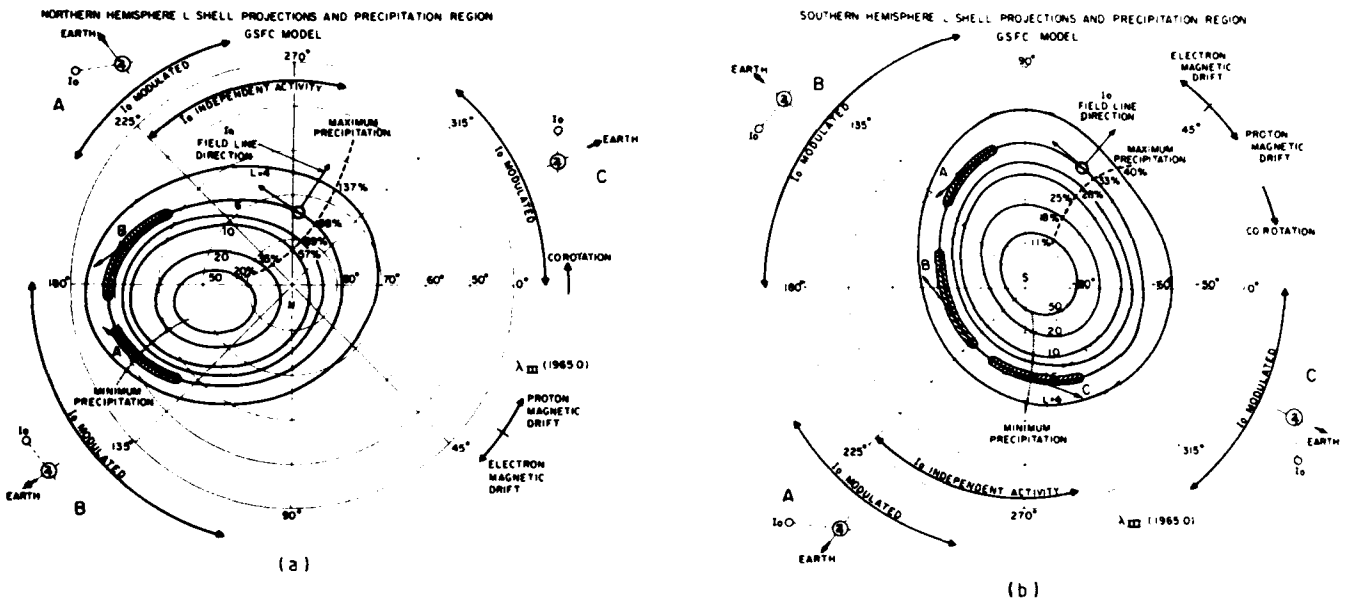

Figure 7. L = constant drift shell intersections with the planetary ionosphere in the (a) northern and (b) southern hemispheres of Jupiter, drawn for the 1965 epoch of system III longitude. Dashed and dotted lines represent zones of maximum and minimum precipitation flux, respectively. The percentage values represent the relative variation of the precipitation function between minimum and maximum along a given L = constant contour for each hemisphere. Circles on the L = 6 contour indicate spots of expected maximum precipitation flux of Io-scattered electrons; the projection of the Io field line and the Earth viewing line perpendicular to B is indicated for each spot. The angles of stable Io-modulated decametric radio emission activity are also shown (Warwick, 1967; Carr and Desch, 1976), a vector diagram indicating the relative phases (Io-Jupiter, Jupiter-Earth) required for the detection of each source. On the L = 6 contour the possible source regions of the Io-modulated decametric emission peaks detected at Earth are marked. The arrows indicate Earth viewing lines perpendicular to B. (Figure taken from Roederer et al. (1977); reproduced by permission of Journal of Geophysical Research.)

The cyclotron soliton model of Cole and Pokhotelov (1980) fits the experimental data very well.

(i) It has extremely efficient particle-to-wave energy conversion, thus allowing the extremely high observed brightness temperatures to be produced.

(ii) It produces high polarizations; the polarization is RH and circular when the field line at the source is directed towards us.

(iii) Lack of evidence of any significant contribution to signal scintillation or Faraday rotation in the Jovian ionosphere/magnetosphere indicates that the source has to be located at some height above that at which the plasma frequency, ω_p, equals 18 MHz. Their location of the source at $\omega_B \gtrsim 9$ MHz, $\omega_p \approx 9$ MHz satisfies this requirement and also results in the field line at the source being tilted more favourably, by 2°-6°, toward the Earth.

On the Cole and Pokhotelov (1980) model the source would be located on the evening side of Jupiter (Figure 7) like the auroral kilometric radiation on Earth. The Voyager observations will confirm or disprove this interpretation, since for the model to be correct there would have to be a brilliant aurora at the foot of the field line.

Possibly all features (power, polarization, emission geometry, beamwidth) of Jovian decametric emission may be explained on the cyclotron soliton model. The main requirement is that the three-dimensional soliton be located on a field line tilted most favourably toward the Earth. Thus the non-Io-related source position lies approximately on a line parallel to the SIII longitude 251° passing through the north magnetic pole. Such a line cuts the L-shells virtually at right angles along a magnetic meridian where the L-shells attain a low geographic latitude and where the field lines on a particular L-shell are therefore most favourably inclined to the Earth. The Io-related sources are situated at similar locations. The link with Io is now more indirect; we visualize heating of the ionospheric plasma as the satellite feeds power down the appropriate field line (in addition, of course, to increasing the flux of energetic particles). Subsequently the heated plasma probably diffuses upward along the field line and ω_p approaches ω_B, making the cyclotron soliton process possible. This corresponds, very approximately, to relabelling the shaded region "A" in Figure 7(a) as "B", and vice-versa, and redrawing the arrows, at right angles to the Io L-shell, in the direction of Earth.

The cyclotron soliton model receives strong confirmation from the "null" result the Voyager flypast where the signal level remained constant during flypast. This is due to the effect of the decreasing distance being annulled by the worsening orientation of the spacecraft relative to the emitting source. For efficient particle-to-wave energy conversion the energetic electrons within an individual soliton have to be phase-bunched; hence the beamwidth (6°) is simply related to the soliton cross-sectional area (~10^5 to 10^6 m^2) transverse to the field line.

6. DETECTION OF DISTANT JUPITER-LIKE PLANETS

Using the Voyager technique of comparing the RH and LH polarized signals and an aerial gain of 10^6 (area ≈ 500 × 500 m) we could attain a flux sensitivity of 10^{-35} W m^{-2} Hz^{-1} and detect a Jovian planet at a distance of 32 light years. Clearly it is perfectly feasible to search for Jupiter-like planets among the stars. For random orientation the majority should be detectable.

Acknowledgments

The authors would like to thank the members of the Space Physics Group at the University of Sheffield (led by Professor T.R. Kaiser) and in particular Mr. A. Strong for their help in this project. The assistance of Mr. P. Hughes, Mrs. Elaine Lycett, Mr. K. Thurston, Mrs. Diane Hallam and Mr. R.D. Cotterill was also appreciated.

The observations were conducted as a student project ably carried out by Mr. T.L.P. Baud, Mr. S.R. Darnell and Miss Frances S. Lochtie (under the supervision of K.B.).

We are indebted to Mr. R.W. Smith for information from the World Data Centre, Appleton Laboratory, Slough.

References

Akasofu, S.-I.: 1979, "Interplanetary energy flux associated with magnetospheric substorms", Planet. Space Sci., 27, 425.

Barrow, C.H.: 1979, "Association of corotating magnetic sector structure with Jupiter's decameter-wave radio emission", J. Geophys. Res., 84 (A9), 5366.

Briggs, B.H., and Parkin, I.A.: 1963, "On the variation of radio star and satellite scintillation with zenith angle", J. Atmos. Terr. Phys., 25, 339.

Budden, K.G., and Uscinski, B.J.: 1970, "The scintillation of extended radio sources when the receiver has a finite bandwidth", Proc. R. Soc. Ser. A, 316, 315.

Bullough, K., Gibbons, W., Baud, T.L., Darnell, S., and Lochtie, F.S.: 1979, "Jovian decametric emissions of unusual intensity" (Preprint).

Carr, T.D., and Desch, M.D.: 1976, "Recent decametric and hectometric observations of Jupiter", in Jupiter (ed. T. Gehrels), p. 693 (University of Arizona Press, Tucson).

Cole, K.D., and Pokhotelov, O.A.: 1980, "Cyclotron solitons - Source of Earth's kilometric radiation", Plasma Phys., 22, 595.

Cronyn, W.M.: 1972, "Density fluctuations in the interplanetary plasma: Agreement between space-probe and radio scattering observations", Astrophys. J., 171, L101.

Fremouw, E.J., and Rino, C.L.: 1973, "An empirical model of average F-layer scintillation at VHF/UHF", Radio Sci., 8, 213.

Gehrels, T. (ed.): 1976, Jupiter (University of Arizona Press, Tucson).

Gosling, J.T., Asbridge, J.R., Bame, S.J., and Feldman, W.C.: 1976, "Solar wind speed variations: 1962-1974", J. Geophys. Res., 81, 5061.

References

Gotwols, B.L., Mitchell, D.C., Roelof, E.C., Cronyn, W.M., Shawhan, S.D., and Erickson, W.C.: 1978, "Synoptic analysis of interplanetary radio scintillation spectra observed at 34 MHz", J. Geophys. Res., 83, 4200.

Readhead, A.C.S.: 1971, "Interplanetary scintillation of radio sources at metre wavelengths - II", Mon. Not. R. Astron Soc., 155, 185.

Roederer, J.C., Acuna, M.H., and Ness, N.F.: 1977, "Jupiter's internal magnetic field geometry relevant to particle trapping", J. Geophys. Res., 82, 5187.

Rufenach, C.L.: 1972, "Power-law wavenumber spectrum deduced from ionospheric scintillation observations", J. Geophys. Res., 77, 4761.

Rufenach, C.L.: 1974, "Wavelength dependence of radio scintillation: Ionosphere and interplanetary irregularities", J. Geophys. Res., 79, 1562.

Rufenach, C.L.: 1975, "Ionospheric scintillation by a random phase screen: Spectral approach", Radio Sci., 10, 155.

Thieman, J.R., and Smith, A.G.: 1978, "Frequency and time dependence of the Jovian decametric radio emissions: A nineteen year high-resolution study", J. Geophys. Res., 83 (A7), 3303.

Warwick, J.W.: 1967, "Radiophysics of Jupiter", Space Sci. Rev., 6, 841.

END

DATE
FILMED

9 — 83

DTIC